THE UNIVERSITY OF CHICAGO

GENETIC MODULATION OF A HUMAN KINASE USING ENGINEERED INTRACELLULAR ANTIBODY FRAGMENTS

A DISSERTATION SUBMITTED TO
THE FACULTY OF THE DIVISION OF THE BIOLOGICAL SCIENCES
AND THE PRITZKER SCHOOL OF MEDICINE
IN CANDIDACY FOR THE DEGREE OF
DOCTOR OF PHILOSOPHY

GRADUATE PROGRAM IN BIOCHEMISTRY AND MOLECULAR BIOPHYSICS

BY
KELLY MICHAEL O'LEARY

CHICAGO, ILLINOIS
JUNE 2025

Abstract

Mechanistic target of rapamycin (mTOR) is a serine/threonine protein kinase that regulates eukaryotic cell growth and metabolism in response to nutrient and growth factor cues. Dysregulated mTOR signaling is implicated in the progression of a wide range of human diseases, including cancer, neurodegeneration, metabolic disorders, and age-related conditions. Despite significant therapeutic potential, efforts to safely and effectively modulate aberrant mTOR activity with small molecules remain hindered by an incomplete understanding of how its substrate recruitment modalities, conformational dynamics, and subcellular spatial functions are coupled to distinct physiological outputs.

To address these limitations, this thesis describes an approach for modular genetic control of mTOR-mediated signal transduction. Herein, a series of synthetic antibody fragments targeting multiple epitopes and conformations of an mTOR substrate recruitment domain were generated using phage display. When genetically encoded as intracellular single-chain variable fragment “intrabodies” in living cells, these binders enabled programmable modulation of mTOR activity with conformational, spatial, and epitope-based precision. A combination of high-resolution crystallographic studies and cell-based functional assays provided key insights into FRB-mediated substrate docking, an allosteric mechanism governing mTOR complex 1 stability, the subcellular regulation of nuclear and cytoplasmic mTOR signaling, and an inhibitory binding site for unconventional modulation of mTOR function. In summary, this work integrates protein engineering, molecular structure, and synthetic biology approaches to establish engineered intracellular antibody fragments as essential tools for investigating the structural and spatial mechanisms driving therapeutically relevant protein kinase activity.

Table of Contents

List of Figures

List of Tables

Abbreviations

4E-BP1	-	Eukaryotic initiation factor 4E binding protein 1
βarr	-	β-arrestin
BSA	-	Bovine serum albumin
BRET	-	Bioluminescence resonance energy transfer
CASTOR1	-	Cytosolic arginine sensor for mTORC1 subunit 1
CASTOR2	-	Cytosolic arginine sensor for mTORC1 subunit 2
CDR	-	Complementarity determining region
CRIM	-	Conserved region in the middle domain
Cryo-EM	-	Cryogenic electron microscopy
DNA	-	Deoxyribonucleic acid
eGFP	-	Enhanced green fluorescent protein
ELISA	-	Enzyme-linked immunosorbent assay
ER	-	Endoplasmic reticulum
Fab	-	Antigen binding fragment
FACS	-	Fluorescence-activated cell sorting
FAT	-	FRAP/ATM/TRAAP
FATC	-	FAT C-terminal
FDA	-	United States Food and Drug Administration
FKBP12	-	FK506 binding protein of 12 kDa
FRB	-	FKBP12-rapamycin binding domain
FRET	-	Fluorescence resonance energy transfer
GAP	-	GTPase-activating protein
GDP	-	Guanosine diphosphate
GPCR	-	G-protein coupled receptor
GTP	-	Guanosine triphosphate

HEAT	-	Huntington/EF3A/ATM/TOR
HG1	-	Hydrophobic groove 1
HG2	-	Hydrophobic groove 2
H2A	-	Histone 2A
IC_{50}	-	Half-maximal inhibitory concentration
IGF1	-	Insulin-like growth factor 1
IgG	-	Immunoglobulin G
K_D	-	Dissociation constant
KRAS	-	Kirsten rat sarcoma virus
mChe	-	mCherry
mTOR	-	Mammalian or mechanistic target of rapamycin
mTORC1	-	mTOR complex 1
mTORC1	-	mTOR complex 2
$mTOR^{FRB}$	-	FRB substrate recruitment domain of mTOR
PBS	-	Phosphate buffered saline
PDB	-	Protein data bank
PI3K	-	Phosphatidylinositol 3-kinase
PIKK	-	Phosphatidylinositol 3-kinase-related kinase
PIP_3	-	Phosphatidylinositol 3,4,5-triphosphate
PKCα	-	Protein kinase C α
PPI	-	Protein-protein interaction
Rotamer	-	Rotational isomer
S6	-	Ribosomal protein S6
S6K1	-	p70 S6 kinase 1
sAB	-	Synthetic antibody
SAbDab	-	Structural antibody database
SASA	-	Solvent accessible surface area

scFv	-	Single-chain variable fragment
SDS-PAGE	-	Sodium dodecyl sulfate polyacrylamide gel electrophoresis
SEC	-	Size exclusion chromatography
SESN	-	Sestrin1/2/3
SGK1	-	Serum- and glucocorticoid- induced protein kinase 1
STAT3	-	Signal transducer and activation of transcription 3
SPR	-	Surface plasmon resonance
TFEB	-	Transcription factor EB
TOR	-	Target of rapamycin
TOR1	-	Target of rapamycin 1
TOR2	-	Target of rapamycin 2
TOS	-	TOR signaling motif
ULK1	-	Unc-51-like autophagy-activating kinase 1

Acknowledgments

This dissertation is dedicated to the loved ones, colleagues, and mentors who played a role in shaping my path through science. Words cannot express my gratitude for your support along the way, but the following acknowledgements will have to do.

I would not be where I am at today without the influence of my PhD advisor, Anthony Kossiakoff, who opened the door to opportunities beyond what I had ever imagined. His guidance, insights, and boundless creativity inspired me to grow every single day and explore basic concepts from new perspectives. To Tony, thank you for giving me a chance, believing in me, and supporting my research endeavors.

The work presented in this dissertation would not be possible without significant contributions made by Tomasz Ślężak. It has been a true pleasure to work together on various projects where his work ethic, dedication to research, and leadership have always been exemplary. I would like to highlight that his generosity, quick-witted humor, and persistent optimism played an important role in making each day fun and exciting, even throughout hardships and setbacks. I am grateful to have Tomasz as a role model but even more so as a lifelong friend. My time at the University of Chicago would not have been the same without him. I was fortunate to share many other friendships with those who spent time in the Kossiakoff lab over the years – thank you to everyone who contributed to the energizing atmosphere and inspiring research environment. Additionally, I want to thank Aleksander Promiński for his friendship, good company, and inspiration as a scientist during his time in Chicago.

My interest in biochemistry arose somewhat fortuitously while attending the University of Wisconsin-La Crosse. I am deeply indebted to two professors, Todd Weaver

and Daniel Grilley, for providing me with an opportunity to participate in their undergraduate research program. Little did I know that it would end up reshaping my entire career trajectory. I would also like to extend my gratitude to the members of my PhD thesis committee, Erin Adams, Engin Özkan, and Geoffrey Greene, for their guidance and valuable insights provided throughout my time at the University of Chicago.

Last but not least, I want to highlight the unconditional support I have received from my loved ones while pursuing my dreams. To my parents, Kathleen and Michael O'Leary, thank you for instilling in me the importance of hard work, but above all, the value of being a good person. I am grateful to you both for raising me the way that you did. To my partner, Julia Michalkiewicz, your unwavering love, encouragement, and patience mean the world to me. You have always been there for me since the day we crossed paths in Chicago. I cannot thank you enough for being a source of strength and joy, even during the most challenging of times.

Chapter 1

Introduction

1.1 Regulation of eukaryotic cell growth and metabolism by mTOR

The understanding of how eukaryotic cells sense and respond to environmental nutrients followed a serendipitous path beginning with a bacterial natural product known as rapamycin. Rapamycin is a macrocyclic lactone produced by *Streptomyces hygroscopicus* that was initially discovered in a soil sample extracted from the island of Rapa Nui (i.e., Easter Island) in 1975 (1–4). The unique pharmacological properties of rapamycin, including potent antifungal and immunosuppressive effects, suggested a common mechanism of action from yeast to humans and prompted a critical search for its molecular target (5). It was found that rapamycin forms a complex with the immunophilin FKBP12 by a mechanism similar to the natural product and immunosuppressant FK506 (6). In the 1990s, two independent research groups identified a set of genes responsible for rendering yeast resistant to the effects of the FKBP12-Rapamycin complex (7, 8). These genes were named target of rapamycin 1 (TOR1) and target of rapamycin 2 (TOR2), thus implicating the evolutionarily conserved TOR kinase as the pharmacological target of rapamycin (9). The mammalian homolog of TOR (mTOR) was discovered soon after, providing a molecular foundation for how cells sense and respond to environmental nutrients through an evolutionarily conserved pathway (10–12). Today, mTOR remains the focus of a large body of research and has been actively pursued as a therapeutic target since its discovery (13). It is important to underscore that our understanding of the mTOR pathway might have faced much larger barriers without the use of rapamycin as a molecular probe.

mTOR is one of six members in the evolutionarily conserved phosphatidylinositol 3-kinase-related kinase (PIKK) family of serine/threonine protein kinases (14). This group of kinases is characterized by large size (2549 to 4128 amino acids), common domain architecture, obligate binding partners, and by their critical roles in metabolism, chromatin remodeling, DNA damage response, or mRNA decay (15). Common structural features of PIKKs include an α-solenoidal Huntington/EF3A/ATM/TOR (HEAT) repeat domain, a FRAP/ATM/TRAAP (FAT) domain, a phosphatidylinositol 3-kinase-related kinase domain, and a FAT C-terminal (FATC) domain from N-terminus to C-terminus (Table 1.1).

Table 1.1 Features of PIKK family members.

PIKK	Domain architecture	AA length	Obligate partners	Cellular role
mTOR	HEAT-FAT-FRB-Kinase-FATC	2549	Raptor, Rictor, mSin1, mLST8	Nutrient-sensitive cell growth
ATR	HEAT-FAT-Kinase-FATC	2644	ATRIP	DNA damage, replication stress
ATM	HEAT-FAT-Kinase-FATC	3056	MRE11, RAD50, NBS1	DNA damage repair
SMG1	HEAT-FAT-FRB-Kinase-FATC-Ins	3661	SMG8, SMG9, UPF1, UPF2	mRNA decay
TRRAP	HEAT-FAT-FRB-Kinase-FATC	3859	SAGA, NuA4	Chromatin remodeling
DNA-PKcs	HEAT-FAT-FRB-Kinase-FATC	4128	Ku70/80	DNA damage repair

Together, PIKKs represent attractive drug targets due to their role in controlling fundamental cellular processes that are commonly dysregulated in diseases. However, their massive size, conformational flexibility, and complex interactions with accessory proteins have hampered efforts to develop highly selective inhibitors (16). Catalytic inhibition via adenosine triphosphate (ATP) competition using small molecule drugs is currently the most potent strategy for PIKK inhibition, but even the most selective ATP-

competitive inhibitors exhibit “off-target” crosstalk with phosphatidylinositol 3-kinase (PI3K) or other PIKK members (17). Therefore, uncovering unique structural or conformational vulnerabilities among PIKKs is of great interest for the design next-generation therapeutic inhibitors with optimal selectivity.

TOR was the first PIKK member described, with mTOR following shortly after (8). The phosphorylation of diverse substrates by mTOR plays a central role in regulating cellular metabolism, growth, and homeostasis and provides a critical linkage between the availability of basic nutrients and coordination of cell growth (18). Functioning as the catalytic component in two distinct multi-subunit complexes, mTOR complex 1 (mTORC1) and mTOR complex 2 (mTORC2), mTOR is the master integrator of signals from nutrients, growth factors, and cellular energy status to control essential processes such as protein synthesis, lipid metabolism, and autophagy (19). As a result of signaling from distinct molecular complexes, the upstream regulators and downstream effectors of the mTORC1 and mTORC2 pathways are exquisitely organized in a modular format to relay pro-growth or starvation cues through independent networks (Figure 1.1). For example, amino acid and growth factor inputs are integrated through separate signaling cascades that ultimately converge on mTORC1 and/or mTORC2.

The molecular sensing of leucine and arginine represents the best described mechanisms of upstream nutrient-dependent regulation in the mTOR pathway. Leucine abundance is directly sensed through its recognition by a stress-responsive cytoplasmic receptor called Sestrin2 (SESN) and by leucine aminoacyl-tRNA synthetase (LRS) (20, 21). On the other hand, arginine abundance is sensed through a cytosolic receptor known

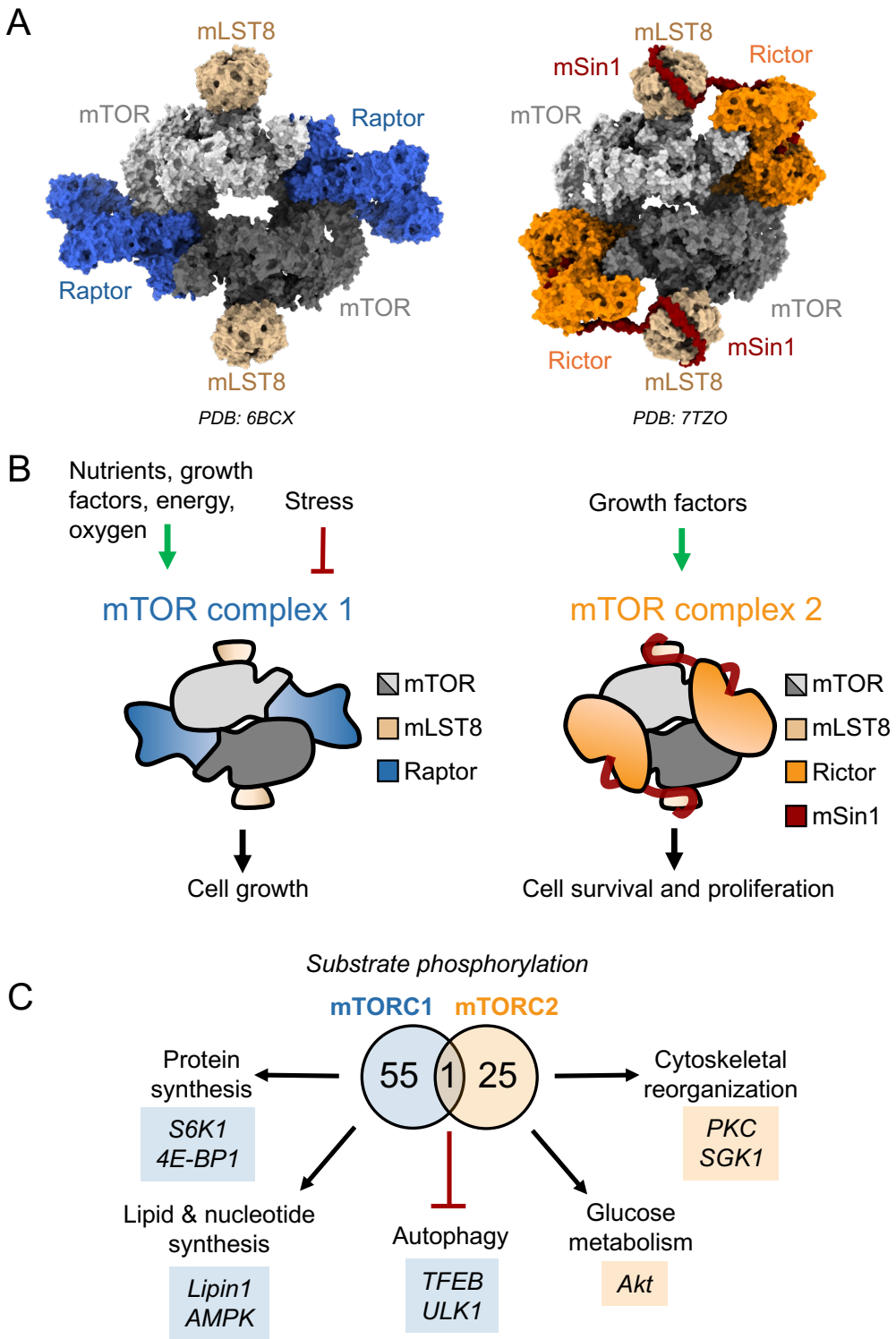

Figure 1.1 Modular basis of mTOR complex assembly and substrate phosphorylation. Figure caption continued on the next page.

Figure 1.1 Modular basis of mTOR complex assembly and substrate phosphorylation. (A) Previously determined high-resolution cryo-EM structures of mTORC1 (left, PDB: 6BCX; 4E-BP1 removed for clarity) and mTORC2 (right, PDB: 7TZO). (B) *Top:* Upstream signals integrated by mTORC1 and mTORC2 signaling assemblies. *Middle:* Cartoon schematics of mTORC1 and mTORC2 assembly. *Bottom:* Differential control of cell physiology and behavior by mTORC1 and mTORC2. (C) Mutually exclusive substrate recruitment and phosphorylation by mTORC1 and mTORC2. Venn diagram represents individual substrates that have been described as direct phosphorylation targets by mTORC1 or mTORC2. The general cellular functions governed by substrate phosphorylation are indicated. This representation is original but is based on information published in the article by Battaglioni et al (2022) *Cell*.

as cytosolic arginine sensor for mTORC1 subunit 1 (CASTOR1) and subunit 2 (CASTOR2) and by transmembrane receptors SLC38A9 and TM4SF5 (22, 23). Regardless of the cognate receptor, all amino acid sensors converge through the GATOR1-GATOR2 axis to mediate Ras-superfamily Rag activation of mTORC1 on the lysosome surface (24–26). The Rag complex is composed of two heterodimers, RagA/B and RagC/D, which are anchored to the lysosome by another complex called Ragulator (27). In the presence of amino acids, guanosine triphosphate- (GTP) bound RagA/B and guanosine diphosphate- (GDP) bound RagC/D interact together with the mTORC1 subunit known as Raptor to promote activation of mTORC1 together with another GTPase activator, Rheb, at lysosomes (28, 29). This fine-tuned pathway represents a key paradigm for nutrient-sensitive regulation of cell homeostasis. mTORC1 activity can be rapidly toggled on or off owing to its recruitment to the lysosome, which is also a master regulator of cell nutrient availability. While mTORC1 exhibits fine-tuned sensitivity to multiple independent amino acid sensor inputs, mTORC2 is rendered insensitive to amino acid signaling. That being said, both mTORC1 and mTORC2 are stimulated by growth factor signaling.

Growth factor signaling to mTORC1 occurs through a separate pathway from amino acid inputs. For example, growth factors, such as insulin or insulin-like growth factor 1 (IGF1,) bind to their cognate receptors and trigger recruitment and activation of PI3K (30). Production of phosphatidylinositol 3,4,5-triphosphate (PIP_3) by PI3K leads to the activation of Akt (31). Akt then phosphorylates tuberous sclerosis complex (TSC) on the TSC2 subunit, which regulates the GTPase-activating protein (GAP) activity of TSC and leads to modulation of the nucleotide-bound state of Rheb (32). TSC represents a major negative regulatory node in the mTORC1 pathway that is relieved in a growth factor-dependent manner.

mTORC2 is activated by growth factors but is less well understood compared to mTORC1. PI3K-mediated PIP_3 production has been suggested to directly activate mTORC2 through two potential models. First, PIP_3 may directly interact with the mTORC2 subunit known as mSin1 to relieve a mechanism of autoinhibition (33, 34). Second, Akt has been proposed to directly regulate mTORC2 activity through phosphorylation of mSin1 at position T86 (35, 36). Nevertheless, it has been established that growth factor-activated mTORC2 phosphorylates Akt at position S473, which represents the best characterized downstream effector of mTORC2 signaling (37–39). Full Akt activation requires phosphorylation at position T308 by phosphoinositide-dependent protein kinase 1 (PDK1) and phosphorylation at position S473 by mTORC2 (40–42). These findings implicated mTORC2 as an indirect regulator of growth factor-induced mTORC1 activation through modulation of the Akt-TSC axis (43). Furthermore, mTORC1 signaling promotes a negative feedback loop through insulin receptor substrate 1 and 2 (IRS1/2), which leads to downregulation of the PI3K-Akt axis and mTORC2 (44). The phosphorylation of other

substrates by mTORC2, including protein kinase C α (PKCα) and serum- and glucocorticoid- induced protein kinase 1 (SGK1), leads to modulation of cytoskeleton dynamics (45, 46). In addition to the canonical amino acids and growth factors described here, myriad other upstream regulators of mTORC1 and mTORC2 have been reported over the years. Together, these findings underscore the complexity of the molecular sensors and circuits that enable cells to dynamically balance their growth and metabolism in response to diverse nutritional cues or nutritional stress (Figure 1.2).

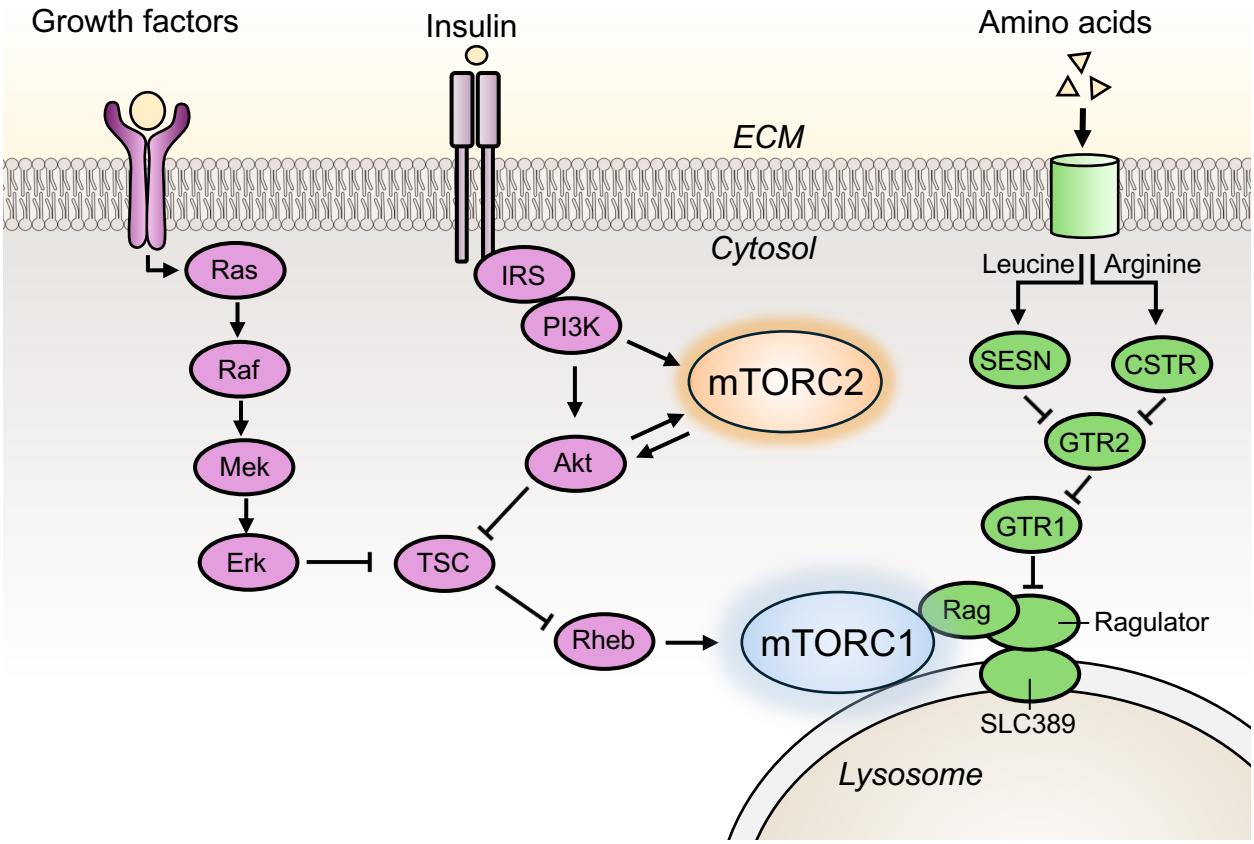

Figure 1.2 Regulation of mTOR signaling by nutrients and growth factors. Signaling pathway schematic for upstream amino acid-dependent (green) and growth factor-dependent (magenta) regulators of mTORC1 (blue) and mTORC2 (orange).

Dysregulated cell growth, proliferation, and migration are implicated in many pathophysiological processes. Hyperactive mTOR signaling is a hallmark of several human diseases, including diabetes, cancer, neurological disorders, and inflammatory disorders (47). These diseases are characterized by loss of control over processes including protein synthesis, cell growth, cell proliferation, or autophagy, which are all key downstream elements controlled by mTORC1 and mTORC2 (48). Furthermore, mTOR dysregulation has been found to promote the cellular aging process, and suppression of mTOR activity has consistently been reported to extend the lifespan and reduce age-related pathologies in diverse eukaryotic model organisms (48). The widespread involvement of mTOR in diverse pathologies underscores its significance as a therapeutic target. As central signaling hubs, mTORC1 and mTORC2 integrate upstream nutrient and growth factor signals to regulate numerous downstream effectors. Conceptually, this centralized positioning renders mTOR a strategic molecular target for controlling cell function, even in the presence of dysregulated inputs, by small molecule therapeutics. However, the implementation of mTOR inhibitors in clinical settings, especially for the treatment of cancers, has shown limited success.

Therapeutic mTOR inhibitors can be divided into three main categories. The first category of mTOR inhibitors includes rapamycin and several rapamycin analogs. Modifying the macrolide ring at positions C16, C32, or C40 represents a basic strategy to derivatize rapamycin for improved physical and pharmacokinetic properties while maintaining potent binding capability. (49). One rapamycin analog, Temsirolimus, was approved by the United States Food and Drug Administration (FDA) in 2007 for the treatment of advanced stage renal cell carcinoma (50). However, rapamycin and its

analogs do not fully inhibit mTOR activity, which may explain their limited efficacy as cancer therapies. mTORC1 signaling is potently inhibited under acute timescales by rapamycin, but it was found that rapamycin inhibits roughly only one third of all mTORC1 substrates (51). Furthermore, rapamycin is unable to inhibit mTORC2 signaling under acute timescales owing to steric hindrance of its binding site (45). However, after prolonged exposure to rapamycin, mTORC2 complex assembly is disrupted and leads to its inhibition. The complex mechanisms by which mTOR is modulated by rapamycin are still being elucidated today.

To circumvent this issue, a second generation of ATP-competitive inhibitors were developed to completely block the catalytic activity of mTOR (52). One of the best described ATP-competitive inhibitors, known as Torin-1, showed high potency (low nanomolar IC_{50}) against mTOR and selectivity for mTOR by approximately 100-fold over other kinases (17). Further drug development efforts resulted in many new compounds, such as AZD8055, which exhibited up to 1,000-fold selectivity for mTOR over other kinases (53). However, even highly selective compounds such as AZD8055 have not made it past clinical trials due to safety profile issues and toxicities (54). Lastly, the third generation of mTOR inhibitors is represented by efforts to combine rapamycin with an ATP-competitive inhibitor through a flexible linker, known as RapaLink-1 (55). This inhibitor displays a unique activity profile but will likely be used as a research tool rather than a conventional therapeutic.

The limited clinical efficacy of mTOR inhibitors underscores our limited understanding of the mechanisms by which mTOR controls cell physiology in health and disease. The concept that certain subsets of downstream mTOR effectors may be responsible for

therapeutic benefits while other subsets may be responsible for toxicities and side effects represents an emerging paradigm in the design of the next generation of mTOR inhibitors. Emphasizing basic research into the molecular mechanisms underlying substrate recruitment and phosphorylation by mTORC1 and mTORC2 remains a promising approach to reveal insight into new therapeutic strategies. However, elucidating the complex processes involved in mTOR-mediated signal transduction has typically required the use of specialized molecular tools, such as rapamycin or catalytic inhibitors, to carry out selective functional perturbations in living cells. The next phase of decoupling mechanisms underlying mTOR substrate phosphorylation will almost certainly require new and customized molecular tools. One can envision that the rational design of inhibitors to enable fine-tuned perturbations to structural, functional, and spatial architectures of the mTOR signaling network might reveal valuable insight into potential therapeutic vulnerabilities.

1.2 Structural mechanisms of mTOR signaling

Like other PIKKs, the functional output of mTOR kinase activity is dependent on its association with accessory binding proteins or core subunit partners. Despite virtually no differences in amino acid sequence or catalytic cleft accessibility, substrate phosphorylation by mTORC1 and mTORC2 is almost entirely mutually exclusive (56). Therefore, the assembly of mTOR into two structurally and functionally distinct multi-subunit complexes represents a crucial mechanism governing how nutrient and growth factor signal transduction is communicated in cells. The molecular basis of mTOR complex assembly was studied intensively for years. Cornerstone findings that 1) mTOR

associates with a subunit called regulatory-associated protein of mTOR (Raptor) in mTORC1 and 2) mTOR associates with subunits called rapamycin-insensitive companion of mTOR (Rictor) and mSin1 in mTORC2 established a highly modular basis of mTOR signaling (45, 57, 58). Furthermore, another cognate subunit known as mLST8 was found to be associated with both mTORC1 and mTORC2 (59). Early cryogenic electron microscopy (cryo-EM) studies revealed that mTOR functions as an obligate homodimer with a rhomboid shape, and that inhibition by rapamycin leads to altered structural integrity of mTORC1 (60). Later, high resolution cryo-EM structures revealed that the architectures of mTORC1 and mTORC2 are similar in that Raptor and Rictor are assembled onto the same general positions in each respective complex (61, 62). These structures provided a molecular description behind the differential sensitivity of mTORC1 and mTORC2 to inhibition by rapamycin. Specifically, Rictor partially occupies the FKBP12-rapamycin binding site in mTORC2, which renders Rictor and FKBP12-rapamycin binding mutually exclusive.

Long before the mTOR architecture was understood, investigations into the mechanisms of how diverse substrates are specifically recruited and phosphorylated by mTOR were a primary focus. mTOR kinase activity exhibits low sequence specificity other than for proline, hydrophobic, or aromatic residues at the +1 position following the phosphorylation site of serine/threonine (51). Therefore, the preference for substrate phosphorylation is highly regulated by specific recruitment mechanisms innate to the associated subunit partners in mTORC1 and mTORC2. The earliest described recruitment mechanism found that a particular amino acid sequence motif is specifically recognized by Raptor in mTORC1. The TOR signaling (TOS) motif was reported for two

different mTORC1 substrates, p70 S6 kinase 1 (S6K1) and eukaryotic initiation factor 4E binding protein 1 (4E-BP1) (63, 64). The TOS motif is described as a five-residue sequence consisting of F-X-Φ-E/D-Φ, where X represents any amino acid and Φ represents hydrophobic amino acids (65). However, TOS-based recruitment is not described for all mTORC1 substrates, indicating that there are more complex mechanisms by which mTORC1 recruits substrates for phosphorylation. For example, transcription factor EB (TFEB) is an important mTORC1 substrate governing autophagy, which lacks a TOS motif and is instead coordinated in a Rag-dependent manner (28).

A second mechanism underlying mTORC1 substrate recruitment was revealed by high resolution structural studies. Crystal structure determination of a truncated mTOR kinase domain in complex with mLST8 revealed that the FKBP12-rapamycin binding (FRB) domain, a small four-helix bundle, is positioned adjacent to the catalytic cleft (66). These results suggested two major concepts. First, FKBP12-rapamycin binding to FRB would severely restrict access to the active site for mTOR substrates. Second, the FKBP12-rapamycin binding site could potentially interact directly with substrates to recruit and stabilize them for phosphorylation in the proximal catalytic cleft. Later on, structural studies of S6K1 and proline-rich Akt substrate of 40 kDa (PRAS40) peptides bound to FRB confirmed these concepts and defined the FRB domain as a critical substrate recruitment site (67). These findings posited that some substrates, such as S6K1, follow a bipartite mechanism of docking onto TOS and FRB. However, other TOS-dependent substrates, such as 4E-BP1, display rapamycin-resistant phosphorylation by mTOR, which suggests that FRB obstruction alone is not sufficient to block catalysis of all mTORC1 substrates (68).

Substrate recruitment by mTORC2 is far less understood than for mTORC1. Interactions between subunits Rictor and mSin1 have been suggested to mediate recruitment and phosphorylation of SGK1, PKCα, and Akt (62, 69). Specifically, the conserved region in the middle (CRIM) domain of Sin1 may directly interact with these substrates. mSin1 also makes interactions with Rictor and mLST8, suggesting that these inter-subunit interactions may also facilitate proper positioning of mSin1-based substrate recruitment (62). However, little is known in regard to particular sequence motifs or structural determinants of mTORC2-specific substrates. Gaining insight into the exact mechanisms by which mTORC2 recruits an independent set of substrates could lead to more effective targeted therapies for diseases driven by mTORC2-specific dysregulation.

1.3 Spatial mechanisms of mTOR signaling

Determining where and with which components mTOR forms active signaling complexes has been a major point of focus since its discovery. The modular basis of its association with distinct multi-subunit assemblies renders this a significant challenge. After years of work, initial models posited that mTORC1 preferentially signals from lysosomes and mTORC2 signals from the inner leaflet of the plasma membrane. However, mounting evidence suggests that mTOR localization is more widespread than previously thought. An emerging paradigm is that compartmentalization of distinct subcellular pools of mTORC1 and mTORC2 signaling assemblies may represent a higher organizational layer enabling cells to more efficiently integrate and respond to diverse nutritional or stress-related cues. How cells couple distinct mTOR complexes with subsets of substrates to particular locations inside the cell remains unanswered.

mTORC1 signaling is canonically described at the surface of lysosomes. This strategic positioning enables the regulatory kinase activity of mTORC1 to control the sensing or liberation of amino acids. Lysosomal mTORC1 activation is enabled by two distinct molecular modules that recruit and promote amino acid- and growth factor- dependent substrate phosphorylation. The first module is the Rag-Ragulator complex. RagA/B and RagC/D heterodimers, which are anchored to the lysosomal membrane by the Ragulator complex, have been established as critical components for docking of mTORC1 in response to amino acid availability (70). The second module is a farnesylated GTPase called RAS homolog enriched in brain (Rheb), which functions under growth factor-dependent TSC regulation (71). In contrast to Rag GTPases, Rheb functions by directly enhancing mTORC1 substrate phosphorylation (72). High resolution structural studies revealed that Rheb-dependent activation of mTORC1 signaling occurs through a direct protein-protein interaction (PPI) formed between GTP-bound Rheb and the N-HEAT, M-HEAT, and FAT domains of mTOR (67). Furthermore, Rheb-induced global conformational rearrangements in the structure of mTOR leads to closing and realignment of key active site residues implicated in catalysis. Together, the amino acid-dependent recruitment of mTORC1 to the lysosome by the Rag-Ragulator complex and the growth factor-dependent allosteric activation of mTORC1 by GTP-bound Rheb constitute a dynamic logic-gated mechanism governing cell growth and metabolism. However, the link between lysosomal localization and mTORC1 functionality goes deeper than simple recruitment and activation mechanisms. Through the phosphorylation of substrates TFEB and Unc-51-like autophagy-activating kinase 1 (ULK1), mTORC1 coordinates the biogenesis of lysosomes and regulates the activation of starvation-induced autophagy

(73). These findings established mTORC1 as both a functional and physical gatekeeper of autophagic regulation. Therefore, delineation of the spatial coupling between mTORC1 and lysosomes represents a milestone in understanding the subcellular regulation of the mTOR signaling network.

The paradigm of lysosomal mTORC1 signaling has been updated in recent years owing to the implementation of novel fluorescence resonance energy transfer (FRET) biosensors and subcellular-targeted inhibitors. A genetically encoded mTORC1 activity reporter (TORCAR), based on intrinsic conformational changes related to the phosphorylation state of 4E-BP1, enabled dynamic studies into mTORC1 activity at selected subcellular locations in living cells. In addition to canonical mTORC1 signaling at lysosomes, this work revealed mTORC1-mediated activity at the plasma membrane and inside the nucleus (74). Later, a nucleus-targeted Akt inhibiting peptide revealed that growth factor-mediated mTORC1 signaling in the nucleus is governed by Akt, providing an important layer of mechanistic insight into noncanonical spatial mTOR regulation (75). These findings have been corroborated by mTOR chromatin immunoprecipitation (ChIP) coupled with mass spectrometry or DNA sequencing. Specifically, mTOR interacts with numerous binding partners associated with chromatin and is found at promoters for genes of RNA polymerase (POL) I and III (76, 77). Furthermore, nuclear mTOR interacts with the androgen receptor and modulates transcriptional networks implicated in cancer metabolism as a consequence of its nuclear localization (78). The question of how mTOR-based scaffolding, interactions, or activity influences transcription from inside the nucleus remains a critical open question.

Similar to the mechanisms of its substrate recruitment, the spatial regulation of mTORC2 signaling is less well understood compared to mTORC1. Owing to its ties with growth factor-induced activation, early models in yeast posited that TOR complex 2 (TORC2) is associated with the inner leaflet of the plasma membrane (79). This description was conceptually satisfying since plasma membrane-bound mTORC2 could be easily integrated into the PI3K-Akt network. This was indeed confirmed, but observations of growth factor-independent mTORC2 activity suggested more intricate layers of regulation than simple PI3K-Akt-mTORC2 activation at the plasma membrane (80). However, studies of mTORC2 in mammalian cells showed many diverse patterns of reticular localization, suggesting that mTORC2 localization may be more widespread throughout the endomembrane system (81). mTORC2 localization has since been described at mitochondria, ribosomes, and inside the nucleus (82–84). Integrating all the evidence together, the question of, “where doesn’t mTORC2 reside inside cells?” becomes more relevant. Location-specific functional studies exploiting compartment-specific recruitment of heterologous Akt, a canonical mTORC2 substrate, demonstrated differential sensitivity to PI3K and growth factor stimulation between plasma membrane and endosomal mTORC2 pools (85). Furthermore, phosphorylation of Akt and SGK1 by mTORC2 preferentially occurs at the plasma membrane and peri-nuclear compartments, respectively (86). Together, these findings suggest that an underlying mechanism of subcellular localization highly influences the substrate phosphorylation, and therefore the functional output, of mTORC2 signaling.

A critical barrier to determining the subcellular localization and functional output of distinct mTOR signaling complexes in cells is the lack of tools capable of eliciting activity

perturbations with spatial resolution. Critical unanswered questions include how compartmentalization of mTOR activity at the plasma membrane, specific endomembrane structures, or inside the nucleus influences nutrient-sensitive cell physiology. Gene knockdowns and small molecule inhibitors lack the capability to perturb mTOR activity at precise subcellular locations and consequently provide a window into "whole cell" signaling phenotypes only. Pioneering studies in the field of subcellular mTOR regulation have consistently relied upon heterologous overexpression of substrates or fluorescent biosensors to measure location-specific mTOR activity. This work has been foundational, but it is important to note that employing heterologous substrates might alter localization or activity patterns relative to the endogenous signaling network. The development of molecular tools capable of eliciting kinase functional perturbations with precise spatial resolution could lower this barrier and enable studies into the subcellular regulation of endogenous signaling networks.

1.4 Molecular tools to dissect mTOR function

As described in the previous chapter, many paradigm-shifting studies in regard to the spatial regulation of mTOR signaling were enabled by the development of customized molecular tools. Rapamycin, although a natural product produced by bacteria, could be considered the first molecular tool harnessed by scientists to discover and explore the biology of mTOR. The next generation of ATP-competitive small molecule mTOR inhibitors revealed further insight into mechanisms of mTOR substrate phosphorylation. Together, chemical inhibitors of mTOR represent a primary category of molecular tools that have been invaluable to probe aspects of mTOR function (Figure 1.3). Another

important approach that enabled insight into the modular basis of mTOR signaling from mTORC1 and mTORC2 is the use of inducible gene knockdowns for Raptor, Rictor, or mLST8 (87, 88). The essentiality of mTOR for embryonic growth renders it a challenging target for complete knockout (89). Nevertheless, our understanding of the mTOR pathway might have faced much larger barriers without the use of inhibitors and gene knockdowns to elicit selective functional perturbations. This concept served as a jumping off point for the development of new molecular tools to dissect this pathway from different perspectives.

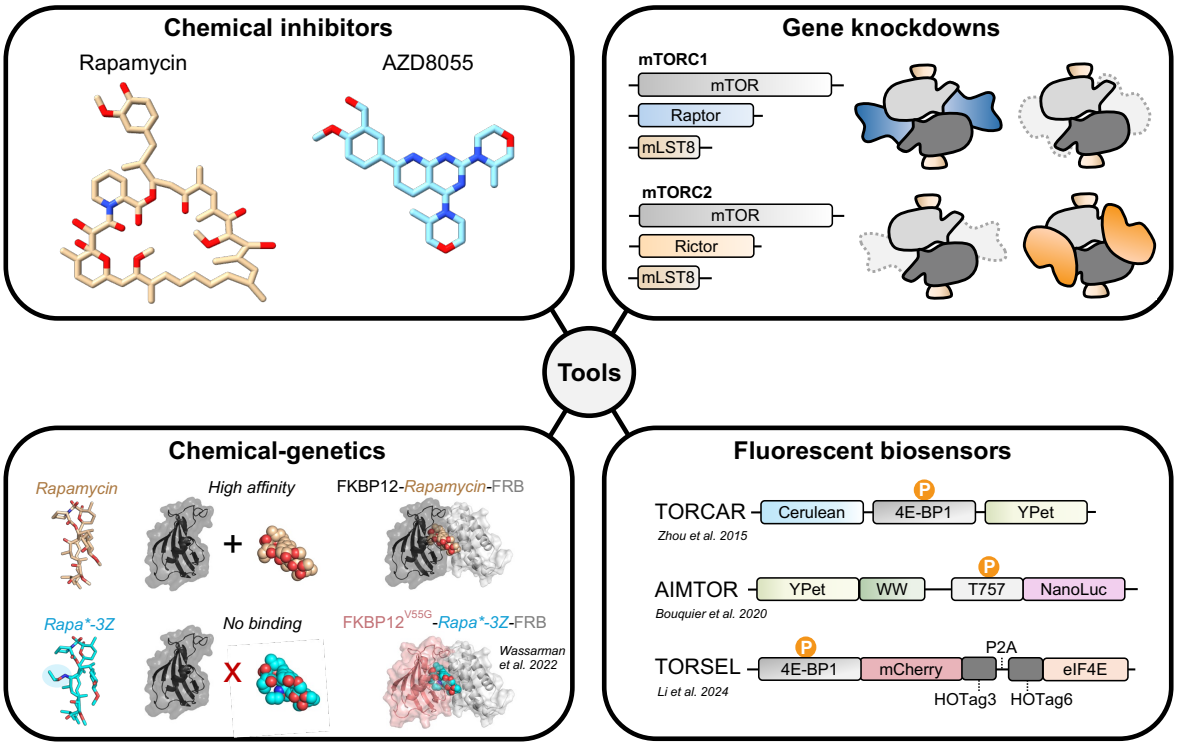

Figure 1.3 Classes of molecular tools to explore mTOR function. *Top left:* Structures of the natural product inhibitor rapamycin and the ATP-competitive inhibitor AZD8055. Structures were generated by ChemSpider and visualized using ChimeraX. *Top right:* Gene knockdowns to investigate mTORC1-specific and mTORC2-specific functionality. *Bottom left:* Chemical-genetic approach developed by Wassarman et al (2022) *PNAS.* (Models made using PDB: 1FAP and PDB: 7U8D). *Bottom right:* Construct maps for FRET or BRET based biosensors developed by Zhou et al (2015) *Cell Rep,* Bouquier et al (2020) *BMC Biology*, and Li et al (2024) *Cell & Bioscience*.

Recently, a novel chemical-genetic system was developed with the goal to enable tissue-restricted inhibition of mTOR by genetically encoding an FKBP12 variant (V55G) and administering a rapamycin analog (Rapa*-3Z) that specifically binds only to the FKBP12-V55G variant (90). This system, termed selecTOR, demonstrated that inhibition of mTOR in different tissues alone can delay larval development in *Drosophila melanogaster*. However, low selectivity between Rapa*-3Z, FKBP12-V55G, and wild-type FKBP12 present a restricted dynamic range that could influence the endogenous mTOR pathway. This limitation creates a barrier against full genetic control over mTOR inhibition. Nevertheless, the selecTOR approach represents the first tool geared toward eliciting tissue-restricted perturbations to mTOR function in living model organisms.

Other recent tool developers endeavored to generate sensitive genetically encodable biosensors with the goal to detect mTOR activity at specific subcellular locations in response to various nutrient or growth factor cues. The first example was demonstrated by TORCAR, a semi-synthetic construct containing full length 4E-BP1 with a cyan fluorescent protein (Cerulean) and yellow fluorescent protein (YPet) attached to each end (Figure 1.3). This system exploits the differential conformational dynamics of 4E-BP1 associated with its phosphorylated and unphosphorylated states mediated by mTORC1 activity to measure FRET between Cerulean and YPet. TORCAR exhibits exquisite sensitivity to growth factor or nutrient stimulation of mTORC1 activity at various subcellular locations and provided critical evidence to push the boundaries of spatial mTOR biology. However, since TORCAR is based on a rapamycin-resistant substrate, 4E-BP1, it does have limitations in exactly which perturbations can be perceived. Other efforts led to the development of AIMTOR, a bioluminescence resonance energy transfer

(BRET) based sensor exploiting a peptide from the mTORC1 substrate ULK1 fused by a linker to a WW domain with YPet and nanoluciferase attached to each end (91). The use of AIMTOR enabled investigations into subcellular pools of mTOR activity in muscle cells in response to leucine and was used to explore mTOR signaling in disease models of mouse neurons. In contrast to activity biosensors, a live-cell mTORC1 sensor (TORSEL) has been generated that detects endogenous or pharmacological inhibition of mTOR activity rather than substrate phosphorylation (92). TORSEL provided insight into histone deacetylase inhibitors that suppress nutrient signaling to mTORC1.

The approaches described above are important examples of how new tools create new opportunities to explore recalcitrant signaling pathways. Pharmacological inhibitors, gene knockdowns, chemical-genetic inhibitors, and fluorescent biosensors each offer valuable insight into the regulation of mTOR signaling. However, a key technological barrier that limits our understanding of how mTOR regulates nutrient-sensitive cell growth is the lack of tools capable of complete genetic control over conformational and spatial perturbations to the mTOR network. The remainder of this thesis will describe the development and implementation of engineered intracellular antibodies (intrabodies) for modulation of mTOR complex assembly and substrate phosphorylation using a genetically encoded platform. The primary advantages of using intrabodies to dissect mTOR function over existing technologies include 1) straightforward epitope-directed engineering against functional sites, 2) propensity to stabilize distinct conformational states, and 3) full genetic programmability for restricted expression in subcellular compartments. These innate properties of intrabodies harbor the potential to elicit

functional perturbations with conformational or spatial specificity, neither of which are possible using existing technologies.

Immunoglobulin G (IgG) based monoclonal antibodies are traditionally derived from animal immunization and hybridoma screening (93). However, this approach is costly, time consuming, and lacks precise control over selection pressures for customized antigen recognition. Phage display is a powerful approach for selecting synthetic antibody fragments (Fabs) *in vitro* with desired recognition properties from large combinatorial libraries containing up to 10^{10} unique variants (94). This method exploits the genetic fusion of a Fab to the pIII coat protein of M13 filamentous phage, thereby directly coupling the phage DNA sequence to the physical coat architecture displaying an encoded Fab (95). The humanized 4D5 Fab scaffold provides a unified framework for construction of powerful synthetic libraries owing to its stability and display level (94). Synthetic sequence diversity in Fab-phage particles can be targeted to complementarity determining regions (CDRs) in the light chain (L1, L2, L3) and heavy chain (H1, H2, H3) using a reduced genetic code to expand the number of diversified positions (96). Using a fully synthetic CDR framework greatly expands the recognition capabilities of unique Fab-phage variants in custom generated libraries (97). Furthermore, restricting sequence diversity to L3, H1, H2, and H3 has been demonstrated to be sufficient for generation of powerful synthetic binders (98).

Libraries are put through a standard iterative sorting procedure for three to five rounds against a target antigen using incremental selection pressures to isolate binders with high affinity and specificity for the target antigen (99). This process typically requires that the target antigen can be recombinantly expressed and immobilized on a solid support

platform, such as streptavidin beads, for the sorting procedure. Gradually reducing the concentration of immobilized target antigen from round to round represents the most basic selection pressure. Other customizable pressures include subtractive or competitive selections to deplete the library for binders against particular domains or conformational states (100). At the end of the sorting protocol, unique binders are identified by sequencing phage DNA and are subsequently cloned to an expression vector to isolate and characterize individual Fab molecules. Compared to traditional antibody discovery approaches, phage display biopanning is rapid, cost effective, and enables fine-tuned control over critical selection pressures leading to the isolation of binders with customized recognition properties. It is important to note that other display-based technologies, such as yeast display or mRNA display, offer similar levels of control

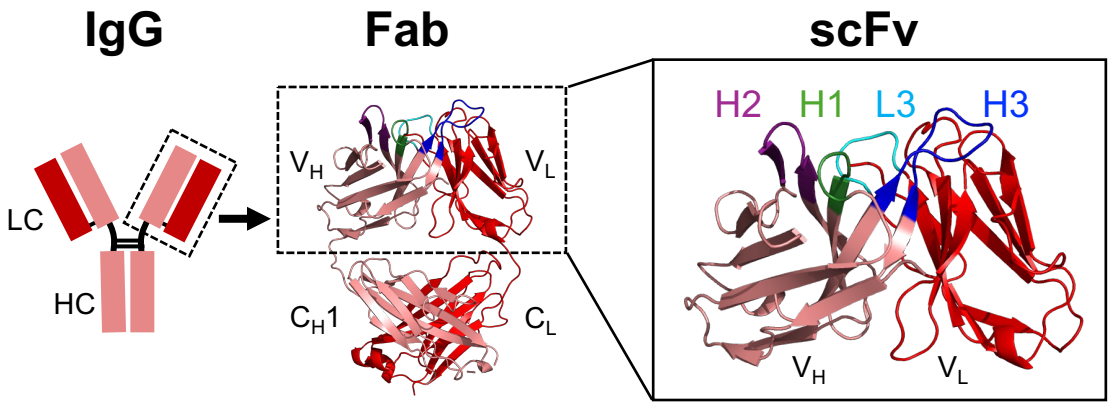

Figure 1.4 Interchangeability between IgG, Fab, and scFv format. IgG molecules are built from two independent chains, known as heavy chain (HC) and light chain (LC), which are covalently linked together via disulfide bond formation. The Fab portion can act as an independent binding module, consisting of a truncated version of the heavy (C_H1-V_H) chain and the full-length light chain (C_L-V_L). Derivatization of a Fab into V_H and V_L domains covalently tethered by a flexible linker represents the basis for scFv reformatting. The scFv format maintains antigen binding properties as CDRs (colored by L3, H1, H2, and H3) are retained, thereby representing a minimalist scaffold for genetic portability into living cells. Model made using PDB: 9DL0.

over selection pressures and are amenable for generating binders in several different antibody mimetic scaffolds (101, 102).

Synthetic antibodies generated via display-based technologies represent a crucial modality for therapeutic modulation of extracellular receptor domains involved in human diseases. While antibody therapeutics are typically limited to the extracellular milieu, intracellular antibody expression has been explored for decades now. The most basic format for intracellular antibody expression is the single-chain variable fragment (scFv), which can be derived from both IgG and Fab molecules (Figure 1.4). The first demonstration of intrabody-based modulation of an important oncoprotein was published in 1994, where researchers modified an scFv targeting the HER2 ectodomain with a signal sequence for retention in the endoplasmic reticulum (ER) lumen (103). Engagement of HER2 by the ER-anchored intrabody prevented its translocation to the plasma membrane, consequently preventing translocation or functionally inactivating oncogenic HER2 signaling from the cell surface. Restricted expression of intrabodies in compartments such as the ER has been one of the most popular methods of intrabody expression due to the oxidizing environment that allows for intra-chain disulfide bonds to form. It has been established early on that cytoplasmic expression of intrabodies leads to unpredictable effects on solubility and stability, potentially stemming from disulfide reduction, thermal stability, or propensity for aggregation (104–106). These findings severely limited further investigations into cytoplasmic expression of scFv binders for targeted knockdown of intracellular protein function. Other formats for intracellular synthetic binders include nanobodies, monobodies, affimers, and DARPins which can circumvent issues related to disulfide bond formation (107, 108).

Intrabodies provide several distinctive advantages over classical perturbation approaches, such as small molecule inhibitors or gene knockdowns. First, synthetic binders can be rapidly generated against multiple epitopes among diverse target antigens, including the binding sites of canonical inhibitors (109). Furthermore, the capability of synthetic binders to engage flat surfaces that are conventionally undruggable by small molecules offers a unique route to explore therapeutic vulnerabilities in recalcitrant disease-correlated proteins (110). Second, the propensity of synthetic binders to stabilize conformational states of their target antigen associated with distinct biological outputs enables insight into elusive conformational vulnerabilities (111). Lastly, full genetic programmability of protein-based modulators provides a route to encode “drug-like” functional perturbations in living cells or organisms. This is an important aspect since genetic knockdowns do not always recapitulate the effect of pharmacological knockdowns (112). Furthermore, incorporation of subcellular localization tags or tissue-specific promoter elements creates opportunities for spatially restricted intrabody-based perturbations in living cells or organisms. These properties underscore the capability for enhanced precision and control by using intrabodies over traditional perturbation approaches.

The utility of intrabodies has been highlighted in recent years through the specific modulation of proteins that are intractable by conventional inhibitors. Monobodies, based on the fibronectin type III domain, have been established as particularly useful synthetic binders for intracellular knockdown of protein function (108). The targeting of signal transducer and activation of transcription 3 (STAT3) using intracellular monobodies exemplified a new approach for control over dysregulated STAT3 activity in cancer (110).

This study showed how synthetic binders can precisely target STAT3 among other members in its family by recognition of a surface lacking conventional drug binding pockets. Furthermore, monobody engagement was shown to impair nuclear translocation and DNA binding, establishing a unique approach to perturb STAT3 activity. Monobodies have also been used to target the recalcitrant therapeutic protein known as Kirsten rat sarcoma virus (KRAS), which is frequently mutated in cancer. KRAS has been considered extremely difficult to target by conventional small molecules inhibitors, often earning the description of “undruggable” (113). While significant efforts have established small molecule inhibitors targeting certain KRAS mutations, there are still many unknowns regarding approaches to develop potent therapeutics to control KRAS (114). The development, functional characterization, and structural determination of various monobodies with selective recognition properties for KRAS mutations or conformations has provided critical insights into potential strategies for small molecule design (115, 116).

In addition to revealing molecular vulnerabilities for challenging therapeutic targets, intrabodies are useful reagents to explore fundamental biological mechanisms that evaded conventional research approaches. One of the most elegant demonstrations of scFv-based intrabody utility is in regard to the β-arrestin (βarr) and G-protein coupled receptor (GPCR) signaling axis. These investigations were enabled by the engineering of a series of synthetic Fabs against multiple isoforms, epitopes, and conformations of βarr, which were shown to allosterically modulate βarr PPIs and βarr-mediated GPCR endocytosis when expressed in scFv format inside living cells (117). This work represents a key milestone in understanding GPCR signaling dynamics owing to the lack of molecular tools geared toward tuning the GPCR-βarr framework in cells. Further studies

have shown scFv-based intrabodies that selectively report βarr-dependent trafficking of GPCR endocytosis, inhibit βarr-dependent GPCR endocytosis, or rescue βarr-dependent GPCR endocytosis in a mutant GPCR model (111, 118, 119). These findings have contributed key insights to inform the paradigm of drug discovery against myriad GPCR targets. Furthermore, the use of scFv-based intrabodies for allosteric modulation of βarr PPIs and conformational dynamics suggests that these tools can be extended toward many other complex targets in the intracellular proteome.

Together, the rapid library-based generation of synthetic binding proteins against desired epitopes or conformational states of a target antigen provides an efficient route to investigate intracellular signaling dynamics when small molecules or gene knockdowns are insufficient. The generation of synthetic Fabs via phage display represents a particularly robust approach owing to capacity for high combinatorial diversity, the relative ease of screening many binders, and the straightforward interchangeability between Fab and scFv format. Furthermore, the superior capability of engineered Fabs as crystallization chaperones enables feasible structure determination pipelines for elucidating mechanisms of target antigen recognition (120). Although intracellular scFv stability can impose issues in functional assays, the advantages of scFv intrabodies clearly outweigh potential drawbacks. The remainder of this thesis will describe the development and implementation of scFv-based intrabodies targeting a conserved substrate recruitment domain involved in mTOR signaling. Through biochemical and cell-based investigations, this work reveals new approaches for genetic control over structural and spatial mechanisms underpinning mTOR-mediated signal transduction.

1.5 Thesis outline

Inherent complexities underlying the regulation of nutrient-sensitive mTOR signal transduction impose fundamental barriers to the strategic discovery of safe and effective small molecule inhibitors. This thesis establishes a modular set of molecular tools for enabling functional perturbations to the mTOR network with unprecedented conformational and spatial specificity. These tools are based on engineered scFv-based intrabodies that possess first-in-class properties in regard to their capability for modulating mTOR complex assembly and substrate phosphorylation with genetically programmable control.

Chapter 2 describes the development of synthetic antibody fragments (Fabs) targeting the FRB substrate recruitment domain of mTOR ($mTOR^{FRB}$). This chapter begins with the engineering and characterization of synthetic Fabs through an epitope-directed phage display biopanning pipeline. High resolution X-ray crystal structure determination established the basis of $mTOR^{FRB}$ substrate recruitment site recognition by two unique synthetic binders, which revealed insights into the promiscuous molecular recognition capability for $mTOR^{FRB}$-mediated protein coordination.

Chapter 3 describes the implementation of drug-like scFv intrabodies targeting $mTOR^{FRB}$ for studies into the conformational and spatial regulation of mTOR function. An allosteric mechanism governing the structural integrity of mTORC1 was revealed by co-immunoprecipitation assays using two unique conformation-specific intrabodies. These intrabodies were modified with subcellular localization tags to enable spatially restricted investigations into cytoplasmic and nuclear mTOR signaling networks. The results described here represent the first example of cytoplasm- or nucleus-restricted inhibition

of mTOR signaling and provide a feasible platform for dissecting the subcellular organization of nutrient-sensitive signaling processes.

Chapter 4 describes the engineering and characterization of Fabs against binding sites located on $mTOR^{FRB}$ that are not targeted by conventional small molecule inhibitors. Crystal structures of two Fabs bound to $mTOR^{FRB}$ revealed the molecular basis for engagement of these unique functional sites. Furthermore, modulation of mTOR complex assembly and substrate recruitment through one of these sites was illustrated through cell-based assays.

Chapter 5 describes the engineering of an antibody-based mTOR inhibition sensor based on recognition of the rapamycin-induced ternary complex of FKBP12 and $mTOR^{FRB}$. Biophysical and structural characterization of a synthetic Fab revealed key molecular recognition properties driving fine-tuned ternary complex specificity, underscoring this binder as a highly unique molecule among structurally characterized complex-specific binders. Implementation of this binder in cell-based assays demonstrated ultra-sensitive detection of endogenous mTOR inhibition by rapamycin.

Together, the engineered synthetic binders characterized in this thesis represent a unique molecular toolkit geared toward elucidating complex signal transduction mechanisms within a recalcitrant therapeutic pathway. This work highlights the utility of synthetic intrabodies for dissecting large and complicated intracellular targets, such as mTOR, and sets the stage for targeting other PIKK members with epitope-directed intrabody modulators. Furthermore, these results should be integrated into the expanding paradigm of drug discovery efforts targeting conformational and subcellular vulnerabilities within the mTOR signaling network.

Chapter 2

Engineered synthetic antibody fragments reveal structural insight into mTOR complex 1 substrate recruitment by the FRB domain

This chapter has been adapted from K. O'Leary, T. Slezak, A. Kossiakoff, Conformation-specific synthetic intrabodies modulate mTOR signaling with subcellular spatial resolution. *Proc. Natl. Acad. Sci. U.S.A.*, in press.

Kelly M. O'Leary[1], Tomasz Slezak[1], and Anthony A. Kossiakoff[1,2,*]

[1]Department of Biochemistry and Molecular Biology, The University of Chicago, Chicago, IL 60637.

[2]Institute for Biophysical Dynamics, The University of Chicago, Chicago, IL 60637.

*Correspondence to: Anthony A. Kossiakoff

2.1 Abstract

The modular assembly of mTOR into structurally and functionally distinct complexes, mTORC1 and mTORC2, critically influences the subcellular localization and biological output of mTOR kinase activity in response to nutrient and growth factor cues. However, mechanisms governing the recruitment and phosphorylation of diverse protein substrates by mTORC1 and mTORC2 are poorly understood. Here, synthetic antibody fragments (Fabs) were engineered against the FRB substrate recruitment domain of mTOR ($mTOR^{FRB}$) to gain insight into sequence and structural determinants underlying the recruitment of FRB-dependent mTORC1 substrates. An epitope-directed phage display campaign yielded seven unique binders with epitopes that compete directly with the FKBP12-rapamycin complex. High-resolution crystal structures of two Fabs, Fab-R3E9 and Fab-R3H8, bound to $mTOR^{FRB}$ revealed striking mimicry in molecular recognition properties when compared with the mTORC1 substrates S6K1 and PRAS40. Structure-guided mutagenesis studies using Fab-R3E9 and Fab-R3H8 revealed that the FRB substrate recruitment site coordinates diverse aromatic and hydrophobic side chains from a few energetically favorable surface pockets, suggesting a general mechanism for the recruitment of diverse substrates. These results highlight the utility of engineered synthetic binders in exploring the molecular determinants of protein-protein recognition at poorly understood functional sites, such as the FRB substrate recruitment domain.

2.2 Introduction

Mechanistic target of rapamycin (mTOR) is a PI3K-related serine/threonine protein kinase that integrates environmental nutrient and growth factor signaling cues to regulate fundamental homeostatic processes (32). mTOR is highly conserved in eukaryotes and evolved to govern how cells utilize basic macromolecular building blocks, such as amino acids, lipids, and carbohydrates, during periods of nutritional stress or abundance (121). Phosphorylation of diverse substrates, such as transcription factors or other kinases, constitutes the basic mechanism underpinning the function of mTOR as a general licensing factor (56). However, the kinase activity of mTOR shows low sequence stringency other than a preference for proline or hydrophobic/aromatic amino acids at the +1 position following serine/threonine phosphorylation sites (51). As a result, mechanisms for selective recruitment of substrates into the active site represent a critical aspect underlying the licensing and activation of diverse downstream components in response to nutrient or growth factor signaling.

mTOR is assembled into two different multi-subunit architectures, known as mTOR complex 1 (mTORC1) and mTOR complex 2 (mTORC2), defined by its association with Raptor and Rictor subunits, respectively (45, 57). mTORC1 and mTORC2 recruit and phosphorylate independent sets of substrates, which suggests that substrate recruitment is a function of the obligate binding partners rather than mTOR itself (56). Specific recruitment of the substrates S6K1 and 4E-BP1 via consensus TOR signaling (TOS) motifs by Raptor in mTORC1 was the first mechanism delineated for mTOR substrate recruitment (63). Later on, the structural basis of mTOR inhibition by FKBP12-rapamycin showed that selective obstruction of the FRB domain is sufficient to prevent

phosphorylation of some mTORC1 substrates, such as S6K1 (66). mTORC2 substrate recruitment is less well understood compared to mTORC1 but appears to be mediated by an accessory binding partner known as mSin1 (69). Understanding the molecular basis of how mTORC1 and mTORC2 recruit and phosphorylate different substrates could potentially provide critical insight into the design of therapies that can decouple deleterious side effects associated with systemic mTOR inhibition.

Selective inhibition of mTORC1 substrate phosphorylation has been suggested to underpin beneficial therapeutic effects, such as promotion of lifespan and healthspan in diverse model organisms (122). The best described mechanisms of recruitment for mTORC1 substrates are in regard to S6K1, 4E-BP1, and TFEB. This chapter will focus on the two-step mechanism of recruitment for S6K1, which was elucidated over the course of decades by multiple independent groups. This mechanism is initiated by docking of the TOS onto a conserved pocket of Raptor (Figure 2.1A). Raptor binds mTOR proximal to the FRB domain, which results in a high localized concentration of TOS-docked substrates. This is an important point since substrate interactions with FRB are typically in the μM range (123). Docking onto FRB positions the substrate proximal to the catalytic cleft, providing specific entry and stabilization for phosphorylation. Insight into FRB-dependent substrate phosphorylation was enabled by the use of FKBP12-rapamycin as a potent inhibitor, which binds and masks the substrate recruitment interface of FRB (Figure 2.1B). While the multi-step mechanism of S6K1 recruitment and phosphorylation may not be broadly applicable to all mTORC1 substrates, it has been confirmed that PRAS40 also exploits TOS and FRB docking to modulate the activity of mTORC1 (Figure 2.1C).

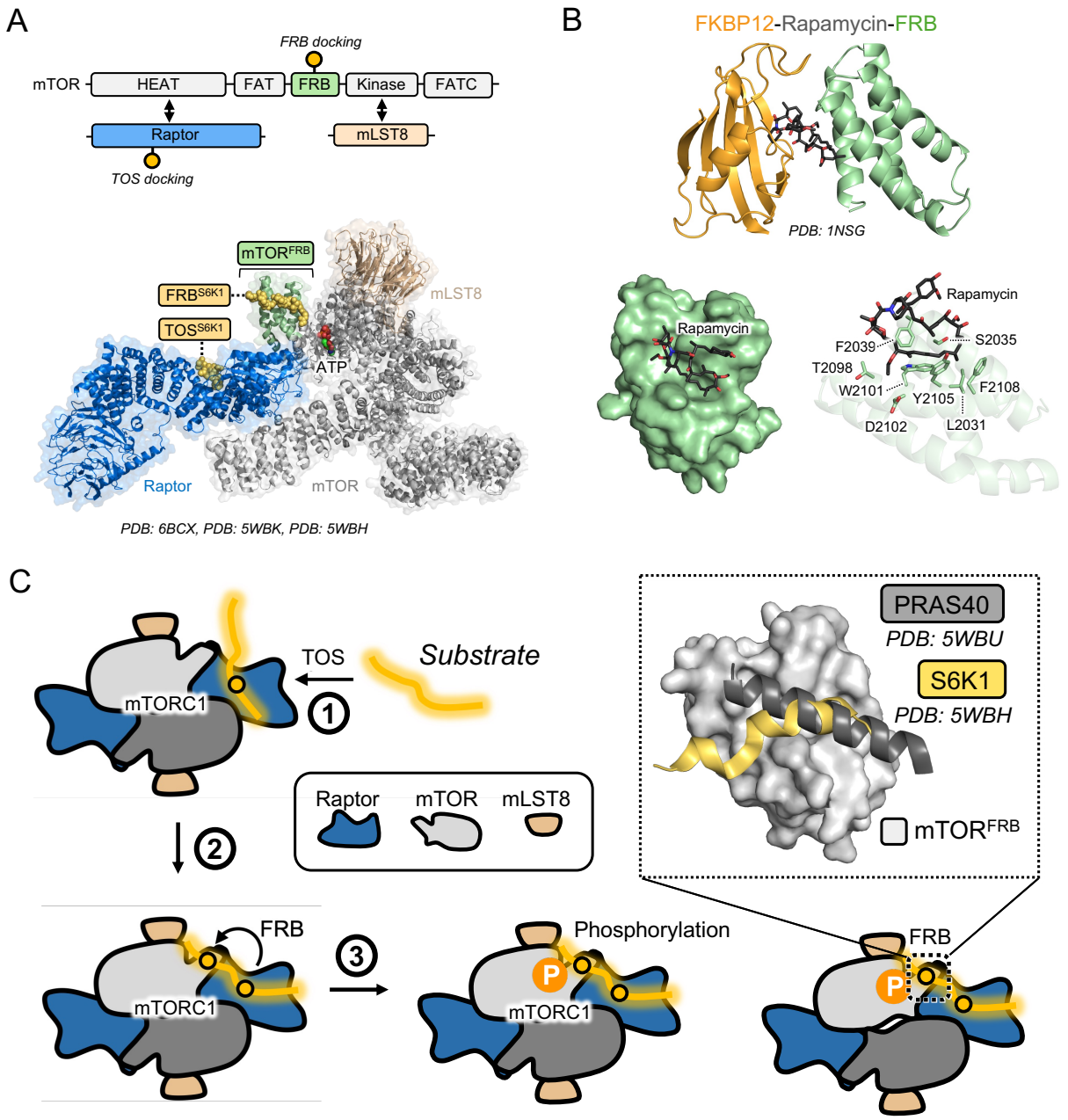

Figure 2.1 Mechanism of TOS- and FRB-dependent substrate recruitment. (A) *Top:* Construct maps for mTORC1 components with substrate docking sites indicated by yellow spheres. The FRB substrate recruitment domain is colored green. *Bottom:* Structural model of the bipartite S6K1 substrate docking domains with peptides visualized in yellow. This model is an alignment of structures from PDB: 6BCX, PDB: 5WBK, and PDB: 5WBH. (B) Structure of the FKBP12-Rapamycin-FRB ternary complex (PDB: 1NSG). (C) Schematic of the two-step docking mechanism based on S6K1. Structurally characterized FRB-docking substrates are shown inside dashed box.

A crucial limitation for delineating the mechanism of recruitment of FRB-dependent substrate docking is in regard to sequence and structural determinants. While TOS-mediated recruitment is defined by a F-X-Φ-E/D-Φ motif, where X represents any amino acid and Φ represents hydrophobic amino acids, no such motif has been described for FRB docking (63). It has been suggested that hydrophobic stretches of amino acids within 15 positions of a serine/threonine phosphorylation site is sufficient for coordination by the FRB substrate recruitment interface (67). However, a consensus sequence motif has not been defined among mTORC1 substrates. To address this limitation, chapter 2 describes the generation of synthetic Fabs against the FRB substrate recruitment site and their implementation in structural and functional studies. The exploration of synthetic protein-protein interactions here expands the paradigm of FRB-mediated molecular recognition and confirms hydrophobic promiscuity as a defining factor for FRB recruitment.

2.3 Results

2.3.1 Phage display selection of synthetic antibody fragments

An epitope-directed phage display campaign was undertaken to generate synthetic Fabs against $mTOR^{FRB}$ that could ultimately be reformatted for scFv-based intrabody expression in living cells (Figure 2.2). Recombinant expression and purification of a fusion between SNAP-tag and $mTOR^{FRB}$ established the target for phage display (124). Site-specific biotinylation of SNAP enabled selective immobilization on streptavidin-magnetic beads throughout the biopanning procedure. Non-biotinylated SNAP-tag was used as a soluble competitor for all steps in the selection process as a simple and effective method to deplete non-specific binders. Incremental selection

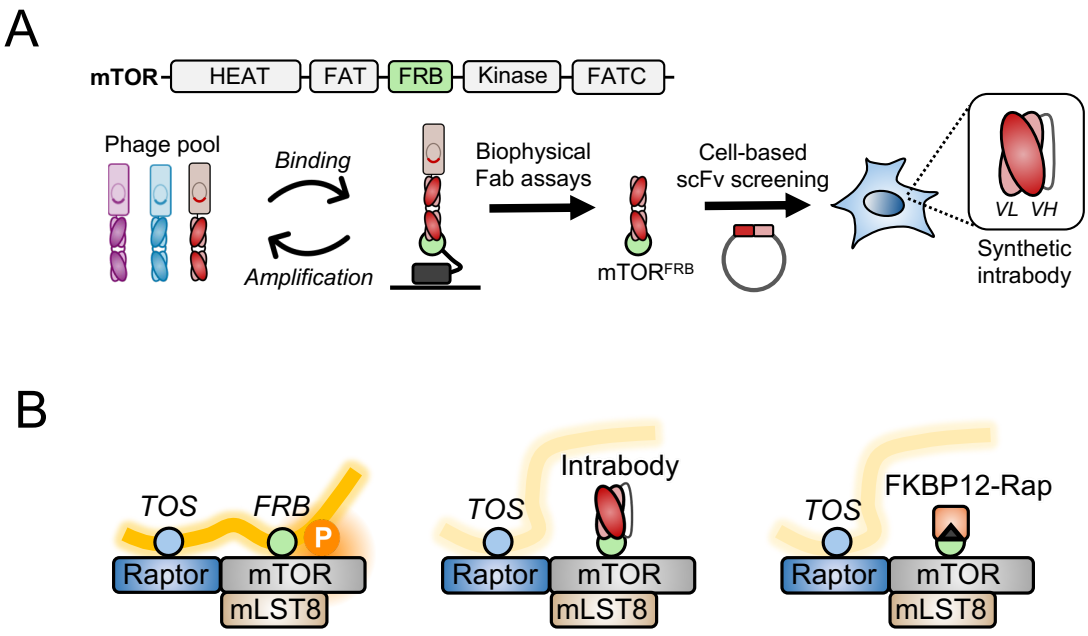

Figure 2.2 Epitope-directed phage display strategy for FRB-specific binders. (A) *Top:* Domain map of mTOR with the FRB highlighted as the target in this selection campaign. *Bottom:* Engineering pipeline from naïve phage library to scFv-screening in cells. (B) Schematic for modulation of FRB-based substrate recruitment by synthetic intrabodies. *Left:* Bipartite substrate recruitment mechanism exploiting TOS-Raptor and the FRB domain of mTOR. *Middle:* Intrabody-based obstruction of the FRB domain. *Right*: Comparison to FRB obstruction by FKBP12-Rapamycin.

pressure was added by gradually dropping the concentration of SNAP-mTOR^{FRB} from round to round, starting at 1 μM and ending at 2 nM throughout five rounds of iterative biopanning. The selection process was monitored using phage enzyme-linked immunosorbent assay (ELISA) and sequencing after rounds four and five. Together, seven unique binders were identified and cloned in Fab format to a the RH2.2 vector for recombinant expression in *Escherichia coli* (Figure 2.3A). These binders were reformatted for expression as scFv molecules to determine intracellular solubility, which is known to be rather unpredictable despite high sequence homology.

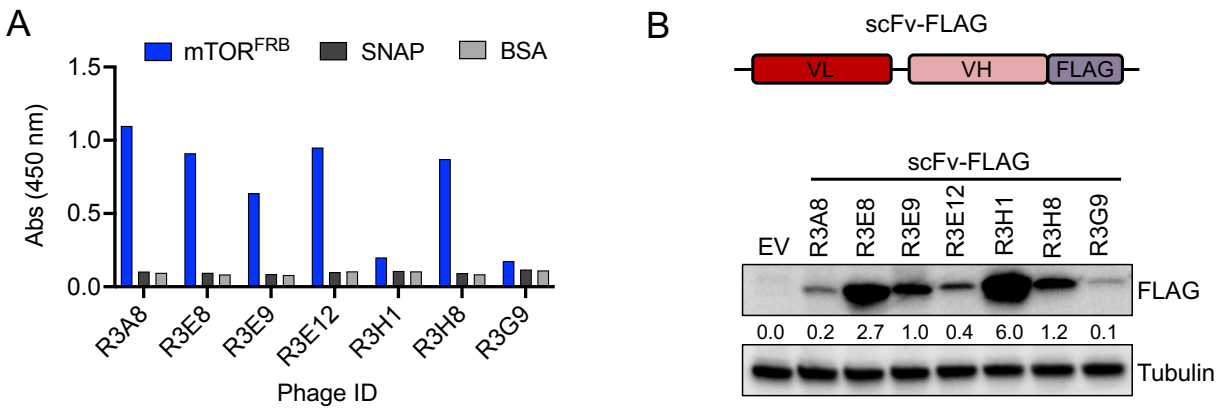

Figure 2.3 Phage ELISA and intracellular scFv expression. (A) Single point phage ELISA analysis for the indicated phage clones against SNAP-FRB, SNAP alone, or BSA. (B) *Top:* Construct design for scFv with a FLAG tag for detection by western blot. *Bottom*: The indicated intrabodies, or empty vector (EV), were transfected in Expi293F cells for 48 hours. Cells were washed once in cold PBS, lysed, and analyzed via western blot. Relative expression levels (normalized to R3E9) are indicated below the FLAG blot.

2.3.2 Binding and epitope-binning characterization

Intracellular expression of all seven intrabody constructs was observed in Expi293F cells (Figure 2.3B). However, the relative expression levels ranged approximately 60-fold with R3G9 displaying the lowest expression and R3H1 displaying the highest expression. No obvious sequence determinants were observed to be correlated with intracellular solubility. With validation of seven unique Fabs that bind mTOR^{FRB} and that can be expressed inside cells in scFv format, the cohort of binders underwent further biophysical characterization to screen affinities and epitopes. Binding kinetics for each Fab against mTOR^{FRB} were measured using surface plasmon resonance (SPR). mTOR^{FRB} was immobilized to the sensor surface via hexahistidine tag and Fabs

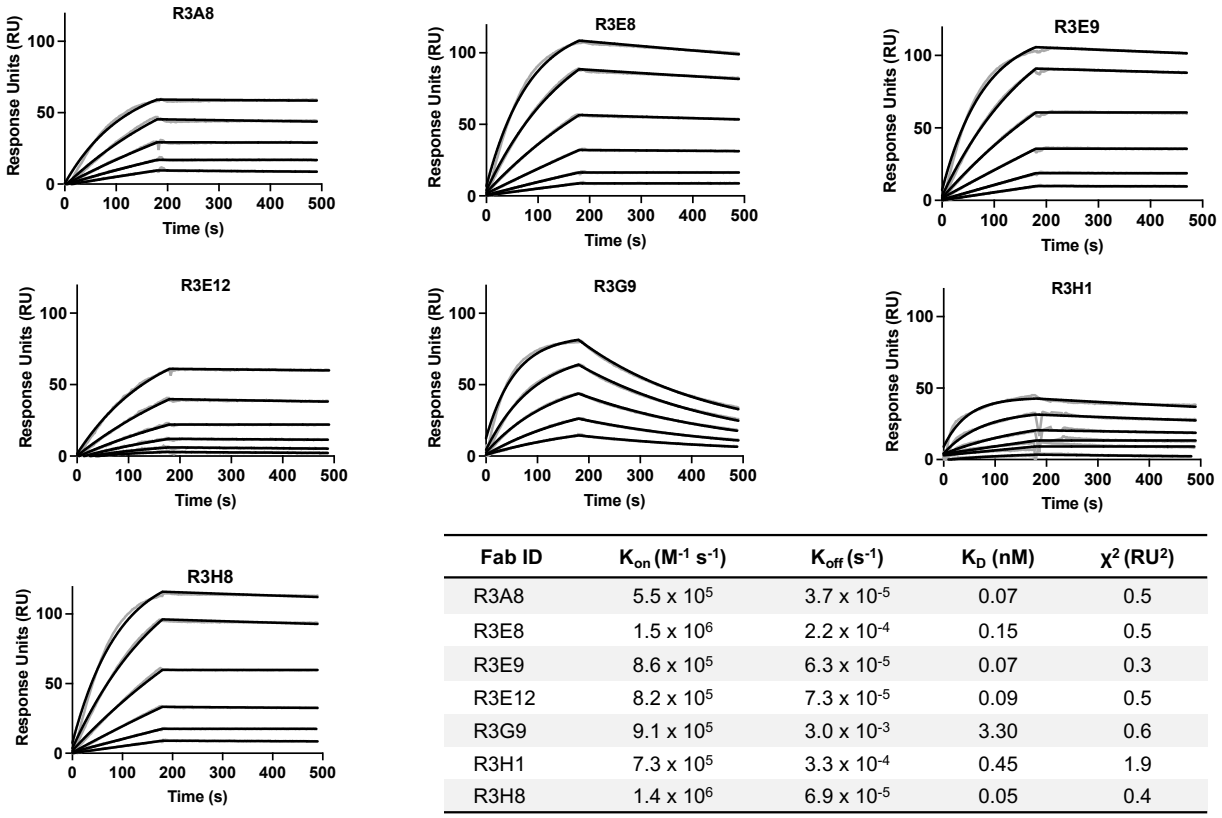

Fab ID	K_{on} (M^{-1} s^{-1})	K_{off} (s^{-1})	K_D (nM)	χ^2 (RU^2)
R3A8	5.5×10^5	3.7×10^{-5}	0.07	0.5
R3E8	1.5×10^6	2.2×10^{-4}	0.15	0.5
R3E9	8.6×10^5	6.3×10^{-5}	0.07	0.3
R3E12	8.2×10^5	7.3×10^{-5}	0.09	0.5
R3G9	9.1×10^5	3.0×10^{-3}	3.30	0.6
R3H1	7.3×10^5	3.3×10^{-4}	0.45	1.9
R3H8	1.4×10^6	6.9×10^{-5}	0.05	0.4

Figure 2.4 Binding kinetics for Fabs against FRB determined by SPR. Multi-point kinetics were determined for each binder as shown by the raw sensorgram and curve fits following a 1:1 binding model. $mTOR^{FRB}$ was immobilized to the sensor surface via hexahistidine tag and Fabs were run as analytes in two-fold serial dilutions.

were injected as analytes. These results displayed a range of sub-nanomolar and low-nanomolar dissociation constants (K_D), from 0.05 nM for R3H8 to 3.3 nM for R3G9, against FRB (Figure 2.4).

All Fabs were tested for binding against the FRB domain from eukaryotic model organisms commonly used in mTOR research studies. These results showed modest cross-reactivity with FRB from *Drosophila melanogaster* by all Fabs and varying degrees of cross-reactivity with FRB (TOR1) from *Saccharomyces cerevisiae* by R3H8 and R3G9

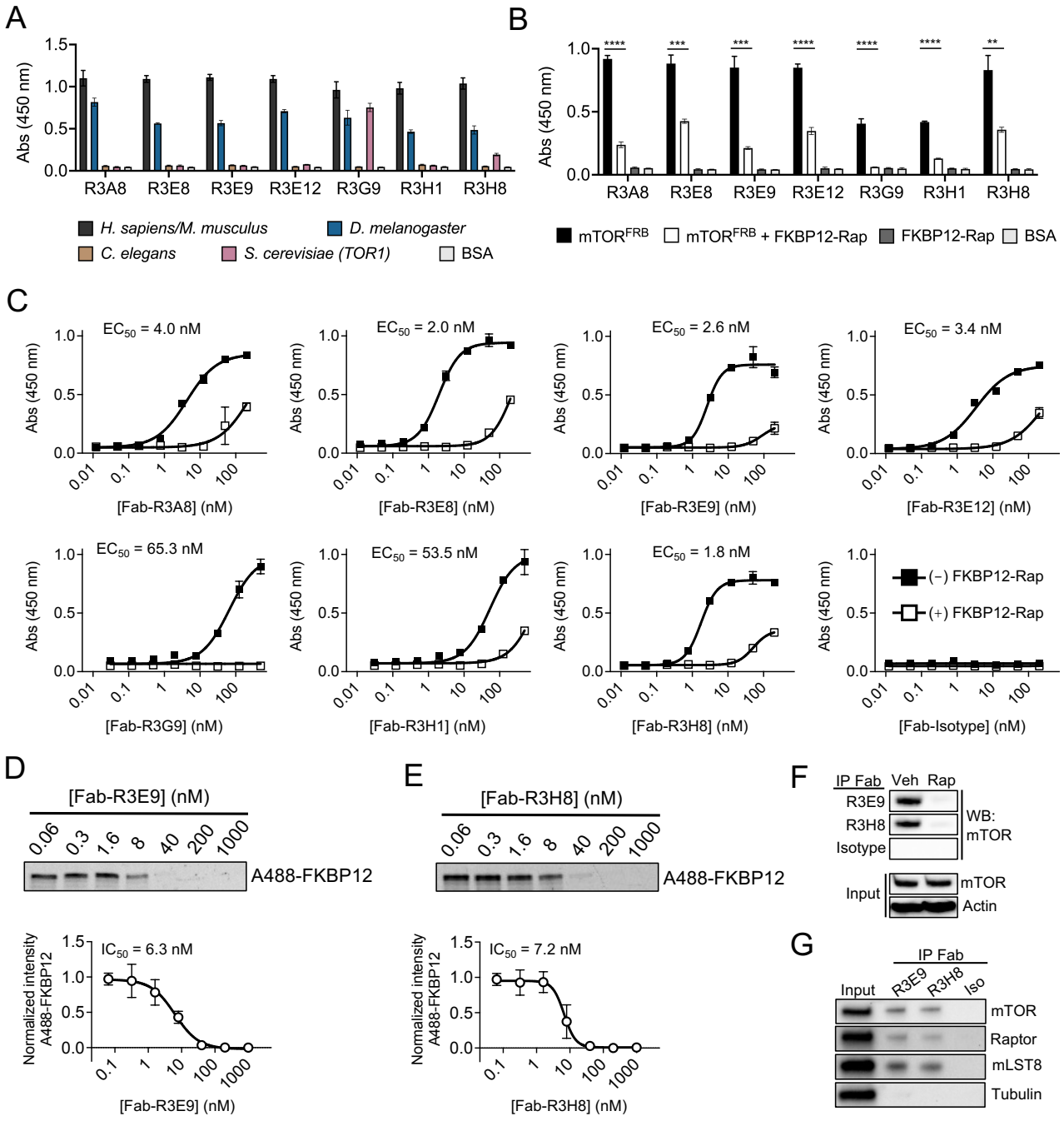

Figure 2.5 Fab characterization and epitope binning. Caption continued on next page.

(Figure 2.5A). Next, epitope binning experiments were performed to determine whether any binders were able to obstruct the substrate recruitment interface of mTOR^{FRB}. Single

Figure 2.5 Fab characterization and epitope binning. (A) Single point ELISA analysis against the FRB domain from the indicated species of eukaryotic model organism (n = 3 independent experiments, mean ± SD). (B) Competitive single point ELISA analysis against FRB using 10 μM FKBP12-Rapamycin as a competitor (n = 3 independent experiments, mean ± SD). (C) Competitive multi-point ELISA analysis against FRB using 10 μM FKBP12-Rapamycin as a competitor (n = 3 independent experiments, mean ± SD). (D) In vitro multi-point competition assay using R3E9, Alexa488 labeled SNAP-FKBP12 (A488-FKBP12) and biotinylated SNAP-FRB (Bio-FRB). 10 nM A488-FKBP12, 10 nM Bio-FRB, and 10 nM rapamycin were incubated together with the indicated concentrations of R3E9 before streptavidin bead enrichment and SDS-PAGE analysis (n = 3 independent experiments, mean ± SD). (E) In vitro multi-point competition assay using R3E9, Alexa488 labeled SNAP-FKBP12 (A488-FKBP12) and biotinylated SNAP-FRB (Bio-FRB). 10 nM A488-FKBP12, 10 nM Bio-FRB, and 10 nM rapamycin were incubated together with the indicated concentrations of R3E9 before streptavidin bead enrichment and SDS-PAGE analysis (n = 3 independent experiments, mean ± SD). (F) Immunoprecipitation-western blot analysis from Expi293F cells treated with vehicle or rapamycin using the indicated biotinylated binders. (G) Immunoprecipitation-western blot analysis from Expi293F cells for detection of mTOR complex 1 components.

point ELISA showed that all Fabs were selectively competed by FKBP12-Rapamycin for binding to $mTOR^{FRB}$, suggesting that they share a common epitope (Figure 2.5B). These results also suggested that the substrate recruitment interface of $mTOR^{FRB}$ possesses an inherent propensity to coordinate protein-protein interactions as no selection pressures were added to obtain binders against this site. Binders were further characterized using multi-point ELISA. Confirming the single point analysis, all binders were selectively competed by the presence of FKBP12-Rapamycin. At this point, a decision was made to move forward with two primary candidates. Fabs R3E9 and R3H8 were selected for further characterization based on binding affinities measured by SPR and ELISA in combination with desirable intracellular expression levels in scFv format. Residual binding signal in multi-point ELISA assays raised the question of whether Fab-R3E9 and Fab-R3H8 epitopes might completely or partially overlap with the substrate recruitment

interface. To answer this question, a new format of in vitro competition assay was developed. This assay was based on the ternary complex formation of Alexa488-labeled SNAP-FKBP12 (A488-FKBP12) and biotinylated SNAP-mTOR^{FRB} (Bio-SNAP). In the presence of rapamycin, these components assemble together and can be specifically enriched using streptavidin beads. Following enrichment, components can be eluted and analyzed via sodium dodecyl sulfate polyacrylamide gel electrophoresis (SDS-PAGE). Using this format, Fab-R3E9 and Fab-R3H8 completely blocked formation of the rapamycin-induced ternary complex, which confirmed that these Fabs occupy and obstruct the substrate recruitment interface (Figure 2.5D and E). These results were

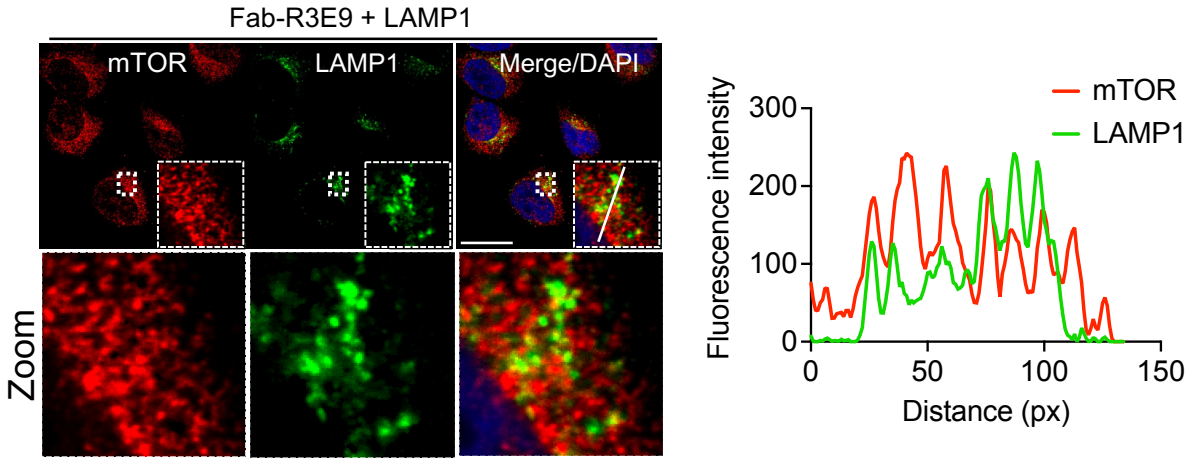

Figure 2.6 Immunofluorescent co-localization of Fab-R3E9 and LAMP1. HeLa cell immunostaining using Fab-R3E9 and anti-LAMP1 antibody. Line trace profile is shown on the right. Scale bar denotes 20.5 μm.

validated in immunoprecipitation assays from Expi293F cells treated with vehicle or rapamycin, which confirmed rapamycin-sensitive recognition of mTOR in a cell-based context (Figure 2.5F). Furthermore, immunoprecipitation studies showed that Fab-R3E9 and Fab-R3H8 engage with and co-purify the mTORC1 components Raptor and mLST8 (Figure 2.5G). In support of engagement with mTORC1 in cells, Fab-R3E9 was used for

immunofluorescent co-staining together with a commercial anti-LAMP1 antibody. These results showed co-localization of Fab-R3E9 and LAMP1, which suggests that Fab-R3E9 can accurately detect active mTORC1 at the lysosomal surface (Figure 2.6). Together, the characterization procedures here resulted in two highly validated Fabs, R3E9 and R3H8, which bind to the substrate recruitment site of the FRB domain in a rapamycin-sensitive manner.

2.3.3 Crystal structure determination reveals molecular basis for recognition of the mTOR^{FRB} substrate recruitment domain

To understand the structural basis for recognition of mTOR^{FRB} by Fab-R3E9 and Fab-R3H8, monodisperse recombinant complexes were purified using size exclusion chromatography (SEC) for high throughput screening in various crystallization conditions (Figure 2.7A). Crystal structures of Fab-R3E9 and Fab-R3H8 were determined at 1.6 Å and 2.0 Å resolution, respectively (Table 2.1). These structures revealed highly similar binding sites on mTOR^{FRB} by Fab-R3E9 and Fab-R3H8, which supported the previous epitope-binning results (Figure 2.7B). To evaluate their capability for engagement of mTORC1 as intrabodies, models of R3E9 and R3H8 in scFv format were generated and docked onto mTOR^{FRB} using a previously determined cryo-EM structure of mTORC1 (PDB: 6BCX). These structural models demonstrated that scFv-R3E9 and scFv-R3H8 can access the mTOR^{FRB} substrate recruitment site and are not obstructed by other components in mTORC1 (Figure 2.7C). Furthermore, buried solvent accessible surface area (SASA) was quantified for all structurally determined mTOR^{FRB}-interacting proteins, which established that scFv-R3E9 and scFv-R3H8 are the most obstructive mTOR^{FRB}

binders characterized to date. These calculations were based on structures of the following PDB identification codes for molecules bound to mTOR^{FRB}: 5WBH (S6K1), 5WBU (PRAS40), and 1FAP (FKBP12-Rapamycin).

Table 2.1 X-ray diffraction data collection and refinement statistics for structures of Fab-R3E9 and Fab-R3H8 bound to mTOR^{FRB}.

	Fab-R3E9•mTOR^{FRB} (PDB 9DL0)	Fab-R3H8•mTOR^{FRB} (PDB 9DBO)
Wavelength (Å)	1.0332	1.0332
Space group	*P 21 2 21*	*P 1 2 1*
Cell dimensions		
a, b, c (Å)	87.613, 110.042, 131.079,	45.055, 69.732, 89.413
α, β, γ (°)	90, 90, 90	90, 90.12, 90
Resolution (Å)	56.31 - 2.0 (2.02 - 2.0)*	45.05 - 1.55 (1.57 - 1.55)
R_{merge}	0.054 (0.955)	0.056 (0.671)
R_{meas}	0.076 (1.351)	0.079 (0.949)
R_{pim}	0.054 (0.955)	0.056 (0.671)
$CC_{1/2}$	0.998 (0.295)	0.994 (0.475)
$I / \sigma I$	8.8 (1.0)	6.8 (1.0)
Completeness (%)	94.32 (99.75)	93.9 (71.0)
Redundancy	2.0 (2.0)	1.9 (1.8)
No. reflections	81,284	75,225
R_{work} / R_{free}	0.2050 / 0.2353	0.2043 / 0.2338
No. atoms		
Protein	8113	4099
Solvent	373	548
Protein residues	1056	529
R.M.S deviations		
Bond lengths (Å)	0.008	0.008
Bond angles (°)	0.99	1.1
Ramachandran favored (%)	97.41	97.9
Allowed (%)	2.59	2.1
Outliers (%)	0	0
Rotamer outliers (%)	1.22	0.44
Clashscore	2.71	1.98
Average B-factor		
Protein	46.18	14.66
Solvent	45.02	34.05

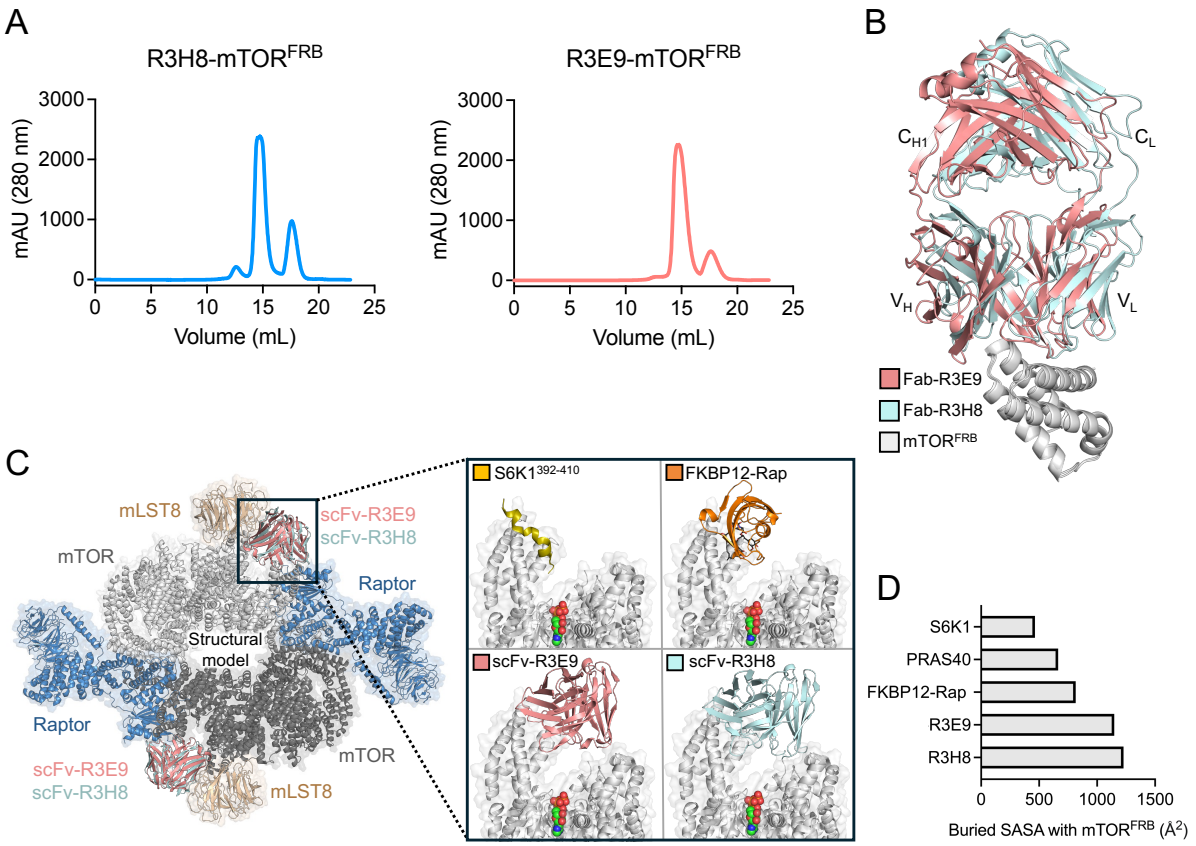

Figure 2.7 Crystal structures of Fab-R3E9 and Fab-R3H8 bound to mTOR^{FRB}. (A) *Left:* SEC profile for the complex of Fab-R3H8 and mTOR^{FRB}. *Right:* SEC profile for the complex of Fab-R3E9 and mTOR^{FRB}. (B) Alignment of crystal structures for mTOR^{FRB} bound by Fab-R3E9 and Fab-R3H8 exhibits nearly identical binding poses. (C) Structural model of mTORC1 (PDB: 6BCX) aligned with scFv models of R3E9 and R3H8. Box inset shows binding poses made by alignments with structures of S6K1-FRB (yellow; PDB: 5WBH), FKBP12-Rapamcyin-FRB (orange; PDB: 1FAP), scFv-R3E9, or scFv-R3H8. (D) Quantification of buried solvent accessible surface area (SASA) on mTOR^{FRB} using structures of S6K1-FRB (PDB: 5WBH), PRAS40-mTORΔN (PDB: 5WBU), FKBP12-Rapamcyin-FRB (PDB: 1FAP), Fab-R3E9-mTOR^{FRB}, or Fab-R3H8-mTOR^{FRB}.

A closer analysis of molecular interfaces between mTOR^{FRB} and Fab-R3E9 or Fab-R3H8 exhibited rich networks of hydrophobic packing interactions and hydrogen bonds (Figure 2.8A and B). Despite highly similar positioning of CDRs L1, L3, H2, and H3, the positional sequence identity is low to none, highlighting the potential of synthetic Fabs to

utilize diverse repertoires of amino acids to mediate recognition of the same binding site. Further inspection of interactions formed at the mTOR^{FRB} substrate recruitment side was performed and mapped onto a multiple sequence alignment of mTOR^{FRB} from multiple eukaryotic organisms. This analysis showed that most of the crucial positions contacted by Fab-R3E9, Fab-R3H8, FKBP12-Rapamycin, S6K1, and PRAS40 are highly conserved from yeast to humans (Figure 2.8C) . This result is not surprising owing to the critical role of this interface in directly interacting with substrates to enable selective phosphorylation.

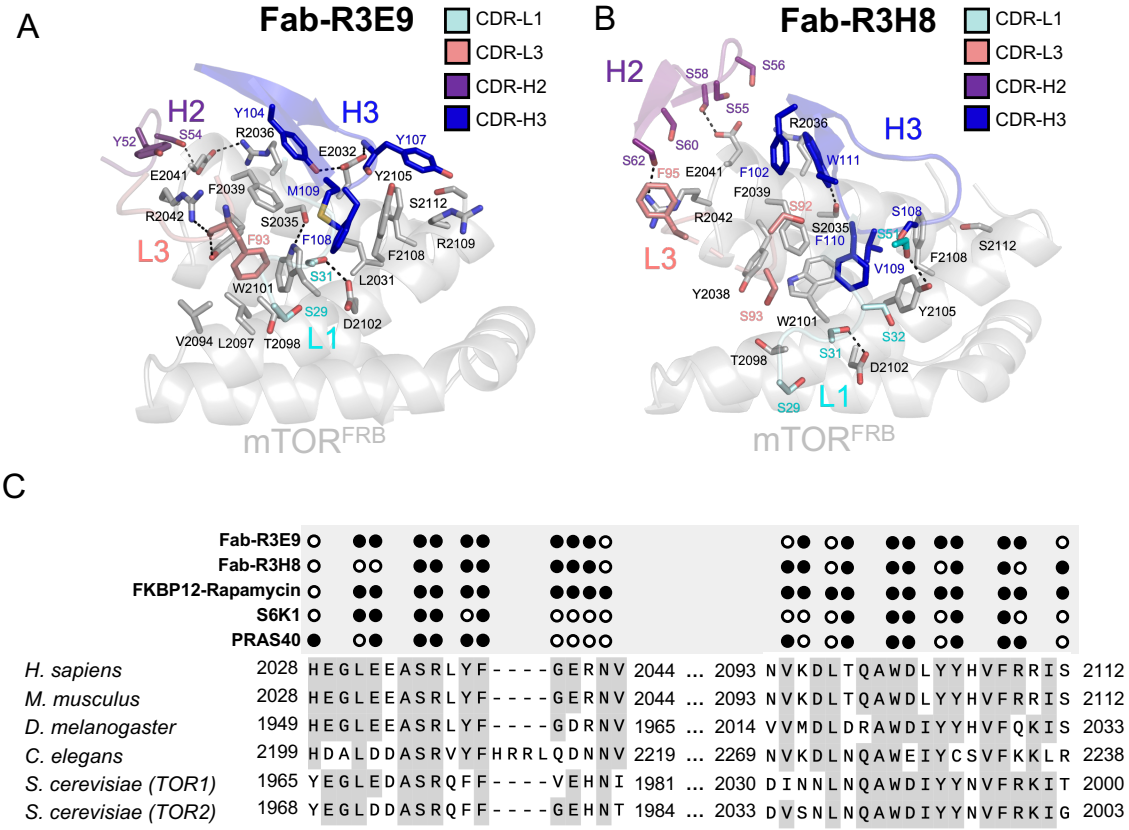

Figure 2.8 R3E9 and R3H8 molecular interface characterization. (A) Side chain interactions formed between Fab-R3E9 CDRs and mTOR^{FRB}. (B) Side chain interactions formed between Fab-R3H8 CDRs and mTOR^{FRB}. (C) Evolutionarily conserved interaction sites with different mTOR^{FRB}-interacting molecules. Multiple sequence alignment made using the following UniProt IDs: P42345, Q9JLN9, Q9VK45, Q95Q95, P35169, P32600. Black circles indicate that a direct interaction is made with that position.

Despite high conservation of positional identity for direct contacts with $mTOR^{FRB}$, the scaffolds and secondary structure characteristics of these $mTOR^{FRB}$-interacting molecules are strikingly different. For example, synthetic Fabs contact $mTOR^{FRB}$ using at least four different CDR loops which are unstructured and can consequently form contiguous contacts using side chains from independent locations in the primary amino acid sequence. In contrast, the regions of S6K1 and PRAS40 that bind to $mTOR^{FRB}$ are α-helical. One might expect that two proteins derived from different scaffolds could still form contacts with the same set of residues on a target antigen, albeit with unique positioning or angle of attack. However, further inspection of molecular recognition characteristic between synthetic and these natural $mTOR^{FRB}$-docking substrates revealed high similarity in the position and orientation of direct side chain interactions (Figure 2.9A). Exceptional similarities between Fab-R3E9 and PRAS40 were observed based on the structural alignment using the PRAS40-$mTOR^{FRB}$ portion of PDB: 5WBU. Here, despite no sequence identity between molecules, four continuous positions contacted by side chains on the hydrophobic side of the amphipathic PRAS40 α-helix are essentially imitated by side chains from the light chain and heavy chain paratope of Fab-R3E9 (Figure 2.9B). Furthermore, structure alignment of Fab-R3H8 with S6K1, based on PDB: 5WBH, exemplified similar characteristics. The S6K1 α-helix bound to $mTOR^{FRB}$ displays a subtle kink. Nevertheless, three continuous residues from CDR-H3 in Fab-R3H8 are inserted into positions directly aligned with hydrophobic residues in the S6K1 amphipathic α-helix (Figure 2.9C). Here, one position is contacted by phenylalanine from both S6K1 and Fab-R3H8, but these interactions stem from opposite sides of the groove they contact. Another example of side chain alignment stemming from displaced α-carbon

positioning is L396^{S6K1} and V109^{R3H8}, where the terminal side chain regions are buried in nearly identical poses.

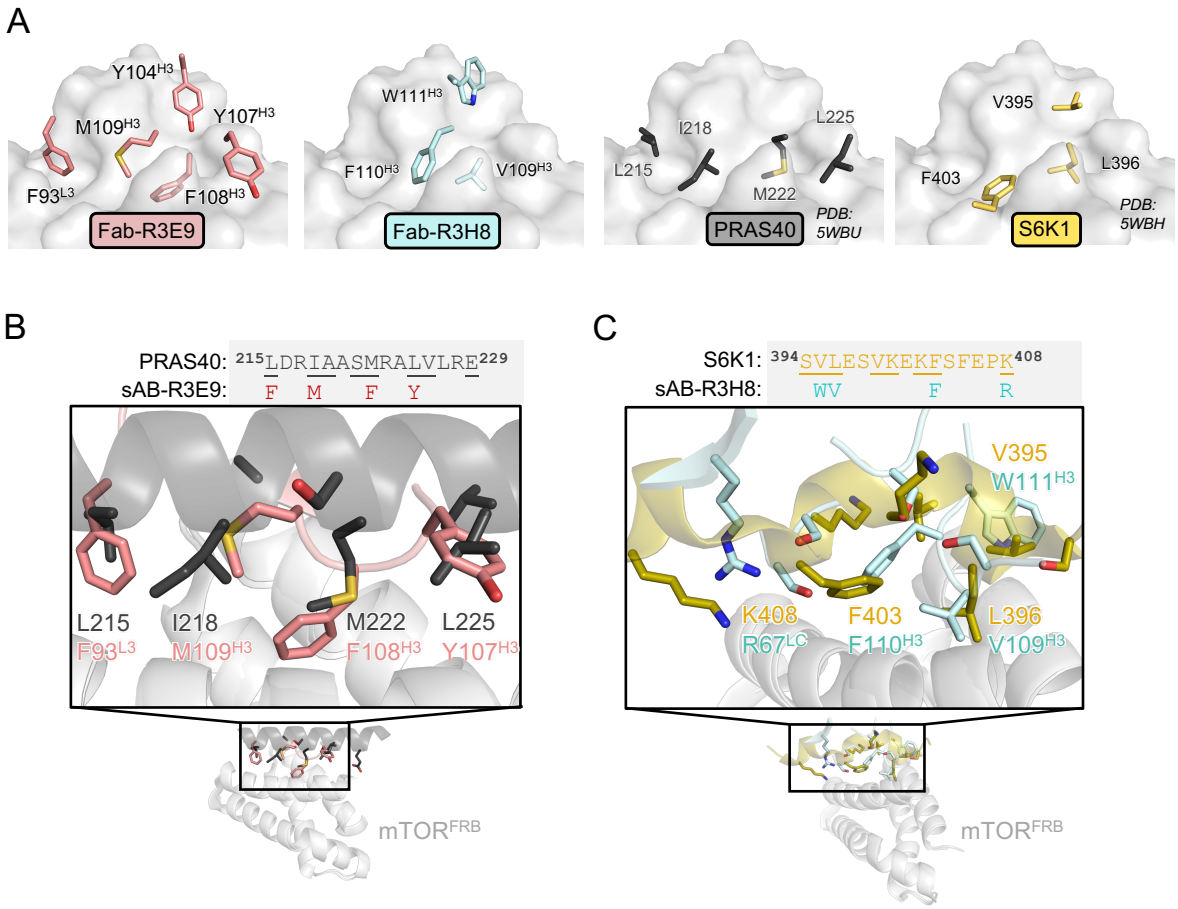

Figure 2.9 Insight into indiscriminate hydrophobic side chain coordination by mTOR^{FRB}. (A) Grey surface representation is the mTOR^{FRB} substrate recruitment interface. Consensus interaction sites for synthetic and natural mTOR^{FRB}-interacting molecules are shown as sticks and labeled accordingly. (B) Structural alignment between Fab-R3E9 and PRAS40 from PDB: 5WBU. (C) Structural alignment between Fab-R3H8 and S6K1 from PDB: 5WBH.

Structure-guided mutagenesis was employed to gain mechanistic insight into the energetic contribution of positionally conserved side chain interactions made by Fab-R3E9 and Fab-R3H8. Directly interacting residues from synthetic Fab paratopes or natural substrates were clustered into five distinct groups based on consensus pocket

burial (Figure 2.10A). There was no sequence identity observed among molecules in four out of these five consensus pockets (Figure 2.10B). The single instance of identity was for phenylalanine side chains by Fab-R3H8 and S6K1 described previously. To understand the molecular basis for this apparent lack of selectivity for hydrophobic side chain coordination, synthetic Fab residues located in the five consensus interaction sites were mutated to alanine and functionally validated using multi-point ELISA. Fab-R3E9 inserts residues into all five of these positions, resulting in generation of the variants $F93A^{L3}$, $Y104A^{H3}$, $Y107A^{H3}$, $F108A^{H3}$, and $M109A^{H3}$. Multi-point ELISA analysis showed that recognition of $mTOR^{FRB}$ by three of these variants was significantly reduced (Figure 2.10C). In particular, $Y104A^{H3}$, $F108A^{H3}$, and $M109A^{H3}$ exhibited more than 10-fold reduction in EC_{50} values, indicating that these side chain interactions contribute significant binding energy. In contrast to Fab-R3E9, Fab-R3H8 inserts residues into three out of the five consensus interaction sites. The Fab-R3H8 variants generated were $V109A^{H3}$, $F110A^{H3}$, and $W111A^{H3}$. Multi-point ELISA analysis showed that recognition of $mTOR^{FRB}$ by all three of these variants was significantly reduced (Figure 2.10D). An EC_{50} value for $F110A^{H3}$ could not be determined from the concentration range used, suggesting that the fold change for this variant over wild-type was much greater than 10-fold. The variants $V109A^{H3}$ and $W111A^{H3}$ exhibited EC_{50} value fold-changes of ~5 and ~15 over wild-type, respectively. Together, this analysis provided molecular insight into the molecular recognition properties of the $mTOR^{FRB}$ substrate recruitment site, which remains controversial in terms of its functionality. These results demonstrate that $mTOR^{FRB}$ protein-protein coordination is relatively indiscriminate toward hydrophobic or aromatic

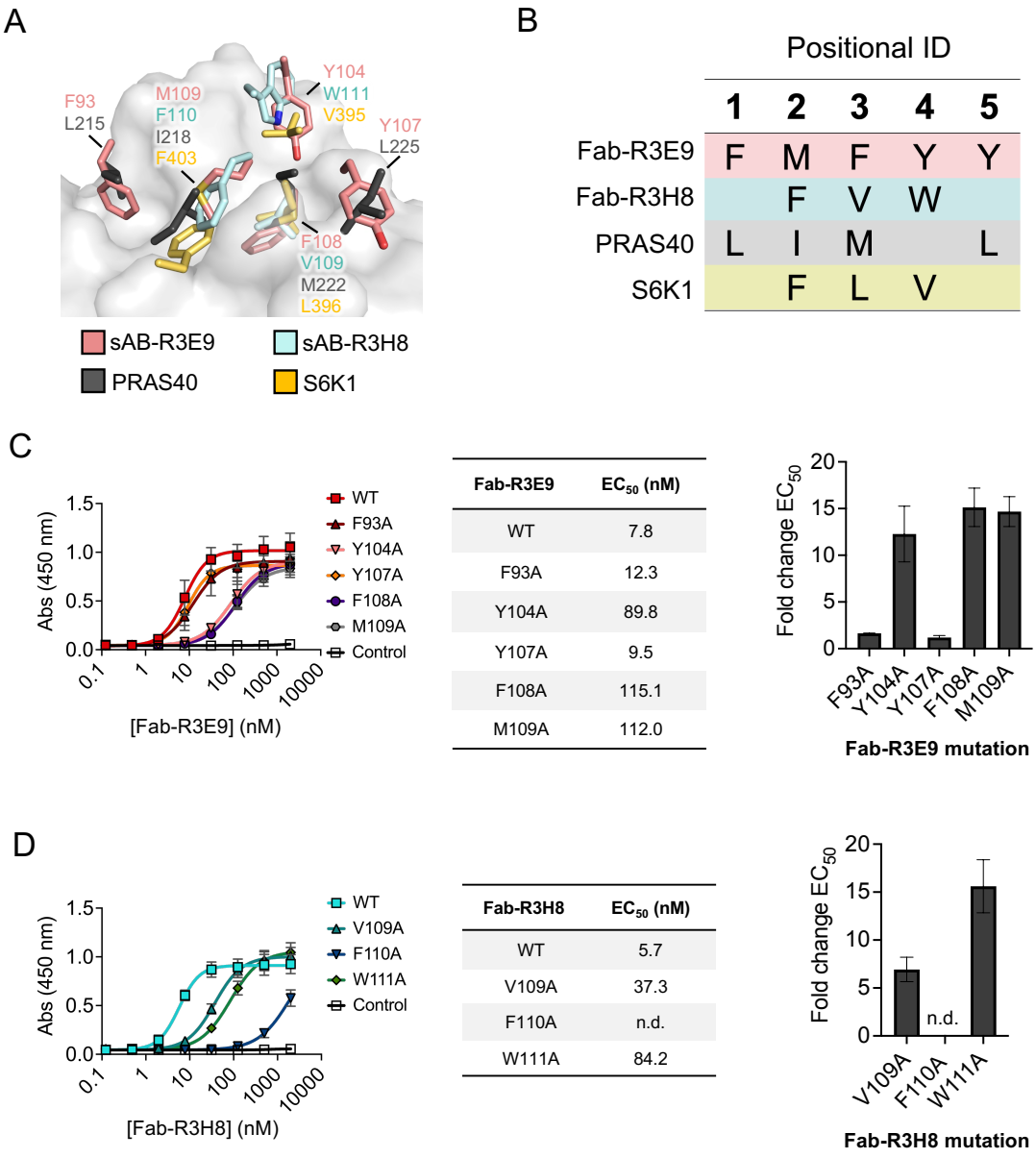

Figure 2.10 Energetic contribution of positionally conserved Fab interactions. (A) Consensus interaction sites revealed by clusters of hydrophobic side chain insertion by Fab-R3E9 (salmon), Fab-R3H8 (pale cyan), S6K1 (yellow; PDB: 5WBH), and PRAS40 (dark gray; PDB: 5WBU). (B) Table of consensus sites categorized by a positional identification code. (C) *Left:* Multi-point ELISA analysis for the indicated Fab-R3E9 variants. *Middle:* EC_{50} values (nM) for the indicated variants (n = 3 independent experiments, mean ± SD). *Right:* Fold change in EC_{50} values for Fab-R3E9 alanine mutations relative to wild-type. (D) *Left:* Multi-point ELISA analysis for the indicated Fab-R3H8 variants. *Middle:* EC_{50} values (nM) for the indicated variants (n = 3 independent experiments, mean ± SD). *Right:* Fold change in EC_{50} values for Fab-R3H8 alanine mutations relative to wild-type. F110A EC_{50} value could not be determined (n.d.).

amino acids. However, structure-guided mutagenesis of Fab-R3E9 and Fab-R3H8 paratopes revealed that their recognition of mTOR^{FRB} depends on the position contacted rather than the side chain chemistry used in each position. The engineering and characterization of synthetic binders against functional interaction sites therefore represents a useful approach to explore and predict potential binding partners.

Previous studies have investigated the requirement of mTOR^{FRB} docking for several mTORC1 substrates using in vitro kinase assays (123). These substrates included TFEB, Lipin1, Maf1, and Grb10 due to the presence of hydrophobic amino acids within 15 positions of their reported phosphorylation sites. Mutation of various hydrophobic side chains to alanine in these peptides was shown to abolish the capability for mTORC1 to phosphorylate the peptides in vitro. These results demonstrated the first example that multiple diverse mTORC1 substrates exploit the FRB domain for transient stabilization to enable phosphorylation nearby in the active site. To investigate whether TFEB, Lipin1, Maf1, and Grb10 employ similar interactions as Fab-R3E9 or Fab-R3H8, structural models were generated using AlphaFold 3 (125). These models showed peptides with random coil or α-helical secondary structures docked to the substrate recruitment interface of mTOR^{FRB} (Figure 2.11A). Analysis of direct side chain interactions showed that each substrate employs side chains with high overlapping positional identity compared to Fab-R3E9 (Figure 2.11B). Similar to the analysis of S6K1 and PRAS40, the tertiary substrate-mTOR^{FRB} architectures differ to varying degrees, suggesting that a consensus linear sequence motif is insufficient to describe the mechanism of mTOR^{FRB}-recruitment (Figure 2.11C). Together, these models contribute even greater sequence diversity into the five positional mTOR^{FRB} consensus interaction sites (Figure 2.11D).

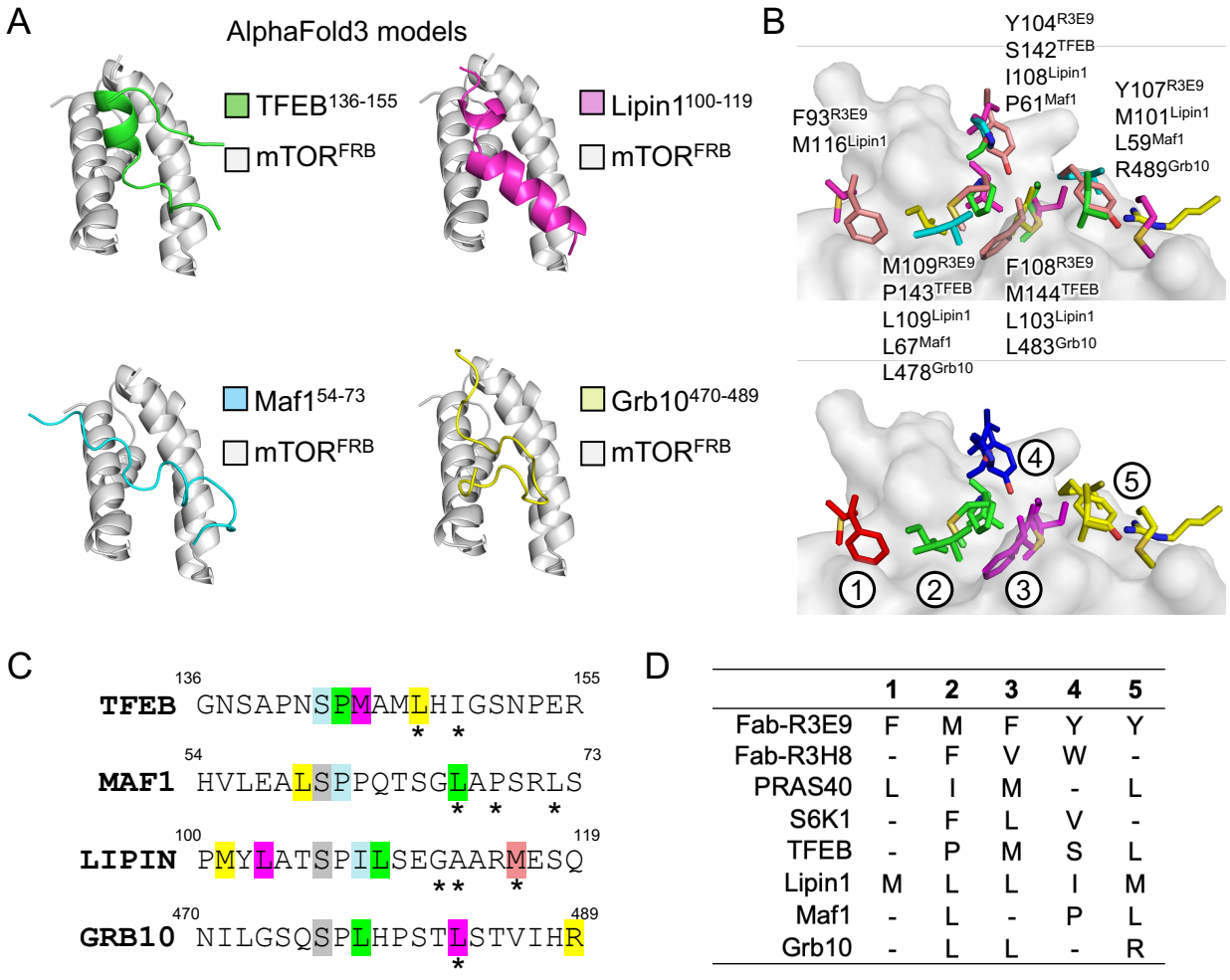

	1	2	3	4	5
Fab-R3E9	F	M	F	Y	Y
Fab-R3H8	-	F	V	W	-
PRAS40	L	I	M	-	L
S6K1	-	F	L	V	-
TFEB	-	P	M	S	L
Lipin1	M	L	L	I	M
Maf1	-	L	-	P	L
Grb10	-	L	L	-	R

Figure 2.11 Synthetic Fabs support models of potential FRB-dependent substrates. (A) AlphaFold 3 models of the indicated mTOR^{FRB}-substrate complexes. (B) *Top:* Side chains from AlphaFold 3 models that align with Fab-R3E9 interactions. *Bottom:* Positional categorization of side chains based on clustered interactions. (C) Sequences of substrates colored by positional identity. Phosphorylation site colored grey. Asterisks mark mutationally validated positions from Yang et al 2017. (D) Table of consensus sites categorized by the positional

2.4 Discussion

Insight into mechanisms underlying substrate recruitment by mTORC1 has been limited by a lack of tools to elicit selective perturbations in cells. While it is clear that

mTORC1 exploits multiple independent mechanisms of recruiting substrates, such as TOS-dependent, Rag-dependent, or TOS- and FRB-dependent docking, distilling the molecular basis for each category could provide useful information to strategically design new therapeutics. For example, until a structural mechanism was described for the role of $mTOR^{FRB}$ in coordinating protein-protein interactions with S6K1 and PRAS40, mTORC1 substrate recruitment was widely considered to occur only through TOS-Raptor interactions. This highlights the critical need for structural and functional delineation of mTOR-substrate recognition, which can be challenging due to disordered structural elements or low affinity of substrate interactions. To address these limitations, synthetic Fabs were generated that selectively bind and obstruct $mTOR^{FRB}$-substrate interactions. Structural and functional studies revealed insight into the flexible molecular code underlying protein-protein interactions coordinated by $mTOR^{FRB}$.

Phage display biopanning against recombinant $mTOR^{FRB}$ resulted in the isolation of seven unique Fabs displaying low- or sub-nanomolar affinities. With no added selection pressures to influence epitope specificities, the epitopes for each of the seven Fabs were found to overlap with the FKBP12-rapamycin binding site, and therefore, the substrate recruitment interface. These results indicate that the substrate recruitment interface of $mTOR^{FRB}$ is particularly immunogenic and supports its proposed role in coordinating protein-protein interactions inside cells. Interestingly, no consensus sequence identity was observed in CDR-H3 between Fabs despite their recognition of the same general epitope.

A major barrier to understanding $mTOR^{FRB}$-mediated substrate recruitment is the lack of information regarding a consensus motif required for selective $mTOR^{FRB}$-substrate

interactions. This is complicated by the fact that not all mTORC1 substrates require $mTOR^{FRB}$ docking for phosphorylation. The best described example of this phenomenon occurs with 4E-BP1, which primarily utilizes TOS-Raptor docking and is phosphorylated in a rapamycin-resistant manner at multiple sites (68). However, for other mTORC1 substrates, such as S6K1, disrupting the $mTOR^{FRB}$ interface is sufficient for potent inhibition (66). Structures of peptides from S6K1 and PRAS40 bound to $mTOR^{FRB}$ have firmly established $mTOR^{FRB}$ as a substrate recruitment domain (67). In light of this advancement, many questions remain open in regard to the selectivity for amphipathic α-helix docking due to low conservation in structural geometry and sequence identity for these interactions.

Crystal structure determination of $mTOR^{FRB}$ bound by two unique synthetic Fabs, Fab-R3E9 and Fab-R3H8, revealed key insight into the molecular basis of $mTOR^{FRB}$-mediated molecular recognition. These structures highlighted properties of inherent promiscuity in $mTOR^{FRB}$-based molecular recognition. Structure-guided mutagenesis studies revealed three major hydrophobic pockets located in the substrate recruitment interface that are critical for coordinating synthetic Fab binding. Importantly, Fab-R3E9 and Fab-R3H8 bind to identical epitopes but have no sequence identity in the direct side chain interactions they form with $mTOR^{FRB}$. When compared with side chain interactions from S6K1 and PRAS40 at these pockets, the positional sequence identity is almost zero. These results demonstrate that elucidating a consensus sequence motif for $mTOR^{FRB}$-based substrate docking might be challenging owing to the capability of $mTOR^{FRB}$ to form energetically favorable interactions with highly diverse hydrophobic and aromatic side chains. These results support the proposition that hydrophobic amino acids within 15

amino acids of a phosphorylation site might be the best indicator for an $mTOR^{FRB}$ substrate recruitment motif (67).

These studies could benefit from analyzing the CDR sequences of a larger pool of synthetic binders, or from engineering mTORC1 substrates to delineate the tolerance for hydrophobic side chains in endogenous $mTOR^{FRB}$-docking peptide regions. However, the inherently weak binding interactions between substrates and $mTOR^{FRB}$ renders this a challenging task. The fact that synthetic Fabs with low nanomolar K_D values are vulnerable to mutations in side chains contacting the center of the substrate recruitment domain suggests a broad relevance for these pockets. An interesting area for exploration could be the evolutionary conservation of $mTOR^{FRB}$-interacting regions between divergent eukaryotic species. Conceptually, these regions might display low sequence conservation, which might not reflect their capability for binding $mTOR^{FRB}$ based on the observations described here. Together, gaining structural and functional insight into substrate-specific interactions with $mTOR^{FRB}$ could provide a foundation to design therapeutic perturbations with higher selectivity within the mTORC1 signaling network. Furthermore, an enhanced understanding of substrate recruitment mechanisms will shed light on nutrient-sensitive regulation of cell physiology by mTOR.

2.5 Materials and methods

Generation of DNA constructs. All PCR and ligation reactions described here were performed using the In-Fusion HD Cloning Kit (Takara Bio). gBlock gene fragments (IDT) encoding FKBP12 and the FRB domain of mTOR (*H. sapiens* and residues corresponding to 2021-2113 for *D. melanogaster, C. elegans,* and *S. cerevisiae* TOR1) were cloned into

the SmaI site of the pEKD40 expression vector bearing C-terminal 6xHis-tags as previously described (126). *H. sapiens* $mTOR^{FRB}$ was also cloned into BamHI/XhoI sites of the pHFT2 expression vector with an N-terminal 10xHis-tag and TEV cleavage site. Synthetic antibody fragment (Fab) PCR inserts were generated by PCR from unique phage clones and ligated into SalI/HindIII sites of the pRH2.2 expression vector (non-tagged) or into SphI sites of the pSFV4 expression vector (AviTag). Mutagenesis was performed according to the QuikChange Site-Directed Mutagenesis Kit (Agilent). Single chain variable fragments were generated by cloning a gBlock fragments encoding Fab-R3E9 or Fab-R3H8 VL and VH domains as previously described (119) into XbaI/BamHI sites of the pSCSTa expression vector. Unique VH domains were cloned into XhoI/BamHI sites and CDR-L3 was mutated by a combination of PCR and In-Fusion ligation.

Protein expression and purification. Expression of SNAP-6xHis, SNAP-$mTOR^{FRB}$-6xHis, SNAP-FKBP12-6xHis, and 10xHis-TEV-$mTOR^{FRB}$ was performed using BL21(DE3) competent *E. coli.* Cells were grown in 2xYT medium to OD_{600}=0.6-0.8, 1 mM IPTG was added, and cells were incubated overnight at 20°C before harvesting by centrifugation. Purification followed a previously described protocol (126). Removal of 10xHis-tag was performed by incubated TEV protease with 10xHis-TEV-$mTOR^{FRB}$ at 1:50 ratio (w/w) overnight at 4°C in the presence of 0.5 μM TCEP. Next day, samples were incubated with TALON resin (Takara Bio) for 1 hour with rotation at 4°C before collecting the flow through for purity analysis by SDS-PAGE. Periplasmic expression of Fabs was performed in BL21 competent *E. coli*. Cells were grown in 2xYT medium to OD_{600} = 0.6-0.8, 1 mM IPTG was added, and cells were incubated for 4 hours at 37°C before

harvesting by centrifugation. Fab purification was performed as previously described (127). Fabs with AviTag were expressed in CVB101 cells following the same protocol above with the exception of adding 50 μM biotin at the time of induction.

Phage display selection. Phage display selection was performed as previously described (127). Prior to library sorting, SNAP-mTOR^{FRB} was site-specifically biotinylated by incubation with SNAP-Biotin (NEB) in the presence of 0.3 mM TCEP for 30 min at 37°C. Biotinylated SNAP-mTOR^{FRB} (Bio-SNAP-mTOR^{FRB}) was immobilized onto Streptavidin MagneSphere Paramagnetic Particles (Promega) for five rounds of phage selection. The selection process consisted of incubation with naïve phage library, washing to remove nonspecific phage, eluting phage, and amplyfing phage in *E. coli* XL-1 blue cells (Stratagene). Before each round, the amplified phage pool underwent competitive and subtractive selection using non-biotinylated SNAP-tag only and empty streptavidin paramagnetic beads for 30 minutes with shaking to eliminate nonspecific binders. The final antigen concentration was dropped systematically from 1 μM to 2 nM from the first to the fifth round (200 nM second round, 50 nM third round, 20 nM fourth round, and 2 nM fifth round). All selection conditions maintained 1 μM of non-biotinylated SNAP-tag to deplete anti-SNAP binders.

Enzyme-Linked Immunosorbent Assays (ELISA). For phage ELISA, SNAP-mTOR^{FRB} (50 nM) was directly immobilized onto high binding 96-well microplates (Greiner Bio). Wells were blocked by incubating with 2% BSA in PBS for at least 1 hour. Individual phage clones were diluted in 0.5% BSA/PBST before being added to the plate for 15

minutes with gentle agitation. Wells were washed three times with 0.5% BSA/PBST and then incubated with Protein L-HRP (Thermo Scientific). The plates were again washed and developed with TMB substrate (Thermo Scientific) followed by quenching with 10% H_3PO_4 and absorbance measurement at 450 nm. For Fab-format ELISA, targets (200 nM) were directly immobilized onto high binding 96-well microplates (Greiner Bio). The wash buffer for all Fab-format experiments was PBS supplemented with 0.05% Tween 20. Plates were washed and blocked with 1% BSA in PBS. For competitive ELISA, competitors alone were incubated first for 15 minutes. Dilutions of Fabs alone or with competitors were prepared in PBS/0.05% Tween 20/0.5% BSA and were added for 20 minutes before washing three times. Secondary detection was carried out by Protein L-HRP (Thermo Scientific) for 20 minutes. Plates were washed three times before adding TMB substrate (Thermo Scientific), quenching with 10% H_3PO_4, and measuring absorbance at 450 nm.

Surface plasmon resonance. The MASS-1 (Bruker) instrument was used for all surface plasmon resonance (SPR) analyses. Ni-NTA sensor surface was used to immobilize $mTOR^{FRB}$ via a 6xHis-tag. Fabs in two-fold dilutions were run as analytes at 30 μl/min flow rate (20°C). Raw data were corrected by double referencing. Analysis was performed with Sierra Analyser (Bruker) using a Langmuir 1:1 binding model for curve fitting. Results were then plotted using GraphPad Prism.

In vitro pulldown assay. SNAP-FKBP12 was site-specifically labeled with SNAP-Surface Alexa Fluor 488 (NEB) according to the manufacturer's protocol. The dilution and

wash buffer for all pulldowns was PBS supplemented with 0.05% Tween 20 and 0.5% BSA. All incubations were performed in the dark at room temperature. Briefly, 10 nM Bio-SNAP-mTOR^{FRB}, 10 nM A488-SNAP-FKBP12, and 10 nM rapamycin were incubated together briefly to allow ternary complex formation. Varying concentrations of sAB-R3E9 or sAB-R3H8 were spiked into each sample and incubated 30 minutes. Next, 10 μL of Streptavidin MagneSphere Paramagnetic Particles (Promega) were added to each samples and incubated with constant rotation for 15 mins. Samples were washed three times in 0.3 mL wash buffer supplemented with 10 nM rapamycin before elution by heating 5 mins in 20 μL 1x sample buffer for SDS-PAGE analysis. A488-SNAP-FKBP12 levels were quantified using Image Lab software to determine IC_{50} values for sAB-R3E9 and sAB-R3H8.

Immunoprecipitation and western blot analysis. To maintain the integrity of mTORC1 assemblies, the lysis buffer used was 0.3% CHAP, 25 mM TRIS, pH 8.0, 150 mM NaCl supplemented with 5 mM EDTA and 1x Halt Protease Inhibitor Cocktail. Briefly, cells were washed one time with ice cold PBS. Cell lysis was carried out on ice for 20 minutes with constant agitation before centrifugation at 14,000 rpm to clarify lysates. Supernatants were transferred to fresh tubes and total protein was quantified by BCA assay (Thermo Scientific). Biotinylated sAB immunoprecipitations were performed for 3 hours with rotation at 4°C. Dynabeads M-270 Streptavidin beads (Invitrogen) were equilibrated in lysis buffer before adding to lysates for 1 hour with rotation at 4°C. Beads were washed five times in lysis buffer before elution by boiling 5 minutes in SDS sample buffer containing 10 mM DTT. Samples were separated via SDS-PAGE at 100V, transferred to

Immobilin-P PVDF Membranes (0.45 μm, EMD Millipore), and blocked for 1 hour at room temperature in blocking buffer (5% BSA in PBS supplemented with 0.1% Tween 20). The following primary antibodies were obtained from Cell Signaling Technology: mTOR (#2972S), Raptor (#2280S), mLST8 (#3274S), Rictor (#2114S), Actin (#4970T), Tubulin (#2148S), and FLAG (#14793S). Antibodies were diluted in blocking buffer and incubated with membranes overnight at 4°C with gentle rocking. Membranes were washed three to four times for five minutes each in wash buffer (PBS supplemented with 0.1% Tween 20) before adding Anti-Rabbit IgG, HRP-Linked Antibody (Cell Signaling Technology, #7074P2) for one hour at room temperature in blocking buffer. Membranes were washed three to four times for five minutes each in wash buffer and then developed using SuperSignal West Pico PLUS Chemiluminescent Substrate (Thermo Fisher Scientific).

Immunofluorescent staining and confocal microscopy imaging. HeLa cells were seeded onto ibiTreat μslide 8-Well slides (Ibidi) and grown in Dulbecco's modified Eagle medium (DMEM) supplemented with 1% Pen-Strep (Gibco) and 10% fetal bovine serum until they reached 80-90% confluency before immunostaining. Imaging was performed using a Stellaris 8 (Leica) confocal microscope. Quantitative analyses were performed using FIJI (128). For mTOR/LAMP1 co-localization immunostaining, HeLa cells were washed once with PBS before fixation for 15 minutes at room temperature in 4% paraformaldehyde. Cells were washed three times in PBS and then permeabilized with 0.2% Triton X-100 for 10 minutes followed by three washes in PBS. Blocking was performed by adding 3% BSA, 0.2% Triton X-100 for 1 hour at room temperature. sAB-R3E9 and anti-LAMP1 (Cell Signaling Technology, #9091T) antibodies were diluted in

1% BSA, 0.2% Triton X-100 and added for 2 hours at 4°C. Cells were washed three times with PBS. Goat Anti-Human IgG, $F(ab')_2$ fragment specific conjugated with Alexa647 and Goat Anti-Rabbit IgG (H+L) conjugated with Alexa488 (Jackson ImmunoResearch) were diluted in 1% BSA, 0.2% Triton X-100 and added for 45 minutes at room temperature. Cells were washed three times with PBS and incubated with 1 µg/µL DAPI (Thermo Fisher Scientific) for 10 minutes before washing again three times with PBS. PBS in 50% glycerol was added as the final step.

Crystallization and structure determination. Fab-R3E9•$mTOR^{FRB}$ and Fab-R3H8•$mTOR^{FRB}$ complexes were purified in in 10 mM HEPES, pH 7.2, 150 mM NaCl by size exclusion chromatography (SEC) using a Sephadex 200 column. Evaluation of SEC purity was performed by analyzing fractions via SDS-PAGE. Pure complexes were concentrated to at least 10 mg/mL for crystallization screening facilitated by the Mosquito Crystal Robot (TTP Labtech). Crystallization conditions for the Fab-R3E9•$mTOR^{FRB}$ complex were 0.2 M Calcium chloride dihydrate, 16% PEG 3350. Crystals were soaked in reservoir solution containing 20% PEG 400 before being flash frozen in liquid nitrogen. Crystallization conditions for the Fab-R3H8•$mTOR^{FRB}$ complex were 0.1 M HEPES, pH 7.5, 4% PEG 400, 2.2 M ammonium sulfate. Crystals were directly flash-frozen in liquid nitrogen for data collection. X-ray diffraction data sets were collected at the 23-ID-D beamline of the Advanced Photon Source at Argonne National Laboratory. Molecular replacement was used to solve crystal structures of Fab-R3E9•$mTOR^{FRB}$ and Fab-R3H8•$mTOR^{FRB}$ using structures of FRB (PDB: 1FAP) and Fab (PDB: 6U8C) in Phaser-MR (129). Models were refined using phenix.refine (130) and manually built using Coot

(131) over iterative alternating cycles. All structural figures were generated using PyMOL. Coordinates have been deposited to the Protein Data Bank (9DBO and 9DL0).

Chapter 3

Conformation-specific synthetic intrabodies modulate mTOR signaling with subcellular spatial resolution

This chapter has been adapted from K. O'Leary, T. Slezak, A. Kossiakoff, Conformation-specific synthetic intrabodies modulate mTOR signaling with subcellular spatial resolution. *Proc. Natl. Acad. Sci. U.S.A.*, in press.

Kelly M. O'Leary[1], Tomasz Slezak[1], and Anthony A. Kossiakoff[1,2,*]

[1]Department of Biochemistry and Molecular Biology, The University of Chicago, Chicago, IL 60637.

[2]Institute for Biophysical Dynamics, The University of Chicago, Chicago, IL 60637.

*Correspondence to: Anthony A. Kossiakoff

3.1 Abstract

Decoupling context-specific functions of pleiotropic signaling molecules is inherently challenging and typically requires specialized molecular tools. Mechanistic target of rapamycin (mTOR) is a cornerstone example of a protein kinase with multifunctional signaling capabilities that are influenced by cognate protein-protein interactions and local subcellular environments. However, elucidating mTOR signaling mechanisms with structural or spatial resolution remains challenging using conventional approaches, such as small molecule inhibitors or gene knockdowns. This limitation was addressed using synthetic intracellular antibody fragments (intrabodies) that recognize distinct conformational epitopes and are capable of modulating mTOR signaling with genetically programmable spatial resolution. Expression of these intrabodies in living cells revealed a conformation-specific allosteric mechanism of regulation for mTOR complex 1 assembly, which was validated by high resolution crystal structure analysis. Furthermore, the ability to genetically tag intrabodies for spatially restricted expression in desired subcellular compartments enabled direct functional perturbations to mTOR in the cytoplasm or nucleus. This work establishes a unique genetic approach for decoupling structural and spatial mechanisms of mTOR signaling using synthetic intrabodies.

3.2 Introduction

Large, multi-subunit protein kinase assemblies govern myriad fundamental cell biological process. A central example of this is the PI3K-related kinase family, which is comprised of 2000-plus amino acid serine/threonine protein kinases that require diverse obligate protein-protein interactions to function properly. A defining member of this family is mechanistic target of rapamycin (mTOR), which controls eukaryotic cell growth and metabolism in response to nutritional cues (32). The modular association of mTOR with cognate subunits, Raptor or Rictor, constitutes the foundation for two structurally and functionally distinct signaling assemblies known as mTOR complex 1 (mTORC1) and mTOR complex 2 (mTORC2), respectively. mTORC1 and mTORC2 integrate different nutrient or growth factor stimuli and phosphorylate mutually exclusive sets of substrates (56).

Canonical descriptions of mTORC1 and mTORC2 posit that they signal from distinct subcellular locations. Lysosomal mTORC1 recruitment has been firmly established to play a role in nutrient- and growth factor-induced regulation of cell metabolism (132). On the other hand, mTORC2 has been described at various endomembrane structures (85). Recent studies have highlighted the distinct signaling capabilities of mTORC1 and mTORC2 in more widespread subcellular locations, including the nucleus (Figure 3.1) (74, 78, 85). These studies were enabled by the development of specialized molecular biosensors, highlighting the critical need for tool development for paradigm-shifting endeavors. This is especially important for studies requiring functional perturbations with the precision of conformational specificity or spatial resolution, which is not afforded by small molecules or gene knockdowns.

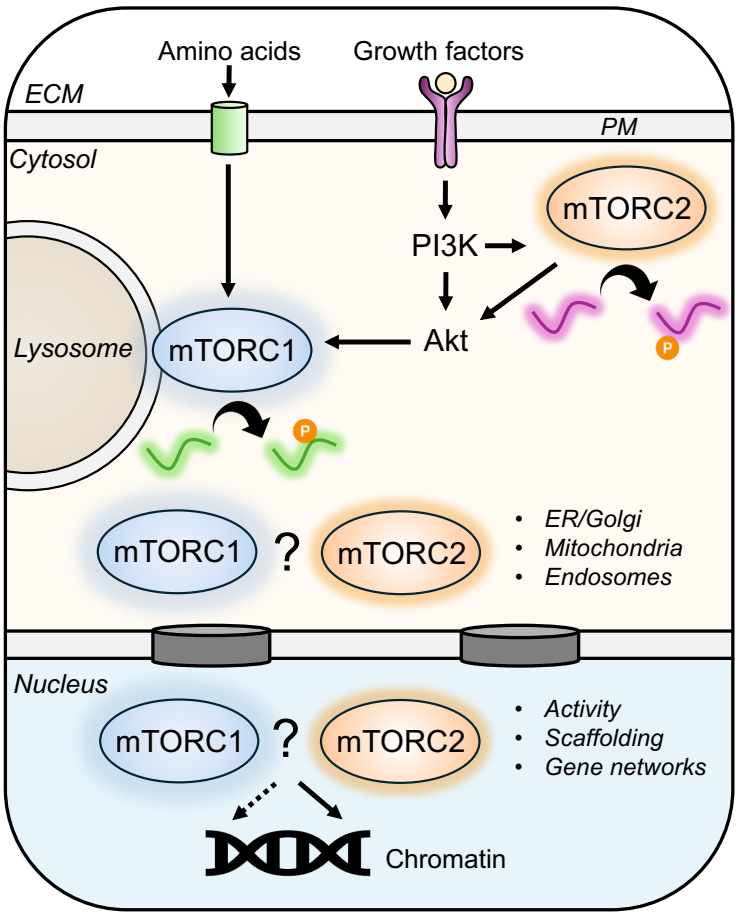

Figure 3.1 Expanding paradigm of subcellular mTORC1 and mTORC2 localization. Generalized cartoon signaling pathway displaying canonical locations for mTORC1 (lysosome) and mTORC2 (plasma membrane) in addition noncanonical locations.

Methods to selectively design therapeutic inhibitors against PIKK members were hampered by a lack of structural insight until the recent cryo-EM resolution revolution. Despite the emergence of high-resolution structures defining the mTOR complex 1 and mTOR complex 2 architectures, these data do not capture the conformational dynamics underlying the regulation of these large, multi-subunit assemblies (62, 123). One example of this is the mechanism of inhibition by rapamycin, which binds together with FKBP12 at

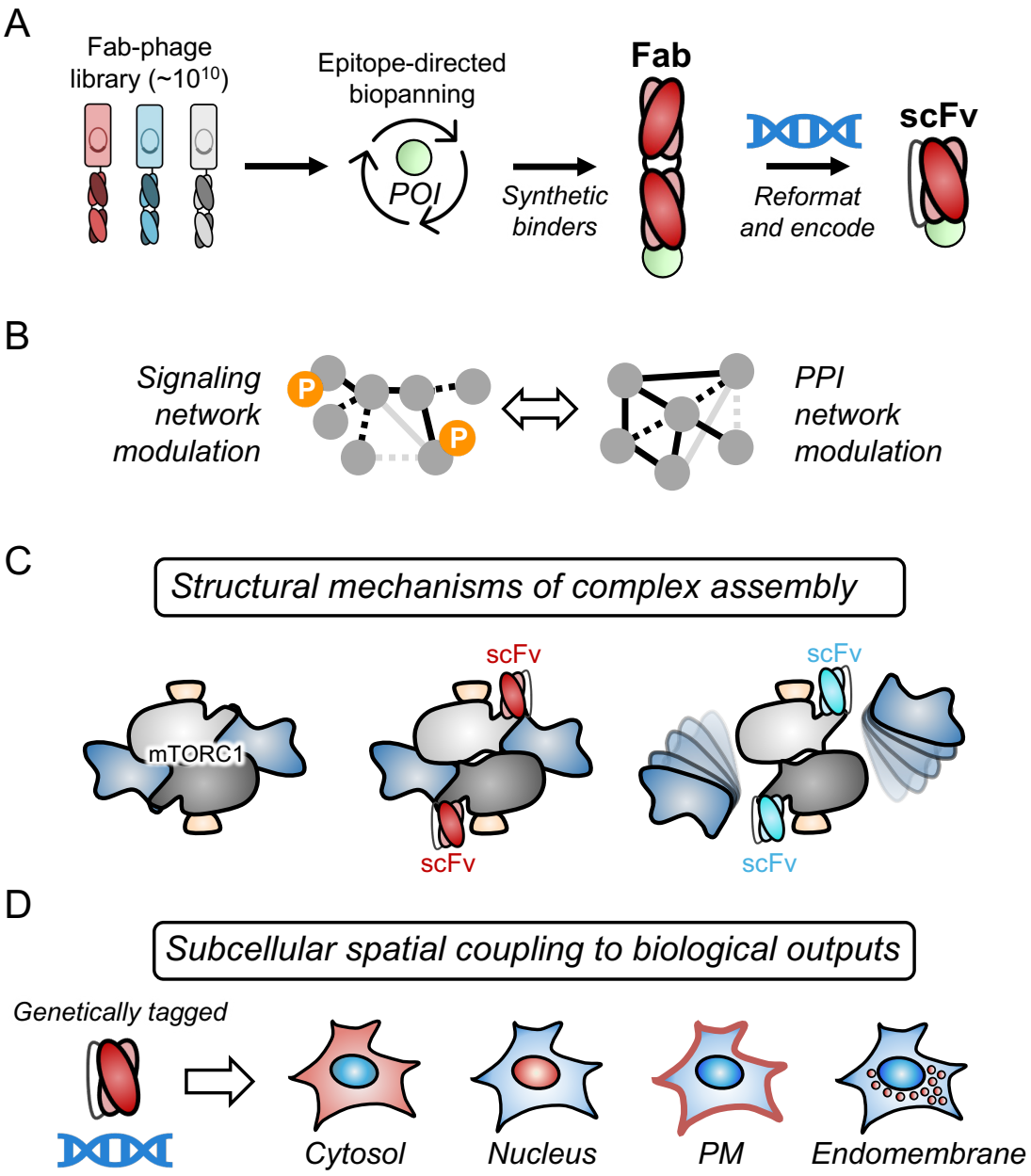

Figure 3.2 Application of intrabodies to dissect structural and spatial mechanisms. (A) Schematic for epitope-directed phage display and Fab-to-scFv reformatting to enable genetically encoded expression in living cells. (B) Potential applications for genetically encoded intrabodies. *Left:* Modulation of intracellular signaling networks in a drug-like manner. *Right:* Modulation of protein-protein interaction networks. (C) Schematic for the use of intrabodies to decouple allosteric or orthosteric binding site interactions. (D) Schematic for the use of intrabodies as genetically encoded and spatially restricted inhibitors at select subcellular locations.

the FRB domain and allosterically destabilizes the interaction between mTOR and Raptor (133). Despite being reported for decades, a molecular mechanism underlying the destabilization of mTOR-Raptor from the allosteric rapamycin binding site has not yet been described.

To circumvent these issues, epitope-directed synthetic Fabs that target the rapamycin and substrate binding site on $mTOR^{FRB}$ were generated and described in chapter 2. This chapter describes implementation of conformation-specific intrabodies for studies into structural mechanisms of mTOR complex assembly and functional mechanisms of subcellular location-specific mTOR signaling (Figure 3.2A-D). Crystal structure analysis revealed subtle conformational changes in $mTOR^{FRB}$ side chain rotational isomers (rotamers) at the epitope-paratope interface in the Fab-R3E9 bound structure compared to Fab-R3H8. These rotamers were correlated with small distortions in two α-helices in the structure of $mTOR^{FRB}$. The intrabody scFv-R3E9 exhibited selective engagement of the rapamycin binding site and co-immunoprecipitation of mTORC1 with no apparent destabilization of the mTOR-Raptor interaction. In contrast, scFv-R3H8 displayed rapamycin-like destabilization of the mTOR-Raptor interaction. Therefore, a novel allosteric mechanism has been described for switchable destabilization of the mTORC1 architecture mediated through subtle side chain and helical rearrangements in $mTOR^{FRB}$.

Signaling assays established scFv-R3E9 and scFv-R3H8 as potent mTOR inhibitors with a mechanism of action similar to rapamycin. The functional utility of scFv-R3E9 and scFv-R3H8 was extended by incorporating endogenous subcellular localization tags to restrict their expression to select subcellular structures. The simplest manifestation of this was performed by anchoring scFv-R3E9 and scFv-R3H8 in the cytoplasm or in the

nucleus to elicit direct functional perturbations with subcellular resolution. These results established a new technological platform for decoupling subcellular signaling networks where small molecules and gene knockdowns fall short. Together, investigations into the subcellular organization of mTOR activity can be made accessible to researchers through simple plasmid-based genetic portability of the synthetic intrabodies described here.

3.3 Results

3.3.1 Discovery of an allosteric mechanism governing the structural integrity of mTOR complex 1

To test whether conversion of Fab-R3E9 and Fab-R3H8 to scFv intrabody format resulted in proper engagement of mTOR, Expi293F cells were transfected with FLAG-tagged scFv constructs for each intrabody. The FLAG tag provided a handle for selective immunoprecipitation of each intrabody followed by analysis via western blot (Figure 3.3A). Compared to empty vector (EV) or a negative control isotype (Iso) intrabody, scFv-R3E9 and scFv-R3H8 pulled down equal amounts of mTOR after enrichment with anti-FLAG purification resin (Figure 3.3B and C). Strikingly, the amount of Raptor that co-immunoprecipitated with scFv-R3E9 was significantly greater than with scFv-R3H8 (Figure 3.3D). To address the third major component of mTORC1, mLST8 levels were observed to be consistent between scFv-R3E9 and scFv-R3H8 and consistent with mTOR levels (Figure 3.3E). These results suggested that scFv-R3E9 and scFv-R3H8 exhibit differential effects on the stability of the mTOR-Raptor interaction despite binding to nearly identical epitopes that were elucidated by high resolution crystal structures (Figure 3.3F and G).

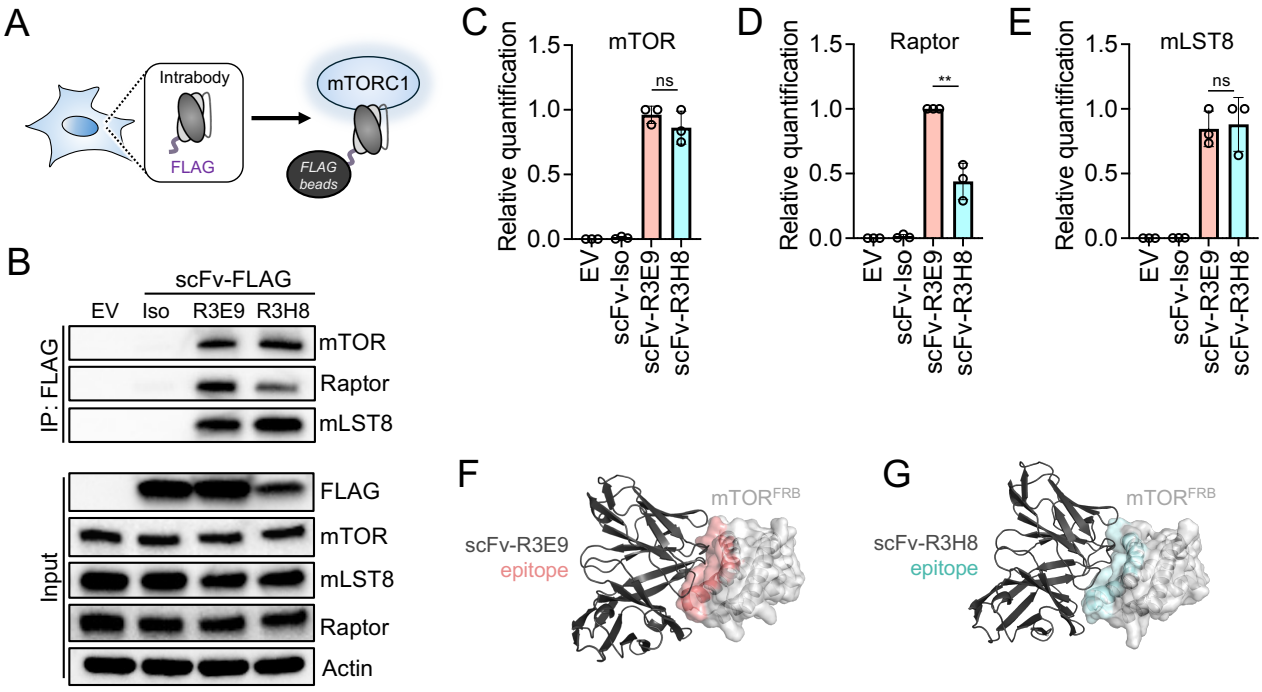

Figure 3.3 Intrabody-based co-immunoprecipitation of mTORC1. (A) Construct design and schematic for intrabody co-immunoprecipitation. (B) Expi293F cells were transfected with the indicated constructs for 48 hours before harvesting for lysis and anti-FLAG enrichment. (C) Quantification of mTOR in the FLAG immunoprecipitation from the experiment in B (n = 3 biological replicates, mean ± SD. ns = not significant, unpaired *t*-test). (D) Quantification of Raptor in the FLAG immunoprecipitation from the experiment in B (n = 3 biological replicates, mean ± SD. $^{**}P \leq 0.01$, unpaired *t*-test). (E) Quantification of mLST8 in the FLAG immunoprecipitation from the experiment in B (n = 3 biological replicates, mean ± SD. ns = not significant, unpaired *t*-test). (F) Structure and location of the scFv-R3E9 epitope. (G) Structure and location of the scFv-R3H8 epitope.

In order to understand the molecular basis for these results, the format of the assay was changed to accommodate pan-mTOR immunoprecipitation from cells expressing scFv-R3E9 or scFv-R3H8. FLAG-tagged intrabody constructs were equipped with T2A-eGFP tags as fluorescent reporters for intrabody expressing cells after transfection. Pure population of these cells were isolated using fluorescence-activated cell sorting (FACS) before performing pan-mTOR immunoprecipitation to analyze the core interactions with all mTORC1 and mTORC2 assemblies via western blotting. Cells treated with vehicle or

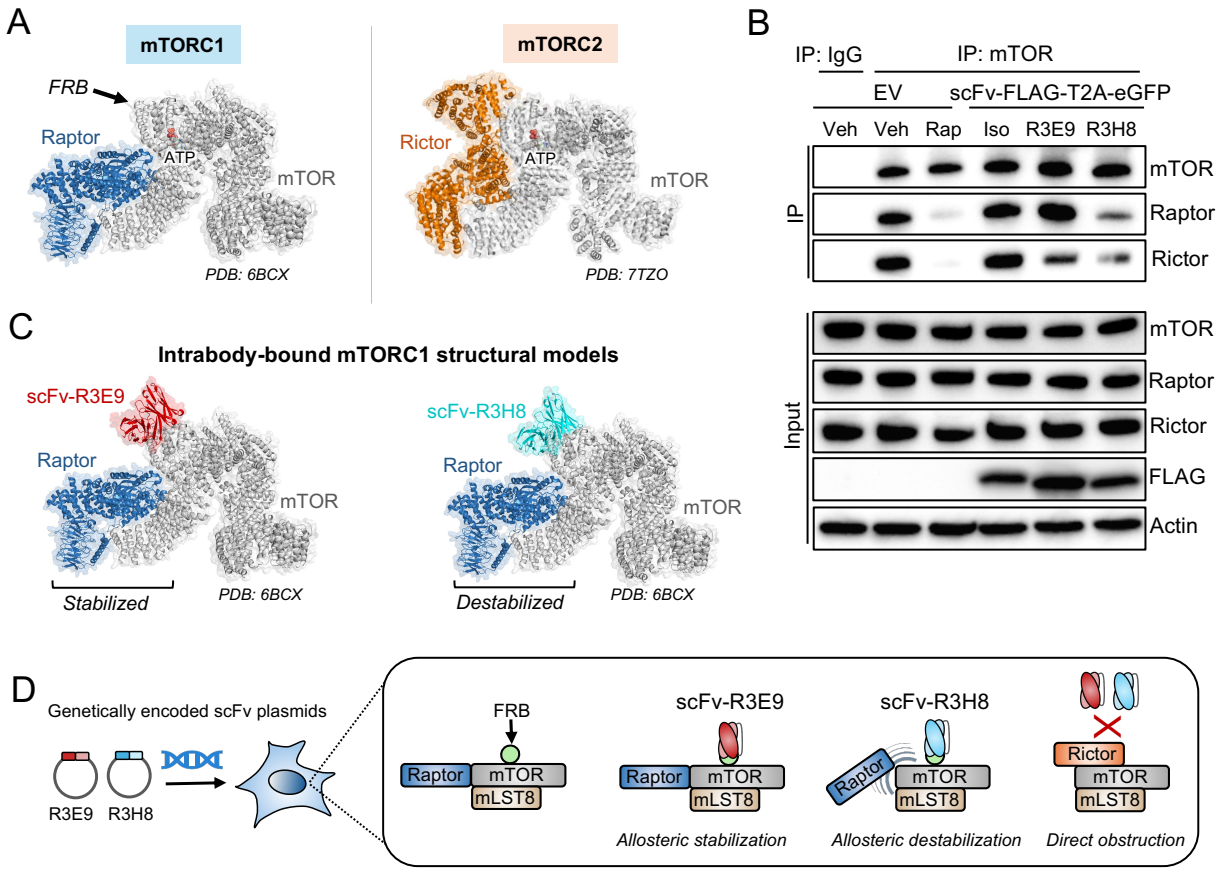

Figure 3.4 Switchable allosteric modulation of the mTOR-Raptor interaction. (A) Previously published cryo-EM structures of mTORC1 (PDB: 6BCX) and mTORC2 (PDB: 7TZO) showing the accessibility and inaccessibility of the FRB domain, respectively. Active site is denoted by ATP (spheres) from PDB: 6BCX. (B) Immunoprecipitation-western blot analysis of mTOR-Raptor and mTOR-Rictor interactions in cells expressing the indicated intrabodies. Empty vector (EV), isotype control (Iso), R3E9, or R3H8 FLAG-T2A-eGFP tagged intrabodies (scFv-FLAG-T2A-eGFP) were transfected in Expi293F cells for 24 hours. FACS was used to isolate eGFP(+) cells. Cells were treated for 24 hours with vehicle or 200 nM rapamycin in the indicated samples (n = 3 biological replicates).

200 nM rapamycin were used as controls to monitor the modulation of mTOR-Raptor and mTOR-Rictor interactions. Rapamycin is a well-characterized allosteric destabilizer of the mTOR-Raptor interaction and an obstructive modulator of the mTOR-Rictor interaction

during prolonged inhibition (133, 134). As expected, Expi293F cells treated with rapamycin for 24 hours showed almost complete loss of Raptor and Rictor compared to the vehicle control in the pan-mTOR immunoprecipitation (Figure 3.4B). These results provided context for rapamycin-based modulation of core mTOR protein-protein interactions in Expi293F cells. Similar to rapamycin, cells expressing scFv-R3H8 showed depletion of Raptor and Rictor in the mTOR pulldown, which can be attributed to allosteric and competitive “rapamycin-like” mechanisms, respectively. Cells expressing scFv-R3E9 showed similar depletion of Rictor but did not exhibit depletion of Raptor. This is particularly intriguing owing to the similar structurally characterized epitopes engaged by scFv-R3E9 and scFv-R3H8, which do not directly interfere with the interaction between mTOR and Raptor (Figure 3.4C). Overall, these results establish a customized genetic platform consisting of conformational intrabody-based probes that report the allosteric modulation of the mTORC1 architecture (Figure 3.4D).

3.3.2 Structural basis for mTOR^{FRB} conformational discrimination by synthetic intrabodies

These findings prompted an investigation into the structural mechanism responsible for the differential allosteric modulation of the mTOR-Raptor interaction by scFv-R3E9 and scFv-R3H8. Owing to the well described allosteric modulation of mTOR-Raptor elicited by FKBP12-rapamycin binding, a structural comparison was made for directly interacting side chains in the paratope-epitope interface for Fab-R3E9 and Fab-R3H8. Rapamycin is a macrocyclic lactone that binds to mTOR^{FRB} only after forming a

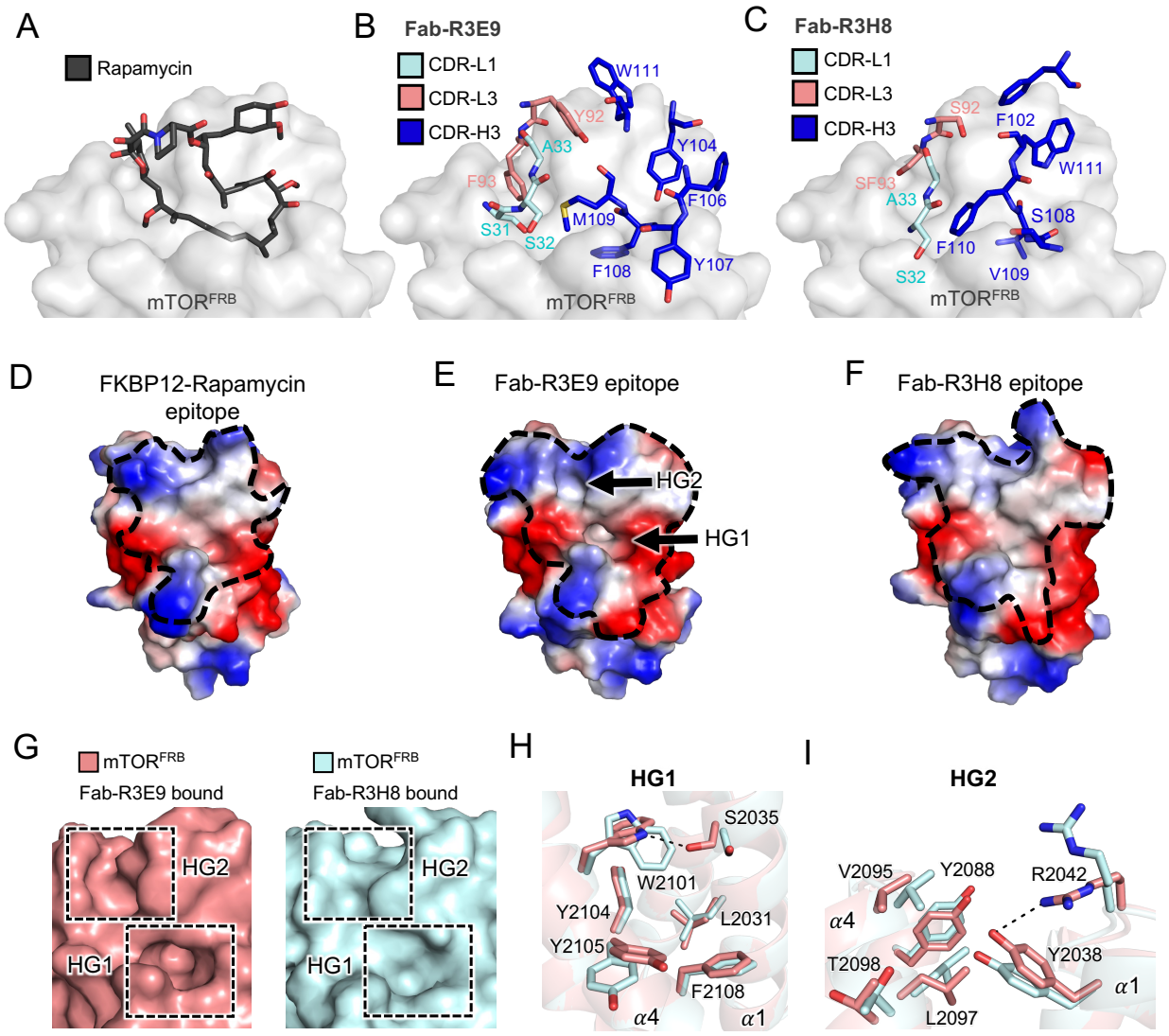

Figure 3.5 Structural comparison of rapamycin, Fab-R3E9, and Fab-R3H8. (A) Binding pose of rapamycin from PDB: 1FAP. (B) Fab-R3E9 residues with similar spatial arrangement as rapamycin. (B) Fab-R3H8 residues with similar spatial arrangement as rapamycin. (D) mTOR^{FRB} surface electrostatics from PDB: 1FAP, (E) mTOR^{FRB} surface electrostatics bound by Fab-R3E9. Hydrophobic grooves 1 and 2 (HG1 and HG2) marked by arrows. (F) mTOR^{FRB} surface electrostatics bound by Fab-R3H8. Epitopes are traced with black dashed line. (G) Surface representations of HG1 and HG2 on mTOR^{FRB} bound by Fab-R3E9 (left, salmon) and Fab-R3H8 (Right, cyan). (H) mTOR^{FRB} side chains that form HG1. (I) mTOR^{FRB} side chains that form HG2.

complex with FKBP12. Rapamycin does not insert many bulky moieties into the hydrophobic interface of the $mTOR^{FRB}$ substrate recruitment domain but instead lays relatively flat across this binding site (Figure 3.5A). Fab-R3E9 and Fab-R3H8 form contacts in a strikingly similar arrangement as the lactone ring from rapamycin (Figure 3.5B and C). However, it is clear from this analysis that the Fab paratope side chain interactions are characteristically different from the lactone ring of rapamycin. Fab-R3E9 and Fab-R3H8 utilize bulky hydrophobic residues, such as phenylalanine, tryptophan, methionine, and valine, to form Van der Waals contacts in shallow hydrophobic pockets located on the surface of $mTOR^{FRB}$. To investigate whether the surface topology of $mTOR^{FRB}$ is modulated by Fab binding, electrostatic potential maps were generated for $mTOR^{FRB}$ bound by FKBP12-rapamycin (PDB: 1FAP), Fab-R3E9, and Fab-R3H8 (Figure 3.5D-F). This analysis demonstrated stark differences in the surface topology for the Fab-R3E9 bound structure of $mTOR^{FRB}$ compared to Fab-R3H8 or FKBP12-rapamycin. This observation aligns with the discrepancy in functional effects for scFv-R3E9, which was found to have a unique allosteric influence on the mTOR-Raptor interaction compared to rapamycin or scFv-R3H8. Specifically, two hydrophobic grooves (HG1 and HG2) were identified in the Fab-R3E9 bound structure that are morphologically altered (Figure 3.5E and G). The molecular basis for $mTOR^{FRB}$ surface modulation by Fab-R3E9 can be described mainly by side chain motions of S0235 and W2101 for HG1 and by R2042, Y2038, V2095, and T2098 for HG2 (Figure 3.5H and I). The formation of HG1 is characterized by broadening and depth extension by ~4 Å to accommodate the side chain of $F108^{H3}$ from Fab-R3E9, which sterically clashes with the canonical $mTOR^{FRB}$ W2101 conformation. HG2 is opened to a lesser extent via Y2038 and V2095 displacement,

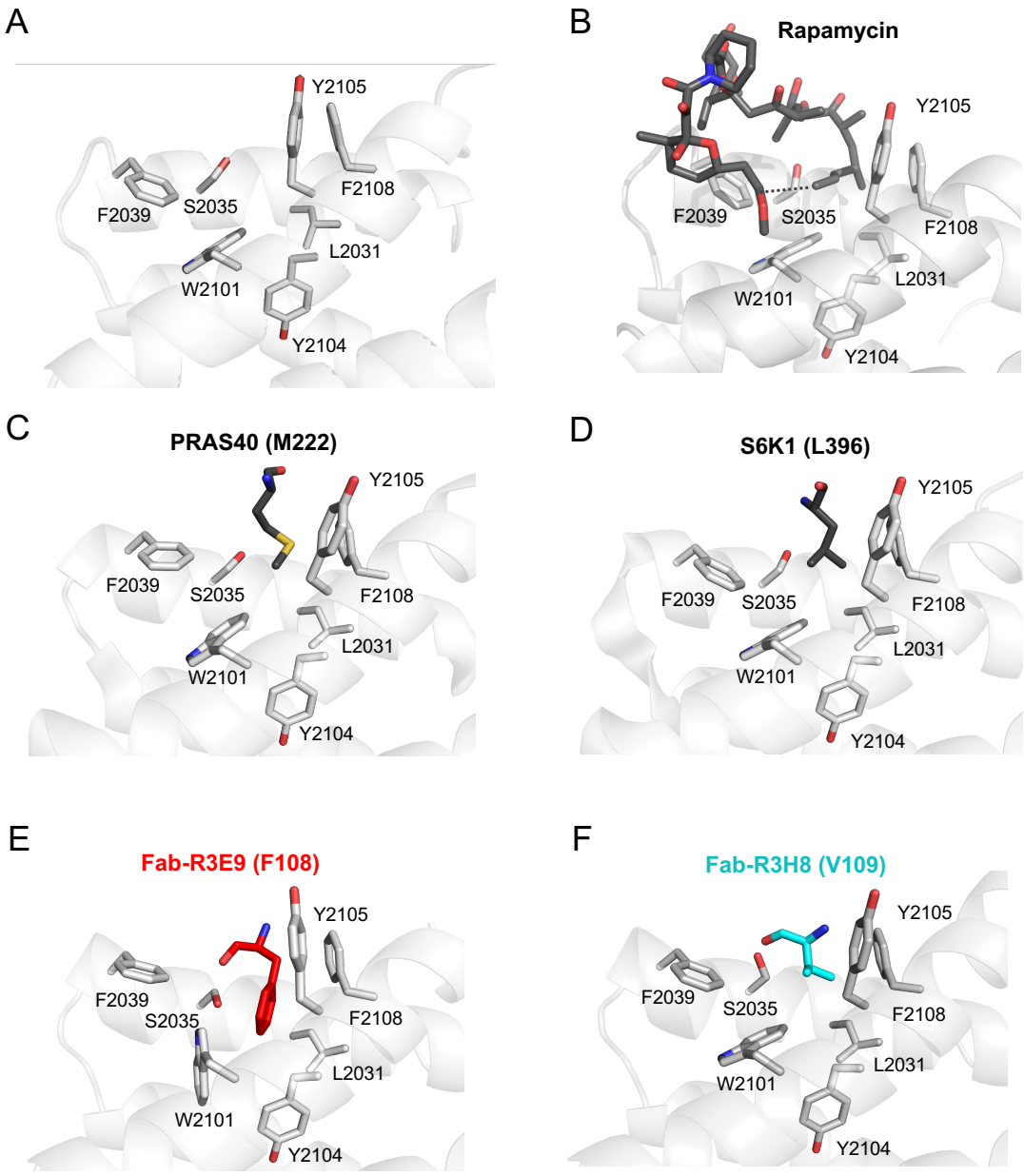

Figure 3.6 W2101 and S2035 rotamers in mTOR^{FRB} structures. (A) Side chains from the previously determined structure (PDB: 1AUE) of mTOR^{FRB} alone that interact directly with substrates or rapamycin. (B) Interaction of rapamycin with mTOR^{FRB} side chains from a previously determined structure (PDB: 1FAP). (C) Interaction of M222 of PRAS40 with mTOR^{FRB} side chains from a previously determined structure (PDB: 5WBU). (D) Interaction of L396 of S6K1 with mTOR^{FRB} side chains from a previously determined structure (PDB: 5WBH). (E) Interaction of F108 of Fab-R3E9 with mTOR^{FRB} side chains. W2101 and S2035 are found in unique rotameric states in this structure. (F) Interaction of F108 of Fab-R3H8 with mTOR^{FRB} side chains.

which represents another unique morphological change compared to $mTOR^{FRB}$ bound by FKBP12-rapamcyin.

To understand the structural basis for HG1 formation, a comprehensive structural analysis for all $mTOR^{FRB}$-bound structures in the protein data bank was performed. Side chains from $mTOR^{FRB}$ that form this pocket are L2031, S2035, F2039, W2101, Y2102, Y2105, and F2108. Side chains in structures of $mTOR^{FRB}$ alone (PDB: 1AUE), $mTOR^{FRB}$-FKBP12-Rapamycin (PDB: 1FAP), $mTOR^{FRB}$-PRAS40 (PDB: 5WBU), and $mTOR^{FRB}$-S6K1 (PDB: 5WBH) were compared to Fab-R3E9 and Fab-R3H8 bound structures (Figure 3.6A-F). This analysis demonstrated that $mTOR^{FRB}$ side chains W2101 and S2035 undergo unique rotational isomerization when bound by Fab-R3E9 but not in any other deposited structures (Figure 3.6E). Based on these findings, the rotation around dihedrals in W2101 and S2035 appear to form the basis for HG1 broadening and depth extension. This can be explained by the bulky planar surface of W2101, which normally forms the bottom of the groove, rotating approximately 30 degrees. This rotation ultimately deepens the groove and allows $F108^{H3}$ from Fab-R3E9 to insert, which would not be compatible with the canonical conformation of W2101. Further analysis of this unique set of side chain rotamers revealed that W2101 and S2035 dihedral angles deviate from energetically favorable conformations. A comparison of tryptophan dihedral angles in the Fab-R3E9 bound structure of $mTOR^{FRB}$ compared to all tryptophans deposited in the protein data bank showed that the rotamer observed here is an extremely rare occurrence (Figure 3.7A). However, the W2101 conformation revealed here is unequivocally resolved in the crystal structure. The 2mFo-DFc electron density map (1σ contour) after refinement for W2101 and S2035 in $mTOR^{FRB}$ bound by Fab-R3E9 and

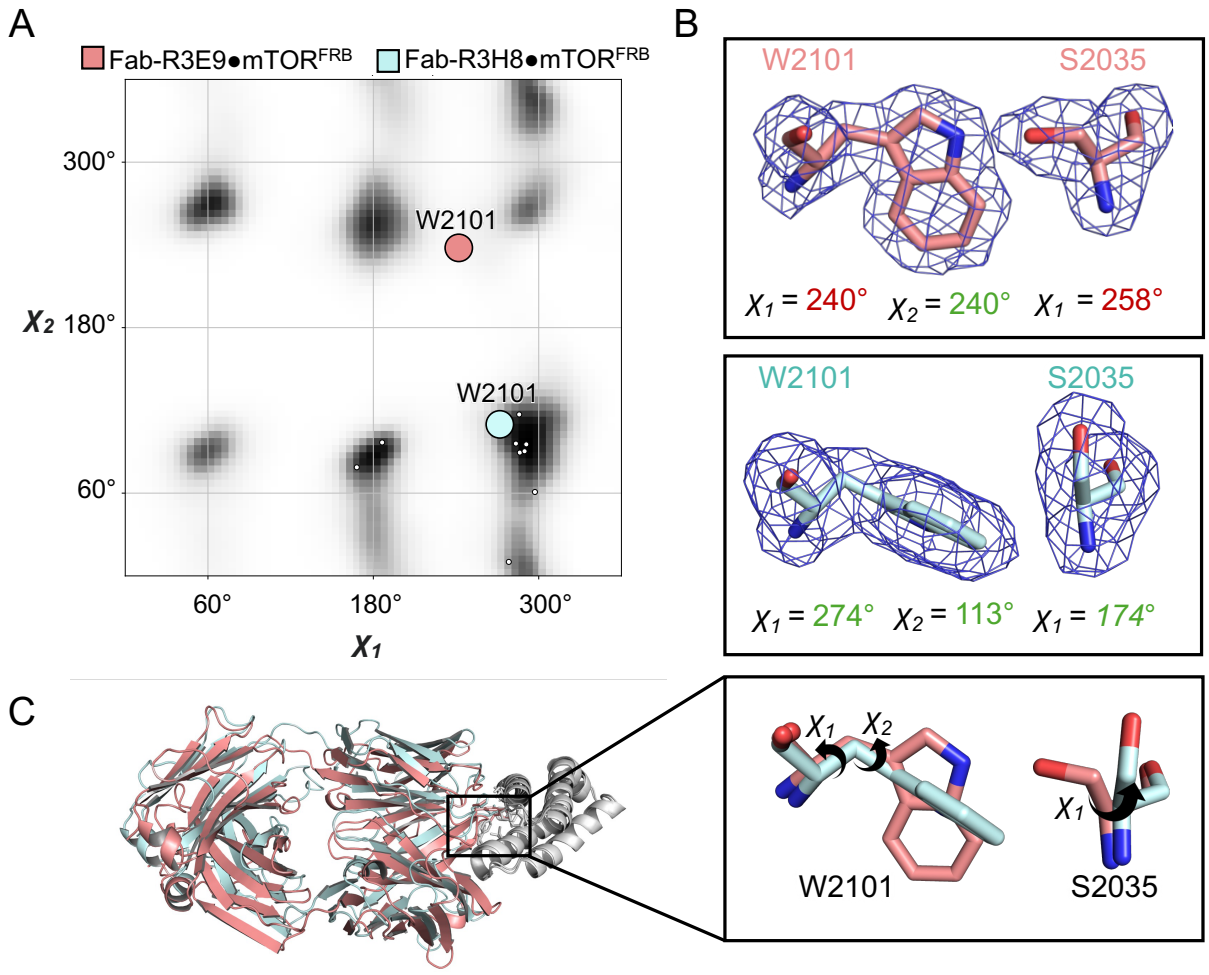

Figure 3.7 Structural basis for high energy rotamer stabilization by Fab-R3E9. (A) Heat map for tryptophan dihedral angles in the protein data bank shown in black. mTOR^{FRB} W2101 dihedrals from structures bound by Fab-R3E9 and Fab-R3H8 are indicated by salmon and cyan circles, respectively. (B) 2mFo-DFc electron density map (1σ contour) after refinement for W2101 and S2035 in mTOR^{FRB} bound by Fab-R3E9 (salmon) and Fab-R3H8 (cyan). (C) Alignment of Fab-R3E9 and Fab-R3H8 structures with W2101 and S2035 rotation shown on the right.

Fab-R3H8 shows clear density for rotation around these dihedrals. The unique side chain conformations under exceptional torsional strain observed in the Fab-R3E9 interface represent a critical aspect of its conformational epitope discrimination (Figure 3.7C).

An obvious question raised here is the following: how does the binding interaction between $mTOR^{FRB}$ and Fab-R3E9 lead to stabilization of W2101 and S2035 in high energy conformations? The energetic penalty of W2101 χ_1 rotation is estimated to be on the scale of 2-3 kcal/mol based on previous studies (135). This may be partially offset by a selective hydrogen bond formed between the high energy rotamer of S2035 with W2101. Furthermore, a nest of aromatic π-π stacking interactions between $mTOR^{FRB}$ (F2039, W2101, and F2108) and Fab-R3E9 ($F93^{H3}$, $F108^{H3}$, and $M109^{H3}$) appears to provide enough energy to pay off the cost of stabilized torsional strain in W2101 and S2035 (Figure 3.8A). Notably, this network of interactions is not observed when $mTOR^{FRB}$ is bound by Fab-R3H8 (Figure 3.8B). Together, the overall conformation of $mTOR^{FRB}$ between Fab-R3E9 and Fab-R3H8 bound structures is similar but exhibits subtle distortions in α-helices termed α3 and α4 (Figure 3.8C). These shifts were quantified and compared to the structure of $mTOR^{FRB}$ bound by FKBP12-Rapamycin (PDB: 1FAP), which demonstrated that Fab-R3E9 stabilizes α3 and α4 in distorted conformations that deviate by 1.6 Å and 1.2 Å, respectively (Figure 3.9D). In contrast, α3 and α4 from the Fab-R3H8 bound structure do not exhibit any differences when compared to α3 and α4 from a previously determined FKBP12-Rapamycin bound structure (PDB: 1NSG). These findings agree with the functional outcomes of rapamycin and scFv-R3H8 binding to

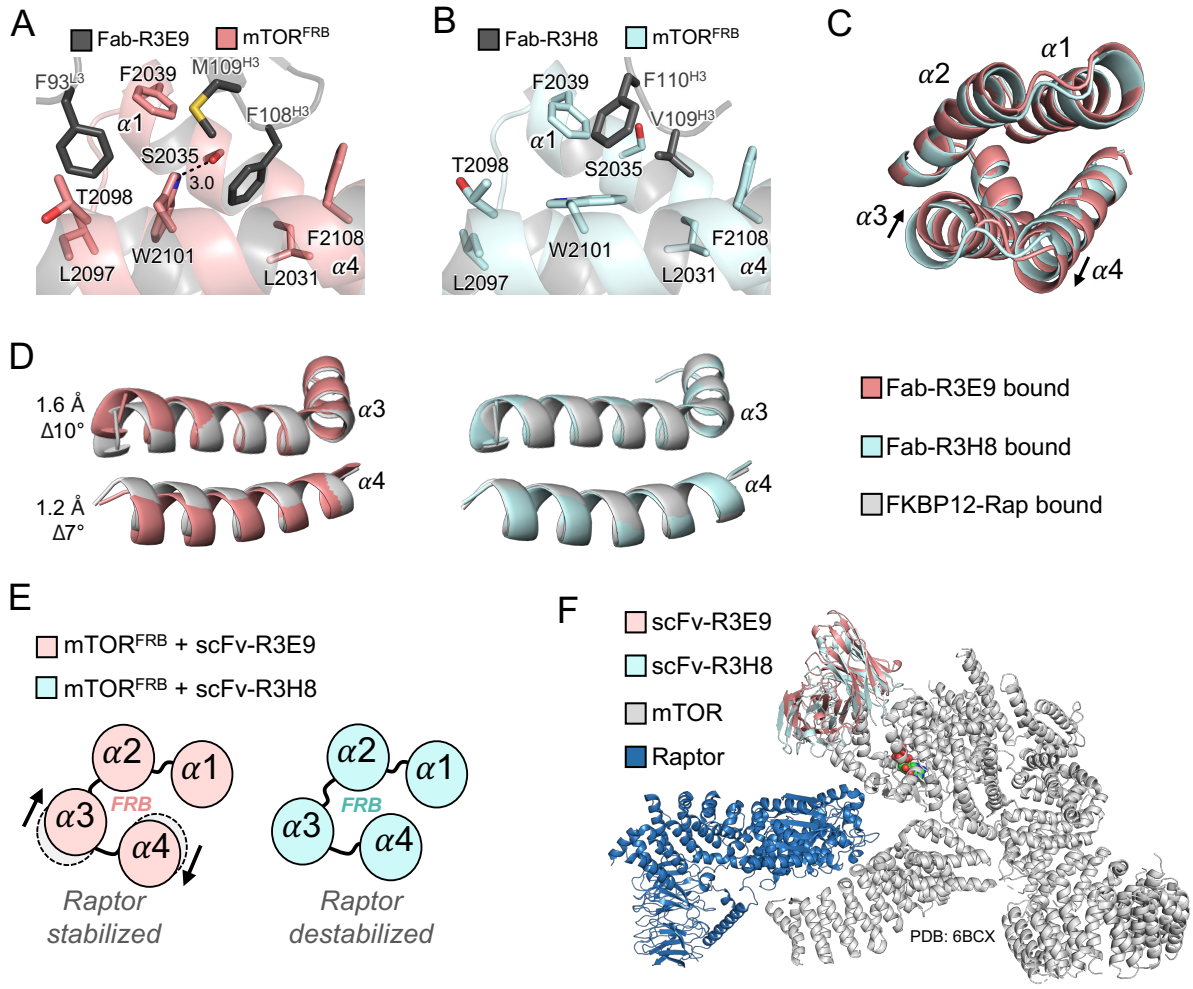

Figure 3.8 Conformations of mTOR^{FRB} correlated with switchable mTORC1 stability. (A) View of aromatic π-π stacking interactions formed in hydrophobic groove 1 (HG1) and 2 (HG2) between Fab-R3E9 (F93, F108 and M109) and mTOR^{FRB} (F2039, W2101, and F2108). (B) View of hydrophobic groove 1 (HG1) and 2 (HG2) with canonical W2101 and S2035 rotamers bound by Fab-R3H8. (C) Structural alignment of mTOR^{FRB} bound by Fab-R3E9 (salmon) and Fab-R3H8 (cyan) exhibiting subtle helical rearrangements, indicated by arrows. (D) Alignment of α-helices, α3 and α4, between the indicated structures using PDB: 1NSG as a reference for mTOR^{FRB} bound by FKBP12-Rapamycin. (E) Model for mTOR^{FRB} conformational states and their functional consequences. (F) Structural model of scFv-R3E9 and scFv-R3H8 bound mTOR^{FRB} aligned with the previously determined structure of mTORC1 (PDB: 6BCX). mLST8 subunit omitted for clarity. ATP is represented by spheres. A clear separation in scFv-R3E9 and scFv-R3H8 binding sites from the mTOR-Raptor interface is demonstrated here.

mTORC1, which both allosterically destabilize the mTOR-Raptor interaction. Therefore, the structural and conformational deviations identified in the structure of $mTOR^{FRB}$ bound by Fab-R3E9 provide a molecular description for the unique allosteric stabilizing effect observed from multiple immunoprecipitation assays. Notably, using scFv-R3E9 and scFv-R3H8 as intracellular conformational probes has revealed in-depth how an allosteric binding site can be functionally decoupled through subtle structural changes.

Owing to the apparent importance of $F108^{H3}$ insertion by Fab-R3E9 for HG1 formation, the hypothesis of whether this interaction is sufficient for allosteric mTOR-Raptor stabilization was tested by mutational studies. $V109^{H3}$ from Fab-R3H8 and $F108^{H3}$ from Fab-R3E9 are inserted into the $mTOR^{FRB}$ epitope from highly similar Cα positions. Therefore, whether the allosteric functionality would be transferred in scFv-R3H8 with a V109F mutation or scFv-R3E9 an F108V mutation was tested. Expi293F cells expressing FLAG-tagged scFv-R3E9, scFv-R3H8, scFv-$R3E9^{F108V}$, or scFv-$R3H8^{V109F}$ were analyzed using anti-FLAG intrabody enrichment for co-immunoprecipitation-western blot. These results demonstrated that scFv-$R3E9^{F108V}$ behaves similarly to scFv-R3E9, indicating that $F108^{H3}$ alone is not sufficient for the allosteric stabilization of mTOR-Raptor (Figure 3.10A). In contrast, scFv-$R3H8^{V109F}$ exhibited minimal binding to mTOR, likely due to the steric clash imposed by the bulky phenylalanine side chain. Together, the cell-based mutational binding assay performed here provides insight into the complex nature of the conformational dynamics of $mTOR^{FRB}$. The intrabodies reported here can be used as conformational probes for intracellular signaling dynamics, but there are still many unknowns in regard to the conformational regulation of mTOR. Whether mTOR

undergoes dynamic structural changes during nutrient-sensitive substrate recruitment and phosphorylation should be investigated in future studies.

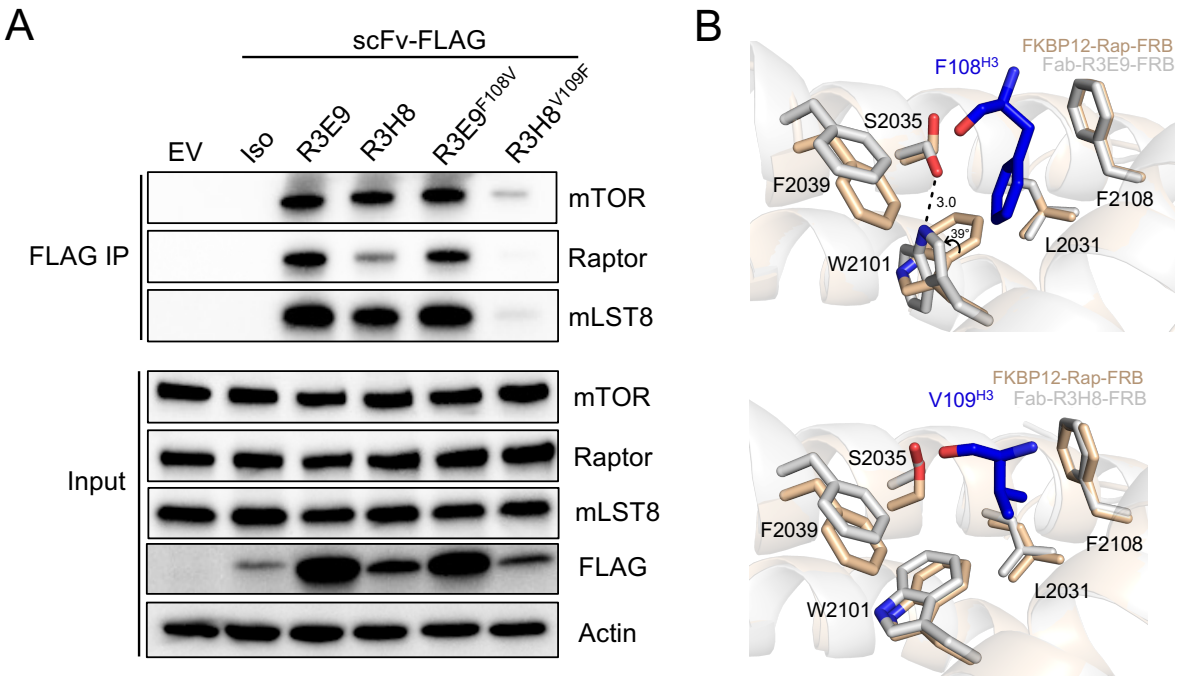

Figure 3.9 F108V mutation is insufficient for scFv-R3E9 allosteric destabilization. (A) Expi293F cells were transfected with empty vector (EV) or the indicated FLAG-tagged intrabody constructs for 48 hours. Cells were harvested and subjected to anti-FLAG immunoprecipitation for western blot analysis. (B) Structural alignment of Fab-R3E9 bound or Fab-R3H8 bound structures with a previously determined structure of $mTOR^{FRB}$ bound by FKBP12-Rapamycin (PDB: 1FAP). This alignment shows the incompatibility of $F108^{H3}$ with the canonical rotamer of W2101 found in all other $mTOR^{FRB}$ structures.

3.3.3 Intrabody-based inhibition of mTORC1 and mTORC2 signaling by a mechanism analogous to rapamycin

A thorough characterization protein-protein interaction network modulation by scFv-R3E9 and scFv-R3H8 established these binders as useful intracellular molecular probes. However, whether scFv-R3E9 and scFv-R3H8 inhibit mTOR substrate phosphorylation is an important question that could extend their applicability in myriad

cell biological systems. mTORC1 exploits multiple independent substrate recruitment mechanisms, such as TOS-dependent recruitment of 4E-BP1, FRB-dependent recruitment of S6K1, or Rag-dependent recruitment of TFEB (28, 63, 123). The mechanism of inhibition for scFv-R3E9 and scFv-R3H8 was hypothesized to be similar to that of rapamycin, based on $mTOR^{FRB}$ obstruction. Therefore, examination of whether scFv-R3E9 and scFv-R3H8 inhibit rapamycin-sensitive FRB-dependent substrate phosphorylation was performed using S6K1 as a model substrate.

Confocal microscopy was used to visualize intracellular expression patterns for eGFP-tagged intrabodies. This analysis showed cell-wide intrabody distribution and low levels of eGFP(+) punctate structures (Figure 3.10A). To investigate effects on the mTOR signaling pathway, intrabody constructs were modified to include FLAG-T2A tags between the scFv and eGFP domains. This construct design results in two independent protein copies of scFv-FLAG and eGFP alone, thereby enabling fluorescent detection of cells expressing intrabodies while ensuring that eGFP does not interfere directly with intrabody activity. Cell signaling was investigated by employing FACS to isolate Expi293F cells transfected scFv-Iso, scFv-R3E9, or scFv-R3H8 (Figure 3.10B). The isolated intrabody expressing cells were compared to cells transfected with empty vector (EV) that were treated with vehicle or rapamycin via western blotting (Figure 3.10C). This experiment demonstrated that intracellular expression of scFv-R3E9 and scFv-R3H8 results in potent inhibition of $S6K1^{T389}$ phosphorylation by mTORC1, similar to inhibition by rapamycin (Figure 3.10D). To confirm that these effects were due to selective masking of $mTOR^{FRB}$ by intrabodies and not altered mTOR or Raptor levels, the total protein levels of mTOR and Raptor were analyzed. This experiment showed that cells expressing scFv-

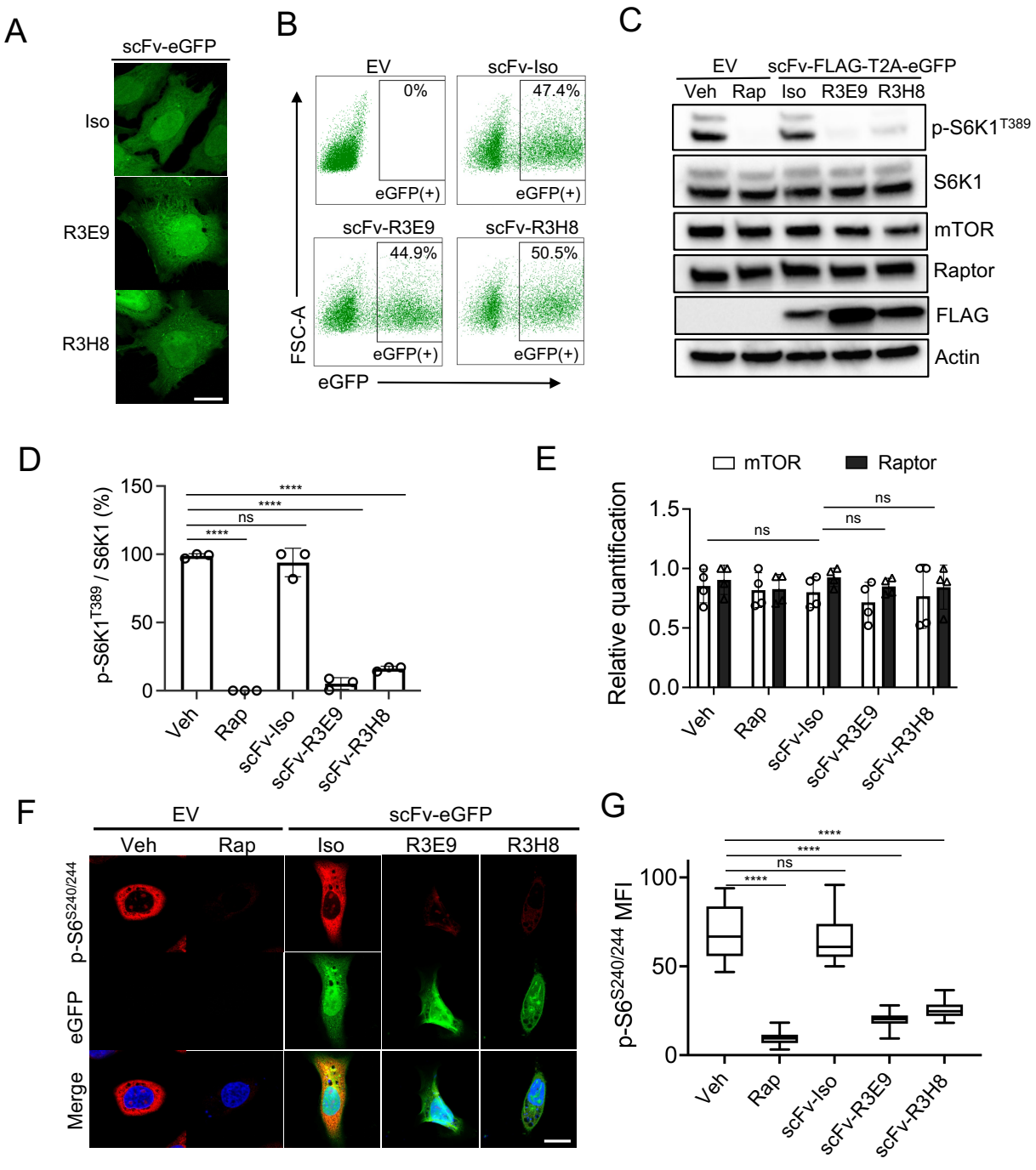

Figure 3.10 Genetically encoded mTORC1 inhibition using intrabodies.
Figure caption continued on the next page.

Figure 3.10 Genetically encoded mTORC1 inhibition using intrabodies. (A) Confocal microscopy visualization of eGFP-tagged intrabodies in HeLa cells. Scale bar denotes 32.3 μm. (B) Expi293F cell isolation using FACS 24 hours post-transfection. Intrabody constructs with C-terminal FLAG-T2A-eGFP tags were used for transfection. (C) Western blot of Epi293F cells isolated by FACS in B. Cells with 24-hour expression of empty vector (EV), isotype control (Iso), R3E9, or R3H8 intrabodies with FLAG-T2A-eGFP tags were compared to 16 hours of vehicle or rapamycin treatment. (D) Quantification of the FACS experiment in C (n = 3 biological replicates, mean ± SD. ns = not significant, ****$P \leq 0.0001$, one-way ANOVA). (E) mTOR and Raptor total protein levels were quantified relative to Actin from the experiment in C (n = 4 biological replicates, mean ± SD. ns = not significant, one-way ANOVA). (F) Analysis of eGFP-tagged intrabody expression and endogenous immunostained p-S6$^{S240/244}$ in HeLa cells using confocal microscopy. Scale bar denotes 20.5 μm. (n = 2 independent experiments). (G) Quantification of endogenous p-S6$^{S240/244}$ levels from the experiment in F (n = 19, 18, 21, 27, and 25 cells. ns = not significant, ****$P \leq 0.0001$, one-way ANOVA with Tukey-Kramer test).

R3E9 or scFv-R3H8 do not exhibit altered protein levels of mTOR or Raptor, suggesting that this did not contribute to the effects observed on S6K1 phosphorylation (Figure 3.10E). The phosphorylation of the main downstream substrate of S6K1, ribosomal protein S6, was next analyzed in HeLa cells expressing scFv-R3E9 and scFv-R3H8 using confocal microscopy (Figure 3.10F). This experiment showed that intrabody expression potently suppresses both downstream nodes in the mTORC1 pathway in a rapamycin-like manner (Figure 3.10G). Together, these studies revealed that intrabodies targeting mTOR^{FRB} inhibit the phosphorylation of rapamycin-sensitive substrates such as S6K1 and S6.

Rapamycin exhibits differential time-dependent mechanisms of inhibition for mTORC1 and mTORC2 (134). This is due to the overlapping binding sites between rapamycin and the mTORC2 subunit, Rictor. The rapamycin binding site is freely accessible in mTORC1, which results in potent inhibition on very short time scales. In contrast, mTORC2 inhibition requires prolonged treatment with rapamycin, which allows

FKBP12-rapamycin to bind newly synthesized mTOR molecules and obstruct the assembly of new Rictor subunits into mTORC2 complexes. To understand whether intrabodies function similar to rapamycin for mTORC1 and mTORC2 inhibition, a simple time course experiment was performed. The pharmacokinetics of intrabody expression are markedly different than administration of cell-permeable organic molecules like rapamycin. Therefore, cells expressing scFv-R3E9 were observed after 24- and 48-hour time points to replicate acute and prolonged conditions of inhibition. This experiment showed that scFv-R3E9 differentially inhibits mTORC1 and mTORC2 after 24- and 48-hour time points (Figure 3.11A). scFv-R3E9 potently inhibited S6K1^{T389} phosphorylation in all conditions tested (Figure 3.11B). In contrast, Akt^{S473} phosphorylation was mildly inhibited after the 24-hour time point and showed stronger inhibition only after 48 hours. These effects were analogous to Expi293F cells treated with vehicle or rapamycin for the same time points (Figure 3.11C and D). Together, these experiments demonstrated that scFv-R3E9 is sufficient to recapitulate the complex mechanisms of mTORC1 and mTORC2 inhibition by rapamycin.

Other mTORC1 substrates, such as 4E-BP1, exhibit resistance mechanisms to rapamycin. For example, mTORC1 phosphorylates 4E-BP1 on multiple sites including T37/46, S65, and T70 (68). However, the sensitivity of these phosphorylation sites to rapamycin is characteristically different, with T37/46 considered as rapamycin-resistant and S65/T70 exhibiting cell line-dependent variation (17). Many open questions remain after decades of investigation into 4E-BP1 and rapamycin. If FKBP12-rapamycin binding to mTOR^{FRB} is sufficient to obstruct entry into the catalytic cleft for some substrates, such as S6K1, how can 4E-BP1 circumvent this blockade? The mechanisms underlying these

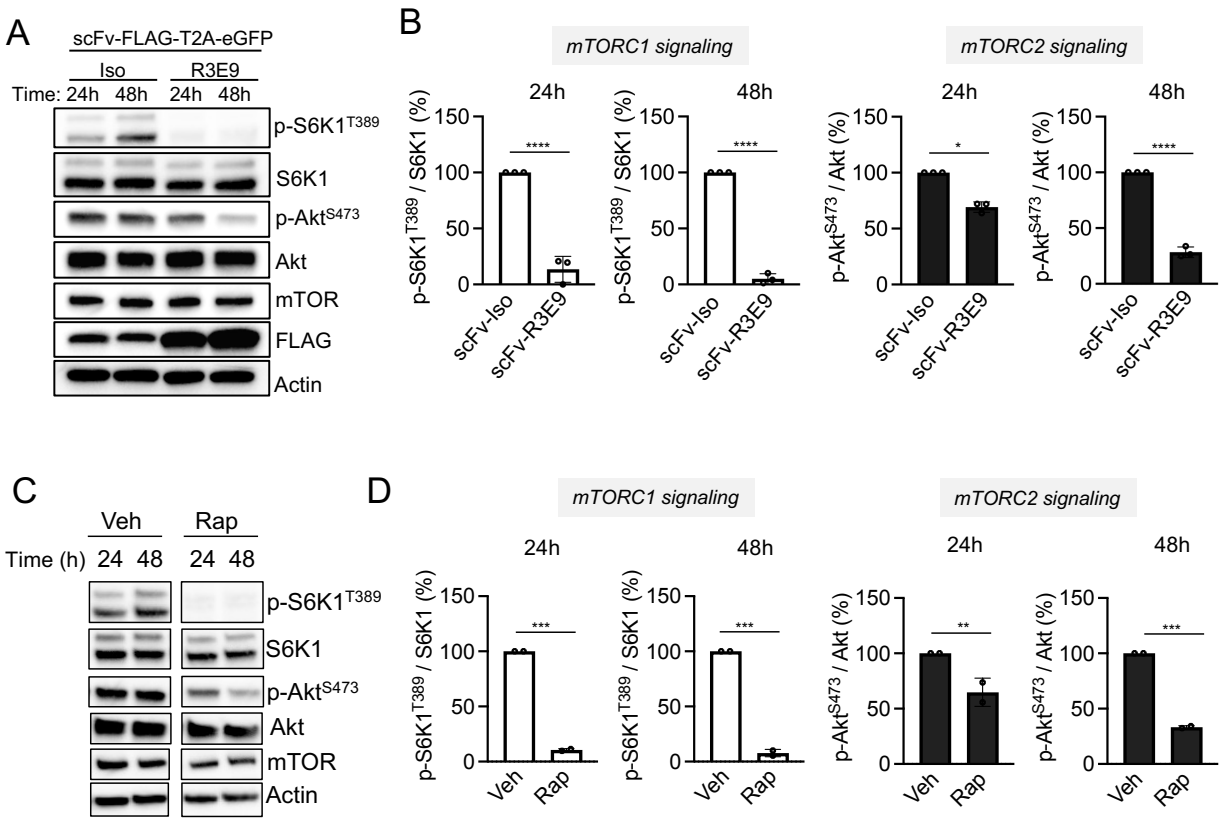

Figure 3.11 Intrabody-based rapamycin-like inhibition of mTORC1 and mTORC2. (A) Expi293F cells transfected with scFv-Iso or scFv-R3E9 were sorted using FACS 24- and 48-hours post-transfection. Samples were analyzed for p-S6K1^{T389} and p-Akt^{S473} levels as mTORC1 and mTORC2 signaling readouts, respectively. (B) Quantification of p-S6K1^{T389} and p-Akt^{S473} levels from the experiment in A (n = 3 biological replicates, mean ± SD. *$P \leq 0.05$, ****$P \leq 0.0001$, one-way ANOVA). (C) Expi293F cells treated with vehicle or 100 nM rapamycin for 24 or 48 hours. Membranes were cropped to remove irrelevant samples. (D) Quantification of p-S6K1^{T389} and p-Akt^{S473} levels from the experiment in C (n = 3 biological replicates, mean ± SD. **$P \leq 0.01$, ***$P \leq 0.001$, one-way ANOVA).

effects of 4E-BP1 resistance are not completely understood. Therefore, intrabodies were used to investigate whether targeting mTOR^{FRB} influences 4E-BP1 phosphorylation in a characteristically different manner from rapamycin (Figure 3.12A).

Different cell lines exhibit high variability in their sensitivity to rapamycin for 4E-BP1 phosphorylation. Expi293F cells were tested using 1-hour or 24-hour treatments with

rapamycin for analysis via western blotting. These results showed modest suppression of S65 phosphorylation after 1 hour, but no effects on both T37/46 and S65 after 24 hours (Figure 3.12B). To test the effects of scFv-R3E9 and scFv-R3H8, FACS was used to isolate cells expressing intrabodies for analysis by western blotting. Similar to previous results, scFv-R3E9 and scFv-R3H8 potently inhibited S6K1^{T389} phosphorylation (Figure 3.12D). In contrast, the effects on 4E-BP1$^{T37/46}$ and 4E-BP1^{S65} were more modest and exhibited high variability between empty vector and eGFP/scFv-Iso controls (Figure 3.12C-F). Critically, a decrease in both 4E-BP1$^{T37/46}$ and 4E-BP1^{S65} phosphorylation was observed for cells expressing eGFP-FLAG or scFv-Iso, which did not occur for S6K1^{T389}. Furthermore, a reduction in total 4E-BP1 levels could be observed in cells expressing eGFP-FLAG or scFv-Iso, which suggests some level of interplay of 4E-BP1 in mediating heterologous overexpression of these plasmid-based negative controls. Therefore, these results should be interpreted with caution as 4E-BP1 phosphorylation was decreased by expression of negative control proteins.

To corroborate this analysis, a different cell line and technique was employed. Confocal microscopy was used to inspect 4E-BP1$^{T37/46}$ phosphorylation in HeLa cells expressing eGFP-tagged intrabodies and was compared to vehicle, rapamycin, or Torin-1 treatment (Figure 3.12G). Rapamycin treatment showed a slight increase in 4E-BP1$^{T37/46}$ phosphorylation while Torin-1 showed complete inhibition (Figure 3.12H). Again, expression of scFv-Iso exhibited a slight decrease in 4E-BP1$^{T37/46}$ phosphorylation compared to the vehicle control. Nevertheless, scFv-R3E9 and scFv-R3H8 showed no

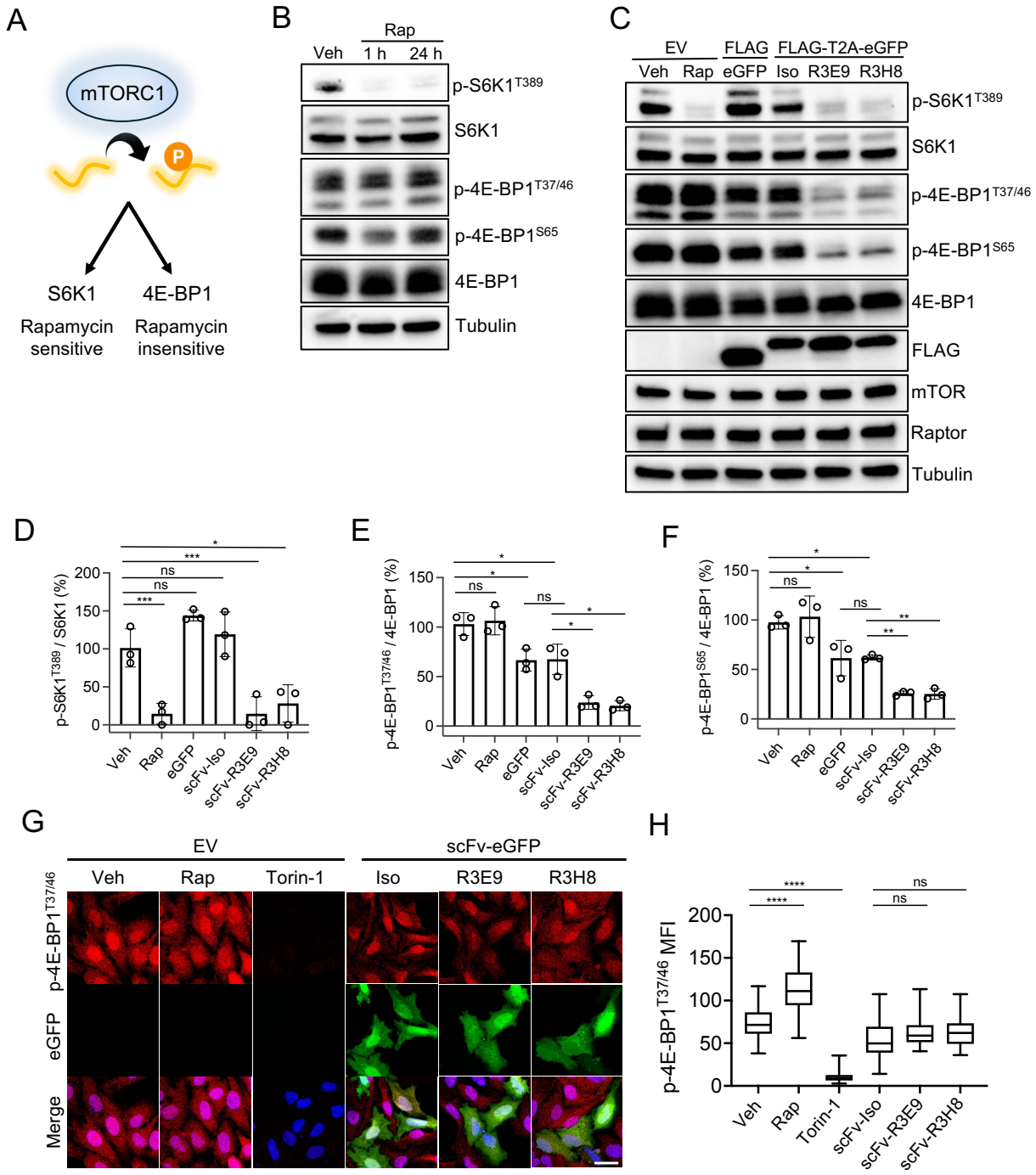

Figure 3.12 Effects of intrabodies on rapamycin-resistant 4E-BP1.
Figure caption continued on the next page.

Figure 3.12 Effects of intrabodies on rapamycin-resistant 4E-BP1. (A) Schematic of differential sensitivity for S6K1 and 4E-BP1 to rapamycin. (B) Expi293F cells treated with vehicle or 100 nM rapamycin for the indicated time points. (C) Western blot of Epi293F cells isolated by FACS. Cells with 24-hour expression of empty vector (EV), eGFP-FLAG, isotype control (Iso), R3E9, or R3H8 intrabodies with FLAG-T2A-eGFP tags were compared to 16 hours of vehicle or rapamycin treatment. (D) Quantification of p-S6K1^{T389} from the FACS experiment in C (n = 3 biological replicates, mean ± SD. ns = not significant, *$P \leq 0.05$, ***$P \leq 0.001$, one-way ANOVA). (E) Quantification of p-4E-BP1$^{T37/46}$ from the FACS experiment in C (n = 3 biological replicates, mean ± SD. ns = not significant, *$P \leq 0.05$, one-way ANOVA). (F) Quantification of p-4E-BP1^{S65} from the FACS experiment in C (n = 3 biological replicates, mean ± SD. ns = not significant, *$P \leq 0.05$, **$P \leq 0.01$, one-way ANOVA). (G) Analysis of eGFP-tagged intrabody expression and endogenous immunostained p-4E-BP1$^{T37/46}$ in HeLa cells using confocal microscopy. Scale bar denotes 32.3 µm. (n = 2 independent experiments). (H) Quantification of immunostained p-4E-BP1$^{T37/46}$ levels in HeLa cells treated with vehicle, 250 nM rapamycin, 250 nM Torin-1, or the indicated eGFP-tagged intrabodies (n = 32, 33, 29, 38, 28 and 29 cells. ns = not significant, ****$P \leq 0.0001$, one-way ANOVA with Tukey-Kramer test).

significant effect on 4E-BP1$^{T37/46}$ phosphorylation compared to scFv-Iso. This suggests that these intrabodies function similarly to rapamycin in some cell lines, such as HeLa, exhibiting strong rapamycin-resistance. Future studies should explore intrabody-mediated effects on 4E-BP1 using stable cell line generation and in diverse cell lines to understand the complex mechanisms of 4E-BP1 recruitment.

3.3.4 Modular design and implementation of subcellular targeted intrabodies

scFv-R3E9 and scFv-R3H8 have the unique capability of mimicking the pharmacological properties of the natural product inhibitor rapamycin. These tools were used to demonstrate similar substrate-specific and time-dependent properties in human cells when compared directly to effects of rapamycin. The human protein-based scaffolding for scFv-R3E9 and scFv-R3H8 harbors additional qualities that cannot be

captured by organic molecules like rapamycin. Specifically, the capability for encoding scFv-R3E9 and scFv-R3H8 within a genetic sequence for delivery into living cells provides unprecedented levels of control over these drug-like molecules. The modular incorporation of fluorescent tags, epitope tags, or cleaving tags enables investigations into cell signaling modulation using approaches such as western blotting or confocal microscopy.

To exert additional control over the inhibition properties of scFv-R3E9 and scFv-R3H8, several different subcellular localization tags were added to enable spatial restriction into selected subcellular structures in living cells. Conceptually, intrabodies can be anchored in different regions of the cell where their engagement with mTOR should result in localized inhibition (Figure 3.13A). These constructs were based on the fusion of scFv-eGFP with localization tags added at either the N-terminus, C-terminus, or both. The tags selected for investigation included nuclear localization signal (NLS), nuclear export signal (NES), plasma membrane binding Lyn Kinase motif (Lyn), or an endosome/lysosome sorting motif (Yxx**ϕ** where x = any amino acid and **ϕ** = bulky hydrophobic amino acids). The efficacy of each tag was visually confirmed using confocal microscopy to analyze the spatial expression of scFv-R3E9 in living cells (Figure 3.13C). These results provided a foundation to elicit functional perturbations to the mTOR signaling network with spatial precision not provided by inhibitors or gene knockdowns. The simplest manifestation of this approach could be the genetic restriction of inhibitory intrabodies to the cytosol or nucleus, resulting in local functional perturbations only inside each respective compartment (Figure 3.13D). Importantly, this cannot be achieved using the current repertoire of molecular tools geared toward mTOR. The ability to decouple

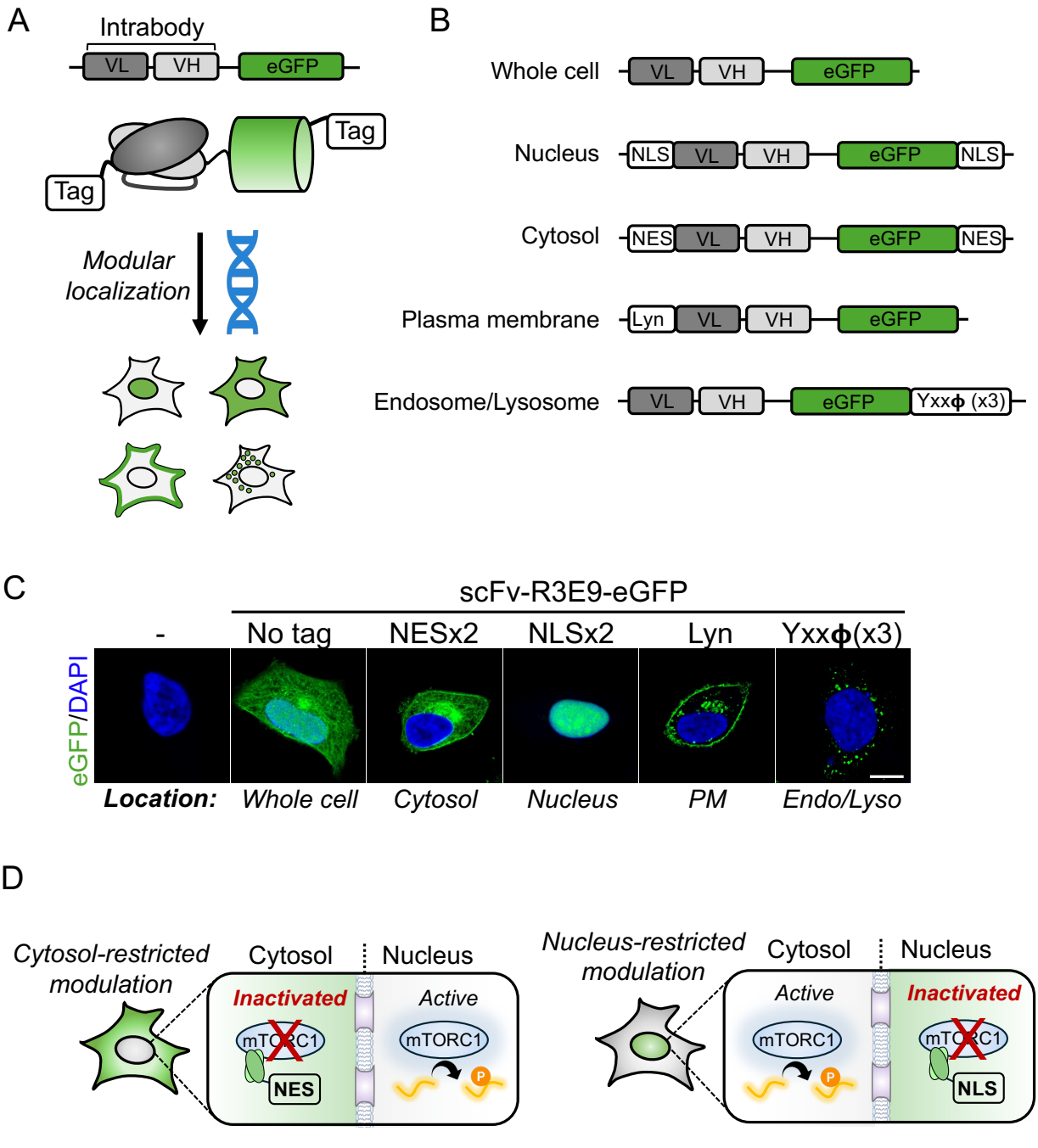

Figure 3.13 Subcellular localization tags for spatially restricted intrabody expression. (A) Schematic for spatially restricted intrabody expression in cells. (B) Construct design for scFv-eGFP fusions with the indicated subcellular localization tags. (C) Confocal microscopy analysis of scFv-R3E9-eGFP equipped with the indicated localization tags in HeLa cells. Scale bar denotes Scale bar denotes 11.5 μm. (D) Schematic for compartment-specific inhibition of mTORC1 signaling enabled by cytosol- or nucleus-restricted intrabody expression.

mTOR protein-protein interactions and substrate phosphorylation events in a subcellular compartment-specific manner could have important biological implications.

A potential limitation of the approach of restricting intrabody localization inside of living cells could be the dynamic translocation of target molecules as a result of intrabody engagement. Conceptually, this might result in localization patterns that deviate from unperturbed cell signaling networks. To test this hypothesis, HeLa cells were transfected with cytosol- or nucleus-restricted eGFP-tagged intrabodies and immunostained to detect endogenous mTOR localization (Figure 3.14). These results demonstrated nuclear-cytoplasmic mTOR ratios of 4.3% and 3.9% in vehicle and rapamycin treated cells, respectively. Cytosolic restriction of scFv-Iso, scFv-R3E9, and scFv-R3H8 decreased the nuclear-cytoplasmic mTOR ratio slightly, but not to significant levels. An important note is that the decrease in nuclear-cytoplasmic mTOR ratio in cells expressing NES-tagged scFv-Iso might reflect potential cross-talk between nuclear export machineries and the mTOR network. These processes are mediated by selective transport of cargo in and out of the nucleus through the nuclear pore complex, which could potentially be involved upstream or downstream in the mTOR signaling network. Nuclear restriction of scFv-Iso showed no significant difference to empty vector cells. In contrast, nucleus-restricted scFv-R3E9 and scFv-R3H8 appeared to increase the nuclear-cytoplasmic mTOR ratio by 4-5% compared to vehicle treated cells (Figure 3.15). This result suggested that engagement of mTOR by NLS-tagged scFv-R3E9 and scFv-R3H8 can indeed alter its localization pattern. However, whether these changes are able to influence mTOR signal transduction remained to be tested.

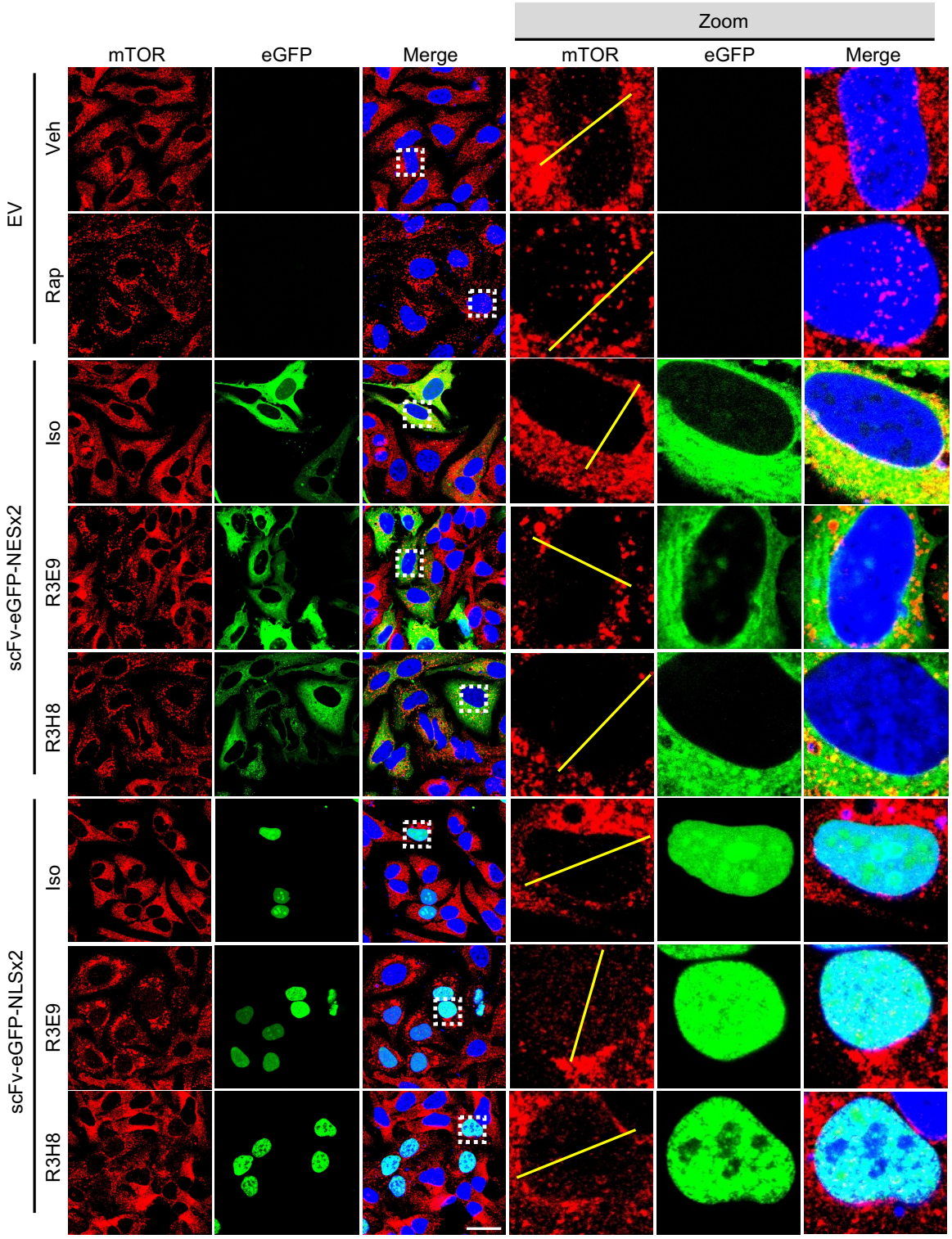

Figure 3.14 mTOR localization in cells expressing spatially restricted intrabodies. HeLa cells expressing the indicated intrabodies for 24 hours were immunostained with an anti-mTOR antibody. Scale bar denotes 32.3 μm. (n = 2 independent experiments

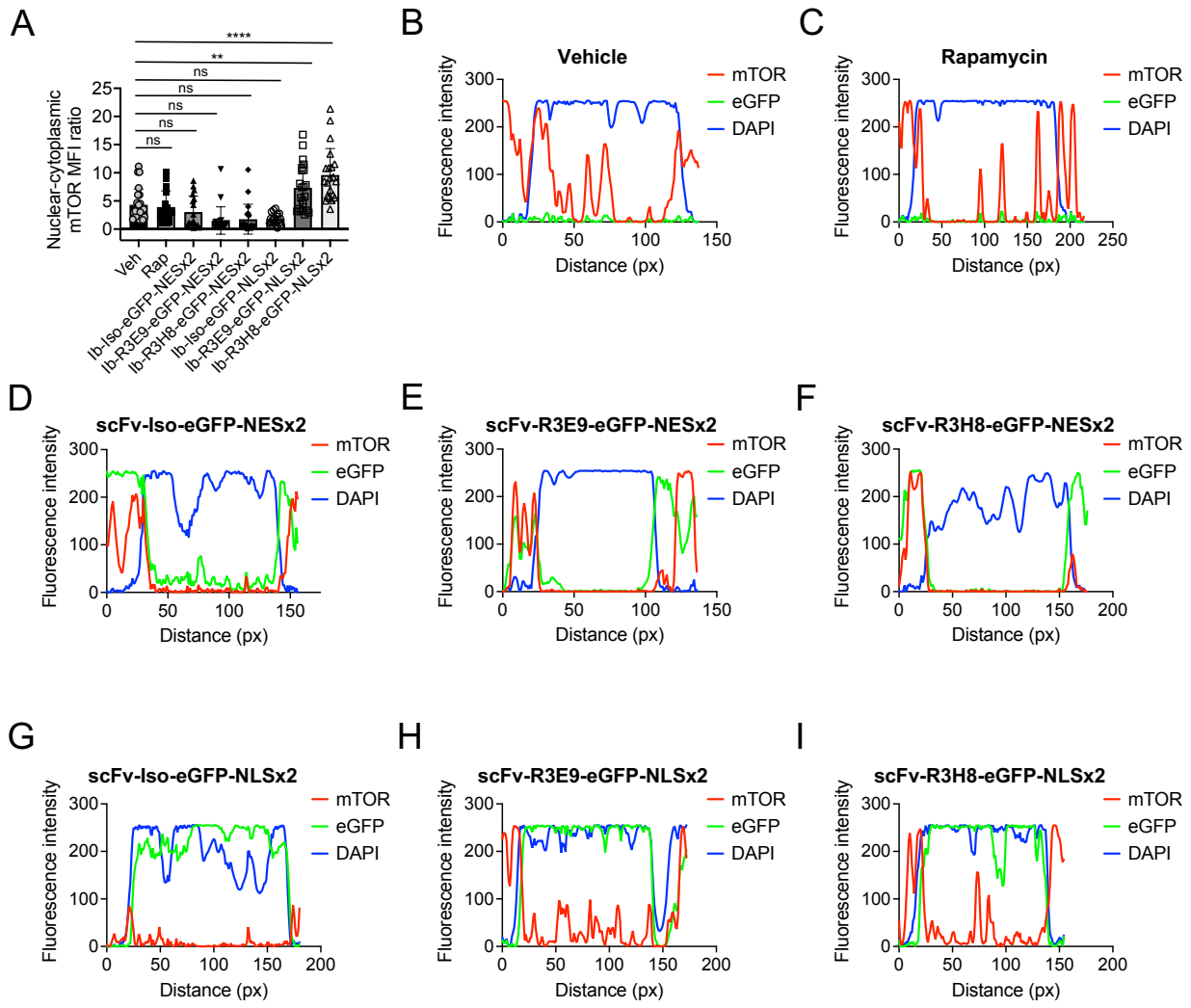

Figure 3.15 Quantification of nuclear-cytoplasmic mTOR translocation. (A) Mean fluorescence intensity (MFI) for the nuclear-cytoplasmic ratio of mTOR from HeLa cells transfected for 24 hours with the indicated constructs (n = 23, 16, 18, 20, 20, 18, 23, and 21 cells from two independent experiments. ns = not significant, $^{**}P \leq 0.01$, $^{****}P \leq 0.0001$, one-way ANOVA with Tukey-Kramer test). (B) Line trace profile from the yellow line shown in Figure 3.14 for vehicle treated cells, (C) rapamycin treated cells, (D) scFv-Iso-eGFP-NESx2, (E) scFv-R3E9-eGFP-NESx2, (F) scFv-R3H8-eGFP-NESx2, (G) scFv-Iso-eGFP-NLSx2, (H) scFv-R3E9-eGFP-NLSx2, and (I) scFv-R3H8-eGFP-NLSx2.

3.3.5 Decoupling cytoplasmic and nuclear mTOR networks through spatially restricted intrabody perturbations

Traditional approaches for investigating cell signal transduction pathways include small molecule inhibitors and gene knockdowns. While these techniques are very powerful in their ability to selectively perturb myriad cellular targets, they lack the capability for subcellular spatial restriction. After thoroughly characterizing scFv-R3E9 and scFv-R3H8 as potent genetically encodable mTOR inhibitors, they were envisioned as spatially restricted inhibitors to elicit mTOR perturbations with subcellular resolution. To understand the inhibitory precision of cytosol- or nucleus-restricted intrabody expression, HeLa cells were transfected with NES- or NLS-tagged intrabodies and immunostained for endogenous $S6^{S240/244}$ phosphorylation levels. The localization of this downstream mTOR component is primarily cytosolic, where direct phosphorylation by S6K1 represents a major mTOR-enabled gateway to activation of protein synthesis (Figure 3.16A). Therefore, the hypothesis of whether nucleus-restricted intrabodies modulate cytosolic signaling events was tested using this feasible system (Figure 3.16B). Phosphorylation of $S6^{S240/244}$ was unaffected by NES-tagged scFv-Iso expression, while NES-tagged scFv-R3E9 and scFv-R3H8 potently inhibited this mTORC1 axis (Figure 3.16B). This was quantified using line trace fluorescence profiles, showing that $S6^{S240/244}$ phosphorylation is suppressed where scFv-R3E9 and scFv-R3H8 localization occurs. In contrast, $S6^{S240/244}$ phosphorylation was not affected by NLS-tagged scFv-Iso, scFv-R3E9, or scFv-R3H8 expression (Figure 3.16D). These results demonstrated that despite a slight alteration in mTOR localization in cells expressing NLS-tagged scFv-R3E9 and scFv-R3H8, the cytosolic activity pattern was not affected.

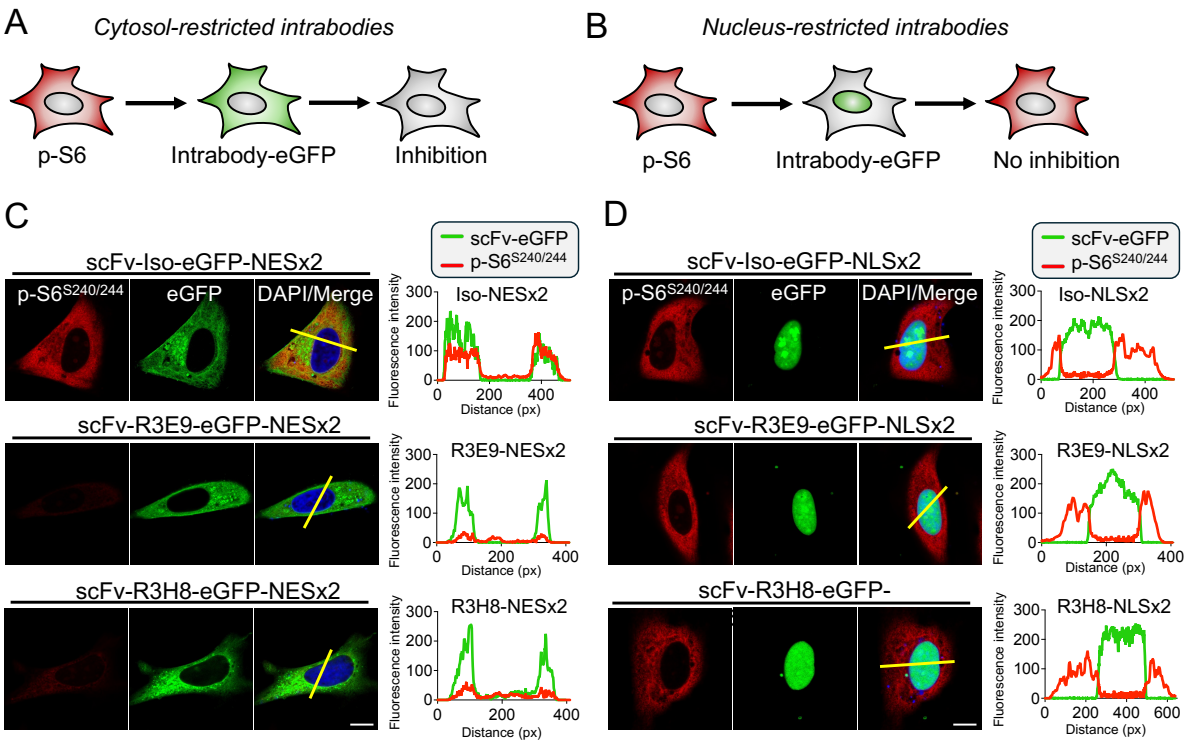

Figure 3.16 Nucleus-restricted intrabodies do not inhibit cytosolic mTOR signaling. (A) Schematic for cytosol-restricted inhibition using NES-tagged intrabodies. (B) Schematic for localization specificity of NLS-tagged intrabodies. (C-D) Endogenous cytosolic mTORC1 signaling was inspected using confocal microscopy. The indicated eGFP-tagged intrabodies were transfected into HeLa. Immunostaining for endogenous $S6^{S240/244}$ phosphorylation was then performed. Scale bar denotes 15.4 µm. Fluorescence intensity profile are shown on the right for traced yellow lines. (n = 2 independent experiments).

These observations provided critical insight into the mechanisms of subcellular inhibition by spatially restricted intrabodies. However, the particular systems analyzed above did not establish inhibitory efficacy of intrabodies inside the nuclear compartment. Despite selective localization to the nucleus, it remained an open question whether they are capable of engaging mTOR and modulating FRB-dependent substrate recruitment. To address this question, a heterologous nuclear substrate reporter construct was

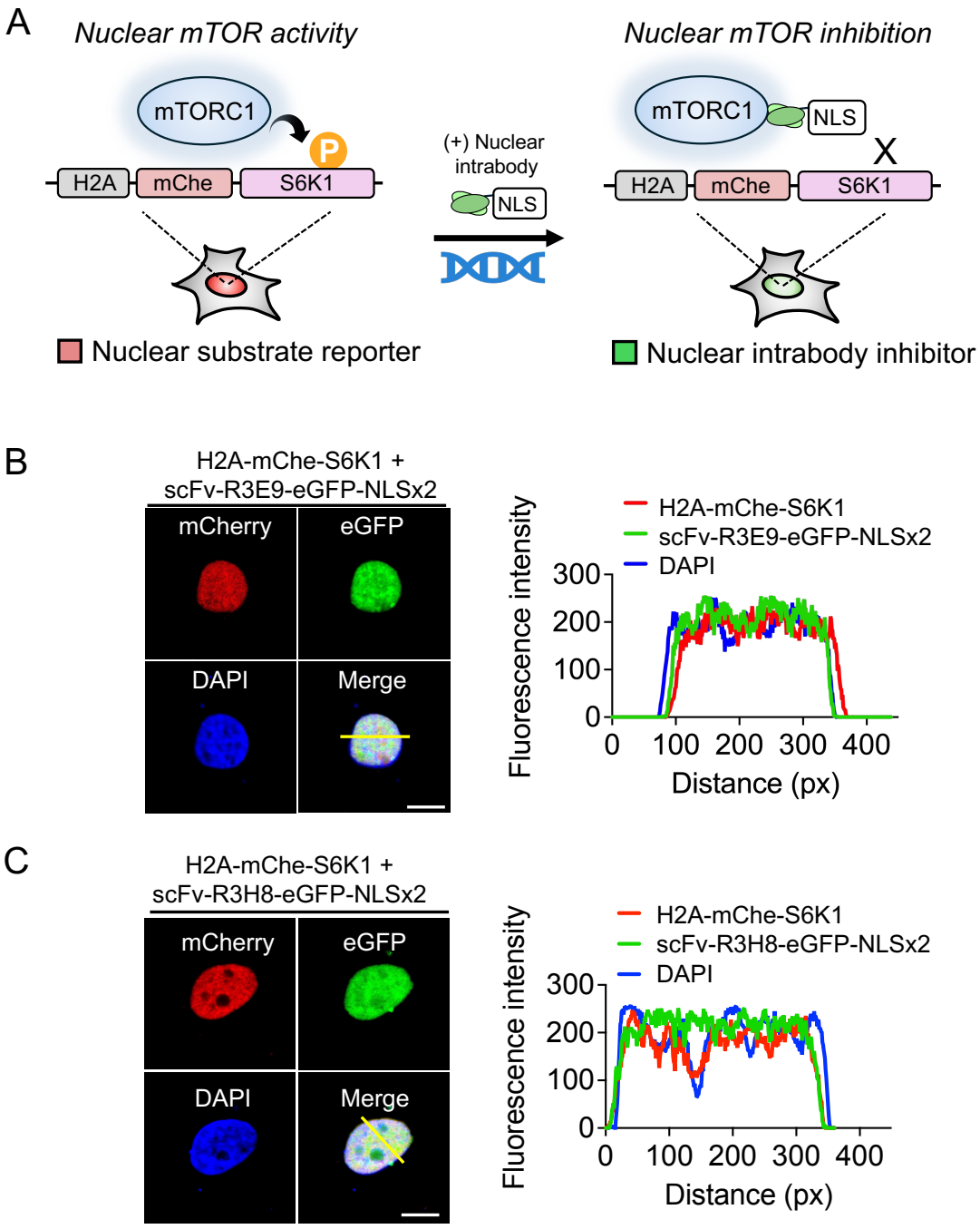

Figure 3.17 A nuclear substrate reporter for mTORC1 activity. (A) Schematic for H2A-mChe-S6K1 as a selective reporter of nuclear mTOR activity based on phosphorylation at position T389. (B and C) *Left:* Confocal microscopy analysis of the indicated constructs transfected in HeLa cells. Scale bar denotes 11.5 μm. *Right:* Fluorescence profile along the yellow line trace located in the merged image.

employed based on a previously reported study of Akt-dependent regulation of nuclear mTORC1 activity (75). This construct includes the full-length sequence of S6K1 with mCherry (mChe) added as a fluorescent tag and histone 2A (H2A) added as a stringent nuclear anchor. Expression of H2A-mChe-S6K1 in living cells thereby results in its localization selectively inside the nuclear compartment. The phosphorylation state of the heterologous S6K1 substrate therefore functions as a direct readout for mTORC1 activity inside the nucleus (Figure 3.17A). To test the hypothesis that nucleus-restricted scFv-R3E9 and scFv-R3H8 are capable of inhibiting mTORC1 inside the nucleus, these constructs were co-transfected along with H2A-mChe-S6K1 into HeLa cells (Figure 3.17A). In order for this system to work, both of the transfected components must exhibit stringent nuclear residency. The localization of H2A-mChe-S6K1 with scFv-R3E9-eGFP-NLSx2 or scFv-R3H8-eGFP-NLSx2 was tested using confocal microscopy, which demonstrated selective nuclear localization of each constructs (Figure 3.17B and C).

Western blotting was employed to examine the phosphorylation state of H2A-mChe-S6K1 in the presence or absence of nucleus-restricted intrabodies. Co-transfection of H2A-mChe-S6K1 with scFv-Iso, scFv-R3E9, or scFv-R3H8 intrabodies equipped with eGFP-NLSx2 tags served as the basis for this approach. Cells expressing scFv-Iso-eGFP-NLSx2 and H2A-mChe-S6K1 exhibited robust phosphorylation of the heterologous reporter at T389, which was selectively ablated by treatment with rapamycin (Figure 3.18A). Furthermore, endogenous S6K1 phosphorylation in these samples was unperturbed in vehicle conditions but ablated by rapamycin treatment. In contrast, cells expressing H2A-mChe-S6K1 together with scFv-R3E9-eGFP-NLSx2 or scFv-R3H8-

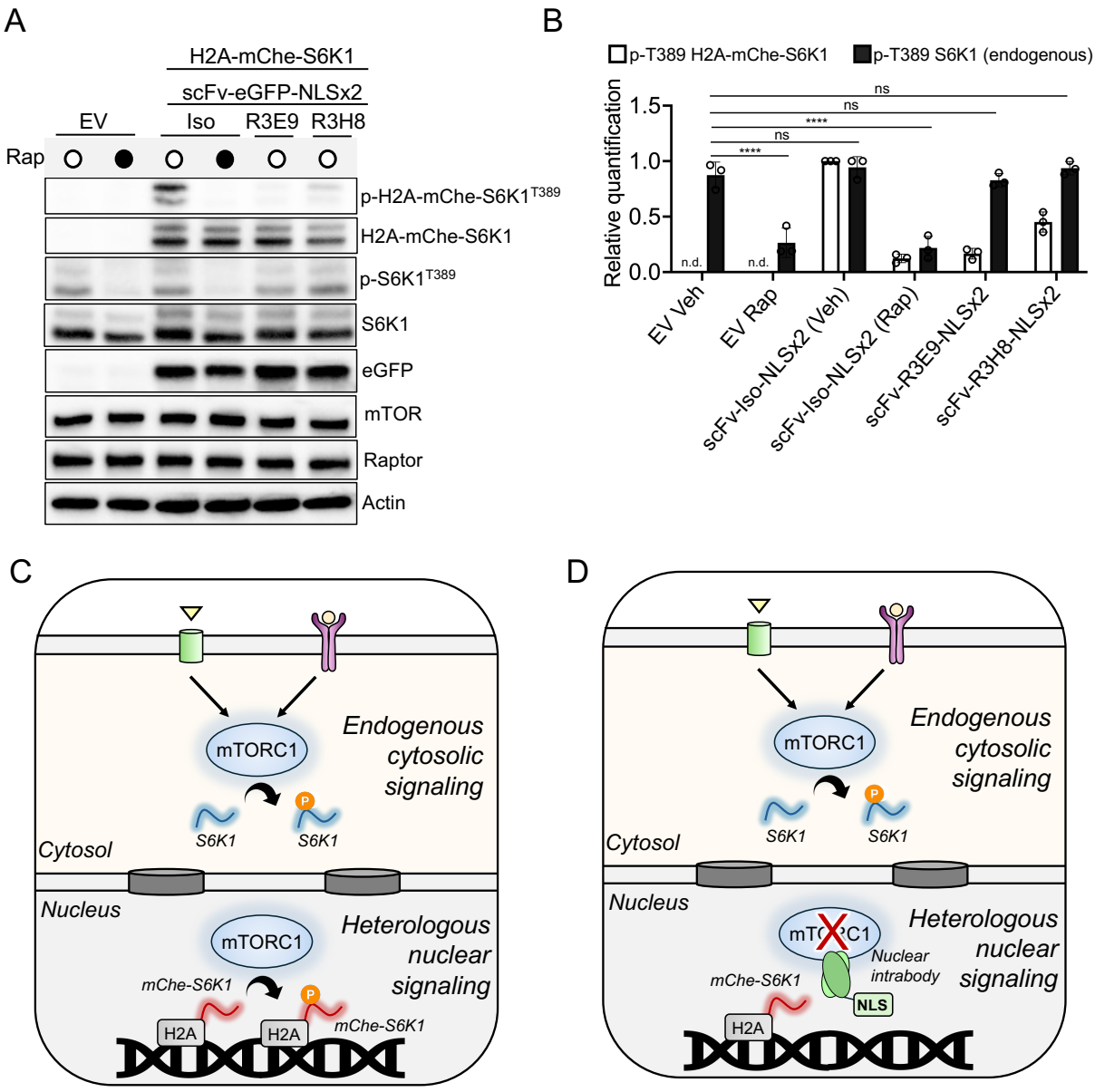

Figure 3.18 Selective mTORC1 inhibition inside the nucleus by intrabodies. (A) HeLa cells were transfected with empty vector (EV), scFv-Iso, scFv-R3E9, or scFv-R3H8 equipped with eGFP-NLSx2 tags. H2A-mChe-S6K1 was co-transfected with the indicated intrabodies for 48 hours. Vehicle or 500 nM rapamycin were administered for 1 hour before harvesting cells for western blot analysis. (B) Quantification of relative H2A-mChe-S6K1^{T389} and S6K1^{T389} phosphorylation levels from the experiment in A. Label of n.d. indicates no data collected for empty vector controls (n = 3 biological replicates, mean ± SD. ns = not significant, ****$P \leq 0.0001$, one-way ANOVA). (C) Schematic for mTORC1 phosphorylation of endogenous S6K1 and H2A-mChe-S6K1 without nuclear inhibition. (D) Schematic of mTORC1 phosphorylation of endogenous S6K1 and H2A-mChe-S6K1 with nuclear inhibition.

eGFP-NLSx2 showed that H2A-mChe-S6K1^{T389} was selective ablated while endogenous S6K1^{T389} was unaffected. These results demonstrated that nuclear modulation of mTORC1 signaling by spatially restricted intrabodies could be effectively decoupled from the cytosolic mTOR network (Figure 3.18C and D). Together, the modular genetically encoded intrabody-based platform developed here showed exceptional capability for precise subcellular targeting of compartment-specific mTOR signaling events.

3.4 Discussion

This chapter has described the implementation of two intrabodies, scFv-R3E9 and scFv-R3H8, as intracellular probes to explore structural and spatial mechanisms of the mTOR signaling network. Chemical and genetic tools have been invaluable throughout decades of work to elucidate the molecular mechanisms underpinning the regulation of nutrient-sensitive cell growth and metabolism by mTOR. This work represents a significant advancement in the development of approaches to dissect complex assembly and signal transduction mechanisms involved in the biological function of mTOR. Conceptually, the intrabody-based methods described here could be applied to other PIKK family members for high-precision studies into their unique complex assembly, substrate phosphorylation, and subcellular regulatory mechanisms.

The biological outputs from mTOR kinase activity are highly dependent on the association of mTOR with obligate binding partners that localize in distinct subcellular locations and recruit specific sets of substrates for phosphorylation. The best described examples of this are Raptor and Rictor, which are the cornerstone subunits in mTORC1 and mTORC2, respectively. The structural basis for the architectural assembly of

mTORC1 and mTORC2 has been resolved, but many questions remain open in terms of molecular mechanisms governing the dynamics and conformational regulation within these complexes. One of the best described examples of the underlying dynamics regulating mTORC1 is potent allosteric destabilization of the mTOR-Raptor interaction by inhibition with the FKBP12-rapamycin complex (133). It has been known for decades that ternary complex formation between mTOR-rapamycin-FKBP12 results in substantial weakening of the interaction between mTOR and Raptor. Interestingly, these effects are opposite to transient nutrient deprivation, which strengthens the mTOR-Raptor interaction (57). Furthermore, chemically crosslinking cells treated with rapamycin reverse the effect of Raptor dissociation in immunoprecipitation studies, suggesting that rapamycin destabilizes Raptor rather than completely dissociating it (57). However, mechanisms describing the structural or conformational pathways leading to these phenomena are still lacking to this day. This highlights the urgent need for molecular probes to reveal conformational insight into the regulation of mTORC1 and mTORC2 dynamics.

Allostery is defined as the regulation of protein function through molecular recognition of a distal site (136). The perturbation of mTOR-Raptor stability through binding of the $mTOR^{FRB}$ substrate recruitment site by FKBP12-rapamycin therefore represents a cornerstone example of allosteric modulation. Notably, Raptor is positioned near the stalk of $mTOR^{FRB}$ but does not exhibit any overlap in binding sites or contact points with the core domain of $mTOR^{FRB}$. Furthermore, comparison of crystal structures of $mTOR^{FRB}$ alone (PDB: 1AUE) or the ternary complex of FKBP12-rapamycin-$mTOR^{FRB}$ (PDB: 1NSG or PDB: 1FAP) shows no obvious conformational changes in the backbone or secondary structure of $mTOR^{FRB}$, which are typically observed as a result of allosteric

binding events. However, emerging evidence shows that allosteric functions are not necessarily correlated with larger enthalpy-driven shape changes to protein structure (137). The lack of global rearrangements in $mTOR^{FRB}$ suggests that dynamic fluctuations elicited by FKBP12-rapamycin binding may be responsible for the allosteric communication between mTOR and Raptor.

Investigating how allostery influences biological mechanisms in a native cellular environment is not trivial and typically requires specialized molecular tools geared toward a protein of interest. Engineered synthetic Fabs are well-characterized tools that are capable of stabilizing their target antigens in distinct conformational states (138, 139). ScFv-based intrabodies have previously been employed as intracellular allosteric probes to reveal crucial insights into GPCR signaling dynamics mediated by β-arrestin (117, 118). In this work, the use of scFv-R3E9 and scFv-R3H8 as conformational probes revealed critical implications on the architectural stability of mTORC1. The structural basis of specificity for distinct conformational states of $mTOR^{FRB}$ by scFv-R3E9 and scFv-R3H8 was delineated using high-resolution crystallographic studies. These results showed that recognition of the same binding site does not necessarily imply stabilization of the same conformational state of $mTOR^{FRB}$. Thus, the results described in this chapter constitute an important example of an allosteric mechanism that has been functionally decoupled through the use of synthetic intrabodies that discriminate conformational epitopes.

How does the intrabody-based stabilization of subtle, but energetically distinct, conformations of $mTOR^{FRB}$ lead to dynamic modulation of the mTOR-Raptor architecture? Allosteric mechanisms are simpler to describe when obvious shape changes are linked to functional output. In this case, the conformational specificity of

scFv-R3E9 and scFv-R3H8 is limited to a small set of side chain motions located in constrained regions of the $mTOR^{FRB}$ epitope (i.e., α3 and α4 helices). The rotation of dihedrals in two key side chains, W2101 and S2035, into conformations with high energetic costs in the R3E9-bound structure stand out as primary deviations from the "canonical" conformation of $mTOR^{FRB}$. The novel side chain conformations likely modulate local contact points and dynamic fluctuations. These movements are correlated with alteration of the $mTOR^{FRB}$ surface pocket HG1, leading to depth extension by ~4 Å and enabling coordination of $F108^{H3}$ from the R3E9 paratope. Furthermore, small distortions to α3 and α4 helices appear to be correlated with accessibility into another surface pocket (HG2), which is characterized by the displacement of V2095 and Y2038 side chains. The biophysical basis of how these distinct conformations of $mTOR^{FRB}$ result in switchable allosteric modulation of the mTOR-Raptor interaction remains unanswered. Insights into the energetics of $mTOR^{FRB}$ side chain motions should be investigated using a combination of molecular dynamics and nuclear magnetic resonance spectroscopy.

ScFv-R3E9 and scFv-R3H8 were also used as tools to enable insights into the regulation of mTOR signaling. Genetically encoding scFv-R3E9 and scFv-R3H8 in multiple human cell lines showed potent modulation of mTOR signaling by a mechanism of inhibition analogous to rapamycin. This was not surprising considering that these intrabodies target the same binding site compared to FKBP12-rapamycin on mTOR. Employing scFv-R3E8 and scFv-R3H8 for cell signal transduction assays showed selective inhibition of S6K1 and S6 but not 4E-BP1, consistent with previous reports of rapamycin. Time-dependent inhibition of S6K1 and Akt in a rapamycin-like fashion provided unequivocal evidence that engagement of the FKBP12-rapamcyin binding site

is sufficient to recapitulate its mechanism of action. Furthermore, these results demonstrated that scFv-R3E9 and scFv-R3H8 intrabodies recapitulate the therapeutic phenotypes associated with rapamycin treatment through a plasmid-based delivery system, which should allow researchers to dissect benefits and toxicities of rapamycin treatment with enhanced precision. While the experiments in this chapter were limited to human cells, scFv-R3E9 and scFv-R3H8 could easily be applied in mouse model systems due to 100% sequence identity between human and mouse $mTOR^{FRB}$. Furthermore, other eukaryotic model organisms, including yeast, fruit flies, and nematodes, have served indispensable roles for exploring mTOR biology. The cohort of synthetic Fabs engineered against human $mTOR^{FRB}$ showed modest levels of cross-reactivity with yeast and fruit fly FRB domains, suggesting that further species-specific engineering endeavors could lead to high-affinity binders for virtually any model organism of interest. The application of intrabodies, such as scFv-R3E9 and scFv-R3H8, for tissue-restricted investigations in living organisms could lead to critical insight into how mTOR function regulates eukaryotic development, growth, or disease with greater accuracy compared to gene knockdowns.

The modular genetically encoded basis of employing scFv-R3E9 and scFv-R3H8 in living cells enabled key insights into the spatial regulation of mTOR signaling. These studies were enabled by spatially restricting the intrabody inhibitors through incorporation of endogenous subcellular localization tags to the plasmid-based constructs. By anchoring the intrabodies to selected locations inside cells, the capacity for mTOR inhibition is also restricted to those locations. The simplest platform envisioned to investigate scFv-R3E9 and scFv-R3H8 as spatial inhibitors was to restrict their expression to the membrane-bound cytosol or nucleus compartments. Adding eGFP and

NES or NLS tags enabled straightforward visualization of cytosolic or nuclear intrabody localization in human cells, respectively. An important observation was that cytosol- and nucleus-restricted intrabody expression slightly altered the nuclear-cytoplasmic ratio of endogenous mTOR molecules. This has been concluded to be a result of mTOR translocation mediated by engaged intrabodies undergoing dynamic nuclear export and import. Nevertheless, the endogenous mTORC1 signaling network was unperturbed by a slight increase in nuclear mTOR levels in cells expressing NLS-tagged intrabodies as measured by endogenous $S6^{S240/244}$ phosphorylation levels.

Lastly, a critical piece of insight enabled by leveraging spatially restricted intrabodies was the capability to selectively inhibit mTOR signaling in the nucleus. Although mTOR has been characterized as having nuclear residency, the role of mTOR in the nucleus is largely undefined. The development of fluorescent biosensors provided the first demonstration that mTOR actively signaling from inside the nucleus (74). However, these tools are limited in their ability to reveal the potential functional outputs of mTOR in the nucleus. This gap in knowledge could be resolved using intrabodies as spatially restricted inhibitors to systematically perturb mTOR function in the cytosol or nucleus and compare the physiological phenotypes. Here, scFv-R3E9 and scFv-R3H8 were used to demonstrate that mTORC1 signaling in the nucleus can be selectively ablated while leaving the cytosolic signaling network untouched. These experiments were performed using a heterologous substrate, H2A-mChe-S6K1, which does not necessarily reflect real physiological outcomes of mTOR activity in the nucleus. Nevertheless, this work provides one of the first examples of employing specialized molecular tools to specifically tune endogenous kinase activity with subcellular spatial resolution. With the

platform established here, scFv-R3E9 or scFv-R3H8 intrabodies can be spatially restricted in diverse cell lines and combined with RNA sequencing, phosphoproteomics, or chromatin remodeling assays to explore unannotated functions of cytosolic or nuclear mTOR activity.

Together, the structural and spatial mechanisms revealed using intrabodies highlights the potential of combining protein engineering, molecular structure, and synthetic biology approaches to better understand recalcitrant therapeutic targets. The particular advantages of using intrabodies stems from their capability to bind canonical functional sites, akin to small molecule drugs, but also to flat surfaces that are typically considered undruggable. This type of engagement results in drug-like functional perturbations to a target antigen of interest. Furthermore, incorporating a small epitope tag to the intrabody provides a handle for pulldowns to reveal the endogenous interactome of the target antigen. Combined together, intrabody-based investigations can be performed to modulate downstream signaling networks and cognate protein-protein interactions with high precision. One could envision that the myriad upstream and downstream nodes within the mTOR pathway might serve as suitable targets for intrabodies to further dissect the complex mechanisms of nutrient-sensitive cell signaling.

3.5 Materials and methods

Generation of DNA constructs. Single chain variable fragments were generated by cloning gBlock fragments encoding Fab-R3E9 or Fab-R3H8 VL and VH domains as previously described (119) into XbaI/BamHI sites of the pSCSTa expression vector. Other unique VH domains were cloned into XhoI/BamHI sites and CDR-L3 was mutated by a

combination of PCR and In-Fusion ligation. C-terminal FLAG tag, eGFP, or FLAG-T2A-eGFP tags were generated by PCR. Intrabody localization tags (NES [LPPLERLTL], c-myc NLS [PAAKRVKLD], SV40 NLS [PKKKRKV], N-terminal Lyn kinase motif [GCIKSKRKDKD], and Yxx**ϕ** [YATFYSGMYQRL]) were generated by a combination of PCR and In-Fusion ligation in each of the eGFP-tagged intrabody expression vectors. Lastly, a gBlock gene fragment encoding histone 2A (H2A), mCherry, and p85 S6K1 was cloned into XbaI/BamHI sites of the pSCSTa expression vector.

Cell culture and transfections. Expi293F cells (Thermo Fisher Scientific) were cultured in Expi293 Expression Medium and handled according to the manufacturer's recommendations. Transfections in Expi293F were performed using the ExpiFectamine 293 Transfection Kit (Thermo Fisher Scientific) following the manufacturer's protocol for 24-48 hours. The step of adding transfection enhancers 1 and 2 was disregarded here. HeLa cells (ATCC) were cultured in Dulbecco's modified Eagle medium (DMEM) supplemented with 1% Pen-Strep (Gibco) and 10% fetal bovine serum. Transfections in HeLa were performed using Lipofectamine LTX Reagent with PLUS Reagent (Thermo Fisher Scientific) according to the manufacturer's protocol for 24-48 hours.

Fluorescence-activated cell sorting. Expi293F cells transiently expressing FLAG-T2A-eGFP tagged intrabodies for the indicated time points were passed through 40 μm cell strainers (Falcon) and sorted using the BigFoot Cell Sorter (2-4 million cells each) into pre-warmed Expi293 Expression Medium. Untransfected Expi293F cells were used as a negative control to establish gates for sorting eGFP(+) cells. After sorting, cells were

centrifuged at 200xg for 5 minutes, resuspended in pre-warmed Expi293 Expression Medium, and cultured at 37°C for one hour before harvesting for immunoprecipitation or western blot analysis.

Immunoprecipitation and western blot analysis. For experiments with cells transfected with H2A-mChe-S6K1, the lysis buffer used was 1x RIPA (EMD Millipore) supplemented with 0.1% sodium dodecyl sulfate and 1x Halt Protease Inhibitor Cocktail (Thermo Scientific). For all other experiments, to maintain the integrity of mTORC1 assemblies, the lysis buffer used was 0.3% CHAP, 25 mM TRIS, pH 8.0, 150 mM NaCl supplemented with 5 mM EDTA and 1x Halt Protease Inhibitor Cocktail. Briefly, cells were washed one time with ice cold PBS. HeLa cells were collected by gentle scraping in ice cold PBS followed by centrifugation. Cell lysis was carried out on ice for 20 minutes with constant agitation before centrifugation at 14,000 rpm to clarify lysates. Supernatants were transferred to fresh tubes and total protein was quantified by BCA assay (Thermo Scientific). Biotinylated Fab immunoprecipitations were performed for 3 hours with rotation at 4°C. Dynabeads M-270 Streptavidin beads (Invitrogen) were equilibrated in lysis buffer before adding to lysates for 1 hour with rotation at 4°C. Beads were washed five times in lysis buffer before elution by boiling 5 minutes in SDS sample buffer containing 10 mM DTT. Anti-FLAG immunoprecipitations were performed by adding 30 µL of Anti-DYKDDDDK G1 Affinity Resin (Genscript) to lysates for 3 hours with rotation at 4°C. Samples were washed five times in lysis buffer before elution by boiling 5 minutes in SDS sample buffer. Samples were adjusted to 10 mM DTT after transferring supernatant to fresh tubes. Pan-mTOR immunoprecipitations were performed by adding

anti-mTOR Rabbit IgG (Cell Signaling #2972, 1:200 dilution) to lysates and incubating overnight with rotation at 4°C. The next day, Protein A Magnetic Beads (Pierce) were equilibrated in lysis buffer and added for 1 hour with rotation at 4°C. Beads were washed five times in lysis buffer before elution by boiling 5 minutes in SDS sample buffer containing 10 mM DTT. Samples were separated via SDS-PAGE at 100V, transferred to Immobilin-P PVDF Membranes (0.45 μm, EMD Millipore), and blocked for 1 hour at room temperature in blocking buffer (5% BSA in PBS supplemented with 0.1% Tween 20). The following primary antibodies were obtained from Cell Signaling Technology: mTOR (#2972S), Raptor (#2280S), mLST8 (#3274S), Rictor (#2114S), p-S6K1^{T389} (#9234S), S6K1 (#2708T), p-Akt^{S473} (#9271T), Akt (#4691T), Actin (#4970T), Tubulin (#2148S), FLAG (#14793S), and eGFP (#2956T). Antibodies were diluted in blocking buffer and incubated with membranes overnight at 4°C with gentle rocking. Membranes were washed three to four times for five minutes each in wash buffer (PBS supplemented with 0.1% Tween 20) before adding Anti-Rabbit IgG, HRP-Linked Antibody (Cell Signaling Technology, #7074P2) for one hour at room temperature in blocking buffer. Membranes were washed three to four times for five minutes each in wash buffer and then developed using SuperSignal West Pico PLUS Chemiluminescent Substrate (Thermo Fisher Scientific).

Immunofluorescent staining and confocal microscopy imaging. HeLa cells were seeded onto ibiTreat μslide 8-Well slides (Ibidi) and grown in Dulbecco's modified Eagle medium (DMEM) supplemented with 1% Pen-Strep (Gibco) and 10% fetal bovine serum until they reached 80-90% confluency before transfection or immunostaining. Imaging

was performed using a Stellaris 8 (Leica) confocal microscope. Quantitative analyses were performed using FIJI (128). For p-S6$^{S240/244}$ (Cell Signaling Technology, #5364), p-4E-BP1$^{T37/46}$ (Cell Signaling Technology, #2855), and mTOR (Cell Signaling Technology, #2983) immunostainings, HeLa cells were first transfected according to the manufacturers protocol. Cells were washed once with PBS before fixation for 15 minutes at room temperature in 4% paraformaldehyde. Cells were washed three times in PBS and then simultaneously permeabilized and blocked by adding 3% BSA, 0.3% Triton X-100 for 1 hour at room temperature. p-S6$^{S240/244}$ Rabbit IgG was diluted in 1% BSA, 0.3% Triton X-100 and added overnight at 4°C. Cells were washed three times with PBS. Goat Anti-Rabbit IgG (H+L) conjugated with Alexa647 (Jackson ImmunoResearch) was diluted in 1% BSA, 0.3% Triton X-100 and added for 1 hour at room temperature. Cells were washed three times with PBS and incubated with 1 µg/µL DAPI (Thermo Fisher Scientific) for 10 minutes before washing again three times with PBS. PBS in 50% glycerol was added as the final step.

Chapter 4

An epitope-directed synthetic intrabody modulates mTOR function through an undruggable interface

Kelly M. O'Leary[1], Duc Anh Le[1], Tomasz Slezak[1], and Anthony A. Kossiakoff[1,2,*]

[1]Department of Biochemistry and Molecular Biology, The University of Chicago, Chicago, IL 60637.

[2]Institute for Biophysical Dynamics, The University of Chicago, Chicago, IL 60637.

*Correspondence to: Anthony A. Kossiakoff

4.1 Abstract

Mechanistic target of rapamycin (mTOR) is an attractive target for therapeutic intervention in several human diseases characterized by dysregulated cell growth, metabolism, or autophagy. However, current mTOR inhibitors are limited by lack of specificity, resistance mechanisms, and on-target side effects, which highlights the urgent need for new strategies to selectively modulate mTOR kinase activity. Here, epitope-directed synthetic intrabodies were engineered to target functional sites located on the FRB substrate recruitment domain of mTOR ($mTOR^{FRB}$) that are not targeted by conventional inhibitors. This engineering approach enabled rapid validation of two non-catalytic interfaces and revealed a previously uncharacterized regulatory site that contributes to mTOR complex stability and function. Crystal structures of two unique binders bound to $mTOR^{FRB}$ combined with cell-based functional assays showed that modulation of mTOR complex 1 can be elicited through direct obstruction of the mTOR-Raptor interaction. Together, these results highlight the broad potential of engineered synthetic intrabodies for expanding the landscape of targetable functional sites to selectively control dysregulated mTOR signaling.

4.2 Introduction

Mechanistic target of rapamycin (mTOR) is a serine/threonine protein kinase in the PI3K-related kinase family that responds to diverse environmental and nutritional cues to regulate basic cell physiological processes (140). mTOR is positioned as a central rheostat in eukaryotic cells where it integrates signals from amino sensors and receptor-mediated growth factor signaling pathways (48). Through a number of activation and specific recruitment mechanisms, mTOR phosphorylates myriad different substrates to license their downstream activity for control of ribosome biogenesis, translation, macromolecule biosynthesis, autophagy, and cytoskeletal dynamics (32). These processes represent fundamental aspects of cell growth that are commonly dysregulated in diseases including cancer, diabetes, neurodegenerative disorders, and other metabolic syndromes (141).

mTOR-mediated signal transduction occurs through the direct formation of many distinct and transient protein-protein interactions. Consequently, the functional output of mTOR activity is highly influenced by its assembly into two different multi-subunit complexes, mTOR complex 1 (mTORC1) and mTOR complex 2 (mTORC2) (142). The architectures of mTORC1 and mTORC2 are defined by mutually exclusive coordination of the obligate binding partners Raptor and Rictor, respectively (45, 57). Raptor is a crucial substrate recruitment modality in mTORC1 that functions by stabilizing TOS sequence motifs in substrates to enable phosphorylation by the mTOR kinase domain (63). Rictor and mSin1 are the defining subunits of mTORC2, but their role in substrate recruitment less well understood compared to Raptor (45). mLST8 is an obligate subunit found in both mTORC1 and mTORC2 that influences mTORC1 kinase activity and mTORC2 assembly

(59, 143). The function of mLST8 is less well understood compared to Raptor or Rictor. Together, gaining molecular insight into the structural and conformational regulation of mTORC1 and mTORC2 signaling could reveal critical targetable vulnerabilities to inform the design of next-generation therapeutics.

The natural product rapamycin was an indispensable tool to discover and elucidate mechanisms of mTORC1 and mTORC2. Rapamycin functions as a molecular glue between mTOR and FK506-binding protein 12 (FKBP12) (144). The FKBP12-rapamycin binding site is freely accessible in mTORC1, enabling rapid inhibition of mTORC1 (57). Rictor masks the FKBP12-rapamycin binding site in mTORC2, leading to insensitivity to rapamycin on short time scales while prolonged inhibition obstructs the assembly of new mTORC2 complexes (134). Importantly, rapamycin inhibits roughly one third of all mTORC1 substrates owing to its non-catalytic mechanism of inhibition (51). In contrast, ATP-competitive inhibitors, such as Torin-1 and AZD8055, block mTOR catalysis and consequently inhibit all activities of mTORC1 and mTORC2 (17, 53). However, these catalytic inhibitors exhibit a large degree of off-target inhibition in other PI3K-related kinases owing to conservation of the catalytic domains (145).

Small molecule development for targeting functional sites different from rapamycin or ATP-competitors has been hindered by a lack of traditional binding pockets implicated in the mTOR activity cycle. The delicately balanced architectures of mTORC1 and mTORC2 and their propensity for allosteric modulation suggest that cryptic binding sites could be exploited for selective modulation. However, small molecule inhibitors are not well suited for binding to relatively flat surfaces found throughout most of mTORC1 and mTORC2. This issue could potentially be circumvented by engineering cell-permeable peptides or

macrocycle-based scaffolds. Therefore, the largest barrier to developing new functional modulators is identification and validation of new druggable binding sites.

Engineering intracellular synthetic binding proteins offers a rapid and feasible solution to explore undruggable functional sites in recalcitrant therapeutic targets. Key examples have been demonstrated using monobodies or scFv-based intrabodies to selectively bind and modulate specific functions in targets including KRAS, STAT3, and β-arrestin (109, 110, 116, 118, 119). These studies describe molecular tools that are capable of revealing insights into therapeutic strategies that are not afforded by traditional small molecule inhibitors or gene knockdowns. However, intrabodies have not yet been exploited to explore new targetable interfaces in the mTOR pathway owing to inherent complexities stemming from the large size of mTOR (289 kDa) and its heterogeneous association with several distinct obligate binding partners.

This chapter describes the engineering and implementation of synthetic intrabodies that target unique binding sites located on the FKBP12-rapamycin binding (FRB) domain of mTOR ($mTOR^{FRB}$). This work was enabled by a competitive phage display biopanning protocol to isolate synthetic binders against multiple $mTOR^{FRB}$ epitopes that are not targeted by current inhibitors. Structural and functional characterization revealed the molecular basis for mTORC1 inhibition by a synthetic intrabody through a mechanism of direct mTOR-Raptor obstruction. This work highlights the utility of engineering synthetic binders against challenging therapeutic targets to enable rapid validation of potential inhibitory sites. Additional engineering strategies could be employed to inform new strategies for highly selective mTORC1 or mTORC2 inhibition.

4.3 Results

4.3.1 Epitope-directed engineering of synthetic antibody fragments for recognition of undruggable surfaces on mTOR^{FRB}

The FRB domain of mTOR is a critical interaction site that facilitates the recruitment and stabilization of certain mTORC1 substrates for phosphorylation (Figure 4.1A). A previous phage display selection campaign against mTOR^{FRB} described in chapter 2 resulted in the isolation of seven unique binders targeting the FKBP12-rapamycin binding site. These results suggested that the substrate recruitment interface is particularly immunogenic as no additional selection pressures were added to guide the selection of binders against this epitope. Here, a competitive phage display biopanning campaign was undertaken to enrich binders against epitopes located outside of the FKBP12-rapamycin binding site. Exploring new sites holds functional relevance in light of the close physical association between mTOR^{FRB}, Raptor, and the catalytic cleft (Figure 4.1B and C).

Briefly, recombinant SNAP-tagged mTOR^{FRB} was site-specifically biotinylated for immobilization on streptavidin magnetic beads throughout the biopanning procedure. Naïve phage libraries were subjected to subtractive selections using individual SNAP-mTOR^{FRB} or SNAP-FKBP12 domains with no rapamycin present. Next, the pre-cleared libraries were enriched for binders against the ternary complex of SNAP-mTOR^{FRB} and SNAP-FKBP12 in the presence of 500 nM rapamycin. This strategy added selection pressures in two discrete ways. First, binders against the highly immunogenic substrate recruitment site epitope were selectively depleted. Second, binders that exhibit sensitivity to the FKBP12-rapamycin-mTOR^{FRB} complex were enriched, which could potentially be

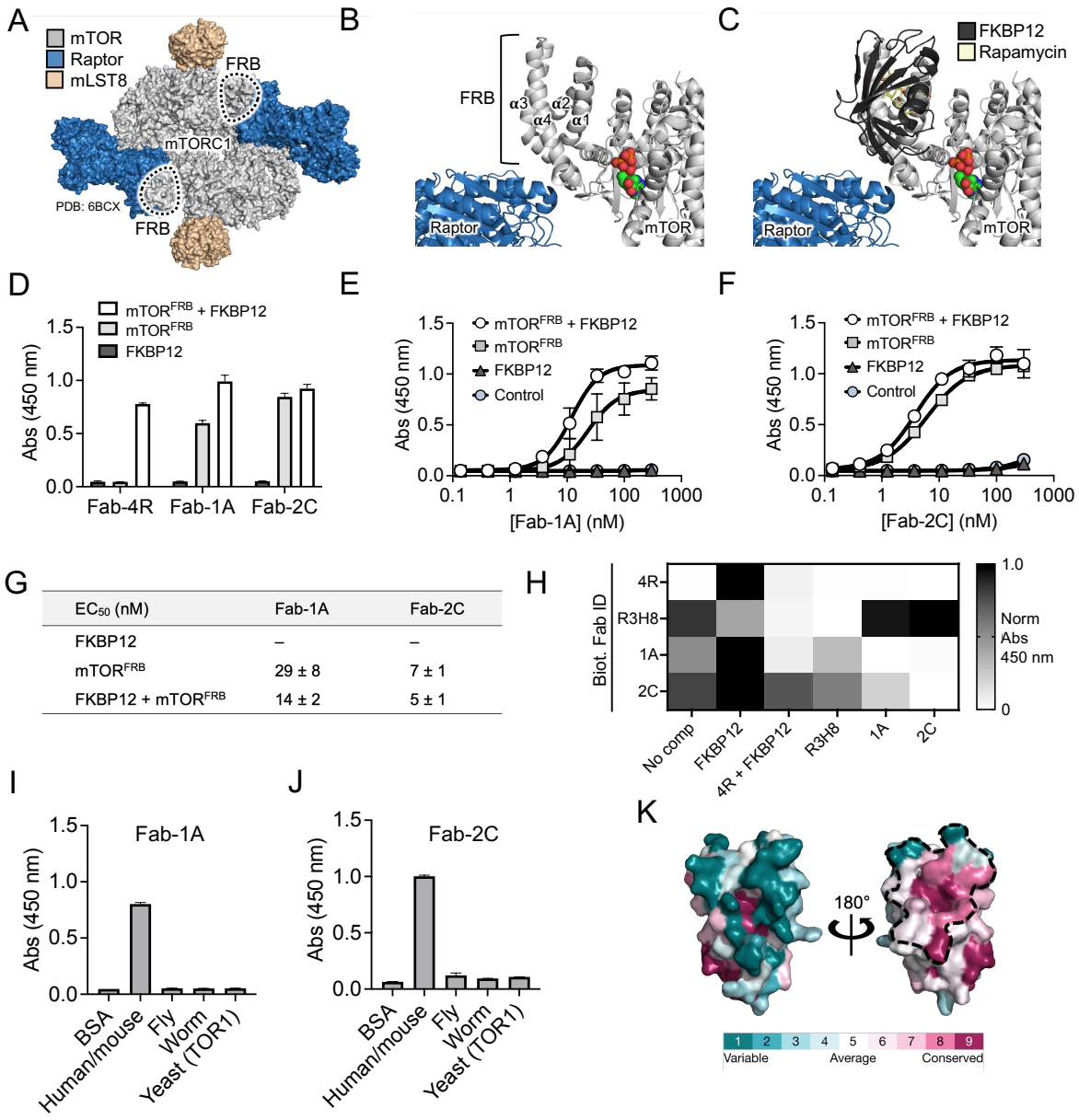

EC_{50} (nM)	Fab-1A	Fab-2C
FKBP12	–	–
$mTOR^{FRB}$	29 ± 8	7 ± 1
FKBP12 + $mTOR^{FRB}$	14 ± 2	5 ± 1

Figure 4.1 Engineering and characterization of epitope-directed Fabs. (A) Location of FRB in the context of mTORC1 (PDB: 6BCX). (B) FRB four-helix bundle. (C) Interaction of FKBP12-rapamycin with FRB. Alignment made using PDB: 1NSG. (D) Single point ELISA analysis of epitope-directed Fabs (n = 3, mean ± SD). (E) Multi-point competitive ELISA for Fab-1A (n = 3, mean ± SD). (F) Multi-point competitive ELISA for Fab-2C (n = 3, mean ± SD). (G) Table of EC_{50} values (nM) for Fab-1A and Fab-2C against the indicated targets. (H) Competitive ELISA epitope binning. Non-biotinylated competitors listed on top. Biotinylated Fabs labeled on left (n = 2). (I-J) ELISA $mTOR^{FRB}$ cross-reactivity analysis (n = 3, mean ± SD). (K) Evolutionary sequence conservation of $mTOR^{FRB}$ visualized using the ConSurf database. Fab-R3E9 epitope is traced in the dashed black line.

manifested by complex-specific or allosteric recognition properties. The process of individual subtractive selections followed by complex-specific enrichment was performed iteratively over five rounds with incremental reduction of target concentrations starting from 1 μM and ending at 10 nM. Phage ELISA coupled with DNA sequencing was used to identify four unique clones. However, only three of these exhibited binding in Fab format. These were named Fab-1A, Fab-2C, and Fab-4R. More details in regard to the selection strategy and characterization of Fab-4R are described in chapter 5.

Single point ELISA was used to characterize the molecular recognition properties of Fab-1A, Fab-2C, and Fab-4R against $mTOR^{FRB}$, FKBP12, or $mTOR^{FRB}$-FKBP12 together in the presence of rapamycin. These results showed no recognition for FKBP12, different degrees of sensitivity for $mTOR^{FRB}$ alone, and similar levels of recognition for $mTOR^{FRB}$-FKBP12 for each Fab (Figure 4.1D). This indicated that Fab-1A, Fab-2C, and Fab-4R may recognize unique epitopes. The characterization and implementation of Fab-1A and Fab-2C will be described in the remainder of this chapter while Fab-4R will be described in chapter 5 owing to its exquisite selectivity for binding only to the ternary complex of FKBP12-rapamycin-$mTOR^{FRB}$. To better understand the binding properties of Fab-1A and Fab-2C, multi-point ELISA was performed using $mTOR^{FRB}$, FKBP12, or $mTOR^{FRB}$-FKBP12 together in the presence of rapamycin as targets (Figure 4.1E and F). This experiment revealed EC_{50} values of 29 nM and 14 nM for Fab-1A binding to $mTOR^{FRB}$ and $mTOR^{FRB}$-FKBP12, respectively (Figure 4.1G). Fab-2C exhibited higher affinities but less sensitivity with EC_{50} values of 7 nM and 5 nM against $mTOR^{FRB}$ and $mTOR^{FRB}$-FKBP12, respectively.

Next, a competitive ELISA assay was performed to characterize the epitopes of Fab-1A and Fab-2C. This assay was based on the detection of biotinylated Fabs using streptavidin-horseradish peroxidase as a secondary detection agent. Consequently, non-biotinylated Fabs could be used as competitive probes to profile different binding sites. These results indicated that Fab-1A and Fab-2C epitopes might be partially overlapped with each other, and that Fab-2C might partially overlap with Fab-R3H8 (Figure 4.1H). Furthermore, a cross-reactivity binding assay using $mTOR^{FRB}$ from various eukaryotic model organisms showed that Fab-1A and Fab-2C are highly specific to human/mouse, which share 100% sequence identity with each other (Figure 4.1I and J). This result is not surprising owing to the lack of evolutionary conservation outside of the substrate recruitment interface (Figure 4.1K). Together, these experiments provided insight into the recognition properties for two new epitope-directed Fabs.

Biotinylated Fab-1A and Fab-2C constructs were tested for recognition of native mTOR assemblies isolated from living cells. HeLa cells were treated with vehicle or 50 nM rapamycin for 1 hour before being harvested for immunoprecipitation. Cell lysates were incubated with biotinylated Fab-1A or Fab-2C before enrichment using streptavidin magnetic beads for western blot analysis. This experiment confirmed that Fab-1A and Fab-2C recognize different epitopes as indicated by the differential capability for immunoprecipitating mTOR in vehicle or rapamycin treated cells (Figure 4.2A). In contrast to its prior characterization using the recombinant $mTOR^{FRB}$ domain, Fab-1A exhibited stable levels of mTOR recognition in the presence or absence of rapamycin while Fab-2C showed large differences (Figure 4.2B). The stark reduction in co-immunoprecipitated Raptor levels in Fab-1A pulldowns suggested that this Fab can bind mTORC1 and reports

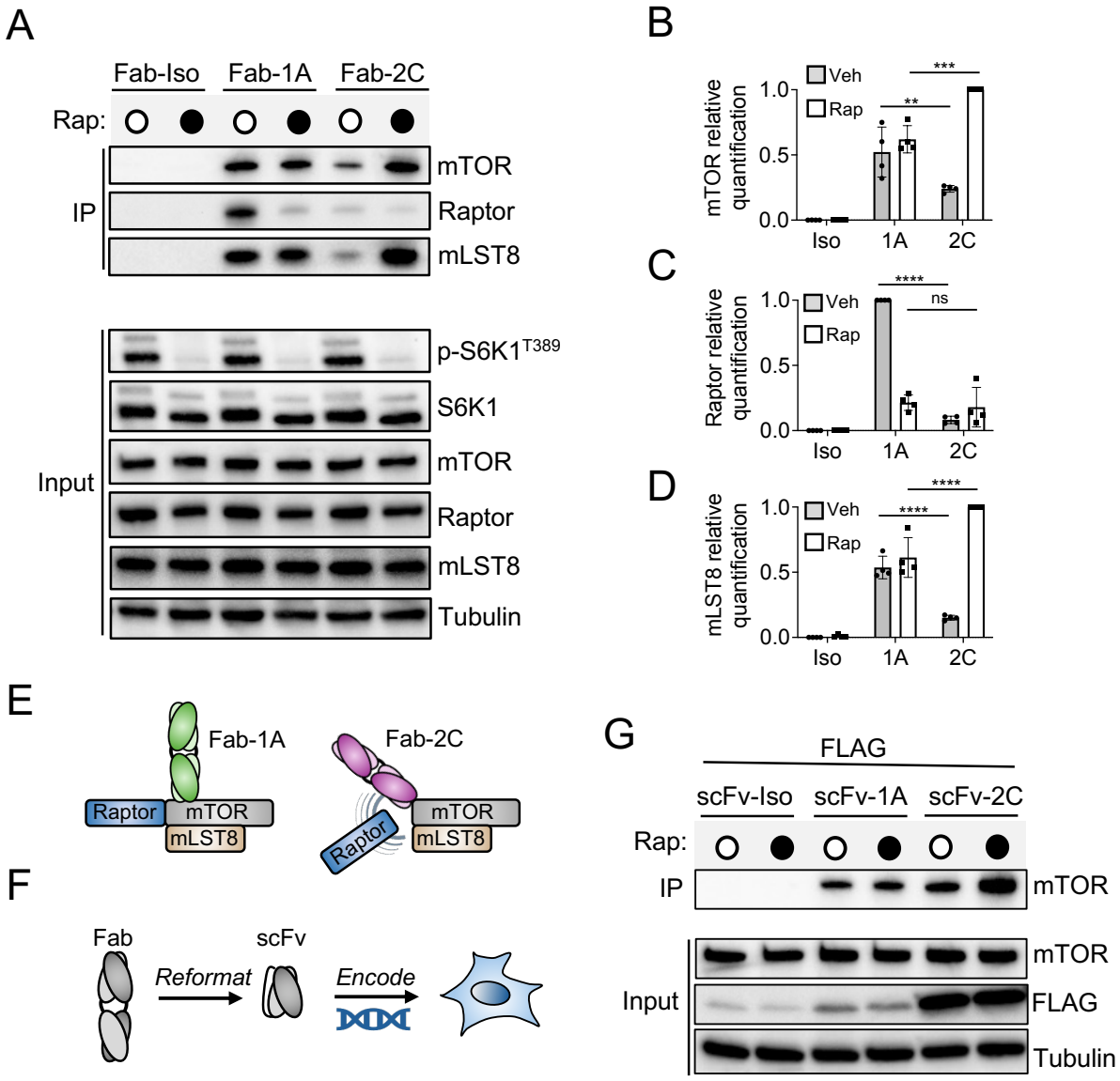

Figure 4.2 Fab-1A and Fab-2C recognition properties for mTORC1. (A) Co-immunoprecipitation of the indicated biotinylated Fabs from HeLa cells treated with vehicle or rapamycin for 1 hour. (B) Quantification of immunoprecipitated mTOR relative to input in A (n = 4 biological replicates, mean ± SD. $^{**}P \leq 0.01$, $^{***}P \leq 0.001$, one-way ANOVA). (C) Quantification of immunoprecipitated Raptor relative to input in A (n = 4 biological replicates, mean ± SD. ns = not significant, $^{****}P \leq 0.0001$, one-way ANOVA). (D) Quantification of immunoprecipitated mLST8 relative to input in A (n = 4 biological replicates, mean ± SD. $^{****}P \leq 0.0001$, one-way ANOVA). (E) Proposed schematic for differential mTORC1 recognition capability by Fab-1A and Fab-2C. (F) Workflow for Fab to scFv intrabody reformatting. (G) Anti-FLAG immunoprecipitation of the indicated FLAG-tagged intrabodies from Expi293F cells treated with vehicle or rapamycin for 1 hour.

the architectural integrity of the mTOR-Raptor interaction (Figure 4.2C). Fab-2C also exhibited differences from its in vitro characterization. Binding of Fab-2C to mTOR in vehicle treated cells was significantly lower than Fab-1A despite its more favorable affinity. However, Fab-2C was capable of selectively engaging mTOR in rapamycin treated cells where it co-immunoprecipitated mLST8 but not Raptor (Figure 4.2D). These results suggest that the Fab-2C epitope could be obstructed by the presence of Raptor within the context of the mTORC1 architecture (Figure 4.2E). Consequently, rapamycin-induced destabilization of the mTOR-Raptor interaction allows Fab-2C to engage its cognate epitope and co-immunoprecipitate the remaining components in mTORC1.

This hypothesis was tested by reformatting Fab-1A and Fab-2C into scFv intrabodies for intracellular expression studies (Figure 4.2F). Expression of intrabody probes inside living cells provides a unique window into molecular recognition properties, particularly in light of the dynamics continuous chaperone-assisted assembly of mTOR into mTORC1 or mTORC2. As a result, epitopes that are obstructed in cell lysates might be transiently accessible within a native and active intracellular environment. Expression of FLAG-tagged scFv-1A and scFv-2C in Expi293F cells treated with vehicle or rapamycin for 1 hour served as the platform to test this hypothesis. Anti-FLAG immunoprecipitation showed that scFv-1A recognition of mTOR was similar to Fab-1A, but scFv-2C exhibited a substantially greater capacity to engage with mTOR in vehicle treated cells compared to Fab-2C (Figure 4.2G). These results suggest a mechanism of recognition consistent with the model proposed in Figure 4.2E whereby the epitope for Fab-2C directly interferes with the cognate mTORC1 subunit Raptor.

While these studies used mTORC1 as a model system to characterize Fab-1A and Fab-2C, it should be noted that the mTORC2 subunit Rictor is coordinated in a highly similar position as Raptor and likely influences the epitope accessibility of Fab-2C as well. Furthermore, the molecular basis for sensitivity to FKBP12-rapamycin remained unresolved. In order to better understand the recognition properties for Fab-1A and Fab-2C, a campaign was undertaken to crystallize these binders complexed with $mTOR^{FRB}$.

4.3.2 Crystal structure reveals molecular basis for recognition of unique functional sites located on $mTOR^{FRB}$

Engineered synthetic Fabs have been exploited as X-ray crystallography chaperones in many different studies to elucidate the structures and conformations of difficult target antigens (120, 146). While antigen stabilization and favorable crystal contact formation are key properties of Fabs as chaperones, there have been further engineering efforts to enhance Fab crystallization properties by reducing surface entropy or promoting specific Fab-Fab crystal contacts (147, 148). The strategy of modifying a small region in the light chain constant domain of human Fabs was found to dramatically enhance their propensity to crystallize. This modification is simply the replacement of seven amino acids in the human Fab scaffold with five amino acids found in the rabbit Fab framework and has been termed “crystal kappa” by the authors. Fab-1A and Fab-2C were modified to include the crystal kappa mutation before initiating crystallization trials. Monodisperse complexes of Fab-1A with $mTOR^{FRB}$ or Fab-2C with $mTOR^{FRB}$ were purified using size exclusion chromatography (Figure 4.3A and B). Pure fractions were pooled and screened in different crystallization conditions where many different crystal

hits were identified (Figure 4.2C). Crystals were fished directly from screens for X-ray diffraction data collection.

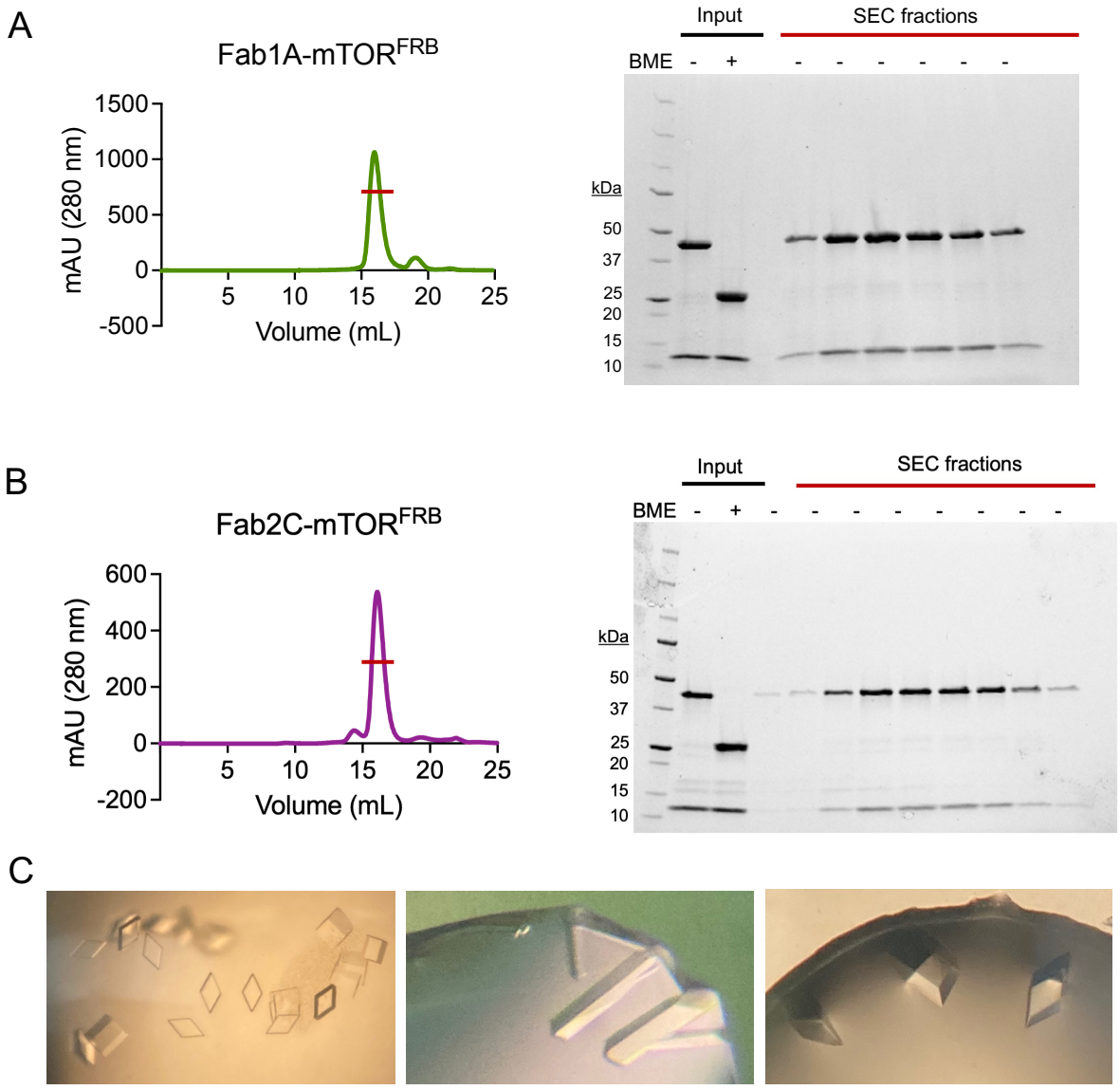

Figure 4.3 Crystallization of Fab-1A and Fab-2C bound to mTOR^{FRB}. (A) Size exclusion chromatogram for the Fab1A-mTOR^{FRB} complex. Red line indicates fractions analyzed by SDS-PAGE. (A) Size exclusion chromatogram for the Fab2C-mTOR^{FRB} complex. Red line indicates fractions analyzed by SDS-PAGE. (C) Crystallization hits observed for Fab1A-mTOR^{FRB} or Fab2C-mTOR^{FRB} complexes from various commercial screens.

Table 4.1 X-ray diffraction data collection and refinement statistics for structures of Fab-1A and Fab-2C bound to mTOR^{FRB}.

	Fab-1A•mTOR^{FRB}	Fab-2C•mTOR^{FRB}
Space group	*P1*	*P 1 21 1*
Cell dimensions		
a, b, c (Å)	64.938, 64.983, 80.302	46.86, 73.441, 91.971
α, β, γ (°)	70.35, 68.34, 71.13	90, 102.78, 90
Resolution (Å)	33.64 - 1.90 (1.96 - 1.90)*	33.40 - 2.18 (2.26 - 2.18)
R_{merge}	0.053 (0.666)	0.104 (0.510)
R_{meas}	0.0756 (0.941)	0.147 (0.722)
R_{pim}	0.053 (0.666)	0.104 (0.510)
$CC_{1/2}$	0.997 (0.540)	0.984 (0.441)
$I / \sigma I$	7.2 (1.2)	5.9 (1.8)
Completeness (%)	97.5 (93.5)	99.90 (99.58)
Redundancy	2.0 (2.0)	2.0 (2.0)
No. reflections	86,739 (2,889)	31,807 (2,879)
R_{work} / R_{free}	0.2220 / 0.2566	0.1899 / 0.2329
No. atoms		
Protein	8,049	4,068
Solvent	392	482
Protein residues	1043	526
R.M.S deviations		
Bond lengths (Å)	0.007	0.002
Bond angles (°)	0.86	0.55
Ramachandran favored (%)	95.42	96.73
Allowed (%)	4.09	2.69
Outliers (%)	0.49	0.58
Rotamer outliers (%)	1.67	1.99
Clashscore	4.6	3.12
Average B-factor		
Protein	45.51	26.8
Solvent	42.68	32.91

*Values in parentheses are for the highest resolution shell

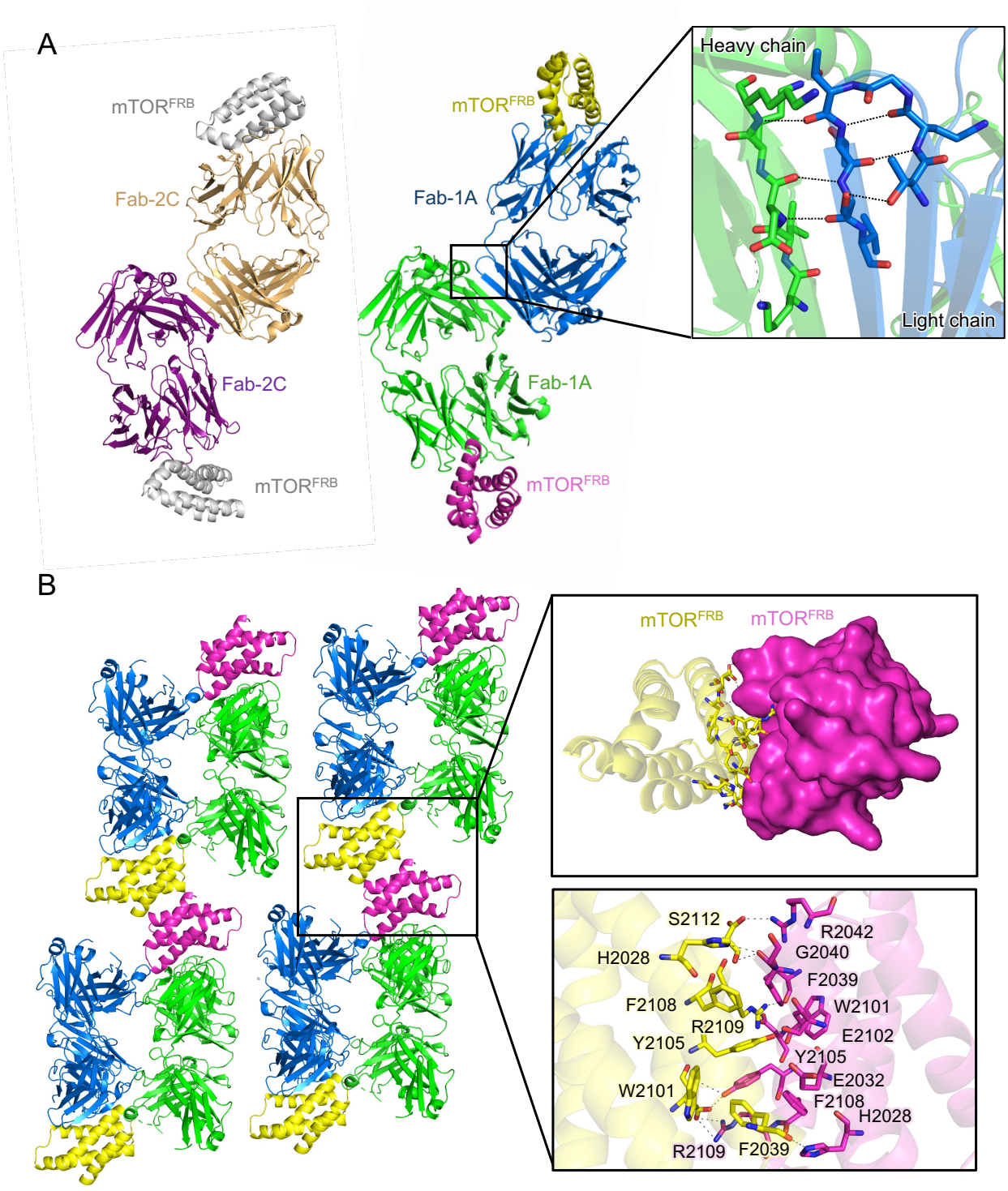

Figure 4.4 Crystal contacts in Fab-1A-mTOR^{FRB} and Fab-2C-mTOR^{FRB} structures. (A) Contacts mediated by the crystal kappa mutated region in Fab-1A and Fab-2C. (B) Antiparallel mTOR^{FRB}-mTOR^{FRB} crystal contacts made through the substrate recruitment interface in the structure bound by Fab-1A.

Crystal structures of Fab-1A and Fab-2C bound to $mTOR^{FRB}$ were determined at 1.90 Å and 2.18 Å resolution, respectively. These data sets were collected from crystals grown in highly similar conditions of 0.2 M ammonium citrate dibasic, 20% PEG 3350 for Fab-1A-$mTOR^{FRB}$ and 0.2 M sodium tartrate dibasic, 20% PEG 3350 for Fab-2C-$mTOR^{FRB}$. The space groups (P1 and P1 21 1) and number of molecules per asymmetric unit (1 and 2) were different between Fab-1A and Fab-2C complexes, respectively. These structures revealed that crystal lattice formation was indeed influenced by the crystal kappa mutation, which facilitated Fab^{HC}-Fab^{LC} contacts in both structures (Figure 4.4A). Furthermore, $mTOR^{FRB}$-$mTOR^{FRB}$ crystal contact formation showed highly specific hydrogen bonding and Van der Waals interactions in the structure bound by Fab-1A (Figure 4.4B). Here, $mTOR^{FRB}$ contacts itself in an antiparallel arrangement solely through its substrate recruitment interface. This has not been observed before and could potentially suggest a mechanism of autoinhibition mediated by the binding of two mTOR molecules through this interface. Notably, the side chains involved in these crystal contacts are also responsible for docking S6K1 and PRAS40. Together, this crystallization campaign demonstrated the utility of engineered Fabs as superior crystallization chaperones.

Closer inspection of the Fab-1A-$mTOR^{FRB}$ and Fab-2C-$mTOR^{FRB}$ structures demonstrated that these binders exploit a combination of hydrogen bonding and Van der Waals interactions and that they do indeed have different epitopes (Figure 4.5A and B). To understand the structural basis for sensitivity to FKBP12-rapamycin, these structures were aligned with a previously determined structure of the FKBP12-rapamycin-$mTOR^{FRB}$

ternary complex (PDB: 1NSG). This analysis showed that Fab-1A binds to mTOR^{FRB} at an epitope sterically disconnected from the FKBP12-rapamcycin binding site (Figure

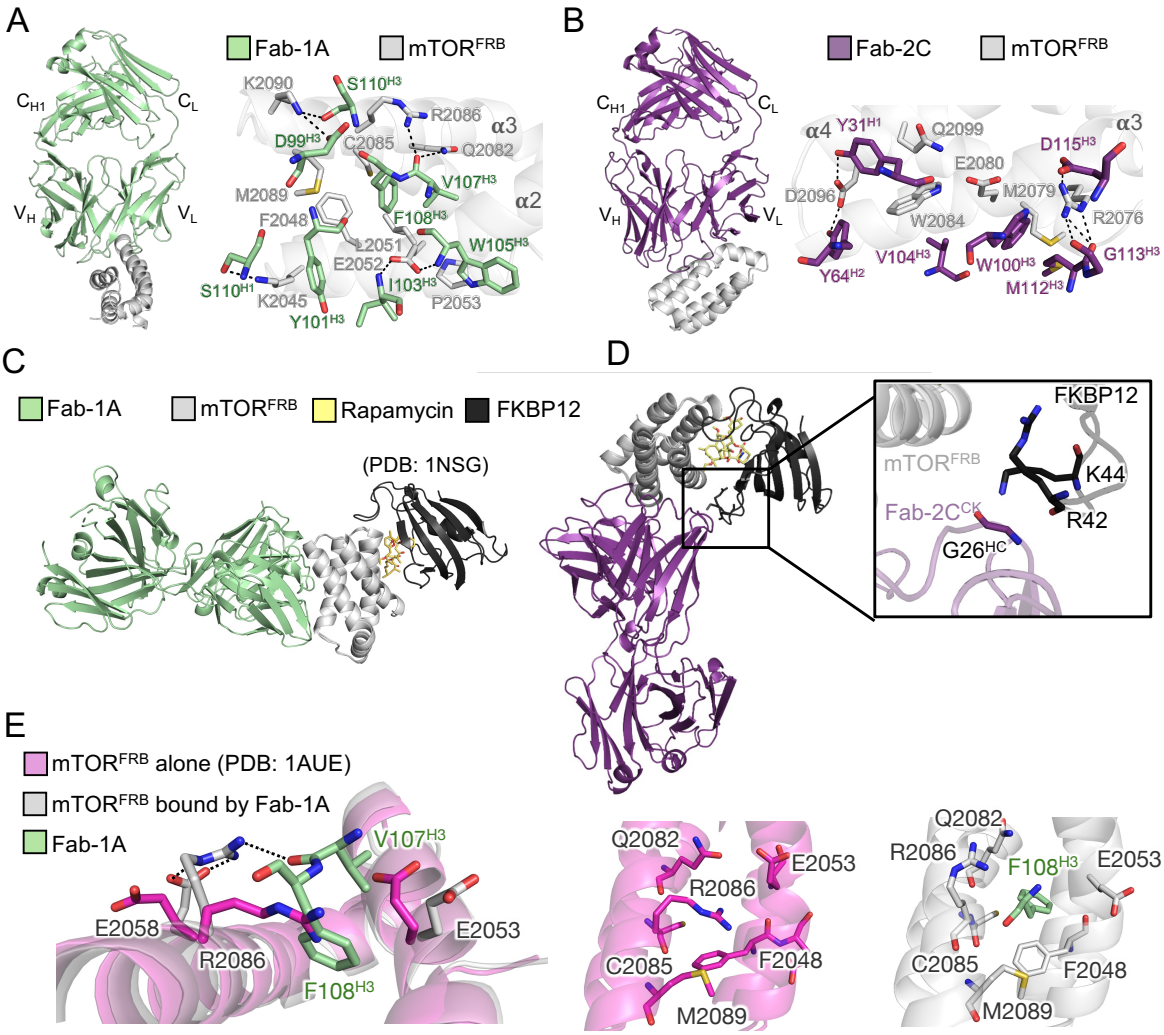

Figure 4.5 Structural basis for Fab-1A and Fab-2C sensitivity to FKBP12-rapamycin. (A) Structure and direct side chain interactions in the Fab-1A-mTOR^{FRB} complex. (B) Structure and direct side chain interactions in the Fab-2C-mTOR^{FRB} complex. (C) Alignment of Fab-1A-mTOR^{FRB} with a previously determined structure of FKBP12-rapamycin-mTOR^{FRB} (PDB: 1NSG) exhibits the distal location of the Fab-1A epitope relative to the FKBP12-rapamycin binding site. (D) Alignment of Fab-2C-mTOR^{FRB} with a previously determined structure of FKBP12-rapamycin-mTOR^{FRB} (PDB: 1NSG) exhibits the potential for interactions formed between FKBP12 and Fab-2C. (E) Alignment of Fab-1A-mTOR^{FRB} with a previously determined structure of mTOR^{FRB} alone (PDB: 1AUE) exhibits the potential for conformational competition between F108^{H3} from Fab-1A and R2086 from mTOR^{FRB}.

4.5C). In contrast, it appeared that Fab-2C might form polar contacts with R42 and K44 from FKBP12 (Figure 4.5D). These findings were particularly intriguing in light of the differential EC_{50} values observed for Fab-1A against $mTOR^{FRB}$ (29 nM) and Fab-1A against FKBP12-rapamcyin-$mTOR^{FRB}$ (14 nM). This suggests that the ternary complex formation of FKBP12-rapamcyin-$mTOR^{FRB}$ could stabilize a particular energetic state of $mTOR^{FRB}$ that is selectively recognized by Fab-1A. This was supported by comparing the Fab-1A-$mTOR^{FRB}$ structure to a previously determined structure of $mTOR^{FRB}$ alone (PDB: 1AUE) (Figure 4.5E). This alignment showed that the R2086 side from $mTOR^{FRB}$ is buried in a shallow surface pocket when $mTOR^{FRB}$ was crystallized alone. In the structure of $mTOR^{FRB}$ bound by Fab-1A, F108 from CDR-H3 is buried inside the same pocket while R2086 is displaced and forms multiple electrostatic interactions with E2058. Together, these results suggest that dynamic side chain reorientation on the opposite side of the $mTOR^{FRB}$ substrate recruitment interface could be a result of allosteric modulation resulting from engagement by FKBP12-rapamycin. These observations establish a hypothesis for the differential recognition capability against $mTOR^{FRB}$ and FKBP12-rapamycin-$mTOR^{FRB}$ by Fab-1A. Future studies should explore the biophysical and energetic basis using nuclear magnetic resonance spectroscopy coupled with molecular dynamics to better understand the altered side chain motions observed here.

The ultimate goal for this chapter is to implement synthetic intrabodies for epitope-specific modulation of mTOR protein-protein interactions and substrate recruitment. To provide a context for the epitopes revealed in crystal structures of Fab-1A-$mTOR^{FRB}$ and Fab-2C-$mTOR^{FRB}$, models of their variable domains (VL-VH) were aligned with a previous cryo-EM structure of mTOR along with variable domains of Fab-R3E9 and Fab-R3H8.

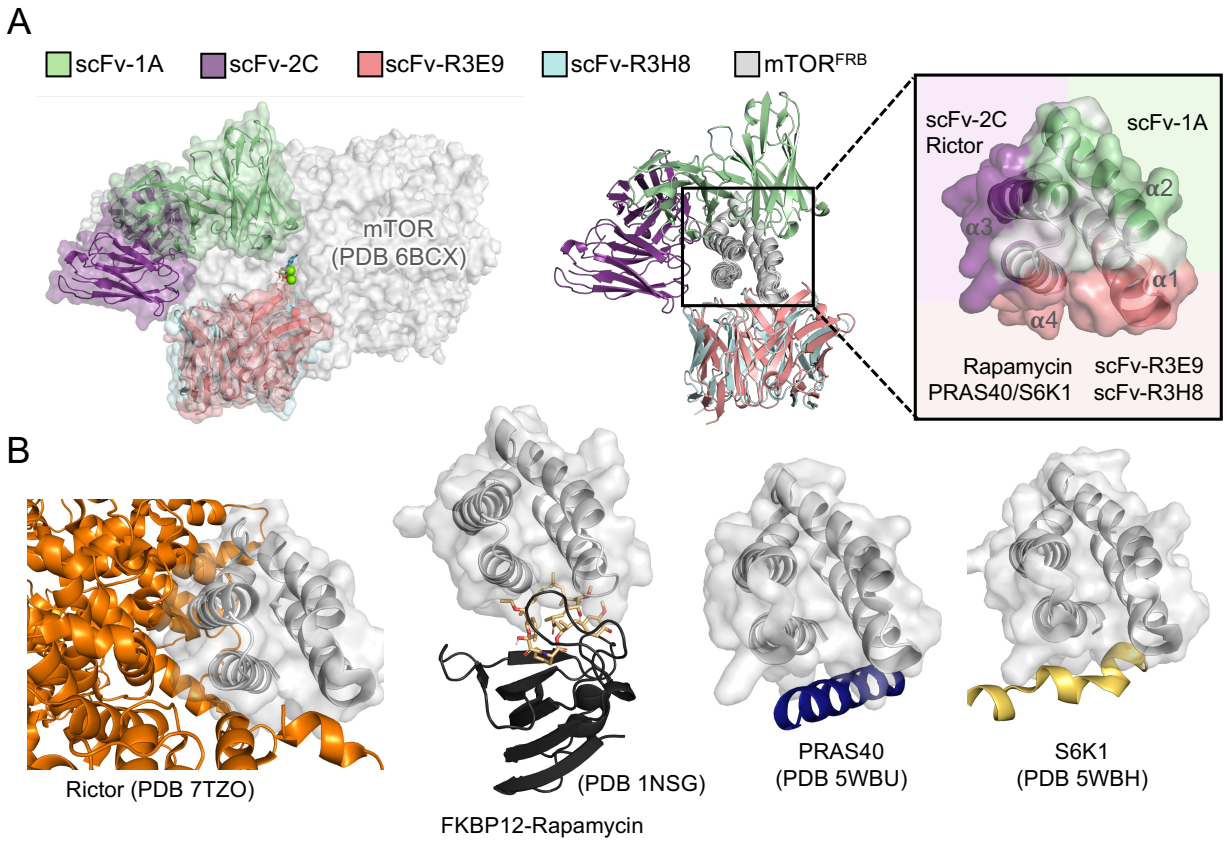

Figure 4.6 Connecting scFv-1A and scFv-2C epitopes with mTOR interaction sites. (A) *Left:* Structural alignment of models for scFv-1A (pale green), scFv-2C (purple), scFv-R3E9 (salmon), and scFv-R3H8 (pale cyan) with a previously determined cryo-EM structure of mTOR (gray; ATP shown as sticks, magnesium shown as spheres; PDB: 6BCX). *Right:* Cartoon representation for alignment of scFv models with $mTOR^{FRB}$. Inset shows epitopes colored on $mTOR^{FRB}$ and lists other structurally characterized proteins known to bind to the same site. (B) Visualization of structurally characterized $mTOR^{FRB}$-interacting proteins. A clear overlap in epitopes for scFv-2C and Rictor can be observed.

This analysis served as a visualization for how three different classes of scFv intrabodies target the small FRB domain located proximal to the mTOR active site (Figure 4.6A). Together, the epitopes for scFv-1A, scFv-2C, scFv-R3E9, and scFv-R3H8 mask most of the solvent accessible surface area surrounding the four-helix bundle of

mTOR^{FRB}. It appears that some surfaces are not amenable to targeting by intrabodies owing to steric hindrance with the active site of mTOR. However, other surfaces, such as the “top” of mTOR^{FRB} are not targeted by these engineered molecules. Nevertheless, a structural bioinformatic characterization showed that the epitope for scFv-1A does not overlap with any other structurally characterized proteins that are known to bind to mTOR^{FRB}. In contrast, the epitope for scFv-2C clearly overlaps directly with the mTORC2 subunit Rictor. Structurally characterized mTOR^{FRB}-interacting proteins only target two general epitopes located directly on mTOR^{FRB}, with one of those being the substrate recruitment interface that was dissected in chapters 2 and 3 (Figure 4.6B).

4.3.3 Modulation of mTORC1 and mTORC2 complex assembly and substrate phosphorylation through an undruggable site

The architectures of mTORC1 and mTORC2 are similar in terms of overall organization but exhibit some key differences in mTOR^{FRB} accessibility. Although Raptor and Rictor bind to mTOR in the same general area, Rictor forms substantial contacts with mTOR^{FRB} along the scFv-2C epitope and also partially occludes the substrate recruitment interface. The latter has been suggested to promote selectivity for mTORC2 substrate phosphorylation by blocking mTOR^{FRB}-based docking of mTORC1 substrates. Models of scFv-1A and scFv-2C were aligned with previously determined cryo-EM structures of mTORC1 and mTORC1 (PDB: 6BCX and PDB: 7TZO). From a global perspective, the epitopes for scFv-1A and scFv-2C appear to be accessible in mTORC1 (Figure 4.7A). However, this alignment revealed that the constant domain of Fab-2C is incompatible with engagement of mTORC1 due to steric clashing with Raptor. This supports the findings

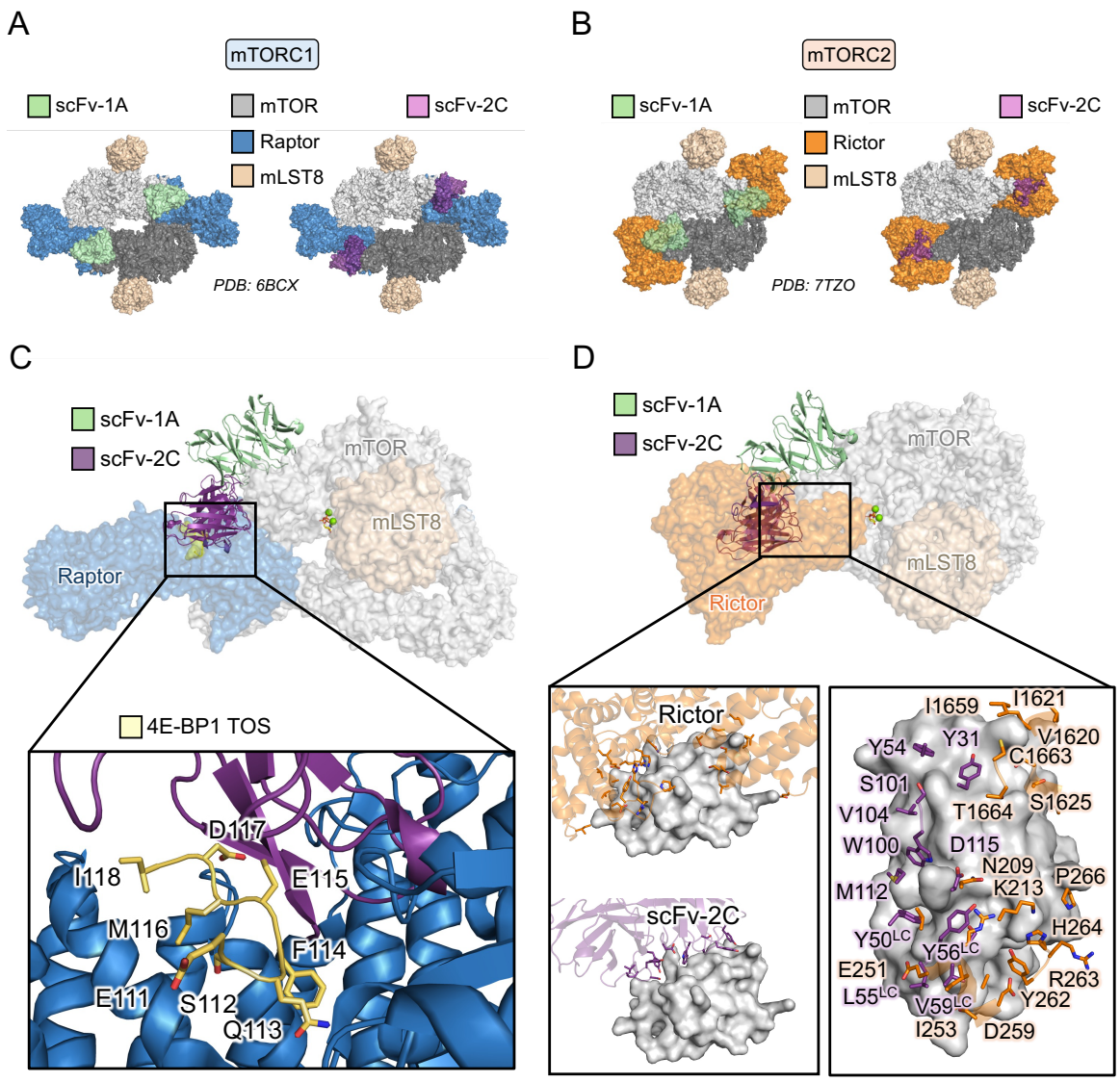

Figure 4.7 Structural models of scFv-1A and scFv-2C with mTORC1 and mTORC2. (A) Alignment of scFv-1A and scFv-2C models with a previously determined structure of mTORC1 (PDB: 6BCX). (B) Alignment of scFv-1A and scFv-2C models with a previously determined structure of mTORC2 (PDB: 7TZO). (C) Zoomed in view of steric clashing between scFv-2C, Raptor, and the 4E-BP1 TOS peptide bound to Raptor. (D) Zoomed in view of steric clashing between scFv-2C and Rictor. Inset shows that scFv-2C and Rictor contact the same general surface area on FRB. Despite contacting the same region, scFv-2C and Rictor employ side chains contacting entirely different local regions within the same binding site. This observation contrasts with the molecular mimicry observed between scFv-R3E9, scFv-R3H8, S6K1, and PRAS40 at the substrate recruitment interface of $mTOR^{FRB}$.

from Fab-based immunoprecipitation studies described earlier in this chapter. In mTORC2, scFv-1A engagement appears unobstructed while scFv-2C competes directly with Rictor for its epitope (Figure 4.7B).

A closer analysis of scFv-1A and scFv-2C aligned with mTORC1 revealed additional clashes between scFv-2C, Raptor, and the TOS docking site on Raptor (Figure 4.7C). This observation is intriguing from two different standpoints. First, the subtle overlap between scFv-2C and Raptor supports a mechanism of mutual exclusivity in their recognition of mTOR. However, the cryo-EM structure used for analysis here represents one static snapshot of the mTORC1 architecture. In living cells, it is likely that mTORC1 undergoes dynamic movements and fluctuations throughout its activity cycle that cannot be accounted for here. Nevertheless, from this particular conformation it is clear that scFv-2C may employ a mechanism of inhibition by competing with both Raptor and with TOS-dependent substrate docking. TOS-mediated substrate recruitment has been described for several mTORC1 substrates, suggesting that scFv-2C could be a useful tool for investigations into substrates that require TOS docking.

The overlap between scFv-2C and Rictor in mTORC2 was analyzed next. Rictor forms extensive contacts with $mTOR^{FRB}$ at regions adjacent to the substrate recruitment site and regions directly overlapping with the substrate recruitment site (Figure 4.7D). This has been suggested to enhance the selectivity of mTORC2 substrate phosphorylation by preventing $mTOR^{FRB}$-based docking of mTORC1 substrates. The epitope of scFv-2C overlaps directly with Rictor contacts formed adjacent to the substrate recruitment site. However, despite targeting the same general surface exposed patch,

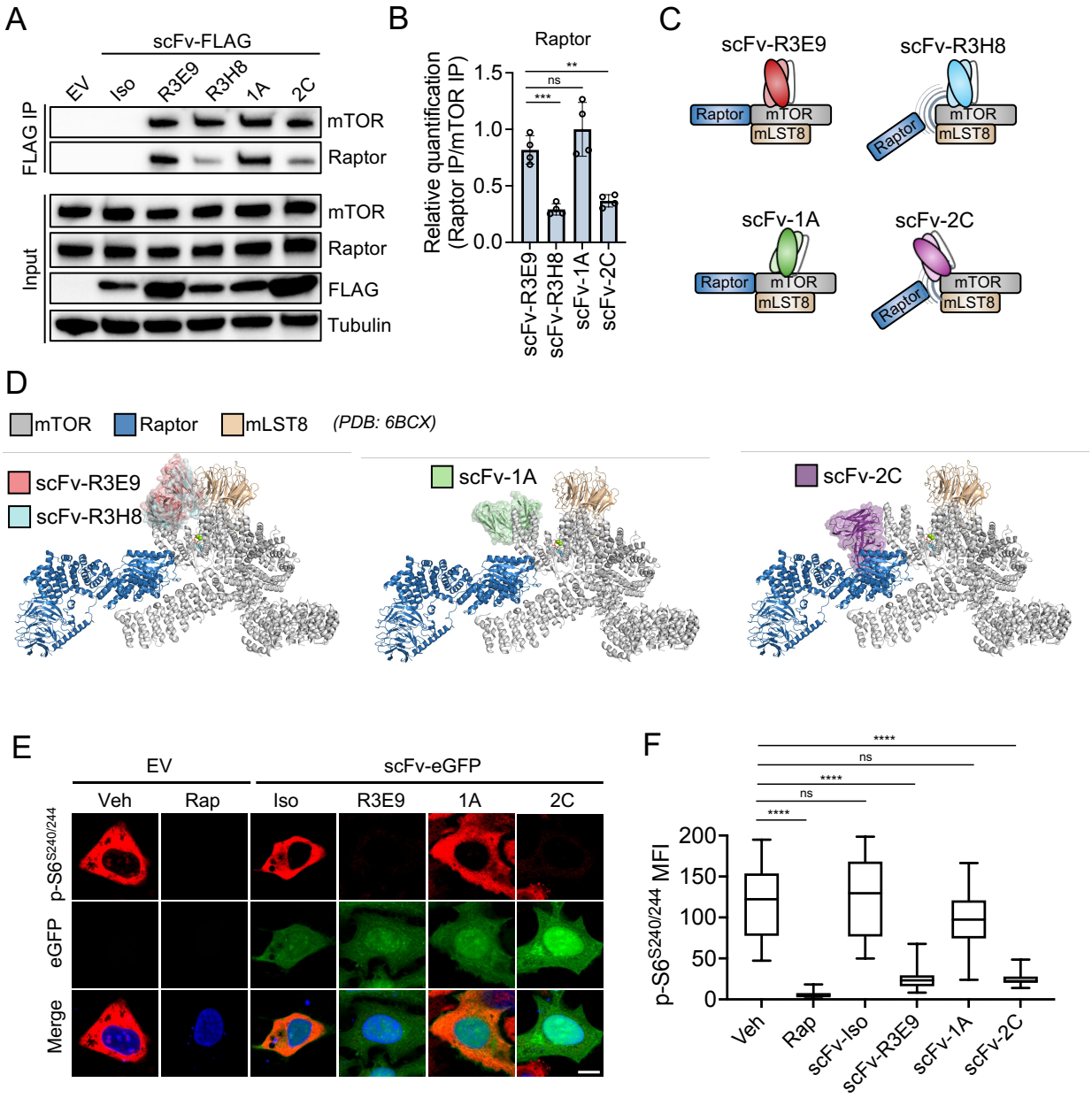

Figure 4.8 Potent modulation of mTORC1 function by scFv-2C. Figure caption continued on the next page.

Figure 4.8 Potent modulation of mTORC1 function by scFv-2C. (A) Anti-FLAG immunoprecipitation from Expi293F cells expressing the indicated constructs for 48 hours. (B) Relative quantification of Raptor relative to mTOR in the FLAG immunoprecipitation from A (n = 4 biological replicates, mean ± SD. ns = not significant, $^{**}P \leq 0.01$, $^{***}P \leq 0.001$, one-way ANOVA). (C) Schematic for the proposed model of intrabody-based modulation of the mTOR-Raptor interaction. (D) Structural models of the indicated scFv intrabodies with a previously determined cryo-EM structure of mTORC1 (PDB: 6BCX, monomeric subunits shown for clarity) (E) Analysis of immunostained p-S6$^{S240/244}$ in HeLa cells expressing eGFP-tagged intrabodies using confocal microscopy. Scale bar denotes 11.5 μm. (n = 2 independent experiments). (F) Quantification of p-S6$^{S240/244}$ from the experiment in E (n = 36, 33, 39, 37, 38, and 34 cells. ns = not significant, $^{****}P \leq 0.0001$, one-way ANOVA with Tukey-Kramer test).

these two molecules employ entirely different structural mechanisms in their recognition of mTOR^{FRB}. This is illustrated in differences of side chain chemistry and positions contacted. Interestingly, no molecular mimicry was observed between these synthetic and natural proteins. In contrast, a high level of mimicry was observed between scFv-R3E9, scFv-R3H8, S6K1, and PRAS40 at the mTOR^{FRB} substrate recruitment interface.

The inhibitory potential of scFv-1A and scFv-2C was assessed using cell-based functional interaction and activity assays. Expi293F cells were transfected with scFv-R3E9, scFv-R3H8, scFv-1A, or scFv-2C for 48 hours before an anti-FLAG immunoprecipitation was performed. This assay was previously used to explore and validate the conformation-specific allosteric modulation of the mTOR-Raptor by scFv-R3E9 and scFv-R3H8. Consistent with previous results, the mTOR-Raptor interaction was stabilized by scFv-R3E9 but selectively destabilized by scFv-R3H8 (Figure 4.8A). These effects were essentially replicated by scFv-1A and scFv-2, respectively, despite being elicited through entirely different recognition mechanisms (Figure 4.8B). These findings were used to propose a general model of allosteric or direct modulation of the

mTOR-Raptor interaction using scFv-R3H8 or scFv-2C (Figure 4.8C). In contrast, scFv-R3E9 and scFv-1A can be used to isolate fully intact mTORC1 assemblies. In light of this model, a series of structural alignments were made to visualize how the engagement of different epitopes by scFv-R3E9, scFv-R3H8, scFv-1A, and scFv-2C leads to differential modulation on mTORC1 complex assembly (Figure 4.8D).

Since these results suggested that scFv-2C modulates mTORC1 interactions, an analysis of mTORC1 signaling was performed next. Confocal microscopy was used to visually inspect endogenous p-S6$^{S240/244}$ phosphorylation levels in HeLa cells transfected with eGFP-tagged intrabodies (Figure 4.8E). These results showed that scFv-2C inhibits mTORC1 signaling with similar potency as rapamycin and scFv-R3E9 (Figure 4.8F). This is a critical finding owing to the unique binding site targeted by scFv-2C relative to rapamycin and scFv-R3E9. The observations made here represent one of the first examples of selective mTORC1 substrate phosphorylation elicited through engagement of a binding site that is not targeted by conventional small molecule inhibitors. Understanding how scFv-2C modulates the phosphorylation of other mTORC1 or mTORC2 substrates could shed light on specific substrate recruitment mechanisms. Owing to the overlap in binding sites, scFv-2C is predicted to obstruct mTORC2 assembly and should therefore inhibit mTORC2 activity similar to rapamycin.

4.3.4 Engineering synthetic antibody fragments for Rheb and CCT/TRiC

As proof-of-concept for the feasibility of rapidly targeting selected nodes within the mTOR signaling pathway, phage display campaigns were carried out against other components involved in mTORC1 activation or mTOR complex assembly. The targets

chosen were Rheb and chaperonin containing tailless complex polypeptide 1/T-complex protein-1 ring complex (CCT/TRiC) subunits CCT1 and CCT2. Rheb is a GTPase that functions downstream of TSC1/2 and growth factor-induced signaling (29). TSC2 exhibits GTPase activating protein (GAP) activity toward Rheb and therefore regulates its nucleotide-bound state (149). In the presence of growth factors, Akt phosphorylates TSC2 and inactivates its GAP activity toward Rheb (150). This relieves negative inhibition on Rheb and allows Rheb to form a direct interaction with mTORC1 at the lysosomal surface where it allosterically modulates alignment of the mTOR catalytic cleft to promote its activity (67). Rheb is an intriguing therapeutic target since it has been described as a selective component for mTORC1 but not mTORC2 activation (Figure 4.9A and B). CCT/TRiC is a critical multi-subunit chaperone that facilitates folding of many proteins in addition to mTOR subunits including mLST8 and Raptor (151). Therefore, it was envisioned that targeted engagement of Rheb or CCT subunits could enable selective modulation of mTOR substrate phosphorylation or complex assembly, respectively.

Recombinant purification of Avi-tagged Rheb, CCT1, and CCT2 and enzymatic biotinylation using the BirA biotin ligase provided high quality targets for phage display biopanning. Targets underwent iterative rounds of incubation with phage library, stringent washing, elution, and amplification with incremental reduction in target concentration for four to five rounds, starting at 1 μM and ending at 10 nM. Phage ELISA and DNA sequencing were used to identify unique phage clones for Fab reformatting and further characterization. Unique binders were expressed and purified as Fabs and validated for engagement with their cognate antigens using multi-point ELISA.

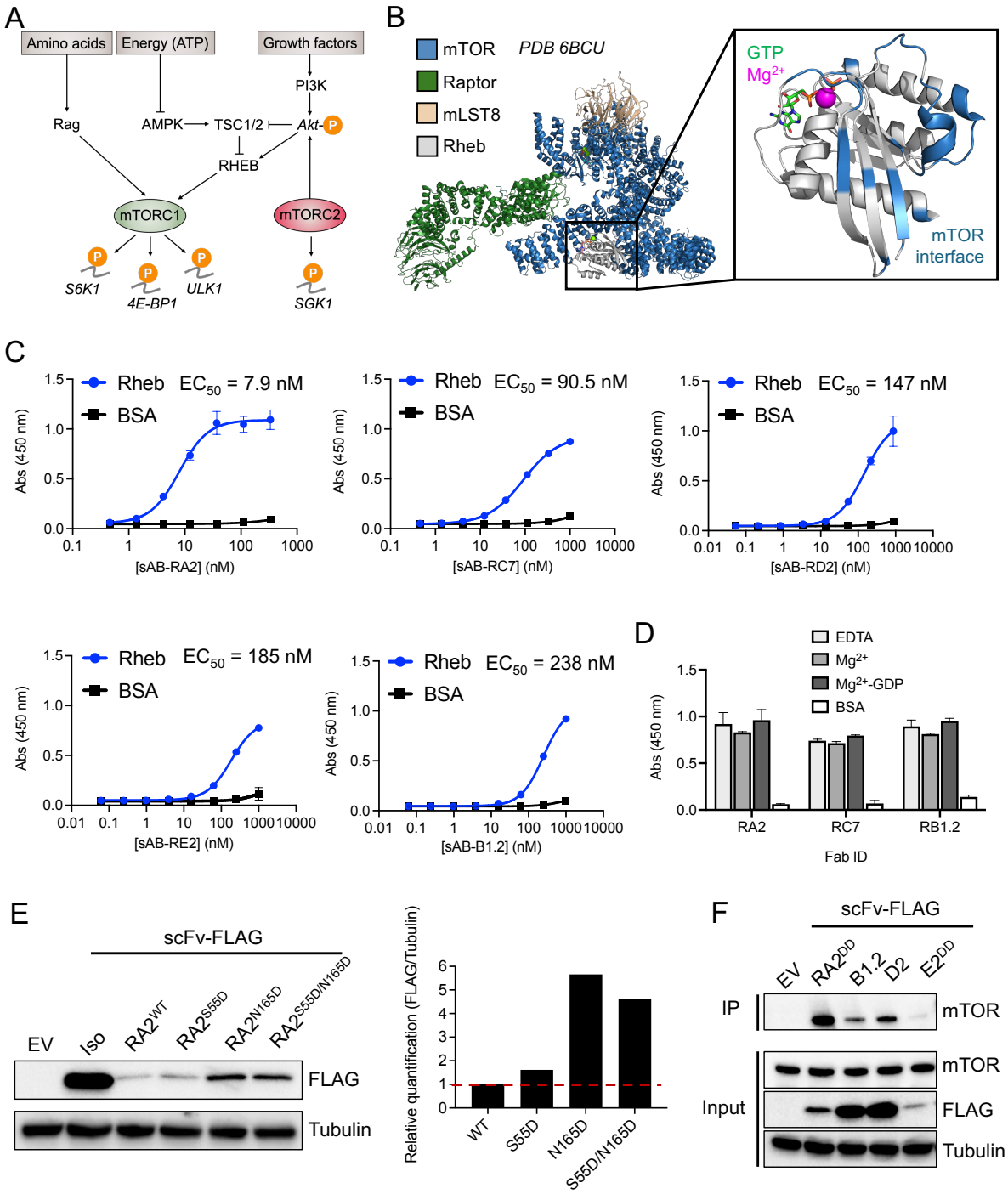

Figure 4.9 Validation of engineered synthetic Rheb binders. (A) Role of Rheb in the mTOR pathway. (B) Previously determined cryo-EM structure of Rheb-mTORC1 (PDB: 6BCU). (C) Multi-point analysis of the indicated Fabs (n = 3, mean ± SD). (D) Single point analysis of the indicated Fabs (n = 3, mean ± SD). (E) scFv engineering for enhanced intracellular expression. (F) Anti-FLAG immunoprecipitation in Expi293F cells expressing the indicated constructs for 48 hours.

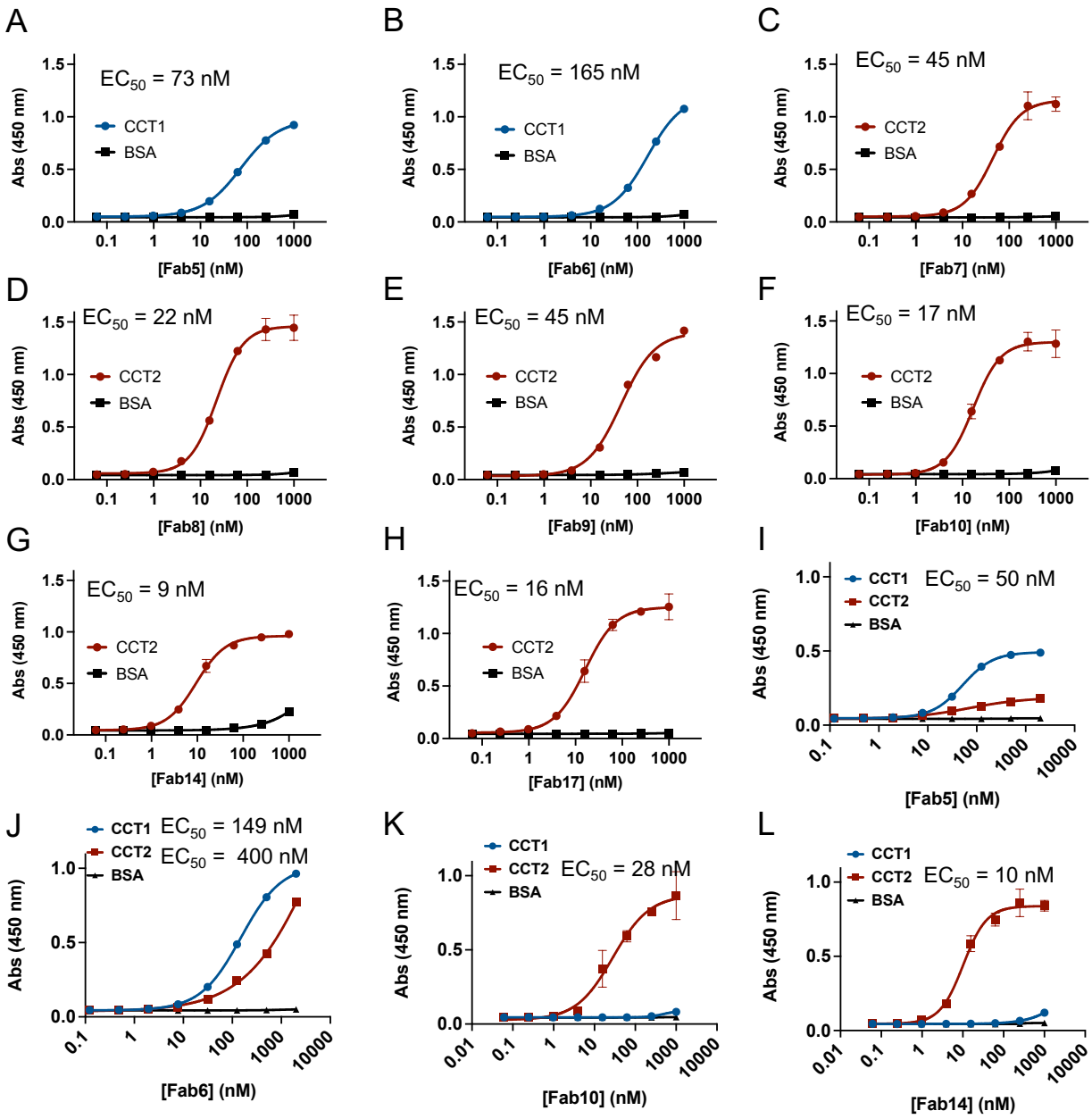

Figure 4.10 Validation of engineered synthetic CCT1/CCT2 binders. (A-B) Multi-point analysis of the indicated Fabs binding to CCT1 (n = 3, mean ± SD). (C-H) Multi-point analysis of the indicated Fabs binding to CCT2 (n = 3, mean ± SD). (I-L) Multi-point analysis of the indicated Fabs binding to CCT1 or CCT2 (n = 3, mean ± SD).

Multi-point ELISA showed EC_{50} values from 7.9 nM to 238 nM for five unique Fabs targeting Rheb (Figure 4.9C). Conceptually, even weak binders in the range of 200-1000 nM could still retain the capability to engage their target in the tightly packed intracellular environment due to high local concentrations. Three of these Fabs exhibited no sensitivity to the ion- or nucleotide-bound state of Rheb, which suggested that their epitopes do not overlap with the nucleotide binding region (Figure 4.9D). Fab-RA2 displayed the strongest binding properties overall but exhibited very poor intracellular expression levels in scFv format. Adding net negative charge to scFv-RA2 through two mutations of serine or asparagine to aspartate improved the intracellular solubility levels of scFv-RA2 (Figure 4.9E). To test whether engagement of Rheb by scFv intrabodies could disrupt the mTOR-Rheb interaction, an anti-FLAG immunoprecipitation was performed in Expi293F cells transfected with intrabodies for 48 hours. These results showed that scFv-$RA2^{DD}$, scFv-B1.2, scFv-D2, and scFv-E2 co-immunoprecipitated various amounts of mTOR. However, these results remain inconclusive until further experiments will be performed to assess whether equivalent amounts of Rheb were pulled down. It is difficult to determine whether the amount of mTOR pulled down is due to the off-rate kinetics of intrabodies or due to selective disruption of the mTOR-Rheb interaction. Nevertheless, these results demonstrated a feasible approach for rapidly engineering synthetic binders against a selected component in the mTOR pathway that can be completed in a matter of weeks.

Multi-point ELISA for two Fabs generated against CCT1 showed EC_{50} values of 73 nM to 165 nM while five Fabs generated against CCT2 showed EC_{50} values from 9 nM to 45 nM (Figure 4.10A-L). These results demonstrated that the selection against CCT2 resulted in the isolation of tighter binders. Although sequence identity between CCT1 and

CCT2 is only 35%, Fab6 exhibited modest cross-reactivity between the two (Figure 4.10J). The affinities were substantially lower than typical “tight” binders but could be sufficient for intracellular engagement of the targets. Overall, this selection served as another example of rapid synthetic binder engineering against critical components in the mTOR pathway. Rheb and CCT1/CCT2 binders should be validated for intracellular target engagement and capability for modulating mTOR function in cells in future studies.

4.4 Discussion

Small molecule drug discovery efforts take on average 12-15 years and can cost up to $2.8 billion (152). This typically consists of screening thousands to millions of new compounds coupled with evaluation of cell modulation. This sort of procedure is useful to screen compounds against novel therapeutic targets. However, there are a number of attractive drug targets that have been known for decades for which small molecule inhibitor development has reached limited success. Examples of oncogenic targets often considered “undruggable” are KRAS, p53, MYC, or SHP2 (153). These examples demonstrate that high-throughput screening technologies are sometimes insufficient to effectively design small molecule inhibitors against a target of interest.

One strategy to address these limitations is to exploit protein engineering to gain molecular insight into vulnerabilities in undruggable targets. This was recently demonstrated by the generation and characterization of monobodies that selectively engage KRAS bearing specific cancer-associated mutations (116). Other studies have shown the feasibility of engineering synthetic binders to engage selected proteolytic epitopes or post-translational modifications of a target antigen (154, 155). Moreover, the

engineering and characterization of $mTOR^{FRB}$ binders described in chapters 2 and 3 demonstrated the utility of targeting specific conformational states. However, a major limitation in drug discovery efforts is the identification and validation of effective druggable interfaces. For promising therapeutic targets that have not reached the level of predicted clinical success, such as mTOR, the discovery of new targetable approaches could reinvigorate drug design efforts.

Here, the FRB substrate recruitment domain of mTOR was exploited to generate epitope-directed synthetic Fabs that bind to sites for which no conventional inhibitors currently exist. Crystal structure determination of Fab-1A and Fab-2C bound to $mTOR^{FRB}$ delineated the structural basis for targeted engagement of two distinct epitopes. Immunoprecipitation studies revealed that the Fab-2C epitope is obstructed by assembly of mTOR into its cognate complexes, which was reversed by acute treatment with rapamycin. This finding suggested that rapamycin-induced destabilization of the mTOR-Raptor interaction provided access to the Fab-2C epitope. Interchangeability between Fab and scFv format enabled rapid investigation into the cellular activity for these binders. This was revealed by cell-based assays to validate the capability for intrabodies to modulate mTOR complex assembly and substrate phosphorylation. These efforts demonstrated potent efficacy mTORC1 inhibition through the direct obstruction of the mTOR-Raptor interaction by scFv-2C. Furthermore, phage display campaigns were performed to rapidly generate synthetic binders against two other targets related to mTOR complex assembly and substrate phosphorylation, Rheb, and CCT/TRiC, which demonstrated the generality and feasibility of this approach.

This approach could be extended to target multiple different components comprising mTORC1 and mTORC2 assemblies. There are many unanswered questions in regard to the specific mechanisms of recruitment and phosphorylation of mTORC1 and mTORC2 substrates. The mutual exclusivity in mTORC1/mTORC2 substrate phosphorylation has been suggested to emerge from interactions by the subunits Raptor, Rictor, and mSin1. However, cell-based dissection of these processes is not trivial. The work described in this thesis demonstrates that synthetic intrabodies can be employed to bind and mask specific epitopes involved in mTOR substrate recruitment. By targeting epitopes located on substrate-recruiting binding partners in mTORC1/mTORC2, intrabodies are capable of revealing crucial insight into how mTOR substrate recruitment mechanisms could potentially be decoupled and exploited from a therapeutic standpoint. Furthermore, insight into how mTORC1 and mTORC2 signaling can be functionally decoupled could be investigated by using synthetic intrabodies to elicit drug-like perturbations against myriad upstream sensors or downstream effectors in the mTOR pathway.

Future studies should investigate the effects of scFv-1A and scFv-2C on mTORC2 assembly by using immunoprecipitation and western blotting. Crystal structure analysis suggests that scFv-2C should be a potent inhibitor of the mTOR-Rictor interaction by an obstructive mechanism of action. Furthermore, investigating the effect of scFv-1A and scFv-2C on mTORC1 substrate phosphorylation should be pursued. Rapamycin and scFv-R3E9/scFv-R3H8 do not inhibit all mTORC1 substrates, such as 4E-BP1. If scFv-2C expression inhibits substrates including 4E-BP1, it could serve as a valuable intrabody-based tool to investigate rapamycin-resistant mechanisms involved in mTOR signaling.

4.5 Materials and methods

Generation of DNA constructs. The In-Fusion HD Cloning Kit (Takara Bio) was used for all PCR and ligation reactions described here. SNAP-tagged FKBP12 and the FRB domain of mTOR (*H. sapiens* and residues corresponding to 2021-2113) were generated by cloning PCR inserts into the SmaI site of the pEKD40 expression vector. A gBlock (IDT) encoding FKBP12-$(G_4S)_4$-FRB was designed and cloned into the SmaI site of pEKD40. These constructs bear C-terminal 6xHis-tags. $mTOR^{FRB}$ was also cloned into BamHI/XhoI sites of the pHFT2 expression vector with an N-terminal 10xHis-tag and TEV cleavage site. Sequences encoding Rheb, CCT1, and CCT2 were designed as gBlocks (IDT) and cloned into the pHFT2 expression vector. The Rheb construct contained the following tags on the N-terminus: 6xHis-tag, AviTag, and TEV cleavage site. CCT1 and CCT2 constructs contained the following tags on the C-terminus: AviTag, TEV cleavage site, 6xHis-tag. Synthetic antibody fragment (Fab) PCR inserts were generated by PCR from unique phage clones and ligated into SphI sites of the pSFV4 expression vector (AviTag). Mutagenesis was performed to incorporate point mutations or the “crystal kappa” sequence into Fab scaffolds according to the QuikChange Site-Directed Mutagenesis Kit (Agilent) (148). Single chain variable fragments were generated by cloning unique VH domains into XhoI/BamHI sites of the scFv-R3E9 construct. CDR-L3 was mutated by a combination of PCR and In-Fusion ligation.

Phage display selection. Phage display selection was performed according to previously protocols (127). Prior to library sorting, SNAP-$mTOR^{FRB}$ and SNAP-FKBP12-$mTOR^{FRB}$ were site-specifically biotinylated by incubation with SNAP-Biotin (NEB)

according to the manufacturers protocol. Biotinylated SNAP-mTOR^{FRB} (Bio-SNAP-mTOR^{FRB}) or SNAP-FKBP12-mTOR^{FRB} (Bio-SNAP-FKBP12-mTOR^{FRB}) underwent solid support immobilization using Streptavidin MagneSphere Paramagnetic Particles (Promega) throughout five rounds of phage display biopanning. Prior to each round of library sorting, phage libraries were incubated with Hisx6-tagged SNAP-mTOR^{FRB} and SNAP-FKBP12 with no rapamycin for 30 minutes at room temperature with constant rotation. TALON cobalt-NTA affinity resin (Takara) was added for 15 minutes. Unbound phage were passed through the resin into a fresh collection tube using centrifugation. The first round of phage panning was initiated by immobilizing 1 μM of Bio-SNAP-mTOR^{FRB} with SNAP-FKBP12 or Bio-SNAP-FKBP12-mTOR^{FRB} onto streptavidin magnetic beads in the presence of 500 nM rapamycin. These targets were incubated together with 2 μM non-biotinylated SNAP for 1 hour with pre-cleared phage libraries. Unbound phage were washed before adding beads to log phase *E. coli* XL-1 blue cells (Stratagene) for infection. Ampicillin (0.1 mg/mL) and M13K07 helper phage (NEB) were added to cells for amplification overnight at 250 rpm shaking at 37°C . Phage precipitation was performed using 20% PEG, 2.5 M NaCl with post-centrifugation cell supernatant (1:5 ratio) for 20 minutes on ice. The concentration of Bio-mTOR^{FRB} or Bio-SNAP-mTOR^{FRB} was incrementally reduced from 1 μM in the first round to 10 nM in the fifth round while maintaining 2 μM non-biotinylated SNAP and performing library pre-clearance against SNAP-FKBP12 and SNAP-mTOR^{FRB} before each round. Eluted phage from fourth and fifth rounds were used to infect cells for individual colony isolation and characterization using single point phage ELISA. Phage clones that exhibited binding were sequenced and reformatted for recombinant Fab expression.

Enzyme-Linked Immunosorbent Assays (ELISA). For phage ELISA, Bio-SNAP-mTOR^{FRB} or Bio-SNAP-mTOR^{FRB} (20 nM) were immobilized for 30 minutes onto neutravidin coated high binding 96-well microplates (Greiner Bio). Plates were washed and blocked for 1 hour with 1% BSA in PBS. Phage were diluted 1:5 in 0.5% BSA/PBST, added to plates for 15 minutes, washed three times with 0.1% BSA/PBST, incubated with 1:5000 diluted Protein L-HRP (Thermo Scientific) for 20 minutes, and washed three times with 0.1% BSA/PBST before addition of the chemiluminescent TMB substrate (Thermo Scientific). Wells were quenched using 10% H_3PO_4 and absorbance was measured at 450 nm. For ELISA using purified Fabs, 200 nM SNAP, SNAP-FKBP12, SNAP-mTOR^{FRB}, or SNAP-FKBP12 with SNAP-mTOR^{FRB} were immobilized directly to 96-well plates. PBS supplemented with 0.05% Tween 20 was used for washing between each step unless indicated otherwise. After target immobilization, the plates were washed with PBS and blocked using 1% BSA in PBS for 1 hour. Fabs were diluted in PBS/0.05% Tween 20/0.5% BSA before incubating for 20 minutes. For competition ELISA, competitors were added first to the plates for 15 minutes before adding biotinylated Fabs directly to wells without washing in between. Secondary detection and absorbance measurement was performed as described above with the exception of using streptavidin-HRP for the competition ELISA experiments.

Cell culture and transfections. The cell lines used in this chapter were Expi293F (Thermo Fisher Scientific) and HeLa (ATCC). These were cultured according to the manufacturer's protocol using Expi293 Expression Medium and Dulbecco's modified

Eagle medium (DMEM) supplemented with 10% fetal bovine serum and 1% Pen-Strep (Gibco), respectively for Expi293F and HeLa. Expi293F transfections were carried out with the ExpiFectamine 293 Transfection Kit (Thermo Fisher Scientific) for 24-48 hours following the manufacturer's recommendations. Transfection enhancers were disregarded here. HeLa transfections in were carried out with Lipofectamine LTX Reagent with PLUS Reagent (Thermo Fisher Scientific) for 24-48 hours following the manufacturer's recommendations.

Immunoprecipitation and western blot analysis. Ice cold PBS was used to wash cells one time before harvesting for immunoprecipitation or western blot analysis. HeLa cells were lifted by trypsin digestion. The lysis buffer used here included 0.3% CHAP, 25 mM TRIS, pH 8.0, 150 mM NaCl, 5 mM EDTA, and 1x Halt Protease Inhibitor Cocktail to maintain the integrity of mTORC1 throughout immunoprecipitation procedures. Cells were incubated with lysis buffer for 20 minutes on ice. Lysates were clarified using centrifugation at 14,000 rpm at 4°C. Total protein quantification was performed using the BCA method (Thermo Scientific). Immunoprecipitations using biotinylated Fabs were carried out for 1 hours with gentle rocking at 4°C. Magnetic streptavidin beads (Invitrogen) were washed three times in lysis buffer and added to cell lysates for 1 hour with rotation at 4°C. Samples were washed using lysis buffer for a total of five times before boiling samples for 5 minutes in SDS sample buffer supplemented with 10 mM DTT. Anti-FLAG immunoprecipitation from Expi293F cells transfected with FLAG-tagged intrabodies were carried out by equilibrating 30 µL of Anti-DYKDDDDK G1 Affinity Resin (Genscript) per sample in lysis buffer. Equilibrated resin was added to cell lysates for 3 hours with gentle

rocking at 4°C. Lysis buffer was used to wash samples five times before adding SDS sample buffer for elution via boiling for 5 minute. After transferring to a fresh tube, each sample was adjusted to a final concentration of 10 mM DTT. SDS-PAGE was performed at 100V. Samples separated on gels were transferred to Immobilin-P PVDF Membranes (0.45 μm, EMD Millipore) at 100V for 1 hour. Membranes were blocked (5% BSA in PBS supplemented with 0.1% Tween 20) for 1 hour at room temperature. Western blot detection was performed using the following primary antibodies from Cell Signaling Technology: FLAG (#14793S), Tubulin (#2148S), p-S6K1^{T389} (#9234S), S6K1 (#2708T), mTOR (#2972S), Raptor (#2280S), and mLST8 (#3274S). Blocking buffer was use dto dilute primary antibodies, which were added to membranes at 4°C for overnight incubation with constant agitation. Wash buffer (PBS supplemented with 0.1% Tween 20) was used to wash membranes were 3-4 times. Anti-Rabbit IgG, HRP-Linked Antibody (Cell Signaling Technology, #7074P2) was diluted in blocking buffer and added at room temperature for one hour before washing 3-4 times. SuperSignal West Pico PLUS Chemiluminescent Substrate (Thermo Fisher Scientific) was used to image membranes.

Immunofluorescent staining and confocal microscopy imaging. IbiTreat μslide 8-Well slides (Ibidi) were used to grow HeLa cells in Dulbecco's modified Eagle medium (DMEM) supplemented with 10% fetal bovine serum and 1% Pen-Strep (Gibco). Cells were transfected once they reached 80-90% confluency. Confocal microscopy imaging was performed on the Stellaris 8 (Leica). FIJI was used for all quantitative analyses (128). Cells were fixed in 4% paraformaldehyde for 10 minutes at room temperature. PBS was used to wash three times before adding 3% BSA, 0.3% Triton X-100 for 1 hour at room

temperature for blocking and permeabilization. 1% BSA, 0.3% Triton X-100 was used to dilute p-S6$^{S240/244}$ Rabbit IgG (Cell Signaling Technology, #5364) before adding overnight at 4°C to fixed cells. The next day, PBS was used to wash three times for five minutes each. 1% BSA, 0.3% Triton X-100 was used to dilute Goat Anti-Rabbit IgG (H+L) conjugated with Alexa647 (Jackson ImmunoResearch) before adding for 1 hour at room temperature. PBS was used to wash three times for five minutes each. DAPI (1 µg/µL, Thermo Fisher Scientific) was added for 10 minutes. PBS was used to wash three times before a final addition of PBS in 50% glycerol.

Crystallization and structure determination. Fab-1A and Fab-2C were modified to incorporate the "crystal kappa" light chain modification prior to crystallization. Fab-1A•mTOR^{FRB} and Fab-2C•mTOR^{FRB} complexes were purified by size exclusion chromatography (SEC) in 10 mM HEPES, pH 7.2, 150 mM NaCl using a Sephadex 200 column. Pure complexes were concentrated to at least 15-20 mg/mL prior to crystallization screening. This screening was facilitated by the use of the Mosquito Crystal Robot (TTP Labtech). Crystallization conditions for the Fab-1A•mTOR^{FRB} complex were 0.2 M ammonium citrate dibasic, 20% PEG 3350. No cryoprotectant was used before flash freezing crystals in liquid nitrogen for data collection. Crystallization conditions for the Fab-2C•mTOR^{FRB} complex were 0.2 M sodium tartrate dibasic, 20% PEG 3350. Again, crystals were flash frozen directly in liquid nitrogen with no cryoprotectant being used. X-ray diffraction data were collected at the Brookhaven National Laboratory NSLS-II Beamline 17-ID FMX. Structures of Fab-1A•mTOR^{FRB} and Fab-2C•mTOR^{FRB} were solved using molecular replacement with previously determined Fab and mTOR^{FRB}

structures (PDB: 9DBO and PDB: 9DL0) as models in Phaser-MR (129). Coot and phenix.refine were used to manually build and refine structures (130, 131). PyMOL was used to generate all structural figures in this chapter.

Chapter 5

An antibody-based mTOR inhibition sensor based on logic-gated molecular recognition of the FKBP12-Rapamycin-mTOR ternary complex

Kelly M. O'Leary[1], Tomasz Slezak[1], and Anthony A. Kossiakoff[1,2,*]

[1]Department of Biochemistry and Molecular Biology, The University of Chicago, Chicago, IL 60637.

[2]Institute for Biophysical Dynamics, The University of Chicago, Chicago, IL 60637.

*Correspondence to: Anthony A. Kossiakoff

5.1 Abstract

This chapter describes a novel approach to study molecular glue-induced interactions using an engineered synthetic antibody with conditionally gated recognition properties. Rapamycin is a potent FKBP12-dependent inhibitor of mechanistic target of rapamycin (mTOR) with promising anti-aging effects in diverse eukaryotic model organisms. However, deleterious metabolic side effects stemming from systemic mTOR inhibition have raised concerns about the therapeutic efficacy of rapamycin. The creation of new therapeutics that exploit the beneficial effects of rapamycin while minimizing toxicities is dependent on a deeper understanding of the molecular mechanisms involved in mTOR inhibition by rapamycin. Here, a customized phage display library sorting procedure was employed to generate a synthetic antibody (Fab-4R) with selective recognition properties for the drug-induced FKBP12-rapamycin-mTOR complex but not FKBP12 or mTOR alone. Biophysical and structural characterization illustrated how Fab-4R recognition is mediated by a two-residue hydrophobic clamp in CDR-H3 positioned directly across the interface of FKBP12 and mTOR. Cell-based immunoprecipitation assays revealed the highly sensitive capability of Fab-4R to engage with the FKBP12-rapamycin-mTOR complex and report the modulation of core mTOR protein-protein interactions. Together, these results establish a novel and versatile molecular tool for fine-tuned sensing of FKBP12-dependent mTOR inhibition by rapamycin.

5.2 Introduction

Eukaryotic cell growth and metabolism are tightly coupled to the abundance of environmental nutrients (18). Cell growth processes require the coordination of many different signaling pathways involving biosynthesis or recycling of basic macromolecules, including nucleic acids, lipids, and proteins (156). Mechanistic target of rapamycin (mTOR) is an evolutionarily conserved PI3K-related serine/threonine protein kinase that integrates signals from nutrients, growth factors, energy, oxygen, and stress to orchestrate the balance between cellular anabolism and catabolism (32). Dysregulated mTOR activity is linked to many human diseases including cancer, diabetes, neurodegenerative disorders, and physiological aging (47). Therefore, the mechanisms by which mTOR senses upstream nutritional cues and transduces them into downstream physiological responses represent a major focus for understanding the physiology of disease progression.

The function of mTOR is dependent on a set of finely balanced cognate protein-protein interactions. mTOR functions as the core catalytic subunit in two structurally and functionally distinct multi-subunit assemblies known as mTOR complex1 (mTORC1) and mTOR complex 2 (mTORC2) (45, 157). mTORC1 is characterized by the association of mTOR with mammalian lethal with SEC13 protein 8 (mLST8) and regulatory-associated protein of mTOR (Raptor) (59). In contrast, mTORC2 is composed of mTOR, mLST8, rapamycin-insensitive companion of mTOR (Rictor), and mammalian stress-activated map kinase-interacting protein 1 (mSin1) (158). Together, these obligate binding partners influence mutually exclusive subcellular localization and substrate recruitment

mechanisms underlying the function of mTORC1 and mTORC2 despite the fact that these assemblies share the same catalytic subunit.

Rapamycin is a macrocyclic lactone natural product that functions as a bifunctional molecular glue by employing specific binding moieties for both FKBP12 and mTOR (144). Rapamycin was one of the first described molecular glue compounds and served as a crucial tool for the discovery of mTOR biology (4, 9, 159). The mechanism of inhibition by rapamycin has been thoroughly described. Similar to the natural product and potent immunosuppressant FK506, rapamycin binds with sub-nanomolar affinity to the peptidylprolyl isomerase FKBP12 (160). The FKBP12-rapamycin complex then binds to the FKBP12-rapamycin binding (FRB) domain of mTOR ($mTOR^{FRB}$) where it obstructs access of some mTORC1 substrates into the active site (66). The non-catalytic basis of this mechanism renders rapamycin an incomplete inhibitor of mTOR function, which has been suggested to be responsible for its unique therapeutic profile relative to ATP-competitive mTOR inhibitors (90).

Inhibition of mTOR by FKBP12-rapamycin also remodels the interactions of core mTORC1 and mTORC2 subunits, Raptor and Rictor, through distinct mechanisms. Engagement of FKBP12-rapamycin with mTORC1 results in rapid destabilization of the mTOR-Raptor interaction (133, 157). Although this phenomenon has been described for decades, the molecular basis underlying allosteric modulation of Raptor by FKBP12-rapamycin remains unresolved. In contrast, mTORC2 is acutely insensitive to rapamycin inhibition because the FKBP12-rapamycin binding site is masked by Rictor (62). Over longer periods of exposure, FKBP12-rapamycin complexes bind to newly synthesized mTOR molecules and obstruct the assembly of Rictor onto mTORC2 (134). However,

some cell lines exhibit resistance to mTORC2 inhibition by rapamycin while others are highly sensitive, illustrating the complex landscape of rapamycin's activity (161). The mechanism of inhibition by rapamycin therefore exploits a complex interplay between structural, temporal, and other unknown factors.

The clinical implementation of pharmacological mTOR inhibitors has met significant barriers. Rapamycin and rapamycin-derived analogs (e.g., Everolimus and Temsirolimus) are approved by the U.S. Food and Drug Administration for treatment of organ transplant rejection, various cancers, and other growth disorders including tuberous sclerosis complex and lymphangioleiomyomatosis (50, 162). However, the complex interplay between rapamycin and tissue-specific pleiotropic mTOR functions can result in on-target toxicities stemming from systemic inhibition. This is exemplified by the potent capability of rapamycin to modulate the immune system, which can lead to beneficial physiological effects in adipose tissue and liver while also impairing wound healing (163–165). Furthermore, both sex- and tissue-specific effects have been observed in regard to dysregulated mTOR activity and response to rapamycin in mice or fruit flies (166, 167).

Currently, there is no tool to selectively isolate mTOR complexes bound by FKBP12-rapamycin from cells, which limits molecular insight into other factors involved in rapamycin-based mTOR functional modulation. Therefore, the development of a high-performance affinity reagent that enables selective purification FKBP12-rapamycin-mTOR complexes could be a valuable research and diagnostic tool. Traditional immunization and hybridoma approaches to generate monoclonal antibodies suffer from time, cost, and lack of control over antigen properties. Without the incorporation of negative selection strategies, the total epitope landscape accessible by animal-generated

antibodies is limited. In contrast, the modular capability of phage display enables fine-tuned control over target antigen properties throughout library sorting procedures. Subtractive selection strategies enable depletion of binders that cover canonical single-domain epitope space, thereby allowing for the enrichment of binders with specific recognition for a protein heterocomplex.

Synthetic antibodies generated by phage display have been consistently exploited as powerful tools to enable studies into the biology and structure of multi-subunit protein complexes. The advantages of using customized antibodies for endogenous immunoprecipitation over heterologous epitope tagged affinity pull-downs are summarized in the following points. First, maintaining the equilibrium of native protein complexes and subpopulations within complexes is critical to avoid stoichiometric artifacts. Second, there is no need to include epitope tags which might alter structural associations. Third, off-the-shelf affinity reagents enable rapid and reproducible analyses that are amenable to genetically unmodified cells or patient-derived tissues.

Here, a customized phage display biopanning strategy was employed that depletes phage bound to FKBP12 or mTOR^{FRB} in a subtractive selection step before enriching the remaining phage pool for binders against the FKBP12-rapamycin-mTOR^{FRB} ternary complex. Fab-4R was identified as a binder with high selectivity for the ternary complex relative to single domain. The molecular basis of FKBP12-rapamycin-mTOR^{FRB} recognition by Fab-4R was delineated using X-ray crystallography, biophysical binding characterization, and cell-based immunoprecipitation assays. This work sheds light on the principles governing logic-gated molecular recognition of a unified epitope comprising two distinct molecular glue-bound antigens. Future endeavors to engineer complex-

specific affinity reagents may benefit from incorporating this generalizable pipeline and could reveal new perspectives into the mechanism of action of poorly understood molecular glue inhibitors.

5.3 Results

5.3.1 Phage display selection of a synthetic antibody fragment with selective FKBP12-Rapamycin gated recognition for mTOR

The FKBP12-rapamycin binding (FRB) domain of mTOR ($mTOR^{FRB}$) and the 12-kDa FK506 binding protein (FKBP12) were used as targets for phage display biopanning. Site-specific biotinylation was performed to generate biotinylated SNAP-tagged $mTOR^{FRB}$ (Bio-SNAP-$mTOR^{FRB}$) and SNAP-tagged FKBP12-$(G_4S)_4$-$mTOR^{FRB}$ (Bio-SNAP-FKBP12-$mTOR^{FRB}$) targets (Figure 5.1A). Immobilization of these targets using streptavidin magnetic beads enabled fine-tuned control over ternary complex formation. The ability to precisely induce FKBP12-$mTOR^{FRB}$ heterocomplex formation by the addition of rapamycin was exploited to engineer conditionally gated binders that interact only with the FKBP12-rapamycin-$mTOR^{FRB}$ ternary complex. Four different sets of library sorting conditions were tested in independent biopanning workflows (Figure 5.1B). To begin each round of biopanning, subtractive selections were performed to deplete phage libraries of binders that recognize accessible epitopes on the individual domains of FKBP12 and $mTOR^{FRB}$. Subsequently, the remaining phage pool was enriched on FKBP12 and $mTOR^{FRB}$ in the presence of 500 nM rapamycin to isolate binders that

A

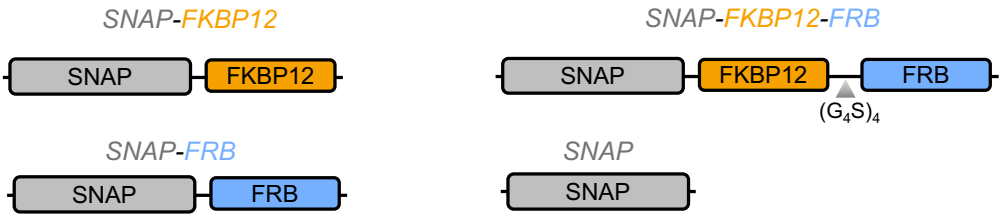

B

	Phage display selection conditions			
	1	2	3	4
Target construct	FKBP12 + FRB	FKBP12 + FRB	FKBP12 + FRB	FKBP12-FRB
Rounds	5	5	5	5
Final [Target]	10 nM	10 nM	10 nM	10 nM
Subtractive selection	–	FKBP12 + FRB	–	FKBP12 + FRB
Competition	SNAP	SNAP	SNAP + Mut	SNAP
Positive selection	500 nM Rap	500 nM Rap	500 nM Rap	500 nM Rap

C

	Selection conditions			
	2		4	
Biotinylated target (500 nM rap)	SNAP-FKBP12 + SNAP-FRB		SNAP-FKBP12-FRB	
Non-biotinylated competitor	SNAP		SNAP	
Library clearance (No rap)	SNAP-FKBP12 + SNAP-FRB		SNAP-FKBP12 + SNAP-FRB	
[Target] (nM)	0	10	0	10

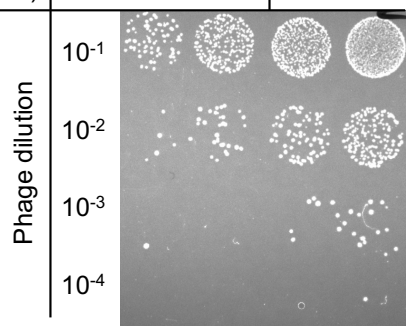

D

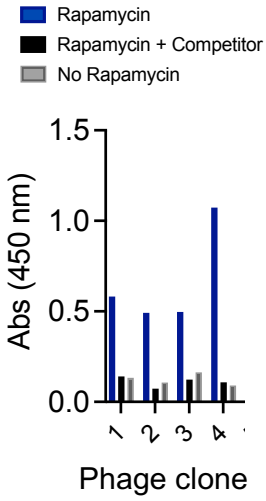

Figure 5.1 Phage display selection strategy for generating complex-specific binders. (A) Construct domain maps for the targets used in phage display. (B) Selection conditions for generating complex-speicfic binders against the rapamycin-induced FKBP12-mTOR^{FRB} complex. (C) Phage titer resulting from five rounds of biopanning from selection conditions 2 and 4. (D) Competitive phage ELISA evaluation of four unique clones identified by DNA sequencing.

recognize epitopes unique to the FKBP12-rapamycin-mTOR^{FRB} complex. This process was repeated for five iterative rounds and exhibited successful outcomes for two out of four selection conditions tested (Figure 5.1C). Four unique phage clones were identified and assessed by phage ELISA for binding to a mixture of FKBP12 and mTOR^{FRB} in the presence or absence of rapamycin (Figure 5.1D). These clones were reformatted for recombinant expression as Fabs and tested for binding properties. Clones 1 and 2 were described in chapter 4 as Fab-1A and Fab-2C, respectively. Clone 3 exhibited no binding in Fab format. Clone 4 will be described in the remainder of this chapter and is referred to as Fab-4R.

These efforts resulted in the isolation of a synthetic antibody fragment (Fab-4R) with highly selective recognition properties for the rapamycin-induced FKBP12-mTOR complex (Figure 5.2A-D). At a concentration of 50 μM, Fab-4R exhibited no binding against individual targets of FKBP12 or mTOR^{FRB} but showed robust binding against FKBP12 and mTOR^{FRB} in the presence of rapamycin (Figure 5.2E). These results confirmed that Fab-4R recognition is highly selective for ternary complex formation. Surface plasmon resonance (SPR) was used to determine binding kinetic parameters for Fab-4R binding to FKBP12-rapamycin-mTOR^{FRB}. This experiment revealed a dissociation constant (K_D) of 8.2 nM between Fab-4R and FKBP12-rapamycin-mTOR^{FRB}, confirming the multi-point ELISA results for this interaction (Figure 5.2F). The association and dissociation curves were fit according to a 1:1 binding model, suggesting that the Fab-4R paratope mediates recognition through a unified epitope spanning the interface between FKBP12 and mTOR^{FRB}. Lastly, multi-point ELISA showed that Fab-4R binds to FKBP12-rapamycin-mTOR^{FRB} with an EC_{50} value of 13.2 nM (Figure 5.2G-I). Here, Fab-

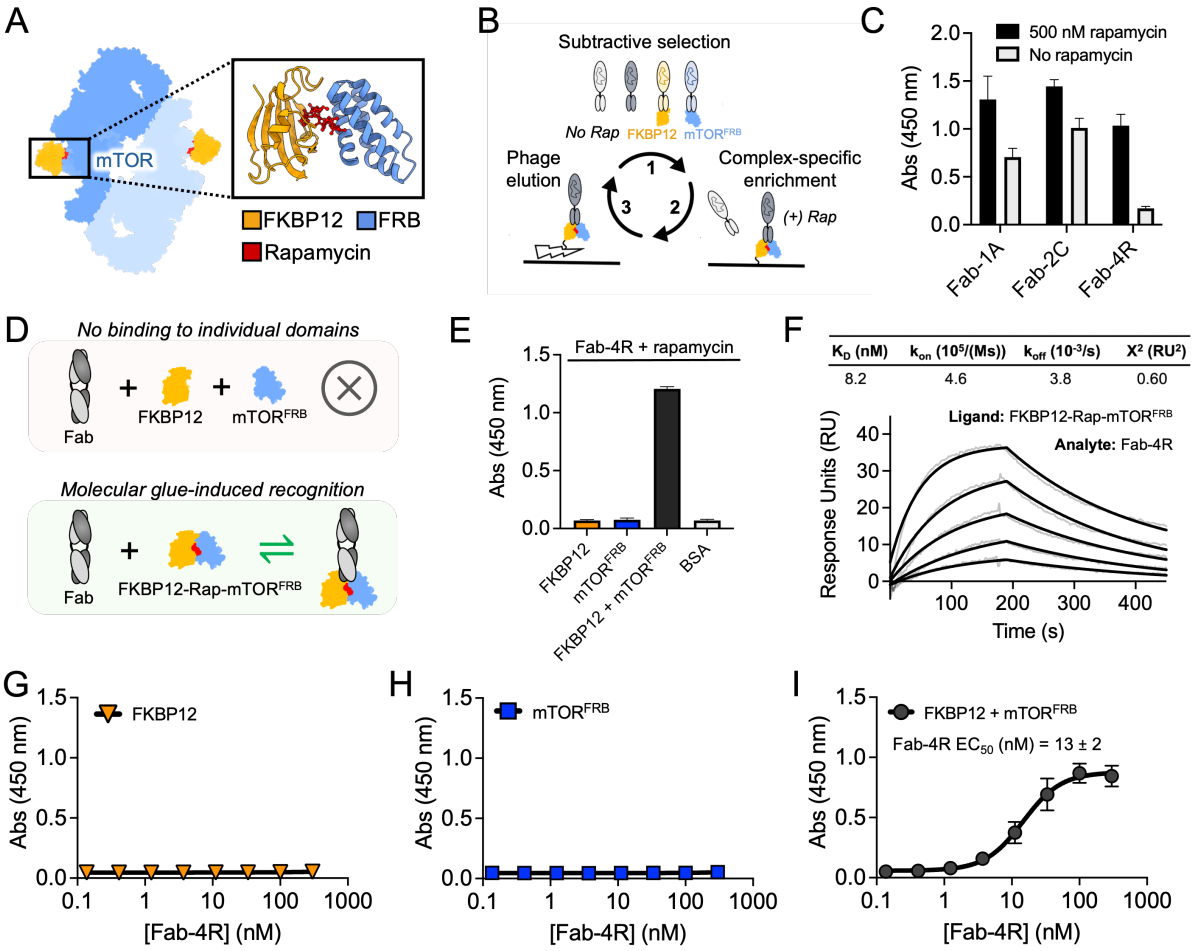

Figure 5.2 A synthetic antibody fragment with rapamycin-gated recognition of mTOR. (A) Representation of the FKBP12-Rapamycin-FRB ternary complex (PDB 6BCX; Raptor and mLST8 omitted). (B) Phage display biopanning strategy for enrichment of binders against the ternary complex of FKBP12, rapamycin, and the FRB domain of mTOR (mTOR^{FRB}). (C) Single point ELISA for the indicated Fabs at 50 nM against FKBP12 and mTOR^{FRB} in the presence of 500 nM rapamycin or no rapamycin (n = 2 technical replicates, mean ± SD). (D) Schematic showing the desired recognition properties for complex-specific binders. (E) Single point ELISA measuring Fab-4R binding at a concentration of 50 μM against the indicated targets in the presence of 500 nM rapamycin (n = 3 technical replicates, mean ± SD). (F) Binding kinetics and multi-point SPR sensorgrams of the interaction between Fab-4R and the ternary complex of FKBP12-rapamycin-mTOR^{FRB}. His-tagged FKBP12 and mTOR^{FRB} were immobilized on the NTI sensor surface. 200 nM rapamycin was included in all samples and the running buffer. (G) Multi-point ELISA for Fab-4R binding against FKBP12 alone in the presence of 500 nM rapamycin (n = 3 independent replicates, mean ± SD). (H) Multi-point ELISA for Fab-4R binding against mTOR^{FRB} alone in the presence of 500 nM rapamycin (n = 3 independent replicates, mean ± SD). (I) Multi-point ELISA for Fab-4R binding against FKBP12 and mTOR^{FRB} together in the presence of 500 nM rapamycin (n = 3 independent replicates, mean ± SD).

4R binding to FKBP12-rapamycin-mTOR^{FRB} was detected at concentrations down to 3.7 nM while no binding was observed against FKBP12 or mTOR^{FRB} alone at Fab-4R concentrations up to 300 nM. Taken together, these results indicated that the dynamic range of Fab-4R recognition selectivity spans approximately four orders of magnitude.

5.3.2 Crystal structure of Fab-4R bound to the FKBP12-Rapamycin-mTOR^{FRB} ternary complex reveals basis of bispecific paratope engagement

Several complex-specific antibodies have been previously reported, but the structural basis of how paratope-epitope interactions mediate selective molecular recognition properties remain poorly understood (168–175). Therefore, the general mechanism by which complex-specific binders engage their cognate epitopes remains unclear. Conceptually, this could be manifested by simultaneously engaging two subunits or by recognizing a state-dependent conformation of one subunit. To gain structural insight into the mechanism of complex-specific recognition, the crystal structure of Fab-4R bound to FKBP12-rapamycin-mTOR^{FRB} was determined at 2.05 Å resolution (Table 5.1). The structure revealed that Fab-4R epitope is located at the vertex of the ternary complex and is completely separated from rapamycin (Figure 5.3A). This region is found on an electrostatically neutral patch spanning the interface of FKBP12 and mTOR^{FRB} (Figure 5.3B). Analysis of direct side chain interactions formed between Fab-4R, FKBP12, and mTOR^{FRB} showed a relatively equal distribution between chains (Figure 5.3C). Fab-4R complementarity determining region- (CDR) L3, CDR-H2, and CDR-H3 form the paratope contacting FKBP12 while CDR-H1, CDR-H2, and CDR-H3 form the paratope contacting mTOR^{FRB} (Fig. 3B). Together, the Fab-4R paratope buries 904 Å^2 solvent

Table 5.1 X-ray diffraction data collection and refinement statistics for the structure of Fab-4R bound to FKBP12-rapamycin-mTOR^{FRB}.

	Fab-4R•FKBP12•Rapamycin•mTOR^{FRB}
Space group	P 1 21 1
Cell dimensions	
a, b, c (Å)	62.7, 72.9, 85.9
α, β, γ (degrees)	90, 103.1, 90
Resolution (Å)	55.7 - 2.05 (2.123 - 2.05)
R_{merge} (%)	8.152 (61.17)
$CC_{1/2}$	99.3 (36.3)
$I / \sigma I$	4.96 (1.33)
Completeness (%)	98.14 (97.97)
Redundancy	1.9 (1.9)
Refinement	
Resolution (Å)	55.7 - 2.05
No. of reflections	46577 (4622)
R-work	0.1796 (0.2813)
R-free	0.2268 (0.3334)
Number of atoms	
Protein	4900
Ligands	65
Waters	557
B-factor	
Protein	35.16
Ligands	28.82
Waters	42.15
R.M.S. deviations	
Bond lengths (Å)	0.007
Bond angles (degrees)	1.23
Ramachandran plot statistics	
Favored (%)	97.44
Allowed (%)	2.56
Outliers (%)	0

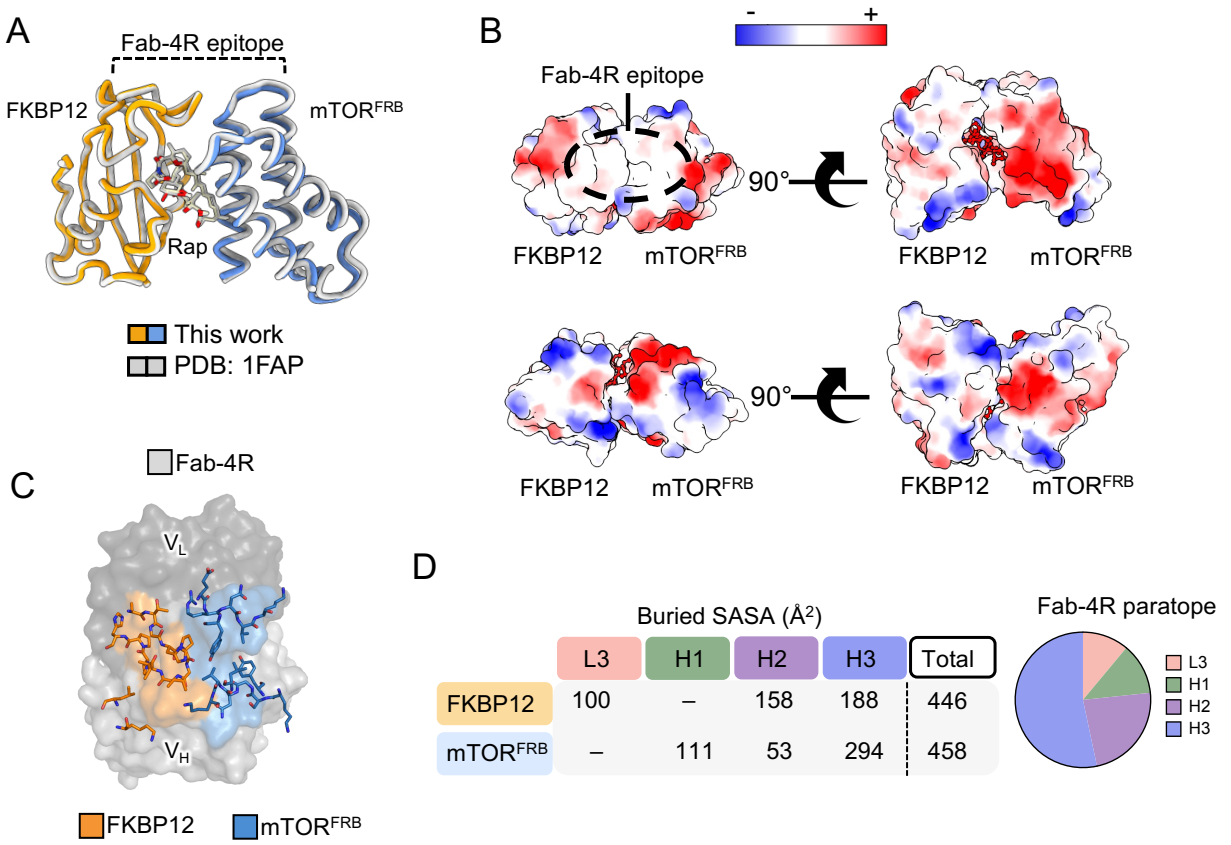

Figure 5.3 Complex-specific Fab-4R epitope characterization. (A) Comparison of FKBP12-rapamycin-mTOR^{FRB} from the structure in this work and from a previously determined structure (PDB: 1FAP). (B) Surface electrostatics show that the Fab-4R epitope is located on a neutral patch. (C) Distribution in direct side chain contacts made by Fab-4R. (D) Quantitative analysis of the Fab-4R paratope and epitope.

accessible surface area (SASA) across a uniform epitope located on the heterocomplex interface of FKBP12 and mTOR^{FRB} (Figure 5.3D).

Analysis of the architecture of the Fab-4R-FKBP12-rapamycin-mTOR^{FRB} complex revealed a delicate balance in CDR positioning over the rapamycin-induced neo-interface between FKBP12 and mTOR^{FRB} (Figure 5.4A). Strikingly equivalent SASA is buried by Fab-4R on each single domain with 446 Å^2 on FKBP12 and 458 Å^2 on mTOR^{FRB}. Given

that an average antibody-antigen interaction buries 1068 ± 314 Å^2, this structural analysis confirms that the sum of all interactions formed between Fab-4R and FKBP12-rapamycin-mTOR^{FRB} falls within the average range (176). In contrast, buried SASA between Fab-4R and the individual domains of FKBP12 or mTOR^{FRB} falls well below the lower end of the average buried SASA range. This supports the results that recognition of FKBP12 or mTOR^{FRB} individual domains by Fab-4R is virtually undetectable. Therefore, the regio-specific balance of paratope-epitope burial alone appears to be a crucial factor driving complex-specific molecular recognition.

Further analyses revealed that a combination of hydrophobic side chain burial and side chain-to-main chain hydrogen bonding is employed by Fab-4R for recognition of the ternary complex. The FKBP12 epitope is mediated primarily by W112^{H3} and S57^{H2} side chain interactions from Fab-4R (Figure 5.4B). Notably, the W112^{H3} side chain is buried (128 Å^2) in a proline-rich loop located on FKBP12 where it forms extensive Van der Waals interactions. W112^{H3} simultaneously forms a hydrogen bond within the hydrophobic pocket to the carbonyl oxygen of I92^{FKBP12}. These interactions appear to be stabilized indirectly by S111^{H3} from Fab-4R, which forms a hydrogen bond with the amide nitrogen of S113^{H3} to form a local kink in CDR-H3. Furthermore, S113^{H3} forms an inter-CDR hydrogen bond with the main chain of S98^{L3}. The proline-rich loop in FKBP12 is also stabilized by a hydrogen bond formed between S57^{H2} and the carbonyl oxygen of G90^{FKBP12}.

The interface between Fab-4R and mTOR^{FRB} originates only one residue downstream with L110^{H3}, which is buried (113 Å^2) into a surface exposed hydrophobic pocket (Figure 5.4C). Additionally, the main chain atoms of L110^{H3} are contacted by a

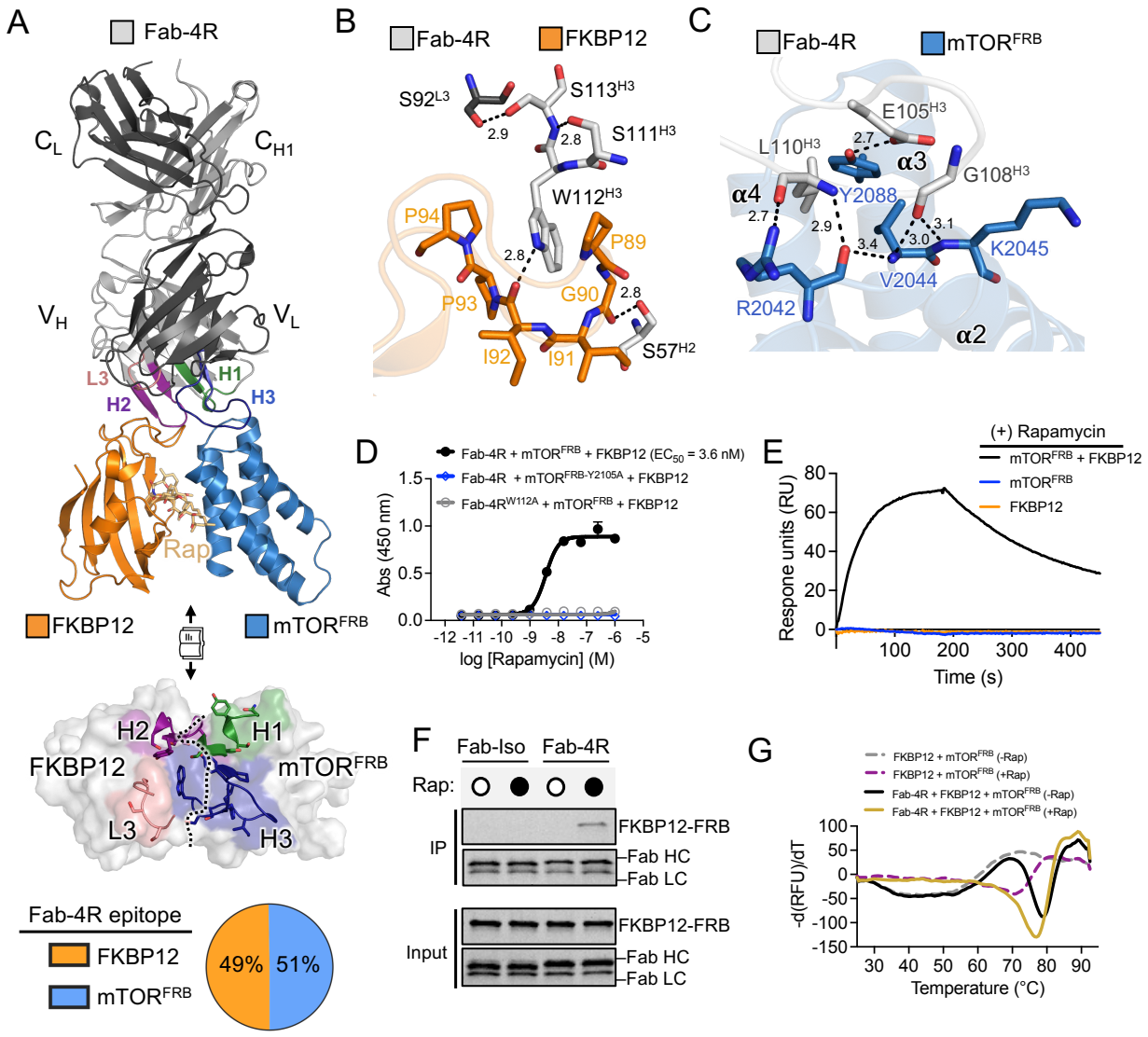

Figure 5.4 A bi-specific paratope in Fab-4R mediates complex-specific recognition. (A) *Top*: Crystal structure of Fab-4R bound to the FKBP12-rapamycin-mTOR^{FRB} ternary complex. *Middle*: Open book view of the Fab-4R paratope (cartoon and sticks) with the FKBP12-rapamycin-mTOR^{FRB} ternary complex (surface). *Bottom*: Percent buried solvent accessible surface area for the Fab-4R epitope between FKBP12 and mTOR^{FRB}. (B) Interactions between Fab-4R and FKBP12. (C) Interactions between Fab-4R and mTOR^{FRB}. (D) Multi-point ELISA rapamycin titration measuring the binding of Fab-4R and mTOR^{FRB} in solution to immobilized FKBP12 (n = 3 technical replicates, mean ± SD). (E) Single point SPR sensorgram for 200 nM Fab-4R binding to mTOR^{FRB}, FKBP12, or mTOR^{FRB} and FKBP12 in the presence of 200 nM rapamycin. (F) In vitro Fab pulldown of a covalently tethered and Alexa488 labeled SNAP-FKBP12-(G$_4$S)$_5$-FRB construct in the absence or presence of rapamycin. G) DSF thermal stability assay for the indicated proteins at 4 μM in the presence or absence of 6 μM rapamycin.

hydrogen bond network formed with $R2042^{FRB}$. The carbonyl oxygen of $L110^{H3}$ is bound by the guanidinium group of $R2042^{FRB}$ while the amide nitrogen of $L110^{H3}$ is bound by the carbonyl oxygen of $R2042^{FRB}$. A main chain-main chain hydrogen bond formed between $G108^{H3}$ and $K2045^{FRB}$ acts as a pseudo-α-helix extension framework on $mTOR^{FRB}$ by mimicking the angle and orientation of intra-α-helical bonds. $E105^{H3}$ forms a hydrogen bond with the hydroxyl group of $Y2088^{H3}$ near the hydrophobic pocket where $L110^{H3}$ is buried. Finally, $Y33^{H1}$ appears to form a planar stacking interaction with $N2093^{FRB}$ (177).

This structure provided critical information to assist interpretations of biophysical binding data for Fab-4R. Rapamycin-dependent recognition of FKBP12 and $mTOR^{FRB}$ was confirmed using multi-point ELISA. At a fixed concentration of 50 nM in solution, Fab-4R showed half maximal binding to FKBP12-rapamycin-$mTOR^{FRB}$ in the presence of 3.6 nM rapamycin (Figure 5.4C). Mutations to abrogate rapamycin binding ($mTOR^{FRB\text{-}Y105A}$) or Fab-4R recognition ($Fab\text{-}4R^{W112A}$) confirmed the specificity of this assay. The Fab-4R epitope spans the interface of FKBP12 and $mTOR^{FRB}$, suggesting that some basal level of affinity must exist between Fab-4R and each individual domain antigen chain. However, no association between Fab-4R and FKBP12 or $mTOR^{FRB}$ was observed by single point SPR at 200 nM in the presence of 200 nM rapamycin (Figure 5.4E). Furthermore, binding of Fab-4R was undetectable to a construct of FKBP12 tethered to $mTOR^{FRB}$ by a 20-residue $(Gly_4Ser)_4$ linker in the absence of rapamycin (Figure 5.4F). This suggested that the binding energy of Fab-4R is insufficient to stably bridge the individual domains of FKBP12 and $mTOR^{FRB}$ together even when they are fixed at a high local concentration. Lastly, Fab-4R did not exert any effect on the thermal stability of FKBP12 and $mTOR^{FRB}$ when incubated together at 4 μM in the absence of rapamycin

(Figure 5.4G). A unified unfolding peak was observed when excess rapamycin (6 μM) was added, suggesting that all three protein components were assembled into a stable complex. The structure-guided biophysical characterization performed here demonstrated that the conditionally gated recognition properties of Fab-4R are mediated by a highly coordinated framework of CDR interactions.

5.3.3 Structure-guided mutagenesis reveals crucial role for a two-residue hydrophobic clamp in ternary complex recognition by Fab-4R

A structural bioinformatics pipeline was employed to gain insight into how the structure of Fab-4R bound to FKBP12-rapamycin-mTOR^{FRB} compares to other high-resolution crystal or cryo-EM structures of antibodies bound to multiple antigens (Figure 5.5A). The Structural Antibody Database (SAbDab) was mined for structures containing Fab, scFv, or nanobody binders in complex with one or more antigens that were determined at ≤ 3.0 Å resolution (178). This resulted in 2,514 total structures. After filtering for structures containing binders that contact two or more antigens simultaneously, this analysis found that 15% of all high-resolution antigen-bound antibody structures exhibit paratope-mediated interactions with two or more antigens (Figure 5.5B). After filtering out repeated structures, the list was reduced to 103 unique structures. These structures were quantitatively evaluated for the fraction of SASA buried in the epitope from each antigen chain (Figure 5.5C and D). This analysis showed that antibodies typically bury SASA with emphasis on one antigen chain (Ag-1) compared to other antigen chains (Ag-2 and Ag-3) found in heterodimeric or heterotrimeric antigen complexes. Specifically, binders bury an average of 72% SASA on Ag-1 compared to 28% SASA on Ag-2 in heterodimeric

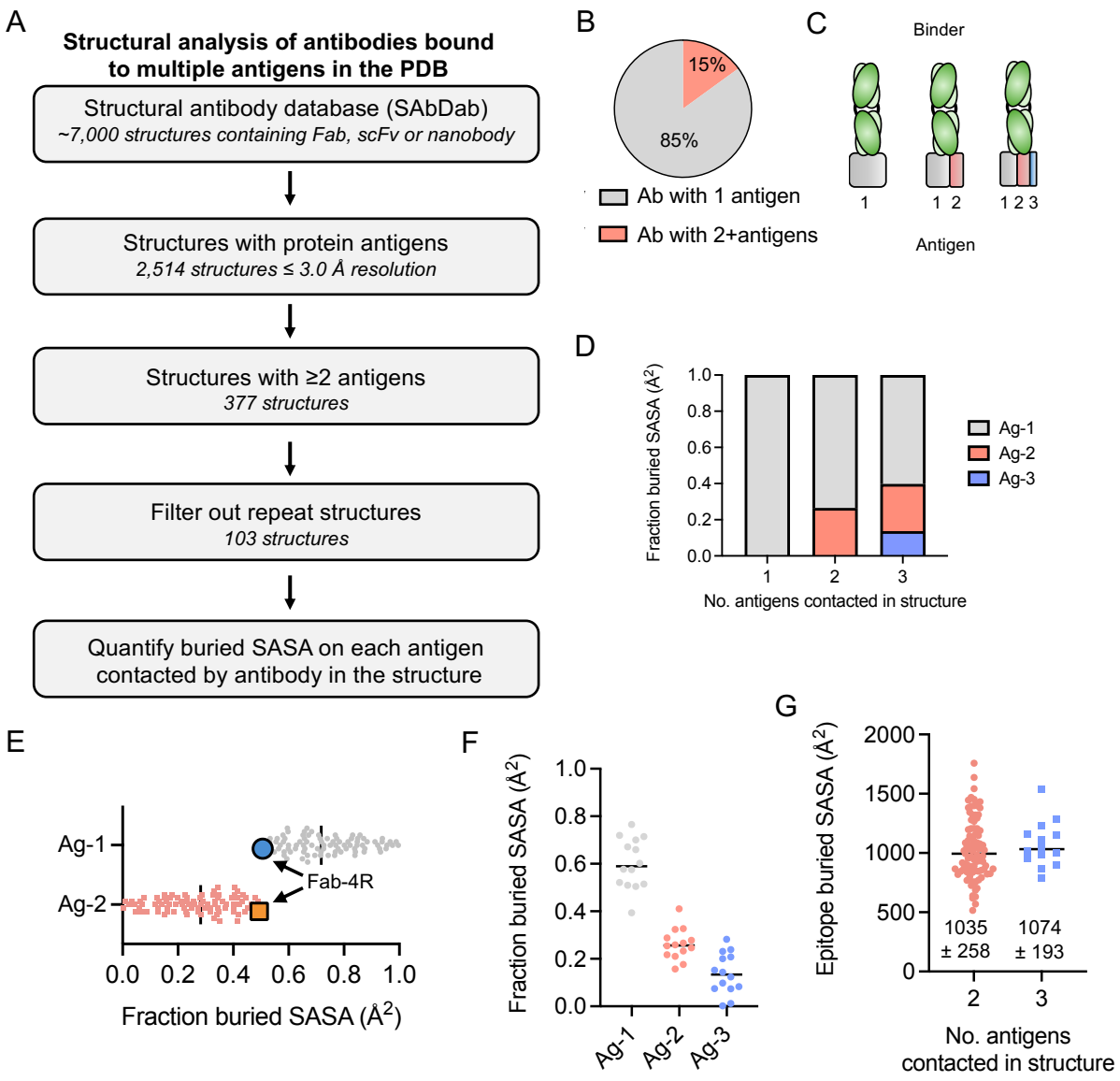

Figure 5.5 Structural analysis of antibodies contacting multiple antigens. (A) Workflow for quantitative assessment of buried epitope solvent accessible surface area (SASA) for binders in SAbDab. (B) Fraction of high-resolution (≤ 3.0 Å) antibody structures that form direct contacts with one antigen (grey) and two or more antigens (red). (C) Schematic for antibody recognition of one, two, or three antigens. (D) Fraction buried SASA for antibodies contacting one, two, or three antigens. (E) Fraction buried surface area between chains in structures of antibodies contacting two antigens. The structure of Fab-4R bound to FKBP12-rapamycin-mTOR^{FRB} is included showing mTOR^{FRB} (blue circle) and FKBP12 (orange square). (F) Fraction buried surface area between chains in structures of antibodies contacting three antigens. (G) Epitope size for structures of antibodies contacting two or three antigens.

antigen complexes while they bury an average of 59% SASA on Ag-1, 26% SASA on Ag-2, and 15% SASA on Ag-3 in heterotrimeric complexes (Figure 5.5E and F). Antigen-based SASA burial for the crystal structure of Fab-4R bound to FKBP12-rapamycin-mTOR^{FRB} described in this chapter is highlighted in Figure 5.5E. This comparison demonstrated that the Fab-4R paratope-epitope distribution is among the most balanced in all antibody structures described to date. Lastly, heterodimeric epitope sizes were quantified on average to be 1035 $\pm$ 258 Å^2 while heterotrimeric epitopes were on average 1074 $\pm$ 193 Å^2 (Figure 5.5G). Both of these values align with the reported average antibody epitope size of 1068 $\pm$ 314 Å^2 (176).

This quantitative pipeline revealed that the high selectivity for ternary complex recognition by Fab-4R is likely mediated by precisely balanced SASA burial between FKBP12 and mTOR^{FRB}. This aligns with the O-ring theory, which posits that binding hot spots in protein-protein interfaces are typically surrounded by a ring of energetically weak interactions that are critical for desolvation near and around the hot spots (179). According to this theory, it was hypothesized that energetically important interactions between Fab-4R and FKBP12-rapamycin-mTOR^{FRB} occur at the center of the epitope near the rapamycin-induced interface between FKBP12 and mTOR^{FRB}. To test this, structure-guided mutagenesis was employed to assess the contribution of Fab-4R paratope side chains that interact with FKBP12 or mTOR^{FRB}. Five paratope side chains located in CDR-H1, CDR-H2, and CDR-H3 were mutated to alanine. This set included Y33^{H1}, S57^{H2}, E105^{H3}, L110^{H3}, and W112^{H3}, which were observed to form direct interactions at the interface between FKBP12 and mTOR^{FRB} (Figure 5.6A). Each alanine variant of Fab-4R was initially validated for binding to FKBP12 and mTOR^{FRB} in the

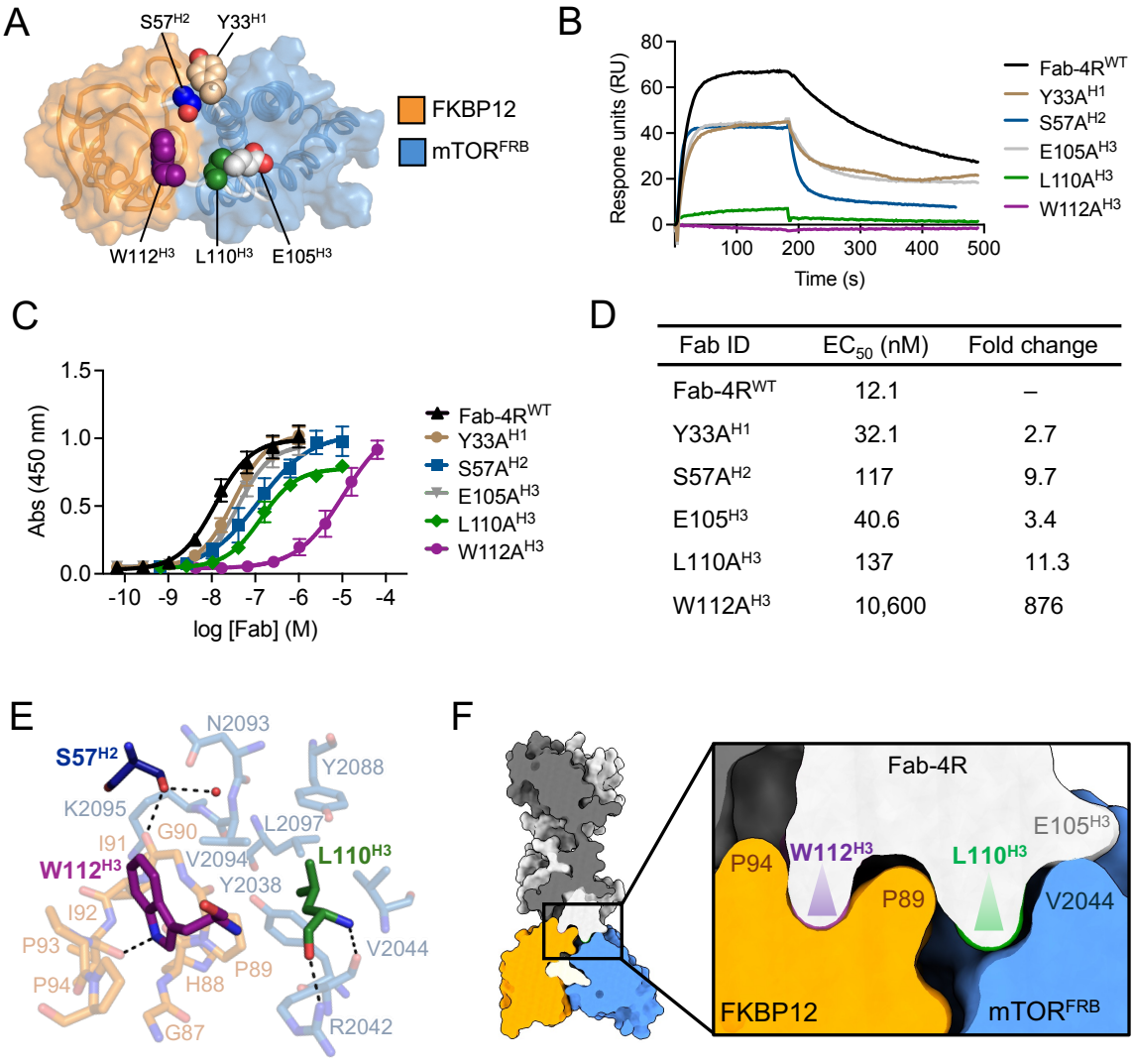

Fab ID	EC_{50} (nM)	Fold change
Fab-4R^{WT}	12.1	–
Y33A^{H1}	32.1	2.7
S57A^{H2}	117	9.7
E105^{H3}	40.6	3.4
L110A^{H3}	137	11.3
W112A^{H3}	10,600	876

Figure 5.6 A two-residue hydrophobic clamp mediates ternary complex recognition. (A) Directly interacting side chains in the Fab-4R paratope (spheres) selected for mutation to alanine. (B) Single point SPR sensorgrams for 200 nM Fab-4R^{WT} or the indicated variants binding to mTOR^{FRB} and FKBP12 in the presence of 200 nM rapamycin. (C) Multi-point ELISA measuring the binding of Fab-4R^{WT} or the indicated variants to FKBP12 and mTOR^{FRB} in the presence of 500 nM rapamycin (n = 3 independent replicates, mean ± SD). (D) EC_{50} (nM) values and fold change over wild-type for the indicated molecules. (E) Structural view of interactions made by S57^{H2} (dark blue), L110^{H3} (green), and W112^{H3} (purple) with FKBP12 (transparent orange) and mTOR^{FRB} (transparent blue). (F) Planar slice through the ternary complex showing the burial of L110^{H3} and W112^{H3} at the rapamycin-induced boundary between FKBP12 and mTOR^{FRB}.

presence of 200 nM rapamycin using single point SPR with 200 nM injections. These results demonstrated that all five of the CDR positions mutated to alanine in Fab-4R contribute toward recognition of the ternary complex with $S57A^{H2}$, $L110A^{H3}$ and $W112A^{H3}$ showing the largest effects (Figure 5.6B). Furthermore, dissociation curves from single point injections for $Y33A^{H1}$, $S57A^{H2}$, and $E105A^{H3}$ exhibited biphasic characteristics. This suggested that the binding equilibrium for these Fab-4R alanine variants should be described using a multivalent model consisting of high affinity and low affinity interactions with multiple dissociation rate constants. However, elucidating multivalent binding mechanisms via SPR is inherently challenging and often resolves rate constants with large uncertainties. Therefore, multi-point ELISA was employed to gain more generalized insights into the interaction between Fab-4R alanine variants and the FKBP12-rapamycin-$mTOR^{FRB}$ complex.

Titration of each Fab-4R alanine variant on immobilized FKBP12 and $mTOR^{FRB}$ in the presence of 500 nM rapamycin exhibited a similar trend as single point SPR with $S57A^{H2}$, $L110A^{H3}$, and $W112A^{H3}$ exhibiting the weakest EC_{50} values (Figure 5.6C and D). These three alanine variants exhibited 10-fold or greater fold change in EC_{50} values relative to wild-type Fab-4R, which indicated that these side chains contribute significant energy toward recognition of the ternary complex. Unsurprisingly, a structural analysis of $S57^{H2}$, $L110^{H3}$, and $W112^{H3}$ side chains revealed a highly coordinated interaction network located directly at the boundary between FKBP12 and $mTOR^{FRB}$ (Figure 5.6E). The extensive burial of $L110^{H3}$ and $W112^{H3}$ into hydrophobic pockets on $mTOR^{FRB}$ and FKBP12, respectively, appears to be the most critical aspect mediating the unique molecular recognition properties of Fab-4R. These residues ultimately form a bi-specific

hydrophobic clamp that latches across the rapamycin-induced interface between FKBP12 and $mTOR^{FRB}$ (Figure 5.6F). $L110^{H3}$ and $W112^{H3}$ side chains contribute 241 $Å^2$ to SASA burial, which amounts to 27% of the total paratope-epitope burial. Therefore, balanced SASA burial between FKBP12 and $mTOR^{FRB}$ in combination with burial of the $L110^{H3}$-$W112^{H3}$ hydrophobic clamp across the FKBP12-$mTOR^{FRB}$ interface represent crucial aspects driving high affinity and selectivity for the ternary complex but not individual domains by Fab-4R.

5.3.4 Fab-4R and scFv-4R selectively report mTOR inhibition through rapamycin-inducible recognition in human cells

A combination of biophysical and structure-guided mutational studies demonstrated exquisite recognition selectivity by Fab-4R for the FKBP12-rapamycin-$mTOR^{FRB}$ ternary complex. The crystal structure for Fab-4R bound to FKBP12-rapamycin-$mTOR^{FRB}$ was docked into a previously determined cryo-EM structure of mTOR (PDB: 6BCX) to investigate whether the Fab-4R epitope is accessible in the context of the mTOR architecture. This analysis revealed that Fab-4R is capable of binding to native cell-derived FKBP12-rapamycin-mTOR complexes (Figure 5.7A). To investigate the efficacy of Fab-4R for isolating endogenous mTOR assemblies bound by FKBP12-rapamycin, cell-based immunoprecipitation studies were performed using both human and mouse cell lines. Expi293F cells were treated with vehicle or rapamycin overnight before co-immunoprecipitation with biotinylated Fab-4R or a negative control biotinylated isotype (Iso) Fab and western blot analysis. This experiment showed that Fab-4R engages mTOR and FKBP12 only in the presence of rapamycin (Figure 5.7B). Furthermore, Fab-4R

recognition was induced by treatment with the rapamycin analogs Everolimus and Temsirolimus but not by the ATP-competitive inhibitor Torin-1, underscoring its specificity for FKBP12-dependent inhibition (Figure 5.7C). Next, Expi293F cells were treated with varying concentrations of rapamycin. This experiment demonstrated that Fab-4R recognition is dose-dependent with an EC_{50} value of 1.4 nM, further highlighting its recognition specificity in a cell-based context (Figure 5.7D and E).

The mTORC1 and mTORC2 architectures are differentially remodeled by inhibition with FKBP12-rapamycin. Raptor is allosterically destabilized by FKBP12-rapamycin while Rictor is competitively obstructed (133, 134). To investigate whether Fab-4R reports mTORC1 and mTORC2 interaction remodeling, Expi293F cells were treated with vehicle or rapamycin before co-immunoprecipitation using Fab-4R. Canonical mTORC1 components including Raptor, PRAS40, and DEPTOR were not observed in the pulldown by Fab-4R. Moreover, canonical mTORC2 components including Rictor, DEPTOR, and mSin1 were not observed in the pulldown either. In contrast, mLST8 was co-immunoprecipitated with mTOR by Fab-4R, which suggests that its association with mTOR is not influenced by rapamycin (Figure 5.7F). Owing to 100% sequence conservation between human and mouse FRB domains and 97% sequence identity between human and mouse FKBP12, Fab-4R was tested for cross-reactivity using immunoprecipitation from human and mouse cell lines treated with vehicle or rapamycin (Figure 5.7G). These results demonstrated that Fab-4R is effective for isolating FKBP12-rapamcyin-mTOR complexes from mice, a critical model organism that has served as the focus for many paradigm shifting studies of rapamycin. The selectivity profile of Fab-4R was compared to Fab-2C, described in chapter 4, by immunoprecipitation from vehicle or

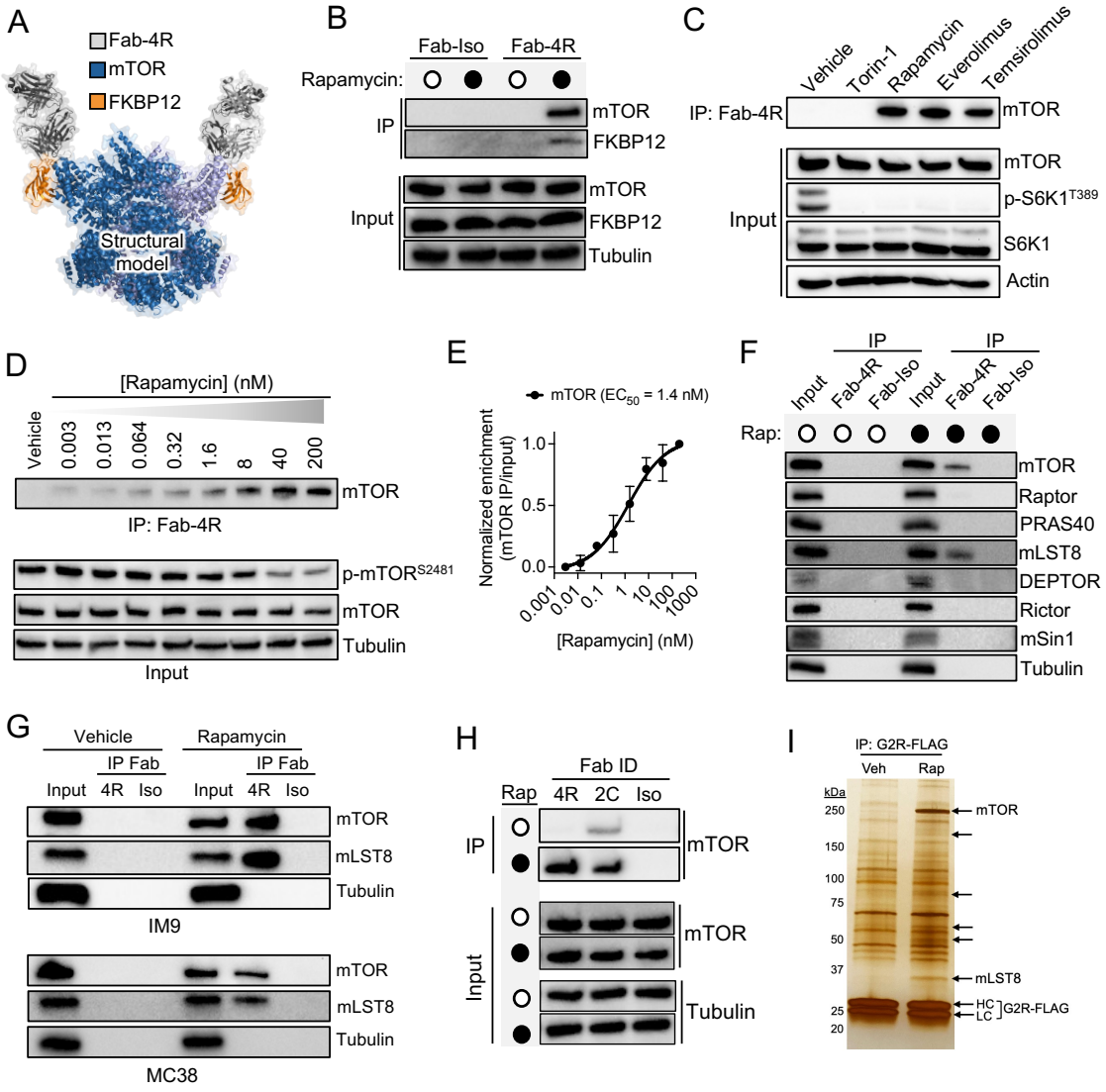

Figure 5.7 Fab-4R reports mTOR inhibition by FKBP12-rapamycin in human cells. (A) Alignment of the Fab-4R-FKBP12-Rapamycin-mTOR^{FRB} crystal structure with mTOR from PDB: 6BCX (Raptor and mLST8 removed for clarity). (B) Immunoprecipitation (IP) using Expi293 cells treated with vehicle or 200 nM rapamycin for 20 hours. (C) IP-western blot using Expi293 cells treated with vehicle, 50 nM Torin-1, or 200 nM of the indicated rapamycin analogs for 20 hours. (D) IP-western blot using Expi293 cells treated with vehicle or the indicated concentrations of rapamycin for 20 hours. (E) Quantification of mTOR from the experiment in D (n = 3 biological replicates, mean ± SD). (F) IP-western blot analysis mTORC1 and mTORC2 components using Expi293 cells treated with vehicle or 200 nM rapamycin for 20 hours. (G) IP from IM9 (human) and MC38 (mouse) cells. (H) Recognition selectivity comparison of Fab-4R and Fab-2C using IP from vehicle or rapamycin treated Expi293F cells. (I) Silver stain SDS-PAGE of anti-FLAG enriched vehicle or rapamycin treated Expi293F cells incubated with FLAG-Fab-4R.

rapamycin treated Expi293F cells. This experiment validated the modest recognition capability of Fab-2C for mTOR in vehicle treated cells and the enhanced accessibility to its epitope in rapamycin treated cells (Figure 5.7H). Fab-4R demonstrated no signal for mTOR in vehicle treated cells and a similar level for mTOR compared to Fab-2C in rapamycin treated cells. Lastly, silver stain gel analysis was used to assess the overall specificity of Fab-4R for vehicle and rapamycin treated cells. This experiment showed the presence of strong bands at molecular weights corresponding to mTOR and mLST8 in addition to at least four other bands in the pulldown from rapamycin treated cells (Figure 5.7I). Future studies employing mass spectrometry could be used to identify additional components in the native assemblies of mTOR bound by FKBP12-rapamycin.

Based on the applications described in this thesis pertaining to the conversion of Fabs to intracellular scFv probes, Fab-4R was reformatted to scFv-4R and transfected in Expi293F cells (Figure 5.8A). Anti-FLAG immunoprecipitation was performed to address the specificity of recognition by scFv-4R in cells treated with vehicle or rapamycin. Similar to the results of Fab-based immunoprecipitations, scFv-4R was found to engage with both mTOR and FKBP12 in a rapamycin-dependent fashion. Furthermore, dose-dependent recognition was observed for mTOR and mLST8 by scFv-4R in cells treated with rapamycin (Figure 5.8B). EC_{50} values of 0.5 nM rapamycin and 1.5 nM rapamycin were observed for the interaction of scFv-4R with mTOR and mLST8, respectively (Figure 5.8C and D). Confocal microscopy was employed to investigate whether intracellular expression of scFv-4R results in modulation of mTORC1 signaling. Analysis of p-$S6^{S240/244}$ phosphorylation levels in HeLa cells transfected with eGFP-tagged scFv-4R or scFv-Iso showed that mTORC1 signaling is not inhibited by expression of scFv-4R

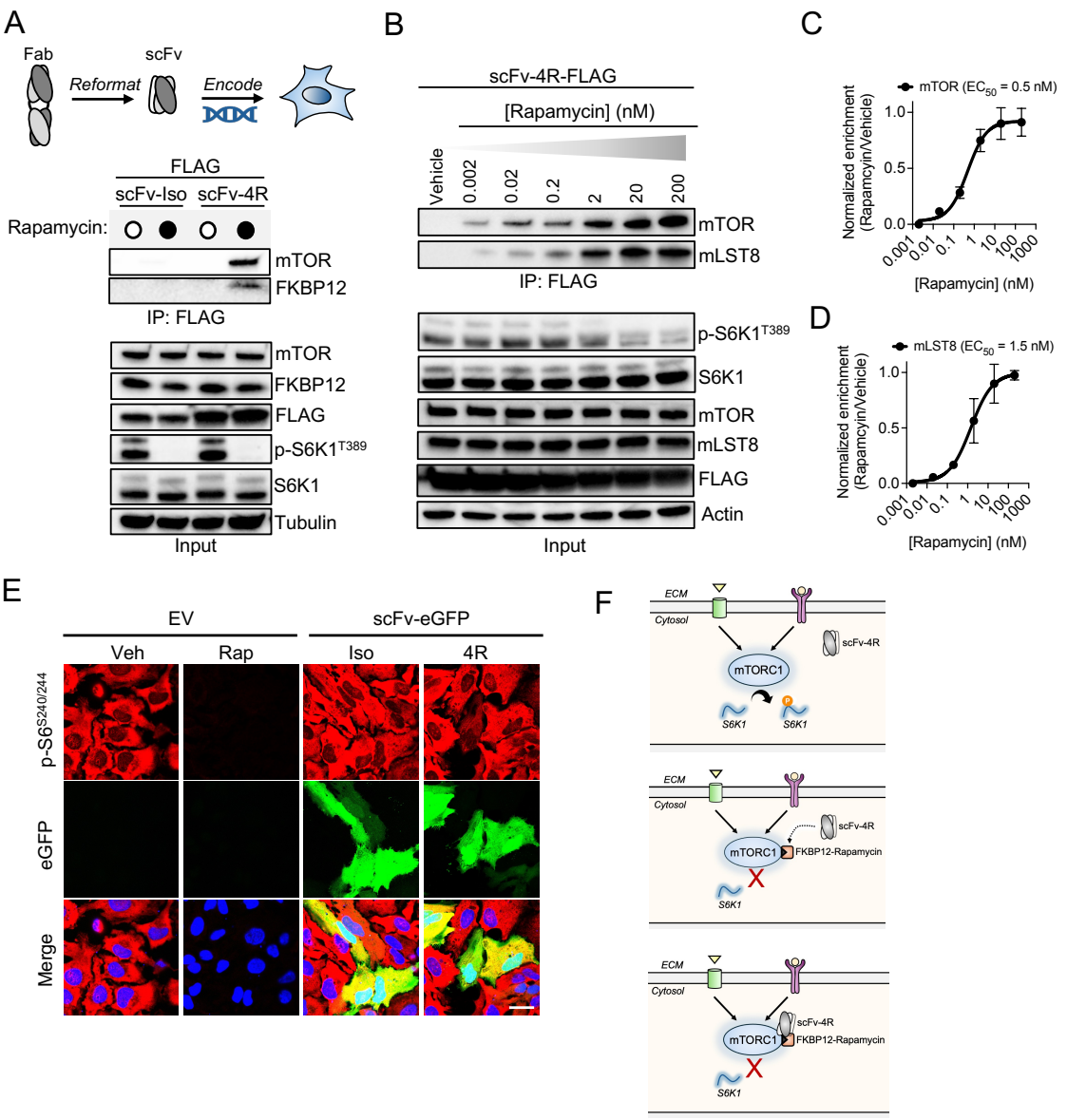

Figure 5.8 Intracellularly expressed scFv-4R reports mTOR inhibition by rapamycin. (A) Expi293 cells were transfected with FLAG-tagged non-targeting isotype control (scFv-Iso) or scFv-4R for 24 hours. Vehicle or 200 nM rapamycin were then administered for 20 hours before anti-FLAG immunoprecipitation (IP) and western blot analysis. (B) Sensitivity of scFv-4R to rapamycin measured by IP-western blot using Expi293 cells transfected with scFv-4R treated with vehicle or the indicated concentrations of rapamycin for 1 hour. (C) Quantification of mTOR in the scFv-4R pulldown from B (n = 3, mean ± SD). (D) Quantification of mLST8 in the scFv-4R pulldown in B (n = 3, mean ± SD). (E) Immunofluorescent confocal microscopy analysis of p-S6$^{S240/244}$ phosphorylation in HeLa cells transfected with the indicated eGFP-tagged intrabodies. Scale bar denotes 32.3 μm. (F) Schematic for rapamycin-inducible recruitment of scFv-4R to the FKBP12-rapamycin-mTOR complex.

(Figure 5.8E). Together, these results demonstrate a novel cell-based platform for direct intracellular sensing and reporting of mTOR inhibition by FKBP12-rapamcyin (Figure 5.8F).

5.4 Discussion

The ability to sense and isolate endogenous drug-bound targets within the human proteome represents a critical barrier to understanding basic pharmacological mechanisms. Common readouts for addressing drug efficacy involve analysis of downstream component phosphorylation, protein levels, or gene transcription. However, these approaches lack the precision to directly address modulation of protein-protein interactions formed by the drug-bound target. This layer of information is especially valuable for the class of small molecules known as molecular glues. Molecular glues function by stabilizing or inducing a desired conditional protein-protein interaction (180). This is typically manifested in molecular glue compounds through utilizing one interface to engage a target protein while employing another interface to recruit an E3 ubiquitin ligase subunit leading to targeted degradation (181). The work described in this chapter focused on one of the earliest discovered molecular glues, rapamycin, which tethers the small peptidylprolyl isomerase FKBP12 to a substrate recruitment domain of mTOR. This relatively simple mechanism of induced proximity mediated by rapamycin leads to potent effects on cellular and organismal physiology.

Although the molecular glue-based tethering function of rapamycin has been thoroughly described, the pharmacological kinetics and phenotypes elicited through rapamycin administration are extremely complex and still being elucidated today. These

complexities are due to the modular nature of mTOR assembly into multiple structurally and functionally distinct complexes, mTORC1 and mTORC2. The FKBP12-rapamycin binding site is freely accessible in mTORC1 but is occluded in mTORC2 by the subunit called Rictor. Consequently, FKBP12-rapamycin is unable to bind directly to mTORC2 in cells but is able to bind and sequester newly synthesized molecules of mTOR before they are loaded into new mTORC2 assemblies. These mechanisms are responsible for the time-dependent inhibition mTORC1 and mTORC2 by rapamycin, whereby mTORC1 is acutely inhibited but mTORC2 inhibition requires typically 24 hours of continuous treatment with rapamycin. Therefore, determining when and which mTOR assembly is bound by FKBP12-rapamycin is not a trivial matter and cannot be elucidated directly from the total pool of mTOR. Furthermore, FKBP12-rapamycin binding to mTORC1 triggers allosteric destabilization of the mTOR-Raptor interaction, adding another layer of complexity to the mechanism of how rapamycin modulates mTORC1 and mTORC2 protein-protein interactions.

The work described in this chapter is based on the engineering of a synthetic antibody with customized molecular recognition properties that enables selective engagement with the rapamycin-induced complex of FKBP12 and mTOR but not FKBP12 or mTOR alone. Library sorting procedures involved iterative rounds of stringent subtractive selections against individual FKBP12 and $mTOR^{FRB}$ domains before phage enrichment in the presence of the FKBP12-rapamcyin-$mTOR^{FRB}$ ternary complex. Using this protocol, one unique phage clone (Fab-4R) was isolated that exhibited highly selective recognition of FKBP12-rapamcyin-$mTOR^{FRB}$ but not FKBP12 or $mTOR^{FRB}$ alone. Rigorous biophysical, structural, and computational analyses revealed critical molecular mechanisms driving

specificity for ternary complex recognition by Fab-4R. Binding assays revealed that the dynamic range for Fab-4R recognition of the ternary complex spans at least four orders of magnitude relative to its recognition of individual domains. In comparison to other structures of antibodies that simultaneously contact two antigens, Fab-4R is among the top ranked antibodies for equal distribution of buried SASA between each antigen. Moreover, the most significant energetic contributions by Fab-4R side chains ($L110^{H3}$ and $W112^{H3}$) were positioned centrally in the paratope-epitope interface and are located directly at the interface between FKBP12 and $mTOR^{FRB}$. Together, these results demonstrated that the regio-specific balance of epitope-paratope interactions and binding hot spots might be a critical aspect for generating binders with precise complex-specificity.

Fab-4R was implemented as a high-performance affinity reagent for isolation of native mTOR assemblies bound by FKBP12-rapamcyin from human cells. Immunoprecipitation studies revealed that Fab-4R reports mTOR inhibition in cells treated with even low picomolar levels of rapamycin. Rapamycin dose-dependent engagement of mTOR was confirmed using Fab-4R. Furthermore, co-immunoprecipitation studies revealed that Fab-4R reports rapamycin-resistant components in FKBP12-rapamycin bound mTOR assemblies, such as mLST8. To expand the scope of these unique recognition capabilities, Fab-4R was reformatted and expressed inside human cells as scFv-4R where its engagement with mTOR was confirmed to be completely rapamycin dependent. Intracellular expression of scFv-4R did not affect mTORC1 signaling, suggesting that this reagent can be genetically encoded in cells or tissues of interest as a selective reporter of intracellular mTOR inhibition by rapamycin.

The molecular recognition properties of Fab-4R suggest that affinity reagents can be broadly engineered for conditionally gated recognition of virtually any protein-protein interaction, including transiently formed complexes or molecular glue-induced complexes. This could be applied to the discovery of new molecular glue compounds that stabilize a particular protein-protein interaction with therapeutic relevance. The additional stabilization contributed by a complex-specific binder could allow for weak drug hits to be observed and characterized which might otherwise be lost in screening efforts. Furthermore, intracellular expression of a molecular glue-stabilizing scFv could stabilize and enhance the pharmacokinetic properties of a molecular glue compound under investigation. Finally, the ability to use complex-specific binders for isolation of endogenous molecular glue-bound target assemblies could enable rapid screening of target protein-protein interaction modulation, thereby providing direct information into the efficacy of a compound under investigation.

Although several complex-specific affinity reagents have been previously reported, the lack of rigorous biophysical or structural characterization imposes barriers to understand the mechanisms driving their recognition specificity. The engineering and characterization of Fab-4R described here provided key molecular insights into this rare class of complex-specific antibodies. This work demonstrated the importance of regio-specific SASA burial for positioning binding hot spots at the interface between molecular glue-bound antigen chains. Furthermore, these results highlight the utility of phage display for engineering synthetic Fabs with customizable recognition properties.

5.5 Materials and methods

Crystallization and structure determination. SNAP-tag was removed from $mTOR^{FRB}$ and FKBP12 by cleavage with Thrombin at room temperature overnight and was subsequently purified by IMAC using TALON resin (Takara). Fab-4R, $mTOR^{FRB}$, and FKBP12 were incubated in 1:1:1 molar ratio with 1 μM rapamycin before purification using size exclusion chromatography on a Sephadex 200 column in HBS. The complex was crystallized using the Protein Complex Suite (NeXtal) screen. Crystal growth was observed in 0.15 M Ammonium sulfate, 0.1 M TRIS pH 8.0, 15% PEG 4000. Hanging-drop seeded crystallization drops were set up by mixing of 1 μL of the complex with 1 μL of reservoir solution containing 0.15 M Ammonium sulfate, 0.1 M TRIS pH 8.0, 17.5% PEG 4000 at room temperature. The crystals were soaked in reservoir solution containing 10% PEG 400 before being flash frozen in liquid nitrogen. The NECAT 24-ID-E beamline at the Advanced Photon Source was used for X-ray diffraction data collection. The structure was solved using molecular replacement with structures of the Fab (PDB: 7MDJ) and FKBP12-rapamycin-$mTOR^{FRB}$ (PDB: 1FAP) using phaser (129). The structure refinements were done using REFMAC (182). Models were manually built Coot (131).

Surface plasmon resonance. Surface plasmon resonance (SPR) experiments were performed using a MASS-1 (Bruker) instrument. $mTOR^{FRB}$, FKBP12, or $mTOR^{FRB}$ and FKBP12 together were immobilized via 6xHis-tags to an Ni-NTA sensor surface. Multi-point kinetic experiments for Fab-4R binding kinetics used FKBP12 and $mTOR^{FRB}$ immobilized in 200 nM rapamycin. The running buffer included 200 nM rapamycin. Fab-4R was diluted in running buffer containing 200 nM rapamycin and was injected as analyte

at 30 μl/min flow rate (20°C). Double reference was used to correct raw data. Sierra Analyser (Bruker) was used for analysis and curve fitting used a Langmuir 1:1 binding model. GraphPad Prism was used to generate plots. Single point injections involved Fab-4R alanine variants diluted in running buffer containing rapamycin and injection at 200 nM.

In vitro pulldown assay. SNAP-FKBP12-mTOR^{FRB} was site-specifically labeled with SNAP-Surface Alexa Fluor 488 (Neb) according to the manufacturer's protocol. In vitro pulldown of the Alexa488 labeled SNAP-FKBP12-mTOR^{FRB} (A488-SNAP-FKBP12-mTOR^{FRB}) was performed as described in chapter 2. Briefly, 20 nM of A488-SNAP-FKBP12-mTOR^{FRB} was incubated with 20 nM biotinylated Fab-4R or biotinylated isotype control Fab (Iso) in the presence or absence of 20 nM rapamycin for 20 minutes. Streptavidin magnetic beads (Promega) were added for 15 minutes and then beads were washed five times and eluted by boiling in SDS sample buffer for five minutes. Pulldown of A488-SNAP-FKBP12-mTOR^{FRB} was assessed via SDS-PAGE visualization in the Alexa Fluor 488 channel of a ChemiDoc Imaging System (Bio-Rad).

Differential scanning fluorimetry. Thermal stability assays were performed and monitored in 384-well plates (Bio-Rad HSP3801) using a real-time PCR instrument (Bio-Rad CFX384). Protein components were incubated at 4 μM in the presence or absence of 6 μM rapamycin for 30 minutes at room temperature. SYPRO Orange dye (Invitrogen S6651) was added to a final concentration of 4x. Temperature was ramped from 25°C to 95°C through 0.5°C/30 second intervals.

Structural bioinformatics analysis of antibodies. The Structural Antibody Database (SAbDab) (178) was mined for structures of antibodies bound to antigens found in the protein data bank (PDB). This set of structures contained Fab, scFv, or nanobody scaffolds and was filtered to remove structures with resolution > 3.0 Å, resulting in a list of 2,514 total structures. For purposes of quantifying buried SASA between binders that simultaneously contact two or more antigen chains, repeat structures were filtered out resulting in a set of 103 unique structures of binders bound to two or more antigens. These structures were subjected to epitope SASA quantification using ChimeraX. Results were plotted in GraphPad Prism.

Generation of DNA constructs. Fabs were cloned into SphI digested pSFV4 vector as previously described (127). Fab-4R alanine mutations were made using site-directed mutagenesis as described in chapter 2.

Phage display selection. Phage display selection was performed according to materials and methods in chapter 4.

Protein expression and purification. Expression of SNAP, SNAP-mTOR^{FRB}, SNAP-FKBP12, and SNAP-FKBP12-mTOR^{FRB} was performed according to the description in materials and methods of chapter 2.

Enzyme-Linked Immunosorbent Assays (ELISA). ELISA binding assays were performed generally as previously described (126). Single point, multi-point, rapamycin titration, alanine scanning ELISA experiments consisted of directly immobilizing target molecules to high binding 98-well microplates (Greiner), blocking plates with 1% bovine serum albumin (BSA) in PBS, adding Fabs diluted in 0.5% BSA in PBS-tween (PBST), detecting Fabs with protein L-horseradish peroxidase (Thermo Scientific), and colorimetric readout using the TMB substrate kit (Thermo Scientific).

Immunoprecipitation and western blot analysis. Immunoprecipitation and western blot analysis were performed as described in chapters 3 and 4.

Cell culture and transfection. Cell culture and transfection of Expi293F and HeLa cells were performed as described in chapters 3 and 4.

Confocal microscopy. Confocal microscopy analysis of p-S6$^{S240/244}$ levels in HeLa cells transfected with eGFP-tagged intrabodies was performed as described in chapter 4.

Chapter 6

Conclusions and future perspectives

6.1 The knowns and unknowns of mTOR signaling

The characterization of rapamycin over 50 years ago marked the initiation of serendipitous endeavors that ultimately led to the elucidation of the mTOR signaling pathway. Rapamycin was first acknowledged for its potent immunosuppressive effects and was eventually approved by the FDA to combat organ transplant rejection. Rapamycin has also played an indispensable role as a molecular tool to enable the discoveries of TOR and mTOR, effectively opening up an entirely new window into how eukaryotic cells sense and respond to environmental nutrients. Studies of the effects of rapamycin in diverse eukaryotic model organisms have exemplified a unique therapeutic profile that is characterized by a combination of benefits and toxicities. The most striking therapeutic benefits are in regard to robust lifespan and healthspan extension in organisms from fruit flies to nematodes to mice. However, significant side effects including immunosuppression, insulin resistance, and hyperlipidemia have imposed barriers to the clinical efficacy of rapamycin as a therapeutic molecule. Today, the therapeutic potential for targeting the mTOR pathway is still of great interest and is being actively pursued by many groups around the world. The work described in this thesis establishes new molecular tools to explore vulnerabilities that could potentially be exploited by the design of next-generation mTOR inhibitors.

One of the most significant barriers to developing safe and effective mTOR inhibitors is the ability to functionally decouple therapeutically beneficial downstream components from those that elicit side effects. The comparison of rapamycin with ATP-competitive

inhibitors represents a cornerstone example of how partial inhibition of mTOR substrate phosphorylation gives rise to a unique therapeutic profile compared to catalytic mTOR inhibition. However, the development of improved targeted therapeutics is currently hindered by an incomplete understanding of the diverse upstream activation and substrate recruitment mechanisms employed by mTORC1 and mTORC2. A promising avenue for gaining insights into this area is the systematic dissection of the distinct molecular and spatial modules that comprise the mTOR signaling network.

Current models posit that canonical mTORC1 activation and signaling occurs from the surface of lysosomes through an intricate molecular framework. This framework positions mTORC1 as a physical and functional gatekeeper of lysosomal biogenesis and autophagy. On the other hand, mTORC2 activation and signaling occurs through various endomembrane surfaces that may intersect with PI3K-Akt activation. Interestingly, inhibition of mTORC1 function has been suggested to be responsible for many of the therapeutic benefits stemming from rapamycin while mTORC2 inhibition has been suggested to mediate deleterious effects. However, emerging evidence is increasingly demonstrating that mTOR signaling is far more widespread throughout the cell than previously appreciated. The results described in chapter 3 of this thesis demonstrate that mTORC1 actively signals from inside the nucleus and that nucleus-restricted intrabodies are sufficient to inhibit nuclear mTORC1 substrate phosphorylation. This proof-of-concept work provides an in-depth validation of new tools to elicit functional perturbations to the mTOR signaling network with unprecedented spatial resolution. Decoding the subcellular organization and interactions of distinct mTOR pools could provide valuable information

to improve therapeutic strategies and reduce undesirable side effects associated with mTOR inhibitors.

Furthermore, elucidating conformational vulnerabilities within the mTOR architecture could enable the design of inhibitors with greater selectivity. The intrabodies described in chapter 4 demonstrated that mTORC1 is amenable to differential allosteric control mediated through conformational discrimination of the FRB domain. Identifying and characterizing other allosteric communication networks within the mTORC1 and mTORC2 architectures could potentially lead to enhanced therapeutic targeting strategies that are capable decoupling of subsets of downstream functional components. These endeavors could be greatly facilitated by the engineering and implementation of intrabody-based molecular tools.

6.2 Molecular recognition properties of engineered synthetic binders in this thesis

Display-based engineering technologies have transformed the field of monoclonal antibody generation. One of the primary advantages of employing phage or yeast display platforms over animal-derived hybridoma approaches is the capability for fine-tuned control over selection pressures and antigen properties. The work described in this thesis was based on the generation of synthetic antibody fragments with customized recognition specificity for multiple epitopes, conformational states, or interactions formed with the FRB substrate recruitment domain of mTOR (Figure 6.1). Implementation of these binders as Fab-based crystallographic chaperones and scFv-based intracellular probes enabled investigations into mechanisms of mTOR signaling with unprecedented resolution. The utility of synthetic intrabodies for dissecting therapeutic vulnerabilities in

signal transduction pathways is relatively straightforward with broad applicability. Similar to small molecule inhibitors or gene knockdowns, the simplest manifestation of intrabodies is to elicit drug-like activity perturbations in living cells based on selective engagement of functional interfaces. However, the genetic programmability and recognition properties of the intrabodies described in this thesis greatly expand the window of opportunity to elicit intracellular functional perturbations with conformational and spatial precision.

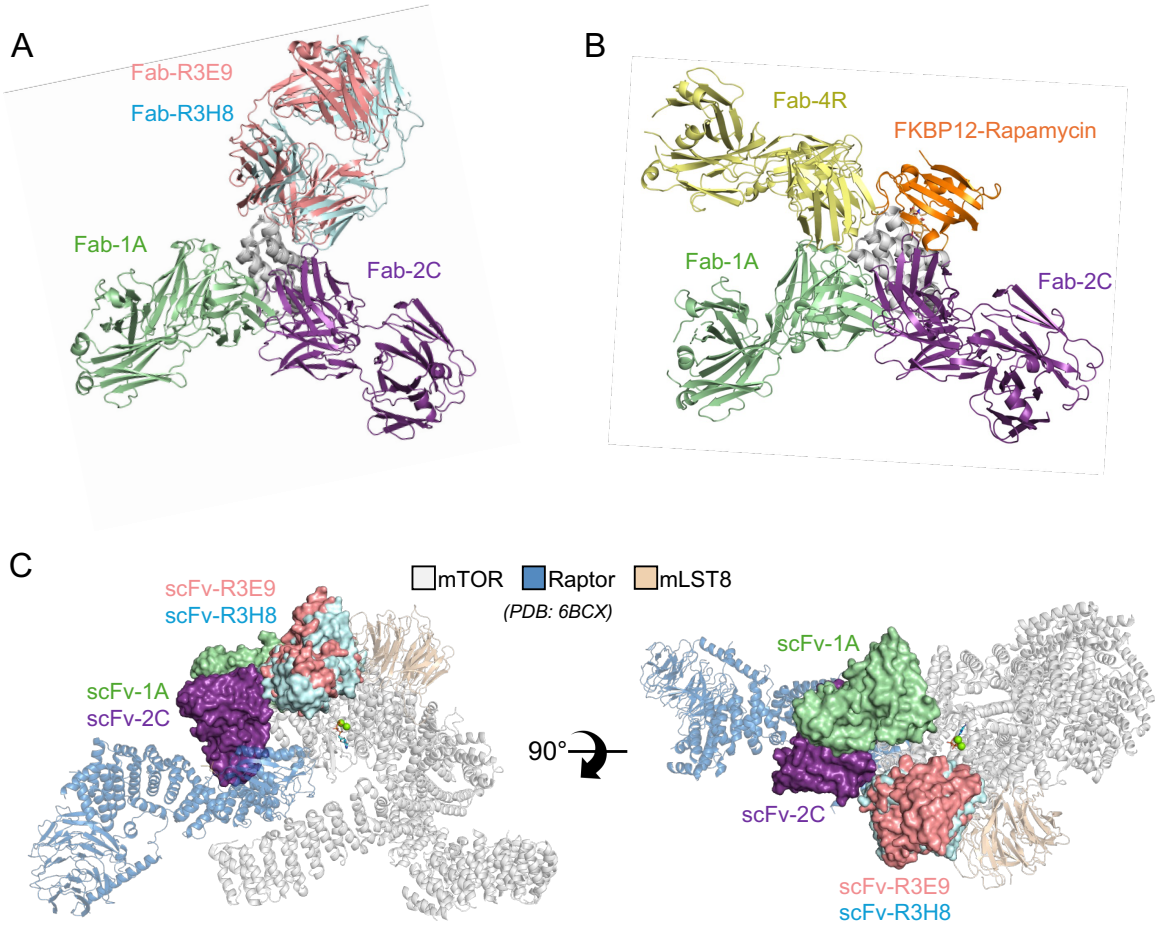

Figure 6.1 Structural view of synthetic binders generated in this thesis. (A) Alignment of crystal structures for the indicated mTOR^{FRB} targeting Fabs. (B) Alignment of crystal structures for Fabs with recognition sensitivity to FKBP12-rapamycin. (C) Structural models for the indicated intrabodies bound to mTORC1 using a previously determined cryo-EM structure (PDB: 6BCX)

6.2.1 Fab-R3H8 and scFv-R3H8

The work described in chapter 2 and chapter 3 is based on synthetic Fabs and genetically encoded scFv-based intrabodies that recapitulate the mechanism of inhibition of rapamycin. These binders were engineered in an epitope-directed phage display pipeline, which resulted in the generation of seven high affinity Fabs that target the substrate recruitment interface of $mTOR^{FRB}$. Rigorous characterization efforts pointed to two primary candidates, Fab-R3H8 and Fab-R3E9. A crystal structure of Fab-R3H8 bound to $mTOR^{FRB}$ revealed that its epitope overlaps with binding sites for FKBP12-rapamycin and for the mTOR substrates S6K1 and PRAS40. This structure also demonstrated that the conformation of $mTOR^{FRB}$ stabilized by Fab-R3H8 is nearly identical other crystal structures of $mTOR^{FRB}$. Implementation of scFv-R3H8 as an intracellular probe showed that engagement of mTOR results in allosteric destabilization of Raptor. This observation indicated that targeted engagement of the $mTOR^{FRB}$ substrate recruitment interface is sufficient to allosterically influence the mTOR-Raptor interaction. Furthermore, scFv-R3H8 exhibited rapamycin-like inhibition of mTOR signaling, thereby validating that obstruction of $mTOR^{FRB}$-based substrate recruitment is an effective mode of inhibition.

6.2.2 Fab-R3E9 and scFv-R3E9

The crystal structure of Fab-R3E9 bound to $mTOR^{FRB}$ revealed a highly similar binding pose as Fab-R3H8. Similar to Fab-R3H8, the Fab-R3E9 epitope overlaps directly with binding sites for FKBP12-rapamycin, S6K1, and PRAS40. However, crystal structure

analysis showed that Fab-R3E9 stabilizes a unique conformational state of $mTOR^{FRB}$. This conformation is characterized by the reorientation of side chains and α-helices, resulting in altered morphology of two hydrophobic grooves, HG1 and HG2, located at the substrate recruitment interface. HG1 morphology in the Fab-R3E9-bound state is formed by significant rotation of dihedrals in the W2101 side chain. Surprisingly, both χ_1 and χ_2 dihedrals of W2101 in the Fab-R3E9-bound state exhibit unusual torsional strain owing to their stabilization in energetically unfavorable geometries. It was hypothesized that W2101 is stabilized in this conformation by an extensive nest of aromatic π-stacking interactions formed with the Fab-R3E9 paratope. Structural alignment of $mTOR^{FRB}$ from crystal structures bound by Fab-R3E9 and Fab-R3H8 demonstrated unequivocal steric incompatibility between $F108^{H3}$ from the Fab-R3E9 paratope and W2101 from $mTOR^{FRB}$ in the Fab-R3H8-bound state. In contrast, HG2 morphology in the Fab-R3E9-bound state is a result of subtle α3 and α4 helix displacement, leading to the separation of V2095 and Y2038 side chains. Together, the coupling between side chain reorientation and α-helix displacement establishes a unique conformational state of $mTOR^{FRB}$ that has not been observed before. Strikingly, implementation of scFv-R3E9 as an intracellular probe revealed opposite effects on the stability of the mTOR-Raptor interaction compared to rapamycin or scFv-R3H8. These results provided critical insight into how an allosteric binding site can be functionally decoupled through subtle conformational rearrangements mediated by intrabody recognition.

6.2.3 Fab-1A and scFv-1A

Additional phage library sorting strategies were employed using $mTOR^{FRB}$ as a target and FKBP12-rapamycin as a soluble competitor. These efforts were undertaken to direct the epitopes of binders against other surfaces of $mTOR^{FRB}$ that are not directly involved in substrate recruitment. Due to the high stringency of subtractive selection pressures throughout the sorting procedures, only three unique functional phage clones (1A, 2C, and 4R) were isolated using this protocol. However, biophysical and structural characterization of these binders revealed markedly distinct modes of recognition against $mTOR^{FRB}$. A crystal structure of Fab-1A bound to $mTOR^{FRB}$ revealed that its epitope is located on the opposite side of the four-helix bundle relative to the substrate recruitment interface. Interestingly, Fab-1A recognition of $mTOR^{FRB}$ exhibited allosteric sensitivity to the presence of FKBP12-rapamycin. The use of Fab-1A as an energetic probe suggested that FKBP12-rapamycin alters the dynamics of $mTOR^{FRB}$ without eliciting obvious changes in the overall conformation of $mTOR^{FRB}$. Implementation of scFv-1A as an intracellular probe showed that it effectively engages with mTOR but does not modulate mTORC1 signaling. This information is extremely valuable as it demonstrates that drug design strategies against the Fab-1A epitope may not be an effective strategy to pursue.

6.2.4 Fab-2C and scFv-2C

Crystal structure determination of Fab-2C bound to $mTOR^{FRB}$ revealed an epitope located adjacent to the substrate recruitment interface, sandwiched in between the epitopes for Fab-1A and Fab-R3E9 or Fab-R3H8. Fab-2C also exhibited sensitivity to FKBP12-rapamycin but to a lesser extent compared to Fab-1A. The molecular basis of

Fab-2C sensitivity was hypothesized to be a result of two hydrogen bonds formed between Fab-2C and FKBP12, rendering Fab-2C slightly complex-specific. Interestingly, the Fab-2C epitope is accessible in the mTORC1 architecture, but immunoprecipitation studies showed that is only capable of engaging with mTOR in cells treated with rapamycin. This result suggested that rapamycin-induced destabilization of the mTOR-Raptor interaction provides accessibility for the Fab-2C epitope. Therefore, Fab-2C essentially functions as an architectural probe that reports the integrity of the mTOR-Raptor interaction. Implementation of scFv-2C as an intracellular probe demonstrated that it modulates the mTOR-Raptor interaction and potently inhibits mTORC1 signaling. These results represent a prototypical example of how intrabodies can be exploited to validate currently undruggable interfaces. Furthermore, this suggested that strategically designed small molecules could be generated and screened for their ability to inhibit mTOR signaling through this site.

6.2.5 Fab-4R and scFv-4R

In contrast to the other binders generated in this thesis, Fab-4R exhibits virtually undetectable recognition for $mTOR^{FRB}$ alone. The engineering of Fab-4R was based on iterative biopanning involving stringent subtractive selections against FKBP12 and $mTOR^{FRB}$ coupled with enrichment against the FKBP12-rapamycin-$mTOR^{FRB}$ ternary complex. Fab-4R represents a prototypical example of the rare class of complex-specific affinity reagents. Rigorous biophysical and structural characterization was used to delineate two energetic hotspots located at the rapamycin-induced boundary between FKBP12 and $mTOR^{FRB}$, thus providing an explanation for the exquisite recognition

specificity of Fab-4R. Furthermore, it is the first example of an antibody that binds selectively to a molecular glue-induced protein complex but not to the individual protein components alone. The utility of Fab-4R as a tool was validated by dose-dependent isolation of endogenous mTOR complexes bound by FKBP12-rapamycin from human and mouse cells. Furthermore, implementation of scFv-4R showed that this reagent can be expressed inside human cells to selectively and sensitively report mTOR inhibition by FKBP12-rapamycin.

6.3 Summary and implications of the results described in this thesis

6.3.1 Substrate recruitment and coordination by the FRB domain

The structural mechanism of $mTOR^{FRB}$-mediated substrate recruitment was described in 2017 through a combination of X-ray crystallography and biochemical signaling assays (67). This study showed that some mTORC1 substrates, such as S6K1 and PRAS40, exploit $mTOR^{FRB}$ as a mode of selective recruitment separate from canonical TOS-Raptor interactions. These S6K1-$mTOR^{FRB}$ and PRAS40-$mTOR^{FRB}$ interactions are both based on amphipathic α-helices docked onto the flat, hydrophobic surface of $mTOR^{FRB}$. A major barrier to understanding the universality of $mTOR^{FRB}$-mediated substrate recruitment is the lack of a singular consensus sequence motif sufficient to predict this type of interaction in mTORC1 signaling.

Crystal structures of two Fabs, Fab-R3E9 and Fab-R3H8, bound to the substrate recruitment interface of $mTOR^{FRB}$ revealed crucial insights into the molecular recognition capability of $mTOR^{FRB}$. The interactions formed by these synthetic binders emulated interactions by both S6K1 and PRAS40 despite the utilization of distinct amino acids from

entirely different secondary structures for recognition. Therefore, these observations suggest that the regiospecific coordination of divergent hydrophobic side chains at defined positions in the substrate recruitment interface is crucial for $mTOR^{FRB}$-mediated substrate docking. This broad molecular recognition characteristic is likely utilized to stabilize many distinct substrates through transient coordination proximal to the active site. Furthermore, these results suggest that delineating a consensus sequence motif for substrates utilizing $mTOR^{FRB}$ as a recruitment hitching post may be difficult owing to the low selectivity for hydrophobic amino acid side chains in the structures analyzed here.

6.3.2 Mechanism of allosteric control over mTORC1 stability

The allosteric destabilization of Raptor by FKBP12-rapamycin was first reported more than two decades ago and is considered a hallmark of the mechanism of inhibition by rapamycin (133, 157). Despite its biological and therapeutic relevance, a mechanistic description for this phenomenon is still lacking today. Here, the implementation of two conformation-specific synthetic intrabodies demonstrated that stabilization of $mTOR^{FRB}$ in distinct conformational states dramatically alters the integrity of the mTOR-Raptor interaction. These results suggested that $mTOR^{FRB}$ may act as a dynamic hub regulating the conformational dynamics throughout the architecture of mTORC1 in addition to its role as a substrate recruitment site. Furthermore, the finding that Fab-R3E9 stabilizes $mTOR^{FRB}$ side chains in energetically unfavorable conformations underscores the capability of synthetic Fabs for revealing phenotypes associated with transiently sampled states that are normally inaccessible using traditional techniques.

6.3.3 Functional decoupling of nuclear and cytoplasmic mTOR networks

The paradigm of subcellular mTOR regulation represents a major shift in understanding how eukaryotic cells dynamically sense and respond to environmental nutrients. It has been known for decades that mTOR licenses myriad downstream components that rewire nuclear circuits and gene transcription. However, recent studies have illuminated that the function of mTOR inside the nucleus may be responsible for a distinct set of biological outputs compared to canonical cytoplasmic mTOR pools (78, 183). The work described in chapter 3 demonstrates a first-in-class example of employing spatially restricted intrabodies for functional inhibition of mTOR signaling with subcellular spatial resolution. This approach represents a significant advancement in the repertoire of molecular tools geared toward manipulating mTOR function and provides enhanced precision compared to small molecule inhibitors or gene knockdowns. While this work utilized a heterologous substrate for proof-of-concept nuclear mTOR inhibition studies, future endeavors should employ RNA sequencing or phosphoproteomic approaches to uncover spatially organized networks under the control of distinct subcellular mTOR pools. Furthermore, genetically encoded intrabodies could be programmed in important eukaryotic model organisms for tissue- or subcellular-restricted mTOR modulation, thereby providing a route for rapamycin-like functional perturbations with unprecedented spatial resolution.

6.3.4 Inhibitory potential of a targeting novel functional site

There are two main classes of therapeutic mTOR inhibitors categorized by their mode of engagement with mTOR. First, rapamycin and rapamycin analogs bind together

with FKBP12 to the $mTOR^{FRB}$ substrate recruitment domain which blocks the entry of some mTORC1 substrates and also allosterically destabilizes the mTOR-Raptor interaction. Second, ATP-competitive inhibitors including Torin-1 and AZD8055 target mTOR catalysis. Despite decades of intensive research efforts, these are currently the only two methods of directly targeting mTOR with small molecules. Chapter 4 of this thesis describes the engineering and implementation of an intrabody that binds and modulates mTOR function through a site that is not targeted by conventional small molecule inhibitors. Pending further investigation of the therapeutic profile for scFv-2C, structure-guided design of cell-permeable compounds that recapitulate the mechanism of scFv-2C could contribute a third class of mTOR inhibitor. Moreover, these results suggest that generating intrabodies against additional functional sites throughout the mTORC1 and mTORC2 architectures could provide a rapid and feasible route to validate more potential inhibitor sites.

6.3.5 Utility of molecular glue-stabilizing antibodies

Molecular glue-based therapeutics are becoming increasingly relevant owing to their capability for degrading oncogenic proteins through induced proximity with E3 ubiquitin ligases. However, the rational design of novel molecular glues is inherently challenging and faces barriers of low hit rates and difficult structure-activity relationship screening. Furthermore, evaluating the efficacy of cognate target engagement by molecular glue compounds in a cellular environment can be difficult due to target heterogeneity or involvement in multi-subunit assemblies. The work in chapter 5 of this thesis describes the engineering of a synthetic Fab with exquisite recognition selectivity

for the rapamycin-induced FKBP12-rapamycin-mTOR^{FRB} ternary complex. Biophysical and structural studies of Fab-4R revealed how finely positioned paratope hot spots at the molecular glue-induced interface of FKBP12 and mTOR^{FRB} mediate high affinity ternary complex recognition while recognition of individual domains is rendered undetectable. Cell-based immunoprecipitation assays demonstrated that picomolar levels of FKBP12-rapamycin engaged with mTOR could be effectively isolated and analyzed. Furthermore, intracellular expression of scFv-4R exhibited a proof-of-concept platform for direct sensing and reporting of mTOR inhibition by FKBP12-rapamycin in living cells. This work serves as a cornerstone example that engineered synthetic antibodies can be exploited to sense and report conditionally induced protein-protein interactions that are central to molecular glue pharmacology.

References

1. C. Vēzina, A. Kudelski, S. N. Sehgal, Rapamycin (AY-22,989), a new antifungal antibiotic. I. Taxonomy of the producing streptomycete and isolation of the active principle. *The Journal of antibiotics* **28 10**, 721–6 (1975).

2. C. Vēzina, A. Kudelski, S. N. Sehgal, Rapamycin (AY-22,989), a new antifungal antibiotic. II. Fermentation, isolation and characterization. *The Journal of antibiotics* **28 10**, 727–32 (1975).

3. H. Baker, A. Sidorowicz, S. N. Sehgal, C. Vēzina, Rapamycin (AY-22,989), a new antifungal antibiotic. III. In vitro and in vivo evaluation. *The Journal of antibiotics* **31 6**, 539–45 (1978).

4. K. Singh, S. C. Sun, C. Vēzina, Rapamycin (AY-22,989), a new antifungal antibiotic. IV. Mechanism of action. *The Journal of antibiotics* **32 6**, 630–45 (1979).

5. K. Garber, Rapamycin's Resurrection: A New Way to Target the Cancer Cell Cycle. *JNCI: Journal of the National Cancer Institute* **93**, 1517–1519 (2001).

6. B. E. Bierer, *et al.*, Two distinct signal transmission pathways in T lymphocytes are inhibited by complexes formed between an immunophilin and either FK506 or rapamycin. *Proceedings of the National Academy of Sciences* **87**, 9231–9235 (1990).

7. R. Cafferkey, *et al.*, Dominant Missense Mutations in a Novel Yeast Protein related to Mammalian Phosphatidylinositol 3-Kinase and VPS34 Abrogate Rapamycin Cytotoxicity. *Molecular and Cellular Biology* **13**, 6012–6023 (1993).

8. J. Heitman, N. R. Movva, M. N. Hall, Targets for Cell Cycle Arrest by the Immunosuppressant Rapamycin in Yeast. *Science* **253**, 905–909 (1991).

9. N. C. Barbet, *et al.*, TOR controls translation initiation and early G1 progression in yeast. *MBoC* **7**, 25–42 (1996).

10. C. J. Sabers, *et al.*, Isolation of a Protein Target of the FKBP12-Rapamycin Complex in Mammalian Cells (∗). *Journal of Biological Chemistry* **270**, 815–822 (1995).

11. E. J. Brown, *et al.*, A mammalian protein targeted by G1-arresting rapamycin–receptor complex. *Nature* **369**, 756–758 (1994).

12. D. M. Sabatini, H. Erdjument-Bromage, M. Lui, P. Tempst, S. H. Snyder, RAFT1: A mammalian protein that binds to FKBP12 in a rapamycin-dependent fashion and is homologous to yeast TORs. *Cell* **78**, 35–43 (1994).

13. F. Meric-Bernstam, A. M. Gonzalez-Angulo, Targeting the mTOR Signaling Network for Cancer Therapy. *JCO* **27**, 2278–2287 (2009).

14. S. Imseng, C. H. Aylett, T. Maier, Architecture and activation of phosphatidylinositol 3-kinase related kinases. *Current Opinion in Structural Biology* **49**, 177–189 (2018).

15. S. K. Althaf Shaik, Evolution of PIKK family kinase inhibitors: A new age cancer therapeutics. *FBL* **25**, 1510–1537 (2020).

16. V. T. Deekshi Angira Althaf Shaik, Structural and strategic landscape of PIKK protein family and their inhibitors: an overview. *FBL* **25**, 1538–1567 (2020).

17. C. C. Thoreen, *et al.*, An ATP-competitive Mammalian Target of Rapamycin Inhibitor Reveals Rapamycin-resistant Functions of mTORC1*. *Journal of Biological Chemistry* **284**, 8023–8032 (2009).

18. H.-X. Yuan, Y. Xiong, K.-L. Guan, Nutrient Sensing, Metabolism, and Cell Growth Control. *Molecular Cell* **49**, 379–387 (2013).

19. R. A. Saxton, D. M. Sabatini, mTOR Signaling in Growth, Metabolism, and Disease. *Cell* **168**, 960–976 (2017).

20. R. L. Wolfson, *et al.*, Sestrin2 is a leucine sensor for the mTORC1 pathway. *Science* **351**, 43–48 (2016).

21. S. Kim, *et al.*, Leucine-sensing mechanism of leucyl-tRNA synthetase 1 for mTORC1 activation. *Cell Reports* **35** (2021).

22. G. A. Wyant, *et al.*, mTORC1 Activator SLC38A9 Is Required to Efflux Essential Amino Acids from Lysosomes and Use Protein as a Nutrient. *Cell* **171**, 642-654.e12 (2017).

23. J. W. Jung, *et al.*, Transmembrane 4 L Six Family Member 5 Senses Arginine for mTORC1 Signaling. *Cell Metabolism* **29**, 1306-1319.e7 (2019).

24. P. Gollwitzer, N. Grützmacher, S. Wilhelm, D. Kümmel, C. Demetriades, A Rag GTPase dimer code defines the regulation of mTORC1 by amino acids. *Nature Cell Biology* **24**, 1394–1406 (2022).

25. L. Bar-Peled, *et al.*, A Tumor Suppressor Complex with GAP Activity for the Rag GTPases That Signal Amino Acid Sufficiency to mTORC1. *Science* **340**, 1100–1106 (2013).

26. T. D. Lama-Sherpa, M.-H. Jeong, J. L. Jewell, Regulation of mTORC1 by the Rag GTPases. *Biochemical Society Transactions* **51**, 655–664 (2023).

27. R. Yonehara, *et al.*, Structural basis for the assembly of the Ragulator-Rag GTPase complex. *Nature Communications* **8**, 1625 (2017).

28. Z. Cui, *et al.*, Structure of the lysosomal mTORC1–TFEB–Rag–Ragulator megacomplex. *Nature* **614**, 572–579 (2023).

29. X. Long, Y. Lin, S. Ortiz-Vega, K. Yonezawa, J. Avruch, Rheb Binds and Regulates the mTOR Kinase. *Current Biology* **15**, 702–713 (2005).

30. A. Glaviano, *et al.*, PI3K/AKT/mTOR signaling transduction pathway and targeted therapies in cancer. *Molecular Cancer* **22**, 138 (2023).

31. M. Ebner, I. Lučić, T. A. Leonard, I. Yudushkin, PI(3,4,5)P3 Engagement Restricts Akt Activity to Cellular Membranes. *Molecular Cell* **65**, 416-431.e6 (2017).

32. G. Y. Liu, D. M. Sabatini, mTOR at the nexus of nutrition, growth, ageing and disease. *Nature Reviews Molecular Cell Biology* **21**, 183–203 (2020).

33. H.-X. Yuan, K.-L. Guan, The SIN1-PH Domain Connects mTORC2 to PI3K. *Cancer Discovery* **5**, 1127–1129 (2015).

34. W. A. Schroder, *et al.*, Human Sin1 contains Ras-binding and pleckstrin homology domains and suppresses Ras signalling. *Cellular Signalling* **19**, 1279–1289 (2007).

35. S. J. Humphrey, *et al.*, Dynamic Adipocyte Phosphoproteome Reveals that Akt Directly Regulates mTORC2. *Cell Metabolism* **17**, 1009–1020 (2013).

36. G. Yang, D. S. Murashige, S. J. Humphrey, D. E. James, A Positive Feedback Loop between Akt and mTORC2 via SIN1 Phosphorylation. *Cell Reports* **12**, 937–943 (2015).

37. W. Fu, M. N. Hall, Regulation of mTORC2 Signaling. *Genes* **11** (2020).

38. D. D. Sarbassov, D. A. Guertin, S. M. Ali, D. M. Sabatini, Phosphorylation and Regulation of Akt/PKB by the Rictor-mTOR Complex. *Science* **307**, 1098–1101 (2005).

39. R. C. Hresko, M. Mueckler, mTOR·RICTOR Is the Ser473 Kinase for Akt/Protein Kinase B in 3T3-L1 Adipocytes *. *Journal of Biological Chemistry* **280**, 40406–40416 (2005).

40. E. Jacinto, *et al.*, SIN1/MIP1 Maintains rictor-mTOR Complex Integrity and Regulates Akt Phosphorylation and Substrate Specificity. *Cell* **127**, 125–137 (2006).

41. A. Szwed, E. Kim, E. Jacinto, Regulation and metabolic functions of mTORC1 and mTORC2. *Physiological Reviews* **101**, 1371–1426 (2021).

42. D. R. Alessi, *et al.*, Characterization of a 3-phosphoinositide-dependent protein kinase which phosphorylates and activates protein kinase Bα. *Current Biology* **7**, 261–269 (1997).

43. A. Ragupathi, C. Kim, E. Jacinto, The mTORC2 signaling network: targets and cross-talks. *Biochemical Journal* **481**, 45–91 (2024).

44. F. Conciatori, *et al.*, mTOR Cross-Talk in Cancer and Potential for Combination Therapy. *Cancers* **10** (2018).

45. D. D. Sarbassov, *et al.*, Rictor, a novel binding partner of mTOR, defines a rapamycin-insensitive and raptor-independent pathway that regulates the cytoskeleton. *Curr Biol* **14**, 1296–1302 (2004).

46. J. M. García-Martínez, D. R. Alessi, mTOR complex 2 (mTORC2) controls hydrophobic motif phosphorylation and activation of serum- and glucocorticoid-induced protein kinase 1 (SGK1). *Biochemical Journal* **416**, 375–385 (2008).

47. E. Dazert, M. N. Hall, mTOR signaling in disease. *Current Opinion in Cell Biology* **23**, 744–755 (2011).

48. V. Panwar, *et al.*, Multifaceted role of mTOR (mammalian target of rapamycin) signaling pathway in human health and disease. *Signal Transduction and Targeted Therapy* **8**, 375 (2023).

49. L. Meng, X. S. Zheng, Toward rapamycin analog (rapalog)-based precision cancer therapy. *Acta Pharmacologica Sinica* **36**, 1163–1169 (2015).

50. E. S. Ali, *et al.*, Recent advances and limitations of mTOR inhibitors in the treatment of cancer. *Cancer Cell International* **22**, 284 (2022).

51. P. P. Hsu, *et al.*, The mTOR-regulated phosphoproteome reveals a mechanism of mTORC1-mediated inhibition of growth factor signaling. *Science* **332**, 1317–1322 (2011).

52. B. Mao, *et al.*, Overview of Research into mTOR Inhibitors. *Molecules* **27** (2022).

53. C. M. Chresta, *et al.*, AZD8055 Is a Potent, Selective, and Orally Bioavailable ATP-Competitive Mammalian Target of Rapamycin Kinase Inhibitor with In vitro and In vivo Antitumor Activity. *Cancer Research* **70**, 288–298 (2010).

54. A. Naing, *et al.*, Safety, tolerability, pharmacokinetics and pharmacodynamics of AZD8055 in advanced solid tumours and lymphoma. *British Journal of Cancer* **107**, 1093–1099 (2012).

55. G. Yang, *et al.*, Dissecting the biology of mTORC1 beyond rapamycin. *Science Signaling* **14**, eabe0161 (2021).

56. S. Battaglioni, D. Benjamin, M. Wälchli, T. Maier, M. N. Hall, mTOR substrate phosphorylation in growth control. *Cell* **185**, 1814–1836 (2022).

57. D.-H. Kim, *et al.*, mTOR interacts with raptor to form a nutrient-sensitive complex that signals to the cell growth machinery. *Cell* **110**, 163–175 (2002).

58. Q. Yang, K. Inoki, T. Ikenoue, K.-L. Guan, Identification of Sin1 as an essential TORC2 component required for complex formation and kinase activity. *Genes & Development* **20**, 2820–2832 (2006).

59. D.-H. Kim, *et al.*, GβL, a Positive Regulator of the Rapamycin-Sensitive Pathway Required for the Nutrient-Sensitive Interaction between Raptor and mTOR. *Molecular Cell* **11**, 895–904 (2003).

60. C. K. Yip, K. Murata, T. Walz, D. M. Sabatini, S. A. Kang, Structure of the Human mTOR Complex I and Its Implications for Rapamycin Inhibition. *Molecular Cell* **38**, 768–774 (2010).

61. C. H. S. Aylett, *et al.*, Architecture of human mTOR complex 1. *Science* **351**, 48–52 (2016).

62. A. Scaiola, *et al.*, The 3.2-Å resolution structure of human mTORC2. *Science Advances* **6**, eabc1251.

63. H. Nojima, *et al.*, The mammalian target of rapamycin (mTOR) partner, raptor, binds the mTOR substrates p70 S6 kinase and 4E-BP1 through their TOR signaling (TOS) motif. *J Biol Chem* **278**, 15461–15464 (2003).

64. S. S. Schalm, D. C. Fingar, D. M. Sabatini, J. Blenis, TOS Motif-Mediated Raptor Binding Regulates 4E-BP1 Multisite Phosphorylation and Function. *Current Biology* **13**, 797–806 (2003).

65. S. S. Schalm, J. Blenis, Identification of a Conserved Motif Required for mTOR Signaling. *Current Biology* **12**, 632–639 (2002).

66. H. Yang, *et al.*, mTOR kinase structure, mechanism and regulation. *Nature* **497**, 217–223 (2013).

67. H. Yang, *et al.*, Mechanisms of mTORC1 activation by RHEB and inhibition by PRAS40. *Nature* **552**, 368–373 (2017).

68. R. Böhm, *et al.*, The dynamic mechanism of 4E-BP1 recognition and phosphorylation by mTORC1. *Molecular Cell* **81**, 2403-2416.e5 (2021).

69. Z. Yu, *et al.*, Interactions between mTORC2 core subunits Rictor and mSin1 dictate selective and context-dependent phosphorylation of substrate kinases SGK1 and Akt. *Journal of Biological Chemistry* **298** (2022).

70. Y. Sancak, *et al.*, Ragulator-Rag Complex Targets mTORC1 to the Lysosomal Surface and Is Necessary for Its Activation by Amino Acids. *Cell* **141**, 290–303 (2010).

71. M. Roccio, J. L. Bos, F. J. T. Zwartkruis, Regulation of the small GTPase Rheb by amino acids. *Oncogene* **25**, 657–664 (2006).

72. N. Parmar, F. Tamanoi, “Chapter 3 - Rheb G-Proteins and the Activation of mTORC1” in *The Enzymes*, (Academic Press, 2010), pp. 39–56.

73. Y. Rabanal-Ruiz, V. I. Korolchuk, mTORC1 and Nutrient Homeostasis: The Central Role of the Lysosome. *International Journal of Molecular Sciences* **19** (2018).

74. X. Zhou, *et al.*, Dynamic Visualization of mTORC1 Activity in Living Cells. *Cell Rep* **10**, 1767–1777 (2015).

75. X. Zhou, *et al.*, Location-specific inhibition of Akt reveals regulation of mTORC1 activity in the nucleus. *Nat Commun* **11**, 6088 (2020).

76. C. R. Dufour, *et al.*, The mTOR chromatin-bound interactome in prostate cancer. *Cell Reports* **38**, 110534 (2022).

77. C. K. Tsang, H. Liu, X. F. S. Zheng, mTOR binds to the promoters of RNA polymerase I- and III-transcribed genes. *Cell Cycle* **9**, 953–957 (2010).

78. É. Audet-Walsh, *et al.*, Nuclear mTOR acts as a transcriptional integrator of the androgen signaling pathway in prostate cancer. *Genes Dev* **31**, 1228–1242 (2017).

79. Sturgill Thomas W., *et al.*, TOR1 and TOR2 Have Distinct Locations in Live Cells. *Eukaryotic Cell* **7**, 1819–1830 (2008).

80. J. R. Knudsen, *et al.*, Growth Factor-Dependent and -Independent Activation of mTORC2. *Trends in Endocrinology & Metabolism* **31**, 13–24 (2020).

81. D. R. Boulbés, T. Shaiken, D. D. Sarbassov, Endoplasmic reticulum is a main localization site of mTORC2. *Biochemical and Biophysical Research Communications* **413**, 46–52 (2011).

82. W. J. Oh, *et al.*, mTORC2 can associate with ribosomes to promote cotranslational phosphorylation and stability of nascent Akt polypeptide. *The EMBO Journal* **29**, 3939–3951 (2010).

83. C. Betz, *et al.*, mTOR complex 2-Akt signaling at mitochondria-associated endoplasmic reticulum membranes (MAM) regulates mitochondrial physiology. *Proceedings of the National Academy of Sciences* **110**, 12526–12534 (2013).

84. M. Rosner, M. Hengstschläger, “Detection of Cytoplasmic and Nuclear Functions of mTOR by Fractionation” in *mTOR: Methods and Protocols*, T. Weichhart, Ed. (Humana Press, 2012), pp. 105–124.

85. M. Ebner, B. Sinkovics, M. Szczygieł, D. W. Ribeiro, I. Yudushkin, Localization of mTORC2 activity inside cells. *Journal of Cell Biology* **216**, 343–353 (2017).

86. C. E. Gleason, *et al.*, Phosphorylation at distinct subcellular locations underlies specificity in mTORC2-mediated activation of SGK1 and Akt. *Journal of Cell Science* **132**, jcs224931 (2019).

87. N. Cybulski, V. Zinzalla, M. N. Hall, “Inducible raptor and rictor Knockout Mouse Embryonic Fibroblasts” in *mTOR: Methods and Protocols*, T. Weichhart, Ed. (Humana Press, 2012), pp. 267–278.

88. D. A. Guertin, *et al.*, Ablation in Mice of the mTORC Components raptor, rictor, or mLST8 Reveals that mTORC2 Is Required for Signaling to Akt-FOXO and PKCα, but Not S6K1. *Developmental Cell* **11**, 859–871 (2006).

89. Y.-G. Gangloff, *et al.*, Disruption of the Mouse mTOR Gene Leads to Early Postimplantation Lethality and Prohibits Embryonic Stem Cell Development. *Molecular and Cellular Biology* **24**, 9508–9516 (2004).

90. D. R. Wassarman, K. Bankapalli, L. J. Pallanck, K. M. Shokat, Tissue-restricted inhibition of mTOR using chemical genetics. *Proc Natl Acad Sci U S A* **119**, e2204083119 (2022).

91. N. Bouquier, *et al.*, AIMTOR, a BRET biosensor for live imaging, reveals subcellular mTOR signaling and dysfunctions. *BMC Biology* **18**, 81 (2020).

92. C. Li, *et al.*, TORSEL, a 4EBP1-based mTORC1 live-cell sensor, reveals nutrient-sensing targeting by histone deacetylase inhibitors. *Cell Biosci* **14**, 68 (2024).

93. C. Zhang, “Hybridoma Technology for the Generation of Monoclonal Antibodies” in *Antibody Methods and Protocols*, G. Proetzel, H. Ebersbach, Eds. (Humana Press, 2012), pp. 117–135.

94. M. Paduch, *et al.*, Generating conformation-specific synthetic antibodies to trap proteins in selected functional states. *Methods* **60**, 3–14 (2013).

95. L. Ledsgaard, M. Kilstrup, A. Karatt-Vellatt, J. McCafferty, A. H. Laustsen, Basics of Antibody Phage Display Technology. *Toxins* **10** (2018).

96. F. A. Fellouse, *et al.*, High-throughput Generation of Synthetic Antibodies from Highly Functional Minimalist Phage-displayed Libraries. *Journal of Molecular Biology* **373**, 924–940 (2007).

97. S. S. Sidhu, *et al.*, Phage-displayed Antibody Libraries of Synthetic Heavy Chain Complementarity Determining Regions. *Journal of Molecular Biology* **338**, 299–310 (2004).

98. K. R. Miller, *et al.*, T Cell Receptor-Like Recognition of Tumor In Vivo by Synthetic Antibody Fragment. *PLOS ONE* **7**, e43746 (2012).

99. M. I. Mustafa, A. Mohammed, Developing recombinant antibodies by phage display technology to neutralize viral infectious diseases. *SLAS Discovery* **29**, 100140 (2024).

100. P. K. Dominik, A. A. Kossiakoff, “Chapter Eleven - Phage Display Selections for Affinity Reagents to Membrane Proteins in Nanodiscs” in *Methods in Enzymology*, A. K. Shukla, Ed. (Academic Press, 2015), pp. 219–245.

101. N. Gera, M. Hussain, B. M. Rao, Protein selection using yeast surface display. *Methods* **60**, 15–26 (2013).

102. M. S. Newton, Y. Cabezas-Perusse, C. L. Tong, B. Seelig, In Vitro Selection of Peptides and Proteins—Advantages of mRNA Display. *ACS Synth. Biol.* **9**, 181–190 (2020).

103. R. R. Beerli, W. Wels, N. E. Hynes, Intracellular expression of single chain antibodies reverts ErbB-2 transformation. *Journal of Biological Chemistry* **269**, 23931–23936 (1994).

104. A. Auf der Maur, D. Escher, A. Barberis, Antigen-independent selection of stable intracellular single-chain antibodies. *FEBS Letters* **508**, 407–412 (2001).

105. A. Wörn, *et al.*, Correlation between in Vitro Stability and in Vivo Performance of Anti-GCN4 Intrabodies as Cytoplasmic Inhibitors*. *Journal of Biological Chemistry* **275**, 2795–2803 (2000).

106. S. Biocca, F. Ruberti, M. Tafani, P. Pierandrel-Amaldi, A. Cattaneo, Redox State of Single Chain Fv Fragments Targeted to the Endoplasmic Reticulum, Cytosol and Mitochondria. *Bio/Technology* **13**, 1110–1115 (1995).

107. T. H. Rabbitts, Intracellular Antibodies for Drug Discovery and as Drugs of the Future. *Antibodies* **12** (2023).

108. O. Hantschel, M. Biancalana, S. Koide, Monobodies as enabling tools for structural and mechanistic biology. *Current Opinion in Structural Biology* **60**, 167–174 (2020).

109. L. Wallon, *et al.*, Inhibition of RAS-driven signaling and tumorigenesis with a pan-RAS monobody targeting the Switch I/II pocket. *Proceedings of the National Academy of Sciences* **119**, e2204481119 (2022).

110. G. La Sala, *et al.*, Selective inhibition of STAT3 signaling using monobodies targeting the coiled-coil and N-terminal domains. *Nature Communications* **11**, 4115 (2020).

111. H. Dwivedi-Agnihotri, *et al.*, “Chapter 12 - An intrabody sensor to monitor conformational activation of β-arrestins” in *Methods in Cell Biology*, A. K. Shukla, Ed. (Academic Press, 2022), pp. 267–278.

112. Z. A. Knight, K. M. Shokat, Chemical Genetics: Where Genetics and Pharmacology Meet. *Cell* **128**, 425–430 (2007).

113. C. Zhu, *et al.*, Targeting KRAS mutant cancers: from druggable therapy to drug resistance. *Molecular Cancer* **21**, 159 (2022).

114. L. Huang, Z. Guo, F. Wang, L. Fu, KRAS mutation: from undruggable to druggable in cancer. *Signal Transduction and Targeted Therapy* **6**, 386 (2021).

115. K. W. Teng, *et al.*, Selective and noncovalent targeting of RAS mutants for inhibition and degradation. *Nature Communications* **12**, 2656 (2021).

116. P. Akkapeddi, *et al.*, Exploring switch II pocket conformation of KRAS(G12D) with mutant-selective monobody inhibitors. *Proc Natl Acad Sci U S A* **120**, e2302485120 (2023).

117. E. Ghosh, *et al.*, A synthetic intrabody-based selective and generic inhibitor of GPCR endocytosis. *Nature Nanotechnology* **12**, 1190–1198 (2017).

118. M. Baidya, *et al.*, Allosteric modulation of GPCR-induced β-arrestin trafficking and signaling by a synthetic intrabody. *Nature Communications* **13**, 4634 (2022).

119. M. Baidya, *et al.*, Genetically encoded intrabody sensors report the interaction and trafficking of β-arrestin 1 upon activation of G-protein–coupled receptors. *Journal of Biological Chemistry* **295**, 10153–10167 (2020).

120. L. J. Bailey, *et al.*, Locking the Elbow: Improved Antibody Fab Fragments as Chaperones for Structure Determination. *Journal of Molecular Biology* **430**, 337–347 (2018).

121. T. J. P. van Dam, F. J. T. Zwartkruis, J. L. Bos, B. Snel, Evolution of the TOR Pathway. *Journal of Molecular Evolution* **73**, 209–220 (2011).

122. J. B. Mannick, D. W. Lamming, Targeting the biology of aging with mTOR inhibitors. *Nature Aging* **3**, 642–660 (2023).

123. H. Yang, *et al.*, Mechanisms of mTORC1 activation by RHEB and inhibition by PRAS40. *Nature* **552**, 368–373 (2017).

124. N. B. Cole, Site-Specific Protein Labeling with SNAP-Tags. *Current Protocols in Protein Science* **73**, 30.1.1-30.1.16 (2013).

125. J. Abramson, *et al.*, Accurate structure prediction of biomolecular interactions with AlphaFold 3. *Nature* **630**, 493–500 (2024).

126. T. Slezak, *et al.*, An engineered ultra-high affinity Fab-Protein G pair enables a modular antibody platform with multifunctional capability. *Protein Sci* **29**, 141–156 (2020).

127. T. Slezak, A. A. Kossiakoff, Engineered Ultra-High Affinity Synthetic Antibodies for SARS-CoV-2 Neutralization and Detection. *J Mol Biol* **433**, 166956 (2021).

128. J. Schindelin, *et al.*, Fiji: an open-source platform for biological-image analysis. *Nat Methods* **9**, 676–682 (2012).

129. A. J. McCoy, *et al.*, Phaser crystallographic software. *J Appl Crystallogr* **40**, 658–674 (2007).

130. P. V. Afonine, *et al.*, Towards automated crystallographic structure refinement with phenix.refine. *Acta Crystallogr D Biol Crystallogr* **68**, 352–367 (2012).

131. P. Emsley, K. Cowtan, Coot: model-building tools for molecular graphics. *Acta Crystallogr D Biol Crystallogr* **60**, 2126–2132 (2004).

132. J. M. Carosi, C. Fourrier, J. Bensalem, T. J. Sargeant, The mTOR-lysosome axis at the centre of ageing. *FEBS Open Bio* **12**, 739–757 (2022).

133. N. Oshiro, *et al.*, Dissociation of raptor from mTOR is a mechanism of rapamycin-induced inhibition of mTOR function. *Genes to Cells* **9**, 359–366 (2004).

134. D. D. Sarbassov, *et al.*, Prolonged rapamycin treatment inhibits mTORC2 assembly and Akt/PKB. *Mol Cell* **22**, 159–168 (2006).

135. R. J. Petrella, M. Karplus, The energetics of off-rotamer protein side-chain conformations11Edited by F. Cohen. *Journal of Molecular Biology* **312**, 1161–1175 (2001).

136. J. Guo, H.-X. Zhou, Protein Allostery and Conformational Dynamics. *Chem. Rev.* **116**, 6503–6515 (2016).

137. C.-J. Tsai, A. del Sol, R. Nussinov, Allostery: Absence of a Change in Shape Does Not Imply that Allostery Is Not at Play. *Journal of Molecular Biology* **378**, 1–11 (2008).

138. S. Mukherjee, *et al.*, Engineered synthetic antibodies as probes to quantify the energetic contributions of ligand binding to conformational changes in proteins. *J Biol Chem* **293**, 2815–2828 (2018).

139. S. K. Erramilli, *et al.*, Conformation-specific Synthetic Antibodies Discriminate Multiple Functional States of the Ion Channel CorA. *Journal of Molecular Biology* **435**, 168192 (2023).

140. S. K. Marafie, F. Al-Mulla, J. Abubaker, mTOR: Its Critical Role in Metabolic Diseases, Cancer, and the Aging Process. *International Journal of Molecular Sciences* **25** (2024).

141. F. Boutouja, C. M. Stiehm, H. W. Platta, mTOR: A Cellular Regulator Interface in Health and Disease. *Cells* **8** (2019).

142. K. Y. Linde-Garelli, K. B. Rogala, Structural mechanisms of the mTOR pathway. *Current Opinion in Structural Biology* **82**, 102663 (2023).

143. Y. Hwang, *et al.*, Disruption of the Scaffolding Function of mLST8 Selectively Inhibits mTORC2 Assembly and Function and Suppresses mTORC2-Dependent Tumor Growth In Vivo. *Cancer Research* **79**, 3178–3184 (2019).

144. J. Choi, J. Chen, S. L. Schreiber, J. Clardy, Structure of the FKBP12-Rapamycin Complex Interacting with Binding Domain of Human FRAP. *Science* **273**, 239–242 (1996).

145. Q. Liu, *et al.*, Kinome-wide Selectivity Profiling of ATP-competitive Mammalian Target of Rapamycin (mTOR) Inhibitors and Characterization of Their Binding Kinetics*. *Journal of Biological Chemistry* **287**, 9742–9752 (2012).

146. P. K. Dominik, *et al.*, Conformational Chaperones for Structural Studies of Membrane Proteins Using Antibody Phage Display with Nanodiscs. *Structure* **24**, 300–309 (2016).

147. H. A. Bruce, *et al.*, Engineered antigen-binding fragments for enhanced crystallization of antibody:antigen complexes. *Protein Science* **33**, e4824 (2024).

148. R. Lieu, *et al.*, Rapid and robust antibody Fab fragment crystallization utilizing edge-to-edge beta-sheet packing. *PLOS ONE* **15**, e0232311 (2020).

149. K. Inoki, Y. Li, T. Zhu, J. Wu, K.-L. Guan, TSC2 is phosphorylated and inhibited by Akt and suppresses mTOR signalling. *Nature Cell Biology* **4**, 648–657 (2002).

150. H. Yang, *et al.*, Structural insights into TSC complex assembly and GAP activity on Rheb. *Nature Communications* **12**, 339 (2021).

151. J. Cuéllar, *et al.*, Structural and functional analysis of the role of the chaperonin CCT in mTOR complex assembly. *Nature Communications* **10**, 2865 (2019).

152. N. Singh, *et al.*, Drug discovery and development: introduction to the general public and patient groups. *Frontiers in Drug Discovery* **3** (2023).

153. X. Xie, *et al.*, Recent advances in targeting the “undruggable” proteins: from drug discovery to clinical trials. *Signal Transduction and Targeted Therapy* **8**, 335 (2023).

154. S. A. Lim, *et al.*, Targeting a proteolytic neoepitope on CUB domain containing protein 1 (CDCP1) for RAS-driven cancers. *J Clin Invest* **132** (2022).

155. M. Riso, *et al.*, Binding mode–guided development of high-performance antibodies targeting site-specific posttranslational modifications. *Proceedings of the National Academy of Sciences* **122**, e2411720121 (2025).

156. J. Zhu, C. B. Thompson, Metabolic regulation of cell growth and proliferation. *Nature Reviews Molecular Cell Biology* **20**, 436–450 (2019).

157. D.-H. Kim, *et al.*, mTOR Interacts with Raptor to Form a Nutrient-Sensitive Complex that Signals to the Cell Growth Machinery. *Cell* **110**, 163–175 (2002).

158. M. Lu, J. Wang, H. E. Ives, D. Pearce, mSIN1 Protein Mediates SGK1 Protein Interaction with mTORC2 Protein Complex and Is Required for Selective Activation of the Epithelial Sodium Channel *. *Journal of Biological Chemistry* **286**, 30647–30654 (2011).

159. G. A. Holdgate, C. Bardelle, S. K. Berry, A. Lanne, M. E. Cuomo, Screening for molecular glues – Challenges and opportunities. *SLAS Discovery* **29**, 100136 (2024).

160. A. M. März, A.-K. Fabian, C. Kozany, A. Bracher, F. Hausch, Large FK506-Binding Proteins Shape the Pharmacology of Rapamycin. *Molecular and Cellular Biology* **33**, 1357–1367 (2013).

161. K. H. Schreiber, *et al.*, Rapamycin-mediated mTORC2 inhibition is determined by the relative expression of FK506-binding proteins. *Aging Cell* **14**, 265–273 (2015).

162. D. Wang, H. J. Eisen, “Mechanistic Target of Rapamycin (mTOR) Inhibitors” in *Pharmacology of Immunosuppression*, H. J. Eisen, Ed. (Springer International Publishing, 2022), pp. 53–72.

163. F. J. Dumont, Q. Su, Mechanism of action of the immunosuppressant rapamycin. *Life Sciences* **58**, 373–395 (1995).

164. K. Makki, *et al.*, Beneficial Metabolic Effects of Rapamycin Are Associated with Enhanced Regulatory Cells in Diet-Induced Obese Mice. *PLOS ONE* **9**, e92684 (2014).

165. Y. Ekici, *et al.*, Effect of Rapamycin on Wound Healing: An Experimental Study. *Transplantation Proceedings* **39**, 1201–1203 (2007).

166. Y. Raynes, J. C. Santiago, F. A. Lemieux, L. Darwin, D. M. Rand, Sex, tissue, and mitochondrial interactions modify the transcriptional response to rapamycin in Drosophila. *BMC Genomics* **25**, 766 (2024).

167. E. L. Baar, K. A. Carbajal, I. M. Ong, D. W. Lamming, Sex- and tissue-specific changes in mTOR signaling with age in C57BL/6J mice. *Aging Cell* **15**, 155–166 (2016).

168. B. R. Curtis, J. G. McFarland, G.-G. Wu, G. P. Visentin, R. H. Aster, Antibodies in Sulfonamide-Induced Immune Thrombocytopenia Recognize Calcium-Dependent Epitopes on the Glycoprotein IIb/IIIa Complex. *Blood* **84**, 176–183 (1994).

169. F. Van Leuven, P. Marynen, J. J. Cassiman, H. Van den Berghe, The epitopes of two complex-specific monoclonal antibodies, related to the receptor recognition site, map to the COOH-terminal end of human alpha 2-macroglobulin. *Journal of Biological Chemistry* **261**, 6933–6937 (1986).

170. K. O. A. Yu, *et al.*, Production and characterization of monoclonal antibodies against complexes of the NKT cell ligand α-galactosylceramide bound to mouse CD1d. *Journal of Immunological Methods* **323**, 11–23 (2007).

171. P. A. Hessian, L. Fisher, The heterodimeric complex of MRP-8 (S100A8) and MRP-14 (S100A9). *European Journal of Biochemistry* **268**, 353–363 (2001).

172. S. Eastman, *et al.*, A study of complexes of class II invariant chain peptide: Major histocompatibility complex class II molecules using a new complex-specific monoclonal antibody. *European Journal of Immunology* **26**, 385–393 (1996).

173. R. A. Gadkari, S. Roy, N. Rekha, N. Srinivasan, R. R. Dighe, Identification of a heterodimer-specific epitope present in human chorionic gonadotrophin (hCG) using a monoclonal antibody that can distinguish between hCG and human LH. *Journal of Molecular Endocrinology* **34**, 879–887 (2005).

174. C. Puttikhunt, *et al.*, Novel anti-dengue monoclonal antibody recognizing conformational structure of the prM-E heterodimeric complex of dengue virus. *Journal of Medical Virology* **80**, 125–133 (2008).

175. Gromowski Gregory D., Barrett Nicholas D., Barrett Alan D. T., Characterization of Dengue Virus Complex-Specific Neutralizing Epitopes on Envelope Protein Domain III of Dengue 2 Virus. *Journal of Virology* **82**, 8828–8837 (2008).

176. P. B. P. S. Reis, *et al.*, Antibody-Antigen Binding Interface Analysis in the Big Data Era. *Frontiers in Molecular Biosciences* **9** (2022).

177. G. J. Bartlett, R. W. Newberry, B. VanVeller, R. T. Raines, D. N. Woolfson, Interplay of Hydrogen Bonds and n→π* Interactions in Proteins. *J. Am. Chem. Soc.* **135**, 18682–18688 (2013).

178. J. Dunbar, *et al.*, SAbDab: the structural antibody database. *Nucleic Acids Research* **42**, D1140–D1146 (2014).

179. J. Li, Q. Liu, 'Double water exclusion': a hypothesis refining the O-ring theory for the hot spots at protein interfaces. *Bioinformatics* **25**, 743–750 (2009).

180. J. M. Sasso, *et al.*, Molecular Glues: The Adhesive Connecting Targeted Protein Degradation to the Clinic. *Biochemistry* **62**, 601–623 (2023).

181. G. Dong, Y. Ding, S. He, C. Sheng, Molecular Glues for Targeted Protein Degradation: From Serendipity to Rational Discovery. *J. Med. Chem.* **64**, 10606–10620 (2021).

182. G. N. Murshudov, A. A. Vagin, E. J. Dodson, Refinement of macromolecular structures by the maximum-likelihood method. *Acta Crystallogr D Biol Crystallogr* **53**, 240–255 (1997).

183. Y. Chen, L. Han, C. R. Dufour, A. Alfonso, V. Giguère, Canonical and Nuclear mTOR Specify Distinct Transcriptional Programs in Androgen-Dependent Prostate Cancer Cells. *Molecular Cancer Research* **22**, 113–124 (2024).